Investigation of the behavior and interaction of ginsenoside Rh2 in model membranes containing cholesterol and sphingomyelin

Ginsenoside Rh2 のコレステロールとスフィンゴミエリン含有モデル膜における相互作用と物性の解明

A Thesis Submitted to the
Graduate School of Science
Osaka University

In Partial Fulfillment of the Requirements for the Degree of
Doctor of Philosophy (Ph.D) in Chemistry

By

Darcy Lacanilao Garza

Department of Chemistry
Graduate School of Science
Osaka University

2022

~ Table of Contents ~

~ List of Abbreviations ~

calcein	2,7-bis[bis(carboxymethyl)aminomethyl] fluorescein
Cho	Cholesterol
ChoGlc	Cholesteryl-β-D-glucoside
DPH	1,6-diphenyl-1,3,5- hexatriene
DPPC	1,2-dipalmitoyl-sn-glycero-3-phosphorylcholine
EC_{50}	Half maximal effective concentration
EDP	Electron density profile
eggPC	Egg phosphatidylcholine
ER	Endoplasmic reticulum
eSM	Egg sphingomyelin
GP or GP_{340}	Generalized Polarization
GR	Glucocorticoid receptor
GRE	Glucocorticoid Responsive Element
GUV	Giant unilamellar vesicle
***K*p**	Partition coefficient
Ld	Liquid-disordered phase
Lo	Liquid-ordered phase
LUV	Large unilamellar vesicle
MD	Molecular dynamics
MLV	Multilamellar vesicle
NMR	Nuclear magnetic resonance
POPC	1-palmitoyl-2-oleoyl-sn-glycero-3-phosphorylcholine
PM	Plasma membrane
PSM	N-palmitoyl-D-erythro-sphingosylphosphorylcholine
r	Anisotropy
Rh2	20(*S*)-ginsenoside Rh2
SAR	Structure-activity relationship
So	Gel phase
SM	sphingomyelin
ss-NMR	Solid-state nuclear magnetic resonance
SSM	N-stearoyl-D-erythro-sphingosylphosphorylcholine
SUV	Small unilamellar vesicle

TEM	Transmission electron microscopy
T_m	Transition temperature
594-neg-SSM	594-neg-N-stearoylsphingomyelin
Δδ (CSA)	Chemical Shift Anisotropy
Δν	Quadrupolar Splitting
λ_{em}	Emission maxima
π – A	Surface pressure – Molecular Area

~ Chapter 1 ~

General Introduction

1. Ginseng (Panax L.) and Ginsenosides

Ginseng (*Panax L.*) is one of the most-utilized herbal medicine documented from the Han Dynasty. The genus *Panax L.* of the Araliaceae family has a Greek etymology that means "all-healing" (Leung and Wong, 2010). Ginseng has been used as a standard health tonic in ancient Chinese medicine to foster somatic and intellectual functioning. It is known to deliver several benefits – from providing bodily refreshment to improving blood circulation. *Panax ginseng* C.A. Meyer (*Panax ginseng*, Asian or Korean ginseng), *Panax quinquefolius* L. (American ginseng), and *Panax notoginseng* (Burkill) F. H. Chen (Sanchi or Chinese ginseng) are the three well-known species of ginseng. With great interest, diverse research on ginseng has led to the discovery of other valuable species from the Araliaceae family (Bai *et al*., 2018). This includes *Panax japonicus* C.A. Meyer, *Panax vietnamensis* Ha & Grushv., *Panax stipuleanatus* Tsai & K.M. Feng, *Panax bipinnatifidus* Seem., *Panax pseudo-ginseng* subsp. *himalaicus* Hara, and many more (Yang *et al.,* 2014).

Today, ginseng supplements are in demand for their numerous therapeutic applications. These dietary supplements alleviate certain diseases and improve cognitive performance. In 2013, the annual sales of ginseng reached approximately $2,084 million worldwide. Ginseng is cultivated in about 35 countries, and approximately 90% of which is grown in South Korea (27, 480 tons), China (44, 749 tons), Canada (6486 tons), and the US (1054 tons) (Baeg and So, 2013). The global industry of ginseng is still projected for market expansion as there is an unremitting demand for functional food. The global distribution of 17 ginseng species is shown in *Fig. 1.1* (Ratan *et al.,* 2021) (Zhang *et al*., 2020).

Figure 1.1. Global distribution of *Panax L.* The genus Panax in the family Araliaceae occurs primarily in the northern hemisphere and is cultivated in 35 countries across the globe. Cited and modified from Ratan *et al.,* 2021, and Zhang *et al*., 2020.

In a bibliometric analysis performed by Xu *et al.* in 2017., an upsurge in research about *Panax ginseng* has occurred from the beginning of the 21st century. Research on ginseng has been performed in 64 countries, and the number of publications has grown exponentially, especially in Asia. Based on publications indexed by the Web of Science™ Core Collection, conventional research domains focus on pharmacology (39%), plant science (26%), and integrative complementary medicine (19%). With several studies carried out on the pharmacological activity of ginseng, research themes involving saponins and ginsenosides drew significant attention. They were the leading keywords on ginseng publications as denoted by the largest circles in *Fig. 1.2.* The purple ring surrounding the keyword nodes signifies high betweenness centrality – an indication of impending transformative discovery and the significant scientific contribution of these topics. And the reason for this is that ginseng saponins, also known as *ginsenosides*, are the bioactive ingredients of ginseng (Ratan *et al.*, 2021) (Hong *et al.*, 2021) (Shi *et al.*, 2019).

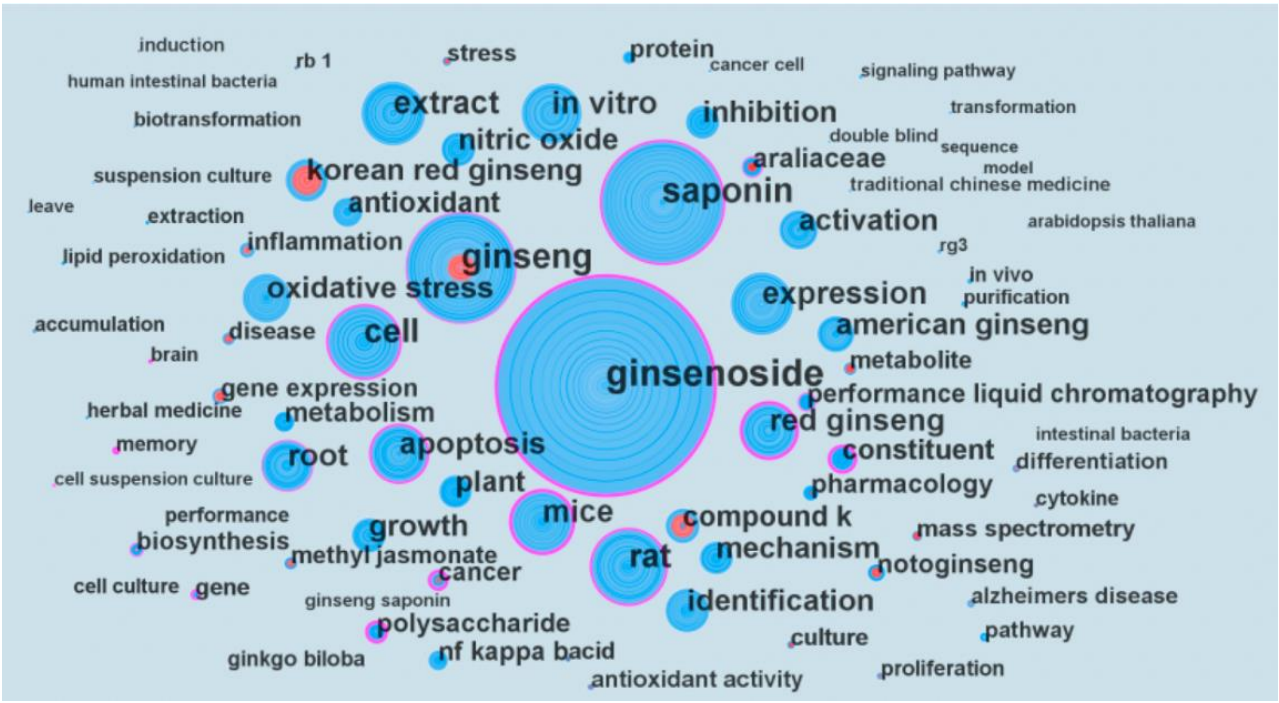

Figure 1.2. Major keywords of *Panax ginseng* research and burst detection result. (Xu *et al.*, 2017)

The primary chemical composition of *Panax ginseng* includes ginsenosides, non-saponins, and miscellaneous (lipids, polysaccharides, *etc.*) (*Fig. 1.3*). Ginsenosides are saponins comprised of a triterpenoid backbone with sugars moieties attached to specific sites, and they are subcategorized based on structural variances. The isolation of ginsenosides in the 1960s provided groundwork in understanding the therapeutic actions of ginseng; since then, much effort has been given to characterize and evaluate the functions of different ginsenosides (Leung and Wong, 2010) (Xiang *et al.*, 2008) (Shibata *et al.*, 1965). Today, there are over 300 ginsenosides reported present in 17 species of *Panax ginseng.* More of these constituents are being discovered, and studied to better comprehend the pharmacological efficacy of ginseng.

In this chapter, the topics reviewed will be limited to the most recognized ginseng botanicals – *Panax ginseng* C.A. Meyer (*Panax ginseng*, Asian or Korean ginseng). First, the subtype classification and structural diversity of ginsenosides will be discussed. In addition, significant findings on the bioactivity of ginsenosides will be tackled.

Progress made regarding the study of its mechanistic action and potential structural-activity relationship will be reviewed in this section as well.

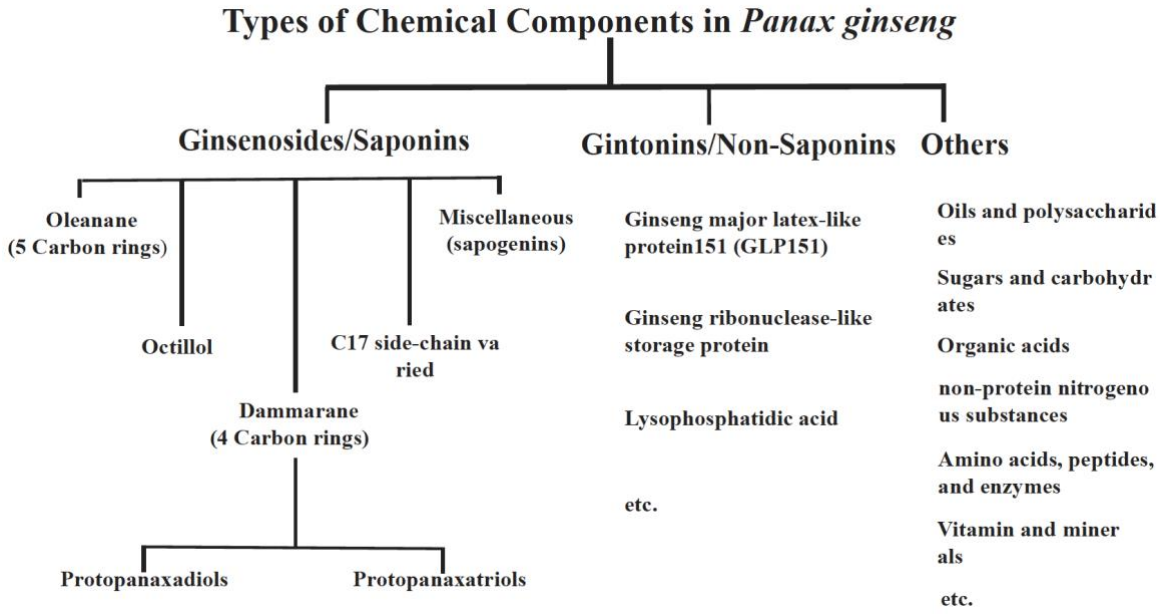

Figure 1.3. Types of chemical components in *Panax ginseng* (Ratan *et al.*, 2021)

1.1. Ginsenosides: subtype classification and structural diversity

Saponins are plant glycosides distributed in over 100 botanical families. These naturally occurring compounds are known for their lathering capacity, surface-active and detergent-like properties, and hemolytic activity. They are also known to bring about the bitterness and astringency of saponin-rich plant materials. In addition, saponins are known for their health-promoting properties such as anticarcinogenic, antioxidative, antitumor, antidiabetic, and hepatoprotective effects (Mohan *et al.*, 2016). These compounds structurally contain a polycyclic backbone with 27-30 carbon atoms, and at least one glycosidic linkage. Furthermore, they are generally classified into the steroidal and triterpenoid varieties based on the nature of their aglycone nucleus (El Aziz *et al.*, 2019). Generally, steroidal saponins possess a spirostan or furostan core with 27 carbon atoms and are primarily isolated in monocotyledons (*Liliaceae, Smilax, Dioscorea, etc*). On the other hand, triterpenoid saponins typically comprise of a 30-carbon dammarane (four-ring) or oleanane (five-ring) nucleus, and are isolated from secondary dicotyledons (*Leguminosae, Panax, etc.*) (Piao *et al.*, 2020).

Saponins are important bioactive components of herbal medicines, including ginseng. Ginseng saponins, termed as ginsenosides, are composed of a triterpenoid backbone with sugar moieties attached to specific sites. The nature and quantity of ginsenosides extracted in different ginseng species are influenced by an array of external factors – farming conditions, climate, portion of the herb, food processing, preservation method, *etc*. Ginsenosides are categorized based on the varying structure of their sapogenin moiety. To date, there are six subtypes, including protopanaxadiol (PPD), protopanaxatriol (PPT), oleanolic acid (OA), ocotillol (OT), C17 side chain varied (C17SV), and miscellaneous types. The first five subtypes will be discussed in this section. Moreover, the most

common monosaccharides attached to ginsenosides are β-D-glucopyranosyl, α-D-glucopyranosyl, β-D-glucopyranuronic acid, α-L-rhamnopyranosyl, α-L-arabinopyranosyl, α-L-arabinofuranosyl, and β-D-xylopyranosyl (*Fig. 1.4*). The nomenclature that was adapted in naming ginsenosides was from the early works of Shibata *et al.*, in 1965 on the structural determination of saponins and sapogenins present in *Panax ginseng.* Here, saponins extracted from the root or rhizome were named 'R' followed by a letter (in alphabetical order) designated based on their polarity and elution in thin-layer chromatography.

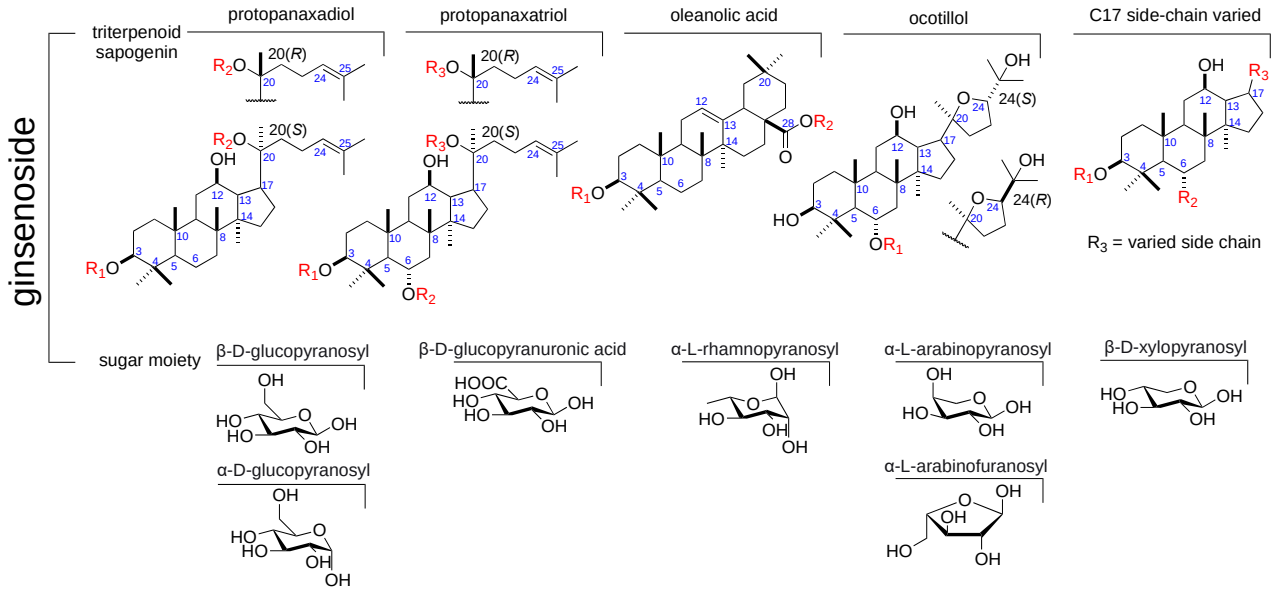

Figure 1.4. Structural classification of various types of ginsenosides. Structures of the five most common triterpenoid backbone – protopanaxadiol (PPD), protopanaxatriol (PPT), oleanolic acid (OA), ocotillol (OT), C17 side chain varied (C17SV). The standard glycosylation sites (C3, C6, and C20), and acyl substituent attachment (C17) are highlighted in red. Structures of the five most common monosaccharides in ginsenoside are shown as well – β-D-glucopyranosyl, α-D-glucopyranosyl, β-D-glucopyranuronic acid, α-L-rhamnopyranosyl, α-L-arabinopyranosyl, α-L-arabinofuranosyl, and β-D-xylopyranosyl.

1.1.1. Subtype classification of ginsenosides

1.1.1.1. Protopanaxadiol (PPD)

A large number of ginsenosides are classified under the protopanaxadiol (PPD) category. It is considered one of the most abundant and well-studied out of the six subtypes. PPD is generally characterized by a four-ring dammarane skeleton, with two β-OH glycosylation sites at the C3 and C20 positions (Qi *et al.*, 2011) (Shi *et al.*, 2019). Another feature is that saccharides are linked in a linear fashion, ranging from single to six sugar units. In some cases, the C6-OH of the terminal glucose in a 3-sugar structure is acylated (Yang *et al.*, 2014). Structural diversity of the PPD backbone becomes apparent with the 20(*S*) and 20(*R*) stereoisomers (Hong *et al.*, 2021).

Examples are shown in *Fig. 1.5*. Ginsenoside Rb1 has two glucose units attached to its C3 and C20 positions, and these sugars have a linear glycosidic linkage. Quinsenoside I is an example of a ginsenoside with 3 sugar units bearing an acyl functional group at C6 of the terminal glucose. Ginsenoside Rg3 is an example of a PPD-type ginsenoside with 20(*S*) and 20(*R*) epimers. However, there are some exceptions to these systems. For example, the *Panax japonicus* isolate, namely chikusetsusaponin FK7, has a glucose unit attached to C19. In addition, chikusetsusaponins VI, FK4, FK5, and FK6 have branched sugar linkages (Yoshizaki and Yahara, 2012) (Kohda

et al., 1991). *Table 1* from the publication of Yang *et al.* shows the names, chemical formula, and ginseng source of the 66 identified PPD ginsenosides.

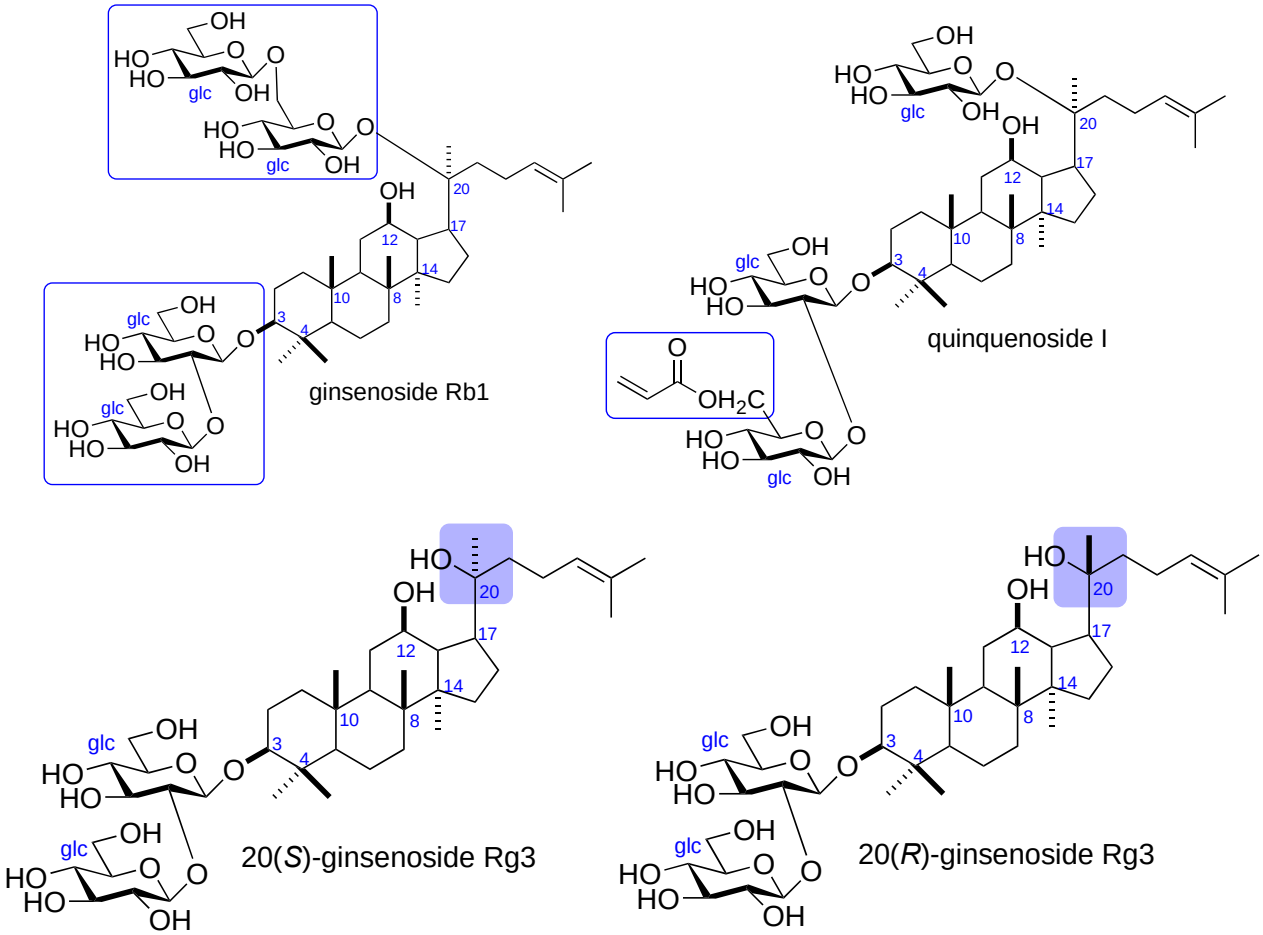

Figure 1.5. Examples of ginsenosides with protopanaxadiol (PPD) backbone.

Table 1.1. Saponins with protopanaxadiol (PPD) backbone isolated from the *Panax* species. (Yang *et al.*, 2014)

No.	Trivial name	M.F.	Source
PPD			
1	Chikusetsusaponin FK7	$C_{48}H_{82}O_{18}$	PJ (fruits)
2	Chikusetsusaponin VI	$C_{59}H_{100}O_{27}$	PpGa (rhizomes)
3	Chikusetsusaponin FK4	$C_{58}H_{98}O_{26}$	PJ (fruits)
4	Chikusetsusaponin FK5	$C_{58}H_{98}O_{26}$	PJ (fruits)
5	Chikusetsusaponin FK6	$C_{53}H_{88}O_{22}$	PJ (fruits)
6	Quinquenoside III	$C_{50}H_{84}O_{19}$	PQ (roots)
7	Yesanchinoside J	$C_{61}H_{102}O_{28}$	PJ (roots)
8	Ginsenoside Rb1	$C_{54}H_{92}O_{23}$	PG (roots)
9	Ginsenoside Rb2	$C_{53}H_{90}O_{22}$	PG (roots)
10	Ginsenoside Rc	$C_{53}H_{90}O_{22}$,	PG (roots)
11	Ginsenoside Rd	$C_{48}H_{82}O_{18}$	PG (roots)
12	m-ginsenoside Rb1	$C_{57}H_{94}O_{26}$	PG (roots)
13	m-ginsenoside Rb2	$C_{56}H_{92}O_{25}$	PG (roots)
14	m-ginsenoside Rc	$C_{56}H_{92}O_{25}$	PG (roots)
15	m-ginsenoside Rd	$C_{51}H_{84}O_{21}$	PG (roots)
16	m-ginsenoside Ra3	$C_{62}H_{102}O_{30}$	PG (roots)
17	m-notoginsenoside R4	$C_{62}H_{102}O_{30}$	PG (roots)
18	Ginsenoside Ra4	$C_{62}H_{102}O_{27}$	PG (roots)
19	Ginsenoside Ra5	$C_{60}H_{99}O_{27}$	PG (roots)

No.	Trivial name	M.F.	Source
PPD			
20	Ginsenoside Ra6	$C_{58}H_{96}O_{24}$	PG (roots)
21	Ginsenoside Ra7	$C_{57}H_{93}O_{23}$	PG (roots)
22	Ginsenoside Ra8	$C_{57}H_{94}O_{23}$	PG (roots)
23	Ginsenoside Ra9	$C_{57}H_{94}O_{23}$	PG (roots)
24	Ginsenoside Rs1	$C_{55}H_{92}O_{23}$	RG
25	Ginsenoside Rs2	$C_{55}H_{99}O_{23}$	RG
26	ginsenoside Rs3	$C_{44}H_{74}O_{14}$	RG
27	20(*R*)-Ginsenoside Rg3	$C_{42}H_{72}O_{13}$	PG (roots)
28	Quinquenoside I	$C_{52}H_{86}O_{19}$	PQ (roots)
29	Quinquenoside II	$C_{62}H_{104}O_{24}$	PQ (roots)
30	Quinquenoside V	$C_{60}H_{102}O_{28}$	PQ (roots)
31	Quinquenoside R1	$C_{56}H_{96}O_{24}$	PQ (roots)
32	Quinquenoside L10	$C_{47}H_{80}O_{17}$	PQ (stems and leaves)
33	Quinquenoside L14	$C_{47}H_{80}O_{17}$	PQ (stems and leaves)
34	Ginsenoside Ra1	$C_{58}H_{98}O_{25}$	PG (roots)
35	Ginsenoside Ra2	$C_{58}H_{98}O_{26}$	PG (roots)
36	Ginsenoside Ra3	$C_{59}H_{100}O_{27}$	PG (roots)
37	Ginsenoside Rb3	$C_{53}H_{90}O_{22}$	PG (roots)
38	Ginsenoside F2	$C_{42}H_{72}O_{13}$	PG (leaves)
39	Pseudoginsenoside Rc1	$C_{50}H_{84}O_{19}$	PsGv (rhizomes)
40	Pseudoginsenoside F8	$C_{55}H_{92}O_{23}$	PpGh (leaves)
41	Vinaginsenoside R17	$C_{47}H_{80}O_{17}$	PV (roots)
42	Vinaginsenoside R18	$C_{47}H_{80}O_{17}$	PV (roots)
43	Gypenoside XIII	$C_{41}H_{70}O_{12}$	PN (fruit pedicels)
44	Gypenoside XVII	$C_{48}H_{82}O_{18}$	PpGh (rhizomes)
45	Gypenoside XV	$C_{52}H_{88}O_{21}$	PN (fruit pedicels)
46	Gypenoside IX	$C_{47}H_{80}O_{17}$	PN (fruit pedicels)
47	Notoginsenoside K	$C_{48}H_{82}O_{18}$	PN (roots)
48	Notoginsenoside D	$C_{64}H_{108}O_{31}$	PN (roots)
49	Notoginsenoside O	$C_{52}H_{88}O_{21}$	PN (flower buds)
50	Notoginsenoside P	$C_{52}H_{88}O_{21}$	PN (flower buds)
51	Notoginsenoside Q	$C_{63}H_{106}O_{30}$	PN (flower buds)
52	Notoginsenoside R4	$C_{59}H_{100}O_{27}$	PN (roots)
53	Notoginsenoside S	$C_{63}H_{106}O_{30}$	PN (flower buds)
54	Notoginsenoside T	$C_{64}H_{108}O_{31}$	PN (flower buds)
55	Notoginsenoside Fa	$C_{59}H_{100}O_{27}$	PN (leaves and seeds)
56	Notoginsenoside Fc	$C_{58}H_{98}O_{26}$	PN (leaves and seeds)
57	Notoginsenoside Fe	$C_{47}H_{80}O_{17}$	PN (leaves and seeds)
58	Notoginsenoside FP2	$C_{58}H_{98}O_{26}$	PN (fruit pedicels)
59	Notoginsenoside L	$C_{53}H_{90}O_{22}$	PN (roots)
60	Vinaginsenoside R7	$C_{53}H_{90}O_{22}$	PV (rhizomes and roots)
61	Saponin I[a]	$C_{47}H_{80}O_{17}$	PN (roots)
62	Notoginsenoside Ft1	$C_{47}H_{80}O_{17}$	PN (Leaves in acid)
63	20(*S*)-Ginsenoside Rg3	$C_{42}H_{72}O_{13}$	RG
64	20(*S*)-Ginsenoside Rh2	$C_{36}H_{62}O_{8}$	PG (stems and leaves)
65	20(*R*)-Ginsenoside Rh2	$C_{36}H_{62}O_{8}$	PG (leaves)
66	Vinaginsenoside R16	$C_{47}H_{80}O_{17}$	PV (roots)

1.1.1.2. Protopanaxatriol (PPT)

Protopanaxatriol (PPT) is the next major subtype of ginseng saponins. A discernable feature between the PPD and PPT backbone is the C6 hydroxyl group of PPT. Aside from the C20 position, the OH-group in C6 is also a glycosylation site in the saponin. In addition, a linear linkage of at most two glycosyl chains is observed in this subtype. The number of sugar units in the PPT type is less than the PPD structures – a maximum of four sugar units are determined in this type. Examples are shown in *Fig. 1.6.* Ginsenosides Rg1 and Re depict the C6 and C20 sugar attachment in the PPT subtype. In addition, Re shows linear glycosylation. Few exceptions to this structure include saponins from *Panax japonicus*, chikusetsusaponin L10, and FK1, having sugar units in C19 (Yoshizaki and Yahara, 2012). Also, yesanchinoside E and vinaginsenoside R4 extracted from the flower buds of *Panax ginseng* have conjoined sugars in C3 (Zou *et al.*, 2002) (Duc *et al.*, 1994). *Table 2* lists the names, chemical formulas, and sources of about fifty PPT ginsenosides (Yang *et al.*, 2014).

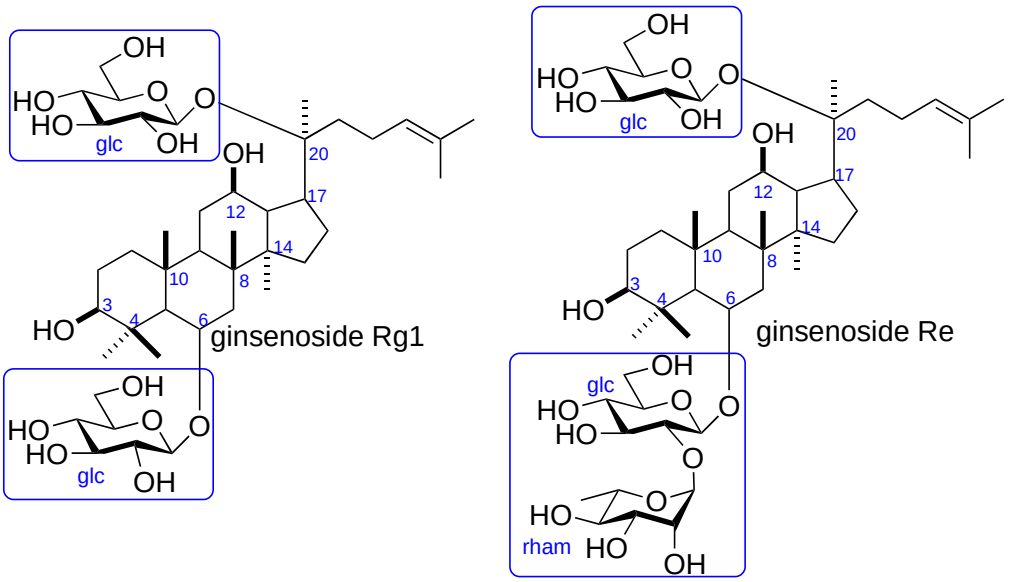

Figure 1.6. Examples of ginsenosides with protopanaxatriol (PPT) backbone.

1.1.1.3. Oleanolic acid (OA)

Ginsenosides with the oleanolic acid backbone are considered a minor subtype – these saponins are less diverse than the others. A distinctive feature of this five-ring oleanane aglycone is the glycosylation at C3 and C28. The presence of a glucuronic acid residue in the C3 sugar chain is also apparent in this type. Today, there are only about 20 ginsenosides with an OA backbone, mostly isolated from *Panax bipinnatifidus* and *Panax stipuleanatus*. An example is ginsenoside Ro (*Fig. 1.7*), extracted from the roots of *Panax ginseng*, bearing glucose units in C3 and C28 (Yang *et al.*, 2014).

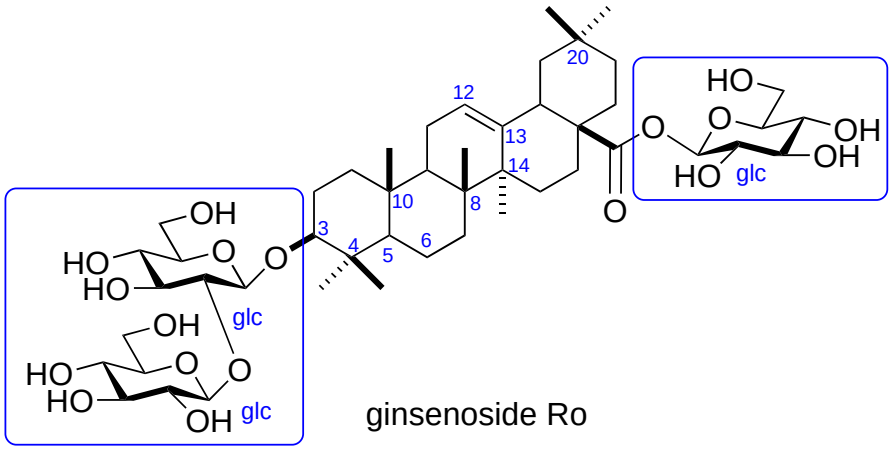

Figure 1.7. Example of a ginsenoside with oleanolic acid (OA) backbone.

Table 1.2. cont. Saponins with protopanaxatriol (PPT) backbone from the *Panax* species. (Yang *et al.*, 2014)

No.	Trivial name	M.F.	Source
PPT			
67	Chikusetsusaponin L10	$C_{36}H_{62}O_9$	PJ (leaves)
68	Chikusetsusaponin FK1	$C_{48}H_{82}O_{18}$	PJ (fruits)
69	Floralginsenoside P	$C_{53}H_{90}O_{23}$	PG (flower buds)
70	Yesanchinoside E	$C_{54}H_{92}O_{23}$	PJ (roots)
71	Vinaginsenoside R4	$C_{48}H_{82}O_{19}$	PV (rhizomes and roots)
72	Ginsenoside Re	$C_{48}H_{82}O_{18}$	PG (roots)
73	Ginsenoside Rf	$C_{42}H_{72}O_{14}$	PG (roots)
74	Ginsenoside Rg1	$C_{42}H_{72}O_{14}$	PG (roots)
75	Ginsenoside Rg2	$C_{42}H_{72}O_{13}$	PG (roots)
76	20-*O*-Glucosylginsenoside Rf	$C_{48}H_{82}O_{19}$	PG (roots)
77	Ginsenoside Rh1	$C_{36}H_{62}O_9$	PG (roots)
78	20(*R*)-Ginsenoside Rg2	$C_{42}H_{72}O_{13}$	RG
79	20(*R*)-Ginsenoside Rh1	$C_{36}H_{62}O_9$	RG
80	Notoginsenoside R1	$C_{47}H_{80}O_{18}$	PN (roots)
81	Notoginsenoside R2	$C_{41}H_{70}O_{13}$	PN (roots)
82	Koryoginsenoside R1	$C_{46}H_{76}O_{15}$	PG (roots)
83	Ginsenoside Re6	$C_{46}H_{76}O_{15}$	PG (roots)
84	Ginsenoside Re1	$C_{48}H_{82}O_{19}$	PG (roots)
85	Ginsenoside Re2	$C_{48}H_{82}O_{19}$	PG (roots)
86	Ginsenoside Re3	$C_{48}H_{82}O_{19}$	PG (roots)
87	Ginsenoside F1	$C_{36}H_{62}O_9$	PG (leaves)
88	Ginsenoside F3	$C_{41}H_{70}O_{13}$	PG (leaves)
89	Floralginsenoside M	$C_{53}H_{90}O_{22}$	PG (flower buds)
90	Floralginsenoside N	$C_{53}H_{90}O_{22}$	PG (flower buds)
91	6′-*O*-Acetyl-ginsenoside Rg1	$C_{44}H_{74}O_{15}$	PQ (roots)
92	20(*S*)-6′-*O*-Acetyl-ginsenoside Rg2	$C_{44}H_{74}O_{14}$	PQ (roots)
93	20(*R*)-6′-*O*-Acetyl-ginsenoside Rg2	$C_{44}H_{74}O_{14}$	PQ (roots)
94	Floralquinquenoside E	$C_{53}H_{90}O_{22}$	PQ (flower buds)
95	Quinquenoside L17	$C_{47}H_{80}O_{18}$	PQ (stems and leaves)
96	Notoginsenoside R3	$C_{48}H_{82}O_{19}$	PN (roots)
97	Notoginsenoside R6	$C_{48}H_{82}O_{19}$	PN (roots)
98	Notoginsenoside M	$C_{48}H_{82}O_{19}$	PN (roots)
99	Notoginsenoside N	$C_{48}H_{82}O_{19}$	PN (roots)
100	Notoginsenoside U	$C_{42}H_{72}O_{14}$	PN (roots)
101	Notoginsenoside Rw1	$C_{46}H_{78}O_{17}$	PN (rhizomes)
102	Notoginsenoside Fp1	$C_{47}H_{80}O_{18}$	PN (fruit pedicels)
103	Notoginsenoside T3	$C_{38}H_{66}O_9$	PN (roots in acid)
104	6‴-*O*-Acetylginsenoside Re	$C_{50}H_{84}O_{19}$	PJ (rhizomes)
105	Ginsenoside F5	$C_{41}H_{70}O_{13}$	PG (leaves)
106	Chikusetsusaponin LM1	$C_{41}H_{70}O_{13}$	PJ (leaves)
107	Chikusetsusaponin LM2	$C_{46}H_{78}O_{17}$	PJ (leaves)
108	Yesanchinoside F	$C_{56}H_{94}O_{24}$	PJ (roots)
109	Chikusetsusaponin L5	$C_{46}H_{78}O_{17}$	PJ (leaves)
110	Pseudoginsenoside Rt3	$C_{40}H_{68}O_{13}$	PpGh (rhizomes)
111	Ginsenoside Re4	$C_{47}H_{80}O_{18}$	PG (roots)
112	Pseudoginsenoside Rs1	$C_{50}H_{84}O_{19}$	PJvm (rhizomes)
113	Ginsenoside-La	$C_{42}H_{72}O_{14}$	PG (leaves)
114	Saponin II[b]	$C_{36}H_{62}O_9$	PG (leaves)
115	Saponin III[c]	$C_{37}H_{62}O_{10}$	PG (leaves)
116	Ginsenoside Rh5 (b)	$C_{37}H_{64}O_9$	PV (roots and rhizomes)

1.1.1.4. Ocotillol (OT)

The ocotillol type, another minor subtype, is derived from the PPT backbone that features a furan ring in C17. Glucose is the primary saccharide attached to C6, and sugar chains exhibit a linear linkage. Commonly, there is a 2'-substitution in the primary glucose unit. Moreover, the majority of the OT-type ginsenosides possess a 24(*S*) configuration (Yang *et al.*, 2014). Examples are 24(*S*) and 24(*R*) pseudoginsenoside F11, isolated from the leaves and rhizomes of *Panax pseudoginseng* subsp. Himalaicus (*Fig. 1.8*). Some exceptions include vinaginsenoside R6

– having a branched chain with two glycosylation at the 2’ and 6’ positions of the primary glucose unit. Moreover, C6-OH of the primary glucose is prone to acetylation – i.e. vinaginsenoside R1 (Duc *et al*., 1994) (Duc *et al*., 1993).

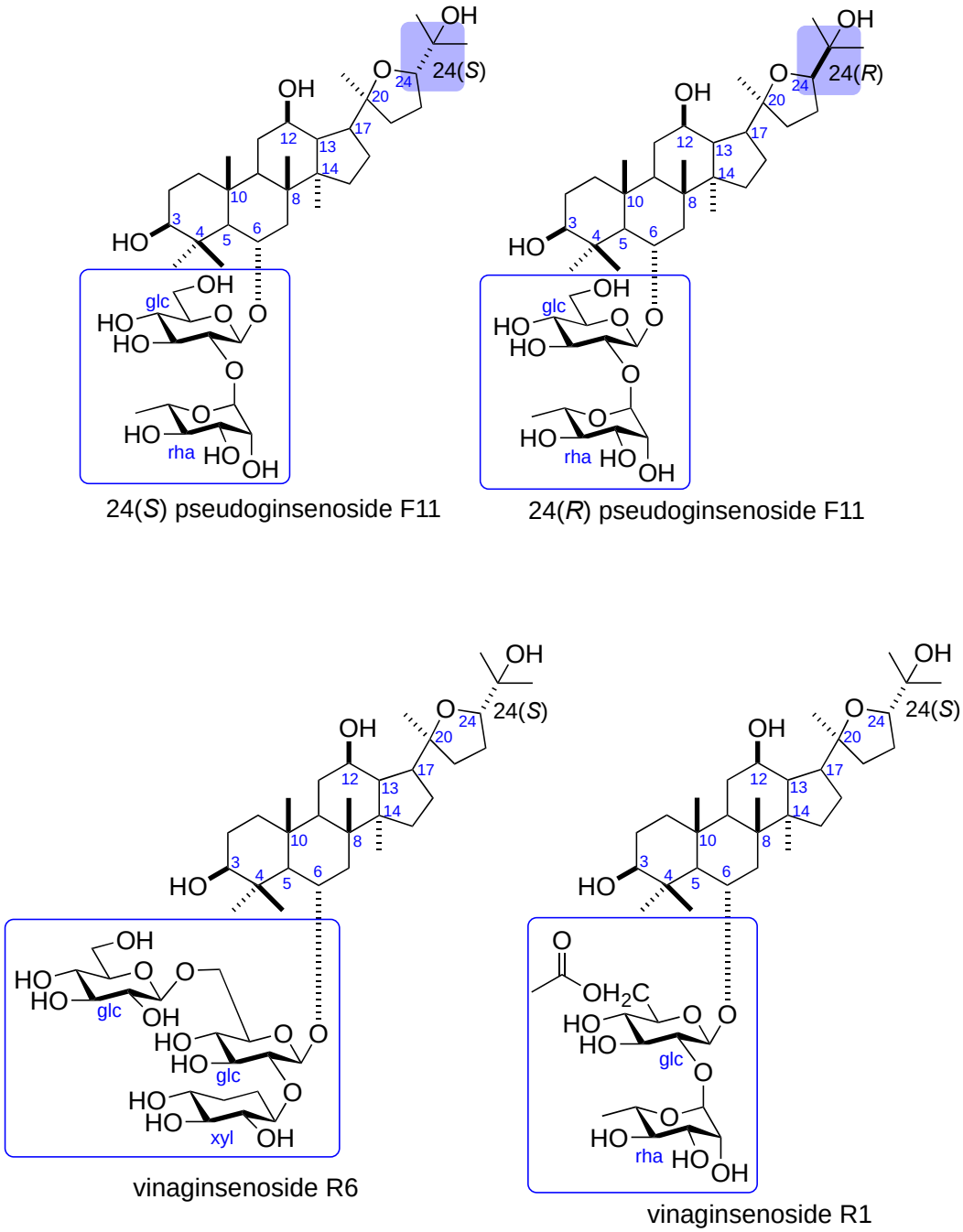

Figure 1.8. Example of ginsenosides with ocotillol (OT) backbone.

1.1.1.5. C17 sidechain varied (C17SV)

Ginsenosides with varying sidechain linked to C17 is the most abundant, with 42.9% fraction of all the subtypes. Newly isolated ginsenosides bearing a C17SV-type sapogenin (C17SV) are garnering attention in different research fields. According to Yang *et al.*, a diversified sidechain is an outcome of different organic reactions such as hydroxylation, methoxylation, peroxidization, dehydration at C20, carbonylation, dehydrogenation, cyclization, oxidation, degradation, rearrangement, or the integration of two or more reactions. The usual derivatization motifs are hydroxylation, dehydration at C20, and peroxidation at C24/C25 position. *Table 3* shows the trivial names and a molecular formula of known C17SV ginsenosides, which are mostly isolated from *Panax ginseng.* Aside from the variable genera, food treatment and processes also contribute to this diversification (Yang *et al.*, 2014).

Table 1.3. cont. Saponins with C17 sidechain varied (C17SV) backbone isolated from the *Panax* species. (Yang *et al.*, 2014)

No.	Trivial name	M.F.	Source
C17 side-chain varied			
151	Chikusetsusaponin L9a	$C_{36}H_{62}O_{10}$	PJ (leaves)
152	Vinaginsenoside R14	$C_{41}H_{70}O_{15}$	PV (rhizomes and roots)
153	Ginsenoside Rh15	$C_{42}H_{70}O_{13}$	PG (stems and leaves)
154	Ginsenoside Rh5 (a)	$C_{36}H_{60}O_{9}$	PG (leaves)
155	Ginsenoside Rh14	$C_{42}H_{70}O_{13}$	PG (stems and leaves)
156	Ginsenoside Rh16	$C_{36}H_{60}O_{8}$	PG (stems and leaves)
157	Ginsenoside Rs4	$C_{44}H_{72}O_{13}$	SG
158	Ginsenoside Rs6	$C_{38}H_{60}O_{8}$	SG
159	Ginsenoside Rg4	$C_{42}H_{70}O_{12}$	PG (leaves)
160	Ginsenoside Rh3	$C_{36}H_{60}O_{7}$	PG (leaves)
161	Ginsenoside Rz1	$C_{42}H_{70}O_{12}$	PG (heated roots)
162	Floralginsenoside C	$C_{41}H_{70}O_{15}$	PG (flower buds)
163	Floralginsenoside A	$C_{42}H_{72}O_{16}$	PG (flower buds)
164	Floralginsenoside Tc (24R or 24S)	$C_{53}H_{90}O_{24}$	PG (flower buds)
165	Floralginsenoside Td (24S or 24R)	$C_{53}H_{90}O_{24}$	PG (flower buds)
166	Floranotoginsenoside B	$C_{53}H_{90}O_{24}$	PN (flowers)
167	Floranotoginsenoside C	$C_{53}H_{90}O_{24}$	PN (flowers)
168	Floralquinquenoside B	$C_{42}H_{72}O_{15}$	PQ (flower buds)
169	Floralquinquenoside D	$C_{42}H_{72}O_{15}$	PQ (flower buds)
170	Ginsenoside SL1	$C_{36}H_{62}O_{11}$	PG (steamed leaves)
171	Ginsenoside I (24S or 24R)	$C_{48}H_{82}O_{20}$	PG (flower buds)
172	Ginsenoside II (24R or 24S)	$C_{48}H_{82}O_{20}$	PG (flower buds)
173	Notoginsenoside C	$C_{54}H_{92}O_{25}$	PN (roots)
174	Floralginsenoside H	$C_{50}H_{84}O_{21}$	PG (flower buds)
175	Floralginsenoside J	$C_{48}H_{82}O_{20}$	PG (flower buds)
176	Floralginsenoside Ka	$C_{36}H_{62}O_{11}$	PG (flower buds)
177	Ginsenoside Pk1	$C_{42}H_{70}O_{12}$	SG
178	Ginsenoside Pk2	$C_{36}H_{60}O_{7}$	SG
179	Ginsenoside Pk3	$C_{36}H_{60}O_{8}$	SG
180	Ginsenoside Rs5	$C_{44}H_{72}O_{13}$	SG
181	Ginsenoside Rs7	$C_{38}H_{62}O_{9}$	SG
182	Notoginsenoside T5	$C_{41}H_{68}O_{12}$	PN (roots in acid)
183	Ginsenoside Rg6	$C_{42}H_{70}O_{12}$	RG
184	Ginsenoside Rh4	$C_{36}H_{60}O_{8}$	Korean RG
185	Vinaginsenoside R10	$C_{36}H_{62}O_{10}$	PV (rhizomes and roots)
186	Vinaginsenoside R11	$C_{41}H_{70}O_{14}$	PV (rhizomes and roots)
187	Floralginsenoside Kb	$C_{45}H_{76}O_{19}$	PG (flower buds)
188	Floralginsenoside Kc	$C_{45}H_{76}O_{20}$	PG (flower buds)
189	Pn-1	$C_{32}H_{54}O_{8}$	PN (leaves)
190	Notoginsenoside R10	$C_{30}H_{50}O_{9}$	PN (roots)
191	Ginsenoside Rg7 (24β)	$C_{42}H_{72}O_{14}$	PG (leaves)
192	Ginsenoside V (24β)	$C_{54}H_{92}O_{24}$	PG (roots)
193	Vinaginsenoside R9	$C_{48}H_{82}O_{19}$	PV (rhizomes and roots)
194	Floranotoginsenoside D	$C_{53}H_{90}O_{23}$	PN (flowers)
195	Gypenoside LXXI (24α)	$C_{53}H_{90}O_{23}$	PQ (leaves)

196	Notoginsenoside Ft3	$C_{47}H_{80}O_{18}$	PN (leaves in acid)
197	Notopanaxoside A	$C_{36}H_{62}O_{10}$	PN (roots)
198	Ginsenoside M7ed	$C_{36}H_{62}O_{10}$	PG (flower buds)
199	Floralginsenoside La (24α)	$C_{48}H_{82}O_{19}$	PG (flower buds)
200	Floralginsenoside Lb (24β)	$C_{48}H_{82}O_{19}$	PG (flower buds)
201	Ginsenoside Rf2 (20R)	$C_{42}H_{72}O_{14}$	RG
202	Notoginsenoside Ft2	$C_{47}H_{82}O_{18}$	PN (leaves in acid)
203	Ginsenoside Rh12	$C_{36}H_{64}O_{10}$	PG (leaves)
204	Vinaginsenoside R12	$C_{36}H_{64}O_{11}$	PV (rhizomes and roots)
205	Vinaginsenoside R21 (24S)	$C_{42}H_{74}O_{16}$	PV (roots)
206	Vinaginsenoside R22 (24R)	$C_{42}H_{74}O_{16}$	PV (roots)
207	Quinquenoside L9	$C_{42}H_{74}O_{15}$	PQ (stems and leaves)
208	Vinaginsenoside R13	$C_{48}H_{84}O_{20}$	PV (rhizomes and roots)
209	Quinquenoside L16	$C_{54}H_{94}O_{25}$	PQ (stems and leaves)
210	Chikusetsusaponin FM1	$C_{53}H_{92}O_{24}$	PJ (fruits)
211	Notoginsenoside-T4	$C_{36}H_{62}O_{11}$	PN (roots in acid)
212	Ginsenoside Rh13	$C_{36}H_{62}O_{9}$	PG (leaves)
213	Ginsenoside ST2	$C_{36}H_{62}O_{10}$	PG (steamed leaves)
214	Saponin VI[a]	$C_{42}H_{72}O_{15}$	PN (roots)
215	Floranotoginsenoside A	$C_{53}H_{90}O_{23}$	PN (flowers)
216	Notoginsenoside ST-5	$C_{47}H_{80}O_{18}$	PN (steamed roots)
217	Yesanchinoside H	$C_{53}H_{90}O_{23}$	PJ (roots)
218	Notoginsenoside A	$C_{54}H_{92}0_{24}$	PN (roots)
219	Majoroside F4	$C_{42}H_{72}O_{14}$	PJvm (leaves)
220	Majoroside F6	$C_{48}H_{82}O_{19}$	PJvm (leaves)
221	Vinaginsenoside R8	$C_{48}H_{82}O_{19}$	PV (rhizomes and roots)
222	Notoginsenoside H	$C_{47}H_{80}O_{19}$	PN (roots)
223	Floralginsenoside B	$C_{42}H_{72}O_{16}$	PG (flower buds)
224	Floralginsenoside D	$C_{41}H_{70}O_{15}$	PG (flower buds)
225	Floralginsenoside E	$C_{42}H_{72}O_{15}$	PG (flower buds)
226	Koryoginsenoside R2	$C_{54}H_{92}O_{24}$	PG (roots)
227	Quinquenoside L3	$C_{47}H_{80}O_{18}$	PQ (stems and leaves)
228	Notoginsenoside R8	$C_{36}H_{62}O_{10}$	PN (roots)
229	Notoginsenoside R9 (20R)	$C_{36}H_{62}O_{10}$	PN (roots)
230	Notoginsenoside Rw2	$C_{41}H_{70}O_{14}$	PN (rhizomes)
231	Ginsenoside Rh20	$C_{42}H_{72}O_{14}$	PG (stems and leaves)
232	Majoroside F5	$C_{48}H_{82}O_{19}$	PJvm (leaves)
233	Bipinnatifidusoside F2	$C_{48}H_{82}O_{20}$	PJvb (leaves)
234	Ginsenoside Km	$C_{36}H_{62}O_{10}$	PG (leaves)
235	Quinquenoside L2	$C_{48}H_{82}O_{19}$	PQ (stems and leaves)
236	Ginsenoside Re5	$C_{42}H_{72}O_{15}$	PG (roots)
237	Ginsenoside Ki	$C_{36}H_{62}O_{10}$	PG (leaves)
238	Yesanchinoside R1	$C_{36}H_{62}O_{10}$	PJ (rhizomes)
239	Yesanchinoside R2	$C_{41}H_{70}O_{14}$	PJ (rhizomes)
240	Vinaginsenoside R24	$C_{48}H_{82}O_{19}$	PV (rhizomes and roots)
241	Quinquefoloside-Lc	$C_{54}H_{92}O_{23}$	PQ (leaves)
242	Quinquefoloside-La	$C_{54}H_{92}O_{23}$	PQ (leaves)
243	Notoginsenoside K	$C_{54}H_{92}O_{25}$	PN (roots)
244	Floralquinquenoside A	$C_{36}H_{62}O_{11}$	PQ (flower buds)
245	Floralquinquenoside C	$C_{42}H_{72}O_{15}$	PQ (flower buds)
246	Floralginsenoside F	$C_{42}H_{72}O_{15}$	PG (flower buds)
247	Notoginsenoside E	$C_{48}H_{82}O_{20}$	PN (roots)
248	Ginsenoside Rh6	$C_{36}H_{62}O_{11}$	PG (leaves)
249	Floralginsenoside O	$C_{53}H_{90}O_{24}$	PG (flower buds)
250	Floralginsenoside G	$C_{50}H_{84}O_{21}$	PG (flower buds)
251	Floralginsenoside I	$C_{48}H_{82}O_{20}$	PG (flower buds)
252	Floralginsenoside K	$C_{48}H_{82}O_{21}$	PG (flower buds)
253	Isoginsenoside-Rh3	$C_{36}H_{60}O_{7}$	PG (fruits)
254	Ginsenoside Rg5	$C_{42}H_{70}O_{12}$	Korean RG
255	(20E)-Ginsenoside F4	$C_{42}H_{70}O_{12}$	Korean RG
256	Ginsenoside SL2	$C_{42}H_{70}O_{14}$	PG (steamed leaves)
257	Ginsenoside ST1	$C_{36}H_{62}O_{10}$	PG (steamed leaves)
258	Notoginsenoside T1	$C_{36}H_{60}O_{10}$	PN (roots in acid)
259	Notoginsenoside T2	$C_{37}H_{62}O_{10}$	PN (roots in acid)
260	Ginsenoside Rg8	$C_{42}H_{70}O_{12}$	PQ (roots)
261	Notoginsenoside ST-1	$C_{36}H_{62}O_{10}$	PN (steamed roots)
262	Notoginsenoside ST-2	$C_{43}H_{74}O_{15}$	PN (steamed roots)
263	Notoginsenoside ST-3	$C_{43}H_{74}O_{15}$	PN (steamed roots)
264	Ginsenoside SL3	$C_{42}H_{70}O_{14}$	PG (steamed leaves)
265	Floralginsenoside Ta	$C_{36}H_{60}O_{10}$	PG (flower buds)
266	Vinaginsenoside R20	$C_{48}H_{80}O_{19}$	PV (roots)
267	Ginsenoside III	$C_{48}H_{80}O_{19}$	PG (flower buds)
268	Notoginsenoside B	$C_{54}H_{90}O_{24}$	PN (roots)
269	Vinaginsenoside R25	$C_{42}H_{70}O_{15}$	PV (rhizomes and roots)
270	Quinquenoside L1	$C_{48}H_{80}O_{18}$	PQ (stems and leaves)

1.1.2. Sugar substituents

Fig. 1.4 shows the common monosaccharide substituents of ginsenosides. These are β-D-glucopyranosyl, α-D-glucopyranosyl, β-D-glucopyranuronic acid, α-L-rhamnopyranosyl, α-L-arabinopyranosyl, α-L-arabinofuranosyl, and β-D-xylopyranosyl. The number,and attachment of these units vary depending on the subtype of ginsenoside. It is proposed that the number and location of sugar moiety affect the biological activities of ginsenosides. The most abundant ginsenosides extracted from different species are often bulky molecules resulting in their poor absorption, low bioavailability, and rapid degradation. Their structures are altered by either acid hydrolysis or enzymatic degradation as they diffuse through the body towards a specific target. Cleavage of sugar typically occurs in a stepwise manner. As bulky ginsenosides are converted into smaller metabolites, their bioavailability and potency enhance to a greater extent (Wong *et al.*, 2015). *Fig. 1.9* shows the stepwise hydrolysis of glucose units in ginsenoside Rb1 leading to the formation ginsenoside CK. In a study done by Niu *et al.*, in vitro analysis of ginsenoside Rb2 by A/J mouse fecal lysate correlated to the pharmacokinetic profile of ginsenoside Rb1. Results showed that ginsenoside Rb1 was hydrolyzed to form ginsenoside Rd, F2, and CK, respectively. A rapid decrease in the concentration of ginsenoside Rb1 was observed, followed by an increase in the concentration of the metabolites. They also concluded that the formation of F2 from Rd is considered the slowest step, while the formation of F2 to CK is instantaneous. Overall, this shows that bulky ginsenosides are less bioavailable than the metabolites with less sugar units.

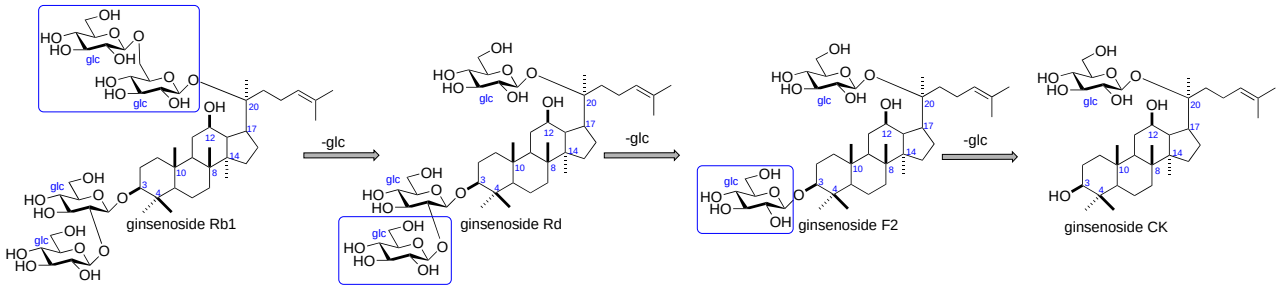

Figure 1.9. Proposed metabolic pathway for the production of ginsenoside CK in A/J mouse fecal lysate (Niu *et al.*, 2013)

1.1.3 S and R configurations of ginsenosides

Another structural feature that extends the diversity of ginsenosides is the presence of *S* and *R* configurations. Varieties of *S* and *R* ginsenosides are present across ginseng species and parts of the plant. The abundance of either structure may also depend on factors such as farming conditions and food processing. For the PPD and PPT saponins, both 20(*S*) and 20(*R*) structures are present depending on the position of the hydroxy group in C20. While OC ginsenosides bearing a chiral center at C24, 24(*S*) isomer is most abundant (Yang *et al.*, 2014). One interesting note is that these epimers produce different pharmacological effects. For the PPD and PPT subtypes, 20(*S*) have greater biological activity than the 20(*R*) configurations (Popovich and Kitts, 2002). An example is 20(*S*) and 20(*R*) ginsenoside Rg3, wherein the 20(*S*) structure has greater hydroxyl scavenging activity, higher efficiency in regulating ion channels, and greater cytotoxic effects (Lee *et al.*, 2008) (Qi *et al.*, 2011). According to Kang *et al.*, the activity of 20(*S*)-Rg3 may be influenced by the unique structural features in the aglycone portion. Here, C12-

OH lies in proximity to C20-OH and the alkene tail, creating a compact structure at the end of the saponin, and influencing the activity of 20(*S*)-Rg3 (Kang *et al.,* 2005). This will be discussed further in the *Structure-Activity Relationship* section.

1.2. Pharmacological Effects of ginsenosides

Pharmacological effects brought by the consumption of ginseng have garnered attention in modern medicine. And these effects are predominantly dependent on the ginsenoside content of the plant. The types of major ginsenosides abundant across ginseng species and specific parts of the herb greatly vary. In addition, marketed ginseng (i.e., fresh, red, white, steamed, acid-processed, fermented, *etc.*) subjected to different processing technologies further diversifies the saponin composition of the product. These factors affecting the diversity of ginsenosides are given emphasis but will not be thoroughly discussed in this manuscript. Instead, most studied pharmacological activities of ginseng saponins will be highlighted in this section.

In traditional Chinese medicine, ginseng is usually described as an "adaptogen," a substance that can overcome various types of stress and restore homeostasis. It has been used as a common tonic to alleviate palpitation, insomnia, cure impotence, diabetes, and other illnesses (Xiang *et al.,* 2008) (Shi *et al.,* 2019). In modern medicine, pharmacological studies reveal that the antioxidant, anti-inflammatory, and immunostimulatory effects from the consumption of ginseng is correlated to the saponins. These effects, and their proposed mechanisms are summarized in *Fig. 1.10.*

One of the well-known effects of ginseng is an improvement in mental performance. In the central nervous system (CNS), ginseng saponins boost cognitive abilities as they improve blood circulation by stimulating the formation and repair of blood vessels. In addition, ginsenosides Rb1, Rg1, Rg3, Rd, and Re suppress neurodegeneration in animal trials and neuronal cell cultures.

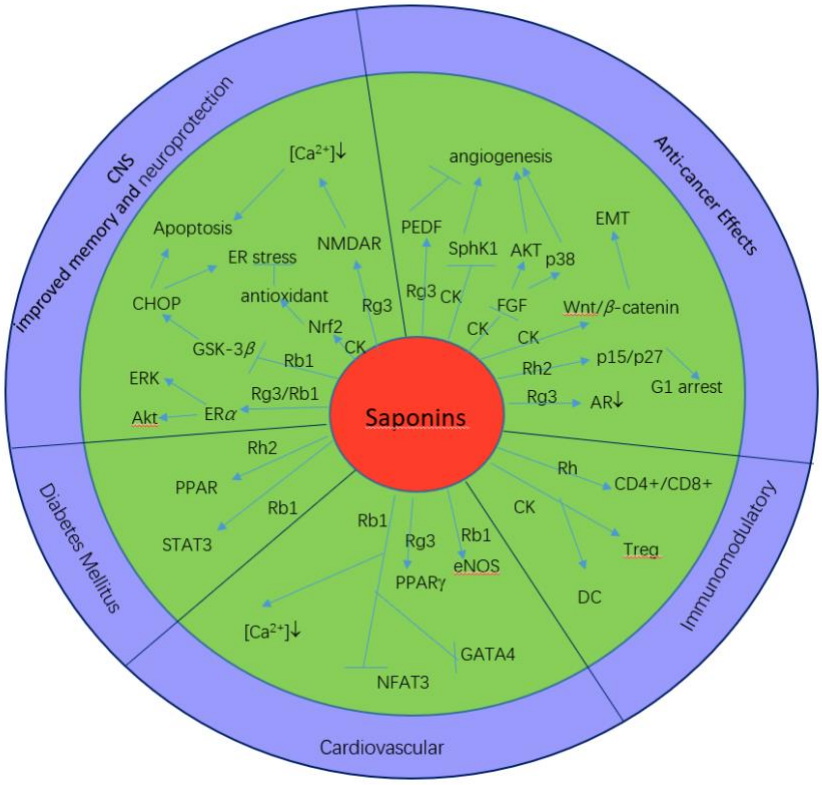

Figure 1.10. Pharmacological profile and mechanism of ginseng saponins (Shi *et al.*, 2019).

Several studies reported the promising anticancer activities of ginsenosides. Signaling pathways for the inhibition of tumor growth in several culture cells collectively converge. These include regulation of the cell cycle, stimulation of apoptosis, and inhibition of angiogenesis and inflammatory response. Interestingly, several ginsenosides also exhibit low toxicity towards normal cells with few side effects, which makes them promising subjects for anticancer research. As an example, Rg3 was found to be a potent chemotherapeutic agent for gallbladder cancer cell lines. Rg3 suppressed the proliferation of gallbladder cancer cell lines NOZ and GBC-SD in a concentration-dependent manner through activation of the p53 pathway, a signaling pathway that responds to cellular stresses (e.g., DNA damage, oxidative stress, *etc.*) consequently triggering cell cycle arrest and apoptosis (Zhang *et al.*, 2015). Another PPD-type ginsenoside, ginsenoside Compound K (CK), suppressed cell migration of human umbilical vein endothelial cell (HUVEC) induced by sphingosine-1-phosphate (S1P). For the anti-inflammatory effect, ginsenosides Rd, Rh1, and Rg3 are some of the ginseng saponins that down-regulate the expression of inducible nitric oxide synthase or iNOS, and cyclooxygenase-2 or COX-2, which are pro-inflammatory molecules (Wong *et al.*, 2015).

Ginsenosides are also known adjuvants for diabetes treatments that increase their efficacy and potency. Ginsenoside Rb1 was found to regulate glucose homeostasis and ameliorate hyperglycemia in animal models and human studies. In Rb1-fed male rats, insulin-induced inhibition of hepatic gluconeogenesis was triggered to a greater extent with the suppression of glucose-6-phosphatase gene expression. Insulin sensitivity and glucose tolerance were improved in these animals through the activation of AMP protein kinase while keeping their food intake constant (Shen *et al.*, 2015). Because of the wide pharmacological activities brought by ginsenosides, they become attractive candidates to the development of several therapeutics.

1.3. Prospective Structure-Activity Relationship of ginsenosides

Due to the structural heterogeneity of ginsenosides, establishing their structure activity relationship (SAR) is useful in predicting their mechanistic actions. Understanding the SAR is also crucial to improve their solubility in the systemic circulation, and improve their membrane/receptor affinity. This discussion is mainly divided into the SAR of the sugar and aglycone moiety of the ginsenosides.

1.3.1. Number and positioning of sugar moieties

Qi *et al.* proposed that the number and position of sugar units in the aglycone of ginsenosides are associated with their anticancer potentials. Ginsenosides with a greater number of carbohydrates (four or more) typically exhibit little to no antiproliferative effects (e.g., Rb1 and Rc). Three sugars on ginsenosides make it weakly antiproliferative, while two to no sugar attachments (Rg3, Rh2, PPD and PPD backbone) have improved antiproliferative effects (Qi *et al.,* 2010). In a study by Niu *et al.*, the bioactivity and bioavailability of Rb1 were reported to depend on the glycosidase activity of mouse intestinal microbiome hydrolyzing Rb1 to smaller metabolites. In vivo conversion of primary ginsenosides in red ginseng, such as Rb1, to bioactive ginsenoside CK was only mediated by bacterial glycosidase as mammalian cells are incapable of ginsenoside hydrolysis. In addition, significant concentrations of ginsenosides F2 and CK were quantified from the blood of A/J mice after the oral administration of Rb1. The structures and proposed metabolic pathway for Rb1 leading to the formation of ginsenoside Rd, F2, and CK through bacterial β-glucosidases is shown in *Fig. 1.9.* Antiproliferative and permeating activities of the ginsenosides were tested in LM1 cells (mouse lung cancer), and Caco-2 cell monolayers, respectively. MTT assay accounted that ginsenoside F2 (IC_{50} 100 μg/ml) and CK (IC_{50} 13 μg/ml) significantly inhibited LM1 cells compared to red ginseng extracts, which were highly composed of primary ginsenoside Rb1 (Niu *et al.,* 2013). Apart from the number of sugar moieties, their position in the triterpenoid backbone is presumed to be significant for the bioactivity of ginsenosides as well. Sugar substituents usually branch at C3, C6, and C20 of ginsenosides. Ginsenosides Rh1 and Rh2 are structural isomers with a β-glucose unit in C6 and C3, respectively. Odashima *et al.* compared the effects of Rh1 and Rh2 in B16 melanoma cells, and despite their structural similarities, Rh2 instigated the inhibition of cell growth and melanogenesis, while Rh1 simply stimulated melanogenesis (Odashima *et al.,* 1985) (Ota *et al.*, 1987). These findings illustrate the correlation of sugar moieties and their position with the antiproliferative activity of ginsenosides.

Similar to other steroids and phytosterols, ginsenosides are proposed to act through receptors in membranes and cytoplasm, or simply diffuse through the plasma or nuclear membranes. Sugar substituents increase the hydrophilic character of ginsenosides, which impacts their cellular absorption. Generally, polar functional groups decrease the permeability of bioactive molecules and their flip-flop rate across the plasma membrane. This decline in permeability is associated to weakened antiproliferative effects (Atkovska *et al*., 2018). In an LC-MS experiment that quantifies the cellular uptake of ginsenosides by Ha *et al.*, relatively less polar ginsenosides (fewer sugar moieties attached, e.g., Rg3, Rk1, Rg5, Rh2, CK) and PPD backbone showed significant cellular uptake in MCF-7 cells. The position of sugar substituents also affects the biological activity of ginsenoside. In molecular dynamics

simulations, sugar units in the C6 position cause steric hindrances to their target proteins and diminish their anticancer potentials (Qi *et al.,* 2010) (Li *et al*., 2009).

1.3.2. Hydroxyl groups

The headgroup of the plasma membrane composed of phospholipids promotes polar interactions with bioactive molecules. This interaction is important for the entry and exit of molecules through the plasma membrane. The number and position of hydroxyl groups in ginseng saponins influence membrane interactions and pharmacological activities (Qi *et al.,* 2010). For example, bioactivities of ginsenosides Rh2 and Rh3 were evaluated in promyelocytic leukemia HL-60 cells. The main structural difference between the two is the absence of an R-OH group in C20 of Rh3. The differentiation induced by Rh2 and Rh3 was at par; however, the potency of Rh2 is higher (Kim *et al.,* 1998).

1.3.3 20(S) and 20(R) isomers

The 20(*S*) and 20(*R*) stereoisomers of PPD ginsenosides further diversify the ginsenosides. This minimal difference in the position of the hydroxyl group has significant effects on the pharmacological activity of ginsenosides. A comparison of the hydroxyl radical (•OH) scavenging activities of 20(*S*)- and 20(*R*)-Rg3 was performed through ESR experiments (structures are shown in *Fig. 1.5*). Results suggest that the 20(*S*)- isomer exhibited greater activity (Kang *et al*., 2005). Furthermore, voltage-dependent channels (Ca^{2+}, K^{+}, Na^{+}) were regulated more efficiently by 20(*S*)-Rg3. In addition to 20(*S*)-Rg3, the 20(*S*)-Rh2 also exhibits greater potency against cancer cells than the 20(*R*) epimer. The antiproliferative effects of 20(*S*)- and 20(*R*)-Rh2 were compared in human colon cancer cells (HT-29) in vitro. In the non-invasive cellular analysis, it was found that the activity of the two saponins is stereoselective and that 20(*S*)-Rh2 diminished the viability of the cells (Jeong *et al.,* 2019). In addition, the reported half-maximal inhibitory concentration of 20(*S*)-Rh2 in A549 cells was 45.7 µM, and 53.6 µM for 20(*R*)-Rh2 (Zhang *et al.,* 2011).

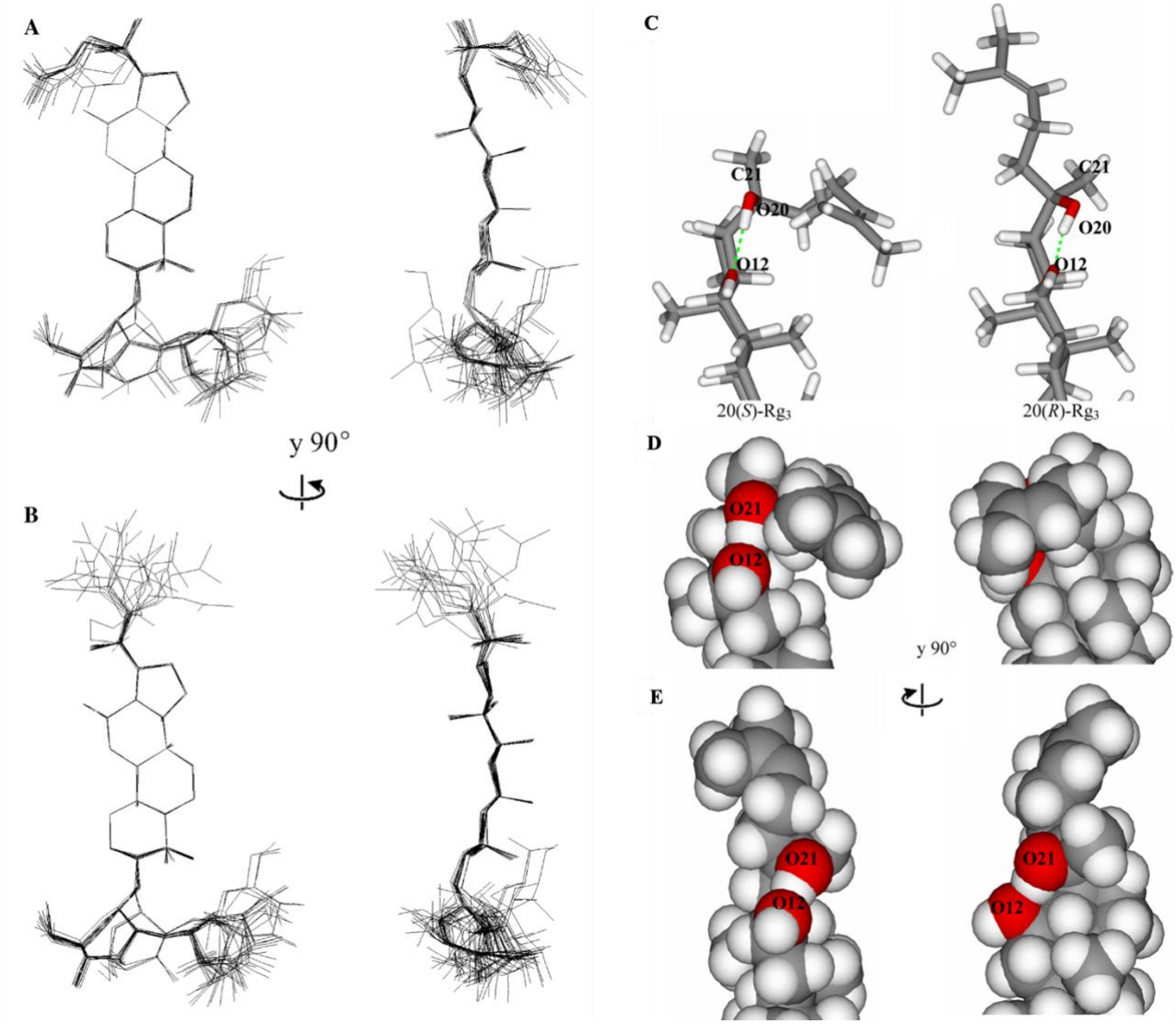

Figure 1.11. Twenty superimposed average structures of (A) 20(*S*)-Rg3 and (B) 20(*R*)-Rg3, respectively; (C) Proximity of hydroxyl groups, HO12 and HO20, and orientation of alkene chains of 20(*S*)-Rg3 and 20(*R*)-Rg3. (D, E) Space-filling representation of 20(*S*)-Rg3, and 20(*R*)-Rg3, respectively (Kang *et al.*, 2005).

According to Kang *et al.*, the stereochemistry of the C12 and C20 hydroxyl groups of PPD ginsenosides, such as Rg3 and Rh2, affects SAR. In 20(*S*) ginsenoside, C20-OH and C12-OH are situated closer to each other, while in 20(*R*), C20-OH is further from C12 hydroxyl. In *Fig. 1.11A* and *1.11B*, the triterpenoid rings of 20-(*S*)Rg3 and 20-(*R*)Rg3 were superimposed to determine their restrained-minimized average structures. Although the sugar moieties are flexible in both structures, their backbone and tail are presumed to have different orientations. The tail of 20(*S*)-Rg3 is postulated to a fixed orientation and to a tight packing towards the triterpenoid backbone. The dihedral angles in the alkene chain/tail of 20(*S*) create a compact shape and are found to converge at 120º for C24-C23-C22-C20 and 170º for C23–C22–C20–C17. On the other hand, the tail of 20(*R*)-Rg3 is more flexible while splaying on random directions (Kang *et al.*, 2005) (Jeong *et al.*, 2004). Since the chiral center of 20(*S*)-Rg3 is geometrically aligned and compact, it was assumed to influence the accessibility to water molecules, as shown in the space-filling models in *Fig. 1.11C and 1.11D.* The hydrogen bond in 20(*S*) is more inaccessible and assumed to have a more stable hydrogen bonding with their receptor. While in 20(*R*)-Rg3, these polar groups are more

exposed to water molecules (*Fig. 1.11C and 1.11E*) which could cause the destabilization of the intramolecular hydrogen bonds and with their receptor.

1.4. 20(S)-Ginsenoside Rh2 (Rh2)

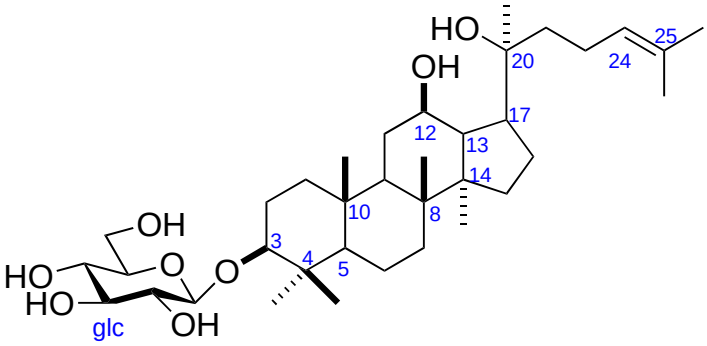

Figure 1.12. Structure of 20(*S*)-ginsenoside Rh2 (**Rh2**)

Ginsenoside Rh2 (Rh2) is a rare type of triterpenoid saponin known for its pharmacological activities (*Fig. 1.12*). In 2016, Rh2 was approved by the China State Food and Drug Administration as a complementary food. Rh2 was first isolated and characterized with its structural isomer ginsenoside Rh1 in 1985. These ginsenosides bear a protopanaxadiol backbone, with β-glucose attached to its C6 and C3 position for Rh1 and Rh2, respectively (Odashima *et al.*, 1985). Their dammarane ring has rough α- and β-faces with several methyl attachments and hydroxyl groups in C12 and C20. Odashima *et al.* compared the effects of Rh1 and Rh2 in B16 melanoma cells, and despite their structural similarities, Rh2 instigated the inhibition of cell growth and melanogenesis, while Rh1 simply stimulated melanogenesis (Odashima *et al.*, 1985) (Ota *et al.*, 1987). This striking difference in their biological effects has led to further scrutinization of Rh2.

Rh2 is undetectable in fresh and white ginseng; however, abundant in red ginseng. Red ginseng accounts for 59% of sales in the South Korean market and is considered the best-selling variety (Shibata, 2001) (Zhang *et al.*, 2020) (Tsuchiya, 2015). This is attributed to the significant quantities of Rg3 and Rh2 in red ginseng. Rh2 is a proposed metabolite of major ginsenosides (e.g., ginsenosides Rb1, Rd, and Rg3) transformed through steaming of fresh or white ginseng at about 95-100^{o}C. The bioavailability of Rh2 is also reported to increase from the bacterial transformation of ginsenosides in the intestinal gut. In human and animal studies, Rg1 is metabolized in the intestinal microflora producing Rg3, Rh2, Compound K, and PPD backbone (Tsuchiya, 2015) (Popovich and Kitts, 2002). A common metabolic pathway is the stepwise deglycosylation of the sugar moieties (Qi *et al.*, 2010). Therefore, the gastrointestinal tract plays an important role in orally administered ginseng supplements, and the smaller metabolites are effectively absorbed from the gut to the circulatory pathways.

1.4.1. Pharmacological effects of Rh2

Rh2 has become well-known in pharmacological research, both in vivo and in vitro studies. To name a few, the variety of therapeutic benefits include anti-obesity, antidiabetic, anti-inflammatory, and anticancer effects (Wong *et al.*, 2015) (Ratan *et al.*, 2021). In an anti-obesity study, low concentrations of Rh2 promote fat accumulation in

mouse adipose tissues (3T3-L1) through the glucocorticoid receptor. However, high concentrations of Rh2 weaken 3T3-L1 adipocyte differentiation – a crucial process in the development of obesity in children and adults. Zhang *et al*. proposed that Rh2 down-regulates the peroxisome proliferator-activated receptor gamma (PPAR-) pathway in cells and obese mice in a dose-dependent manner. This effect makes Rh2 a potential formulation against obesity in vivo (Zhang *et al.,* 2020). SGLT1 is a protein that transports glucose and galactose across the luminal side of enterocytes. Along with Rg3, F2, and Compound K, Rh2 was reported to inhibit sodium/glucose cotransporter 1 (SGLT1) in human embryonic kidney 293 (HEK293) transfected with SGLT1. Although these saponins constrain the activity of SGLT1, they are reported to be absorbed in the gut through passive diffusion or other active transporters and not through SGLT1 interactions (Gao *et al.,* 2017). In addition, diabetic cardiovascular complications in rats with type 1 diabetes (streptozotocin-induced model) were alleviated with Rh2 (Bai *et al*., 2018). The anti-inflammatory effects of Rh2 were explored in several studies as well. The condition of mice with lipopolysaccharide-induced acute lung injury (LPS-induced ALI) improved upon the inclusion of Rh2 in their diet. It was hypothesized that Rh2 inhibited inflammation through the TLR4/PI3K/Akt/mTOR, Keap1/Nrf2/HO-1, and Raf-1/MEK/ERK signaling pathways (Hsieh *et al.,* 2018).

One of the widely studied bioactivities of ginsenosides is their anticancer potentials which are correlated to their anti-inflammatory effects. Interestingly, most ginseng saponins render marginal genotoxicity and cytotoxicity in normal cell lines, increasing their chemotherapeutic potentials (Li *et al.,* 2009) (Li *et al.,* 2020) (Xu *et al.,* 2016). Rh2 was described as a candidate in preclinical studies against liver, breast, prostate, pediatric acute myeloid leukemia cancer, *etc*. (Chen *et al*., 2016) (Ratan *et al.,* 2021). Cancer combination therapy studies also revealed the promising effects of incorporating Rh2 in current cancer medications, as its amphiphilic nature allows the formation of nanostructures, making it a potential adjuvant of drug carriers (Zare-Zardini *et al.,* 2018) (Kikuchi *et al.,* 1991). The oral administration of Rh2 in mice bearing human ovarian cancer cells (HRA) resulted in significant attenuation of HRA tumor growth. Consequently, daily oral administration or subcutaneous inoculation of 120 μM Rh2 in these mice prolonged their survival by roughly 40% (Kikuchi *et al.,* 1991). Similarly, nude mice transfected with pediatric leukemia experienced prolonged survival time, and leukemia cells underwent apoptosis through suppression of Bcl-2 with Rh2 (Chen *et al.,* 2016). Along with Rg3, Rh2 was reported to prevent the proliferation of prostate cancer cells through the downregulation of mitogen-activated protein kinases (MAPK) (Dinda *et al.,* 2010). Recurrence of tumor growth is inhibited through improved immunomodulatory response by Rh2 as a drug adjuvant and found to trigger CD4+/CD8a+ T-lymphocyte infiltration in tumor tissues (Shi *et al.,* 2019). Other anticancer activities of Rh2 are summarized by Chen *et al.* in *Table 1.4.*

Table 1.4. Summary of the anticancer activities of Rh2 (Chen *et al.*, 2016)

Compounds	Activities	Mechanisms
Ginsenoside Rh2	Antiproliferation	G_1 phase arrest [105]; induces cell differentiation and reduces telomerase activity [106]; induces Ca^{2+}-dependent mitochondrial apoptosis pathway [107]; induces autophagy [78]; activates NF-κB signaling pathway and upregulates TNF-α [108]; reduces Akt/mTOR signaling [109]
	Active tumor suppressors	Increases the expression level of DR4 death receptor [65]; upregulates miRNA-128 expression [110]; activates p53 [64]
	Inhibit cellular metabolism	Induces AMPK and p38 MAPK activation. AMPK determines apoptotic sensitivity of cancer cells to Rh2 [111]
	Inhibit tumor growth	Inhibits EGFR signaling through PI3K/Akt/mTOR signaling pathways [112] and upregulation of miR-491 [113]; augment of TGF-β receptor signaling [114]
	Antiangiogenesis	Inhibits angiogenesis and lymphangiogenesis and downregulates JAM expression [115]
	Synergy and attenuation	Synergies with cisplatin, betulinic acid, CTX, daunomycin, vinblastine, docetaxel, paclitaxel, and mitoxantrone [116, 117]; reverses P-gp-mediated MDR [118]
	Prevent tumorigenesis	Decreases the tumor incidence in N:GP(S) newborn mice injected with benzo(a)pyrene model [103, 119]

1.4.2. Proposed cellular uptake mechanisms of ginsenosides and Rh2

Pharmacokinetic studies of bioactive molecules investigate (1) dosing and initial adherence, (2) kinetics, and (3) elimination in systemic circulation (Doogue and Polasek, 2013). The cellular uptake mechanism is one of the crucial stages along a molecule's course in the system. According to Wong *et al.*, the cellular mechanism of ginsenosides can be narrowed to (i) interaction with steroidal receptors, (ii) genomic and non-genomic pathways, and (iii) alterations of the microRNAs. Because of their steroid-like skeleton, several ginsenosides were reported to exhibit steroid-like cellular activities and interact with the plasma membrane and/or compete for functional ligands (Popovich and Kitts, 2002). Based on various experiments and molecular docking studies, ginsenosides mediate steroid receptor-dependent and -independent pathways, as illustrated in *Fig. 1.13*. In panel A, ginsenosides compete in the steroid receptor binding against native ligands; consequently, forming ginsenoside-receptor complexes that either translocate to the nucleus, and triggering transcriptional pathways or cytoplasmic non-transcriptional responses. Ginsenosides were also reported to instigate receptor-dependent responses; however, ginsenoside-receptor binding is not evidenced; therefore, an understudied pathway may be involved (Wong *et al.*, 2015).

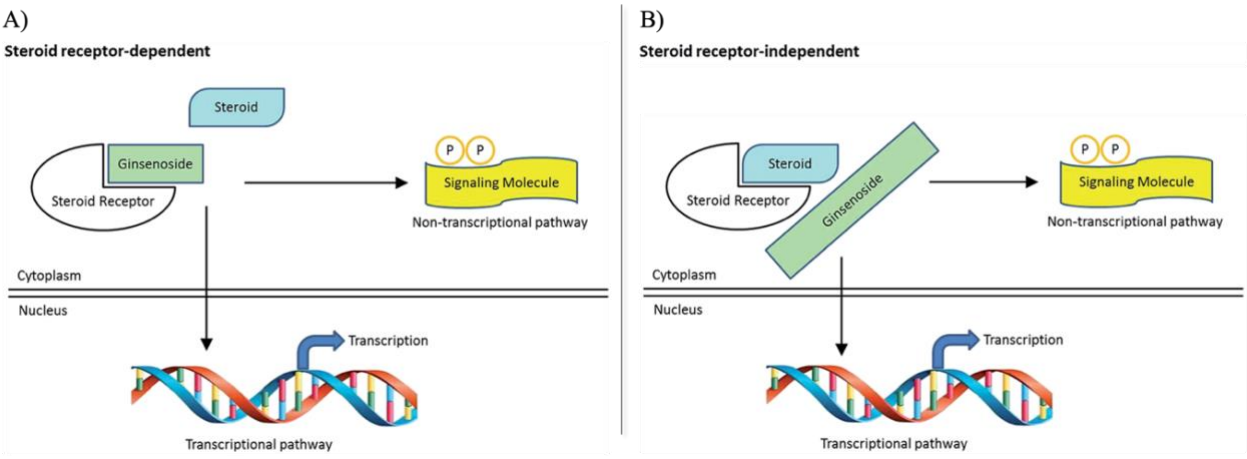

Figure 1.13. Proposed signaling pathways taken by ginsenosides. A) steroid receptor-dependent pathway; B) steroid receptor-independent pathway. (Wong *et al.*, 2015)

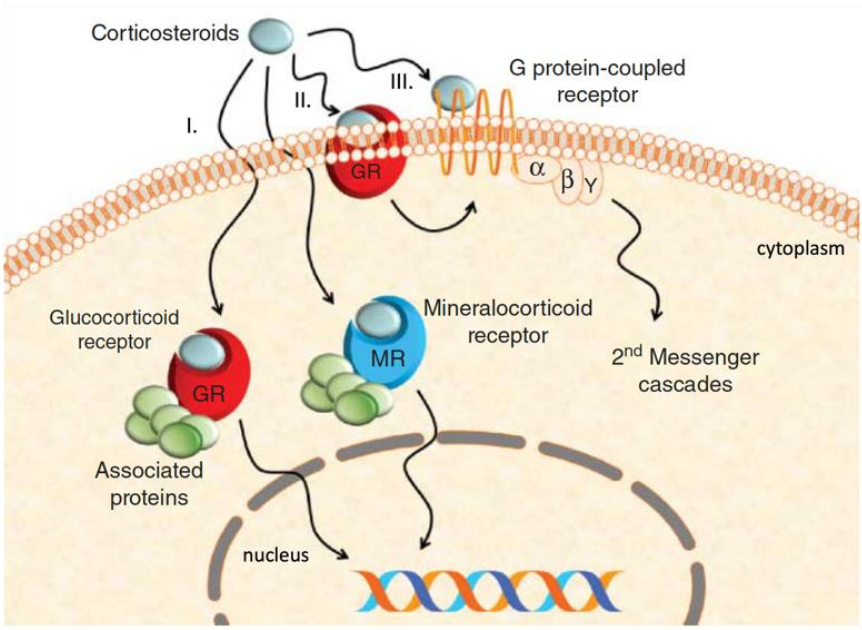

Figure 1.14. Proposed receptor (mineralocorticoid and glucocorticoid) recognition and binding of corticosteroid. Cited and modified from Tasker and Joëls, 2015.

The unknown steroid receptor-independent responses instigated by ginsenosides in reference to Wong *et al.* may be correlated to the other signaling pathways of corticosteroids. In *Fig. 1.14*, corticosteroids diffuse through the plasma membrane, bind to mineralocorticoid (MR) or glucocorticoid receptor (GR) in the cytoplasm, cross the nucleus, and stimulate gene transcription. This is referred to as the '*classical*' corticosteroid transcription effects characterized by delayed onset, which takes minutes to days. While in *Fig. 1.14-II* and *III*, membrane-embedded receptors are activated by the steroid as it initially binds to the plasma membrane and regulates secondary messenger cascade, and G-protein coupled receptor-dependent signaling. This is referred to as the '*rapid*' and non-transcriptional effects of corticosteroids (Tasker and Joëls, 2015), which may be adapted by ginsenosides as well.

Rh2 was reported to possess a similar gross shape to the synthetic glucocorticoid dexamethasone. It was postulated that Rh2 adapts the same cellular mechanism as dexamethasone, and GR may also be involved in its mechanistic actions (Nakata *et al.*, 1998) (Oh *et al.*, 1999) (Jia *et al.*, 2004) (Karra *et al.*, 2019). In a study performed by Lee *et al.*, ginsenosides Rh1 and Rh2 were investigated for their interactions with GR. Immunocytochemistry assay showed that Rh2 was at par with dexamethasone in increasing nuclear translocation and confirmed that Rh2 induced transactivation of the glucocorticoid responsive element (GRE) (Lee *et al.*, 1996) (Lee *et al.*, 1998). The cell-cycle analysis performed by Popovich and Kitts also confirmed the apoptotic activity of Rh2 or dexamethasone-treated THP-1 cells, as evidenced by the build-up of sub-G cells after 24 hours (Popovich and Kitts, 2002).

Similar to these steroidal hormones, Rh2 may interact with biomembranes in a bimodal manner to exert its biological activities. An important take on these assumptions is that both pathways involve the interaction and diffusion of Rh2 through the plasma membrane.

1.4.3. Membrane and Lipid Interactions of Rh2

A common denominator to the proposed cellular mechanisms in the previous section is the binding and diffusion of saponin through the plasma membrane. In their anticancer activities, saponins are reported to induce changes in the properties of the plasma membrane such as pore formation, total lysis, activation of receptors, and pathways through raft binding. Collective illustrations of these pathways are summarized by Lorent *et al.* in *Fig. 1.15.*

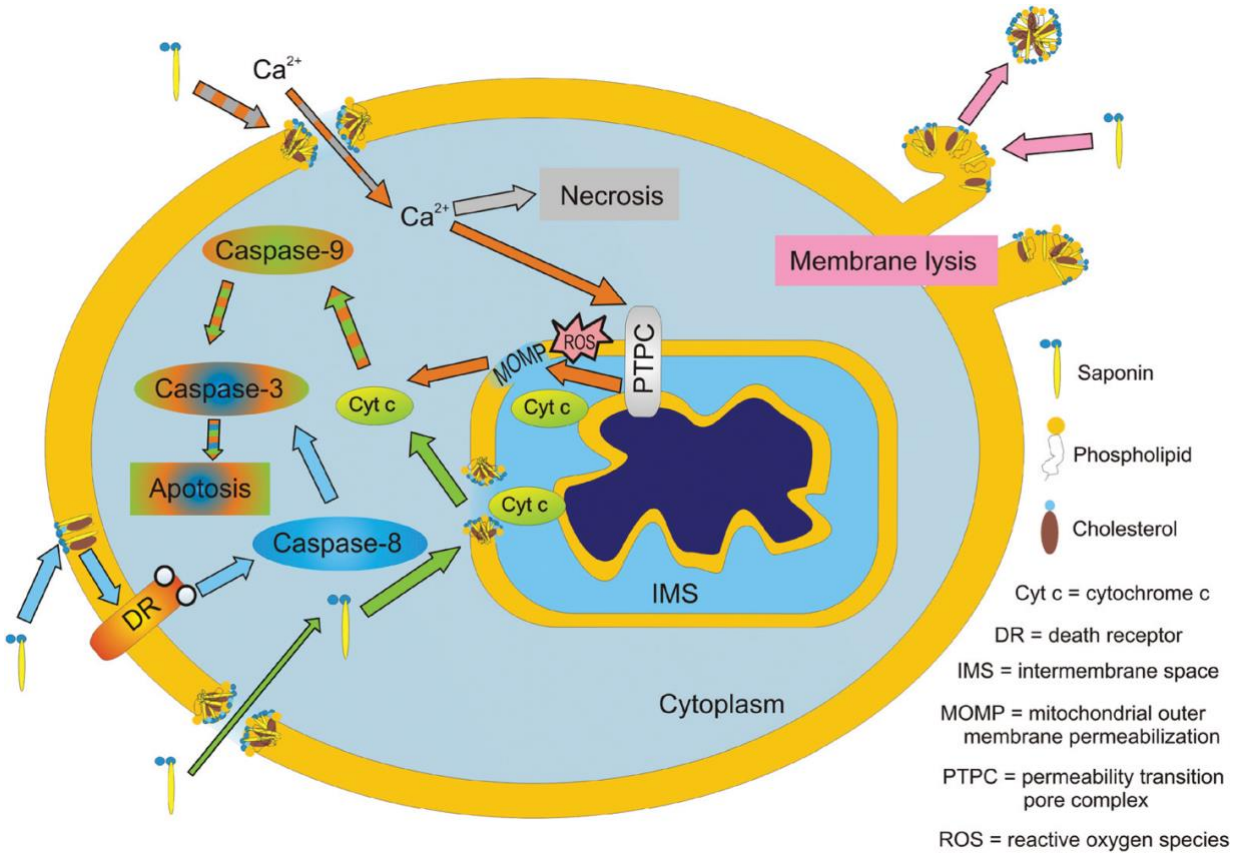

Figure 1.15. Proposed pathways of different cellular effects (e.g., lysis, necrosis, and apoptosis) induced by saponins (Lorent *et al.*, 2014).

One of the actions of saponins is through *lipid rafts*, which are ordered micro- or nanodomains in the membrane enriched with cholesterol and sphingolipids (Bangham *et al*., 1962) (Yi *et al.*, 2009). Lipid rafts serve as a platform for initial membrane binding and signal transduction of drugs and proteins (Jacobson *et al*., 2007) (Lingwood and Simons, 2010). Several saponins are reported to accumulate in lipid rafts; subsequently, altering their properties prior to targeting receptors or regulating signaling pathways. Rh2 was reported to induce apoptosis through the disruption of lipid rafts and activation of death receptors, as shown in the *blue pathway* in *Fig. 1.15* (Lorent *et al.*, 2014). The following experiments depict that the membrane interaction and activity of Rh2 may be influenced by different membrane composition and physical states.

In human epidermoid carcinoma cell lines (A431) treated with Rh2 resulted in a concentration- and time-dependent lipid raft and caveolae (a special-type of the raft that is characterized by a small invagination in the plasma membrane) disruption and internalization. In addition, Akt activity was attenuated and led to cell apoptosis (Park *et al.,* 2010).

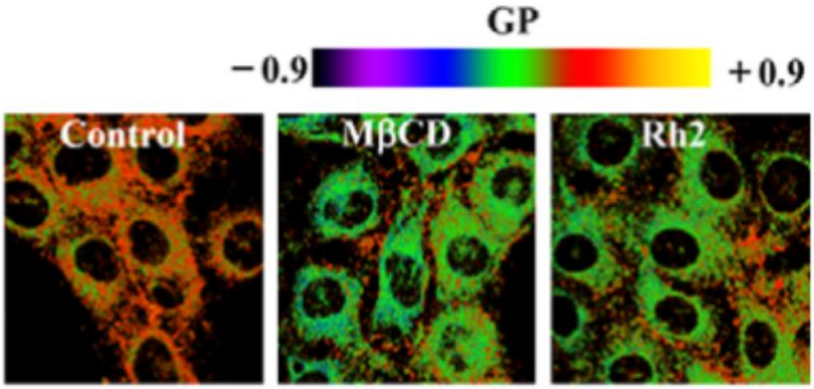

Figure 1.16. HeLa cells treated with 10 mM MβCD or 50μM Rh2 for 1h at 37°C, stained with C-laurdan. GP images of HeLa cells were obtained using two-photon microscopy (Yi *et al.,* 2009).

In *Fig. 1.16*, human cervical cancer (HeLa) cells were stained with carboxyl-laurdan (C-laurdan), and incubated with methyl-β-cyclodextrin (MβCD) or Rh2. C-laurdan is a two-photon dye that emits fluorescence at 400–460 nm in raft membranes and 470–530 nm in non-raft membranes. The intensity of the dye was converted to a generalized polarization (GP) image with pseudocolors. An increase in GP indicates the presence of ordered membrane, whereas low GP indicates disordered membrane. The GP images of HeLa cells showed that high GP domains disappeared upon cellular exposure with ginRh2 as well as MBCD; consequently, activating cell death receptors in HeLa cells. These results indicate that ginRh2 increases the membrane fluidity and might be a lipid raft disruptor (Yi *et al.,* 2009).

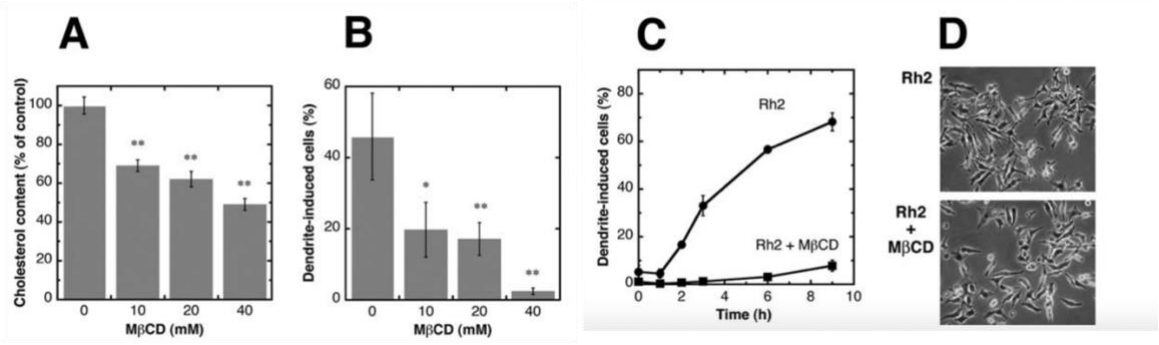

Figure 1.17. The depletion of cholesterol, and disruption of lipid rafts in B16 cells by MβCD consequently suppresses dendrite formation by Rh2. A) Cholesterol content of cells treated with 10 to 40 mM MβCD; B) Percentage of dendrite-induced cells with 18.5 μM Rh2 after treatment with MβCD; C) Percentage of dendrite-induced cells with Rh2, and Rh2 pre-treated with MβCD; D) Morphology of cells treated similarly as C) (Jiang *et al.,* 2010).

In the early studies of Jiang *et al.,* Rh2 was reported to alter the fluidity of B16 melanoma cell membrane. In *Fig. 1.17*, the formation of dendrite relative to the concentration of cholesterol in B16 cells was examined. Dendrites are considered major antigen-presenting cells in T-cell immune responses, and Rh2 are known to induce their production. In *Fig 1.17A* and *B*, increasing the concentration of MβCD reduced the amount of membrane

cholesterol and reduced the dendrite formations. *Fig 1.17D* shows the lack of dendrites in cells treated with MβCD. These suggest that cholesterol is involved in the cellular interaction and dendrite induction of Rh2 (Jiang *et al.*, 2010).

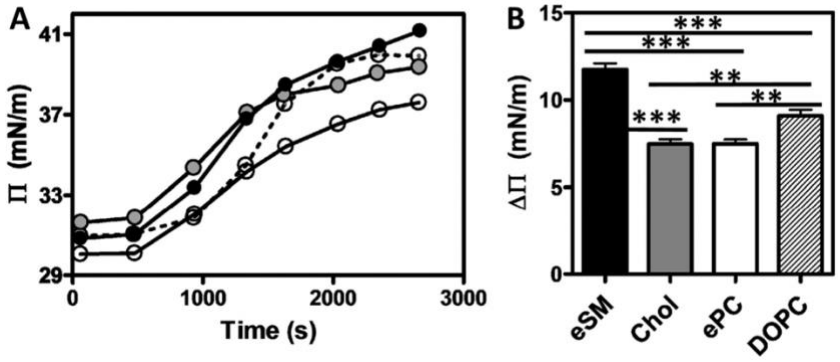

Figure 1.18. Adsorption kinetics of pure lipids (eSM (black), Chol (grey), eggPC (white), DOPC (dotted line)). A) Plot of surface pressure vs time (π – t) (B) Difference between the final and initial surface pressures (Δ π) (Verstraeten *et al.*, 2019).

Verstraeten *et al*., examined the interaction of Rh2 with eSM (egg sphingomyelin), ePC (egg phosphatidylcholine), DOPC (1,2-dioleoyl-*sn*-glycero-3-phosphocholine), and cholesterol through adsorption kinetics via Langmuir monolayer method. Lipids were suspended at the water-air interface, and Rh2 (10 μM final concentration) was injected into the buffer. Surface pressure (π) was measured as a function of time with a constant film area. Changes in surface pressure upon the adsorption of Rh2 from the subphase to lipid monolayer were observed with the following preference: *eSM > DOPC > ePC and Chol* monolayers as depicted in *Fig. 1.18A* and *B*. These imply that Rh2 may have a preference for membrane sphingomyelin (Verstraeten *et al.*, 2019), and contradicts findings of the cholesterol-dependent effects of Rh2. Overall, the presented experiments suggest that the membrane activity of Rh2 is potentially selective towards membrane components; however, this aspect must be investigated further.

1.5. Methods in Membrane Studies

Since the lipid-driven effects of ginsenosides in the plasma membrane were reported, it is equally crucial to investigate the membrane interactions of these saponins aside from their receptor-elicited responses. This section presents the established biophysical techniques carried out to investigate the molecular interactions of saponins and membranes. In addition, this section rationalizes the use of model membranes in the experiments performed and highlights a few of the established lipid-driven membrane effects of saponins.

1.5.1. Model membranes

Over the years, model membranes have been used to apprehend the role of lipids in the membrane interactions of bioactive molecules. In tandem with appropriate biophysical techniques, studies with model membranes are useful in understanding the pharmacokinetic properties of molecules (e.g., transport, biodistribution, accumulation, *etc.*) (Peetla *et al.*, 2009). In addition, investigation at the atomistic level using model membranes helps discern the SAR of several compounds. The heterogeneity and complexity of the plasma membrane make it unsuitable for most

biophysical techniques. The plasma membrane is mainly segregated into lipids, proteins, and carbohydrates. Moreover, lateral and trans-bilayer asymmetry is prominent in the plasma membrane in terms of composition and fluidity (e.g., coexisting liquid-ordered and -disordered phases). For example, the use of live cells in infrared and nuclear magnetic resonance spectroscopic techniques result in unresolved spectra because of the complexity of the membrane. On the other hand, model membranes are a 'simple' system that mimics the fluidity of biological membranes. The components of models can be varied according to the desired experimental approach. As an example, to study the sterol-dependent effects of saponins, model membranes enriched with different types of sterols (e.g., cholesterol, ergosterol, *etc.*) can be utilized. This provides information on lipid-molecule interactions, which may be challenging to determine in a complex membrane (Furlan *et al.*, 2020).

The lipid composition of model membranes can be customized depending on the requisite properties of the membrane in biophysical techniques. Membrane lipids are classified into three groups based on their chemical structures: glycerol-based phospholipids, ceramide-based sphingolipids, and sterols. Glycerophospholipids are subdivided into different groups based on the hydrophilic head groups. Most abundant types are phosphatidylcholine (PC), phosphatidylethanolamine (PE), phosphatidylserine (PS), and phosphatidic acid (PA), while phosphatidylinositol (PI) and cardiolipin are present in smaller quantities. Hydrophobic tails of phospholipids with varying chain length and saturation further diversify their structure and physical properties. The backbone of sphingolipids is comprised of a ceramide moiety with saturated- or trans-unsaturated hydrophobic chains. Sphingomyelin is the most abundant type of sphingolipid and can be further classified depending on the length and saturation of its acyl chains. Cholesterol hydrophilic hydroxyl group attached to a bulky steroid core. Cholesterol is most abundant in the mammalian plasma membranes, while sitosterol and stigmasterol in plant membranes. Sterols are known to influence the packing of the membranes and are essential in the formation of lipid rafts (van Meer *et al.*, 2008) (Escriba *et al*., 2008).

Aside from lipid composition, the fluidity of model bilayers can also be varied depending on the overall temperature, pressure, and hydration of the membrane. Moreover, structural properties, such as the length of the hydrocarbon tails and the composition of the headgroup influence phase states (Kranenburg and Smit, 2005). There are two extreme membrane phase behavior – the gel and fluid phases (*Fig. 1.19*). Sphingolipids tend to adapt a gel or solid-like phase (So). The saturated acyl chains of sphingolipids display trans configuration and are elongated at the maximum, giving rise to an extremely compact lipid network. On the other hand, unsaturation and trans-gauche configuration of phospholipids give rise to a less elongated lipid chain and favor the formation of a liquid-disordered (Ld) phase. The transition between So and Ld phases occur at the thermotropic phase transition (Tm). The addition of sterols in a lipid bilayer forms the liquid-ordered (Lo) phase. Cholesterol in So bilayers disrupts and reduces the packing of the lipid chains. In the case of an Ld bilayer, the addition of cholesterol enhances hydrophobic interactions between the sterol core and the hydrophobic lipid chains which increases the overall packing of the membrane (van Meer *et al.*, 2008) (Eeman and Deleu, 2010).

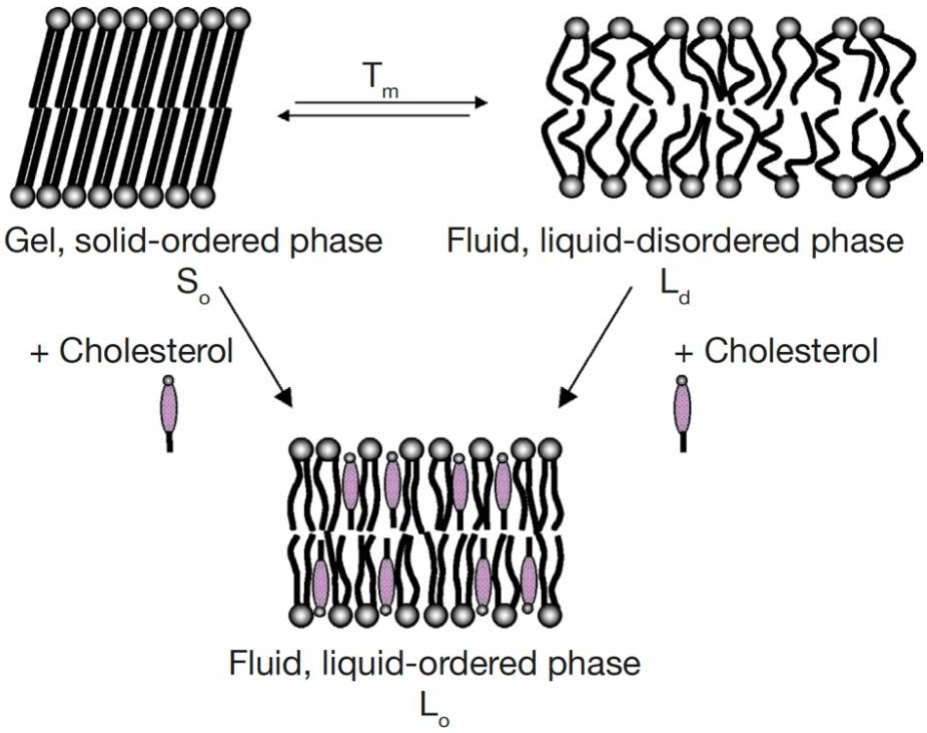

Figure 1.19. Different physical states adopted by a lipid bilayer in aqueous media: gel phase (So), liquid-disordered (Ld), and liquid-ordered (Lo) phase (Eeman and Deleu, 2010).

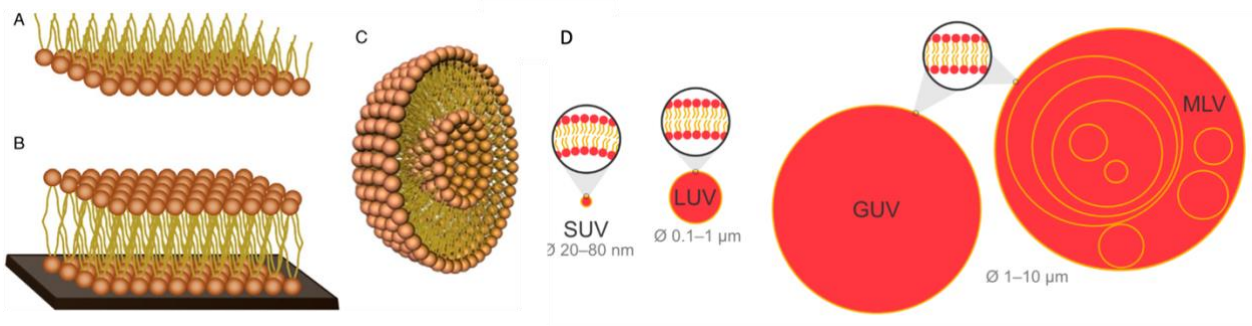

Figure 1.20. Different lipid assemblies of model membranes used in biophysical studies. A) Monolayer: lipids oriented at the air–water interface; B) Supported bilayer: lipids deposited on solid surfaces. C) Liposomes (Deleu *et al.*, 2014); D) Diameter (ø) range of different liposomes: small unilamellar vesicle (SUV), large unilamellar vesicle (LUV), giant unilamellar vesicle (GUV), and multilamellar vesicle (MLV). (Furlan *et al.*, 2020).

Fig. 1.20 illustrates the different types of model membranes used in biophysical studies. Lipid monolayer (*Fig. 20A*) represents the outer half of biological membranes and is considered the simplest model to study penetration and lipid specificity of bioactive compounds. A monolayer is typically formed by dispersing a lipid mixture dissolved in organic solvents over an aqueous solution in the Langmuir trough. As the organic solvent is volatilized, the lipids assemble at the air-water interface – the polar moiety/headgroup locates on the water interface, while the non-polar moiety/acyl chains locate on the air interface (Deleu *et al.*, 2014). The absorption kinetics of an exogenous molecule is evaluated by injecting the compound into the aqueous subphase, allowing it to diffuse freely and interact with the monolayer. Supported lipid bilayers (SLBs) (*Fig. 1.20B*) are bilayers fixed at the interface between the hydrophilic solid substrate (e.g., glass, mica, or silicon) and an aqueous solution. SLBs can be used to

investigate the lipid dynamics of the membrane, such as changes in fluidity and morphology of membranes upon the introduction of exogenous agents. The general method to deposit bilayers onto the solid substrate is via the vesicle-fusion method. Vesicles introduced to the solid substrate rupture, trigger the rupture of neighboring vesicles, and transform into a bilayer patch (Tero, 2012) (Peetla *et al.*, 2009).

Liposomes are the most versatile model membranes formed through the self-assembly of lipids in an aqueous solution (*Fig. 1.20C*). These models are flexible, enclosed systems in which membrane diameter and curvature can be modulated. In addition, liposomes contain an intraluminal cavity within which water-soluble reagents can be encapsulated. This property has been exploited in drug delivery approaches and permeabilization studies. Liposomes are commonly used to examine pore and domain formations, fluidity changes, and membrane adhesion elicited by exogenous molecules. Different liposomal preparations can generate vesicles with varying sizes and membrane curvatures. As shown in *Fig. 1.20D*, different types of liposomes include small unilamellar vesicles (SUVs, 20 to 80 nm), large unilamellar vesicles (LUVs, 0.1-1 μm), giant unilamellar vesicles (GUVs, 1-10 μm), and multilamellar vesicles (MLVs, 1-10 μm). There are several protocols for the preparation of liposomes. MLVs are formed from the hydration of lipid films followed freeze-thaw cycles. These multilayered assemblies can be converted to single bilayers of varying diameters (LUVs or SUVs) through a filter extrusion and sonication. GUVs are generated via electroformation or gentle swelling of lipid films (Furlan *et al.*, 2020).

1.5.2. Biophysical Techniques in Membrane Studies

1.5.2.1. Hemolytic and Liposome Leakage Assay

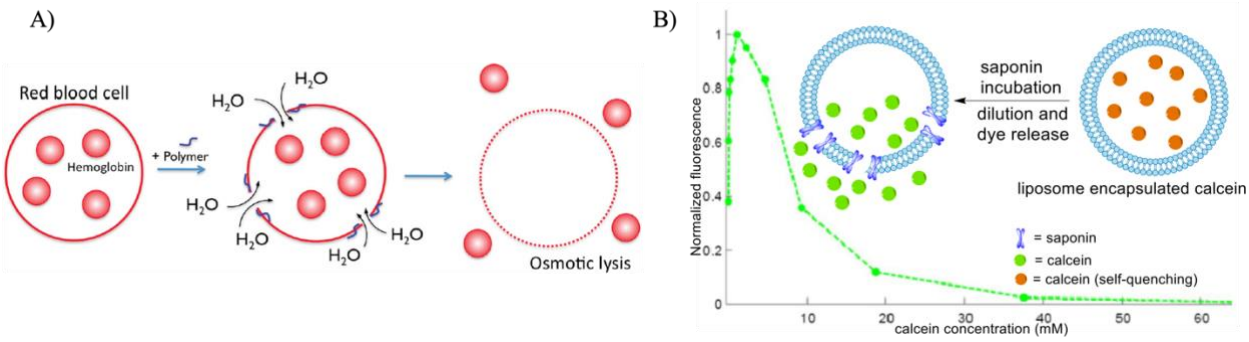

Figure 1.21. Proposed mechanism of A) polymer-induced hemolysis (Sovadinova *et al.*, 2011); B) saponin-induced calcein leakage in model membranes

The hemolytic assay is an initial metric for the toxicity of bioactive molecules and peptides. The mechanism of the rupture of red blood cells induced by polymers is shown in *Fig. 1.21A*. This involves the formation of nano-sized pores smaller than hemoglobin leading to the influx of small solutes into the cells and causing an irreversible rupture or destabilization of the cell (Sovadinova *et al.*, 2011). Hemolysis is spectrophotometrically monitored by measuring the absorbance of released hemoglobin at 415 nm. This all-or-none rupture mechanism is comparative to other pore-forming agents such as saponins. However, note that the exact pore-forming mechanism for different agents varies. In the case of saponins, their hypothesized general mechanism for the rupture of red blood cells follows: (i) formation of insoluble complexes with membrane cholesterol leading to the formation of pores

(Gauthier *et al.,* 2009); (ii) interaction with the water channel, aquaporin, leading to the influx of water molecules in the cells (Winter, 1994).

Calcein leakage assay is a standard protocol that examines the extent of damage induced by an external agent on the model membrane. Calcein is a moderately water-soluble fluorescent dye widely used in cell studies. It exhibits self-quenching at high concentrations of about 60 mM and above (Salassi *et al.,* 2018). The experimental setup uses calcein-filled liposomes incubated with bioactive molecules, peptides, or polymers. Disruptive effects of an agent can lead to pore formation, lamellar phase disorder, or total membrane disruption, which effectively discharge calcein out of the membrane and to the aqueous solution (*Fig 1.21B*). The measured fluorescence emission (λ_{ex} 472 nm; λ_{em} 512 nm) of released calcein is correlated to the activity of the external agent (Claereboudt *et al.,* 2018) (Fukuma *et al.,* 2017). Since there is control over the lipid composition of model membranes, this assay can also be utilized to determine the lipid-dependent activity of an agent.

Aside from the transient pore-formation or total disruption of the membrane, Shimanouchi *et al.* reported that gel or liquid-crystalline phases affect the permeability of calcein across neutral phospholipid membranes. In addition, liposome diameter and temperature could affect diffusion through the membrane. Since calcein has four carboxylate ions at physiological pH (~7.4), this may influence its interaction with polar and charged lipid headgroups, thereby also affecting permeability (Shimanouchi *et al.,* 2009).

1.5.2.2. Fluorescence Anisotropy and Polarization Measurements

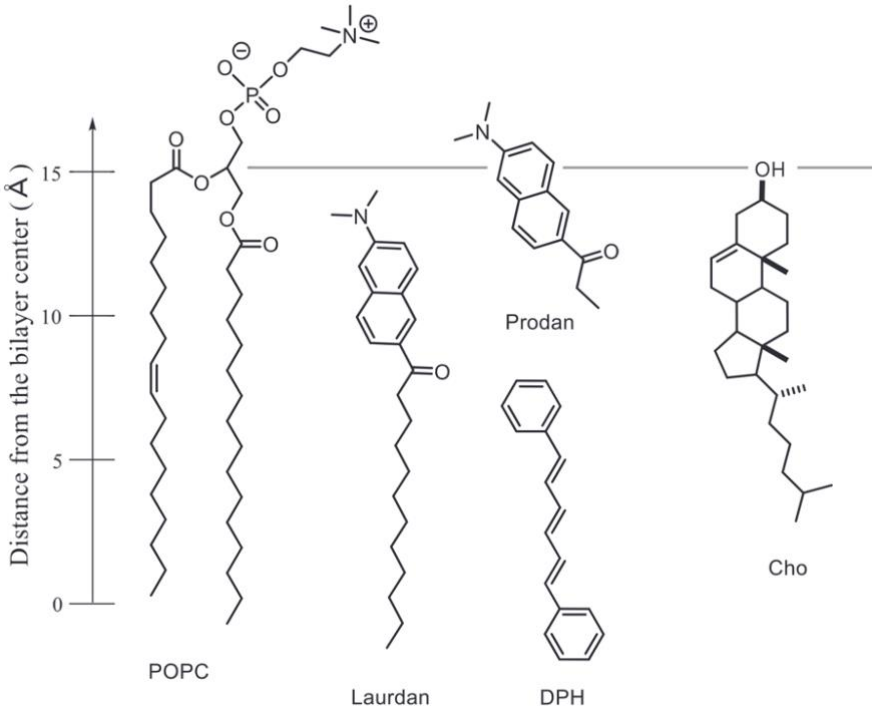

Figure 1.22. Fluorescence probes and their proposed locations along the depth of bilayers relative to POPC and cholesterol (Ondevilla *et al.,* 2021).

The lipid dynamics in artificial membranes can be examined through several fluorescent spectroscopic techniques. Among the widely used probes are 1,6-diphenyl-1,3,5- hexatriene (DPH), 6-lauroyl-2-dimethylaminonaphthalene

(laurdan), and 6-propionyl-2-dimethylaminonaphthalene (prodan). These probes assemble at different depths in the lipid bilayer depending on their structure and major functional groups (*Fig. 1.22*). DPH is one of the fluorescent probes used to observe structural and dynamical features of the hydrophobic region of the bilayer (Furlan *et al.*, 2020). On average, DPH spontaneously inserts into the bilayers and orients parallel to the lipid tails. The steady-state anisotropy of DPH describes the microviscosity, packing, and order of the membrane interior. Upon the introduction of an external agent into the liposome suspension, changes in the rotational diffusion of acyl chains of the membrane lipids can be monitored by DPH fluorescence anisotropy. In principle, a linearly polarized beam excites DPH molecules within the transition moments parallel to the incident polarization vector. The resulting fluorescence intensity passes through a moving polarizer set in parallel (I_{VV}) and perpendicular (I_{VH}) directions relative to the excitation beam. The fluorescence anisotropy, *r*, is calculated from the two measurements (Zhao and Lappalainen, 2012). In a rigid local environment, the mobility of DPH molecules is restricted and gives a high anisotropy value. On the other hand, the high mobility of DPH in a fluid environment would give low anisotropy values. This parameter would report for the ordering or disordering effects of an agent on the hydrophobic chains of lipids. However, in some instances, the interpretation of fluorescence anisotropy values is not as straightforward as it is about membrane ordering. An example is an experimentation and molecular dynamic simulations on POPC bilayers probed with DPH and incubated with itraconazole (ITZ) molecules. It was found that ITZ molecules inside the bilayer locate below the headgroup, parallel to the membrane surface. This orientation of ITZ increases the gap between lipids and results in membrane disorder and bimodal distributions of DPH in the membrane. First, DPH molecules are forced deeper into the membrane and cause tail ordering. Second, DPH molecules orient predominantly perpendicular to the bilayer normal (Poojari *et al.*, 2019). Therefore, DPH did not only report for the changes in the packing of the lipid chains but also changes in the orientations of the probe itself in the bilayer upon the addition of an external agent. Overall, DPH can effectively characterize membrane ordering and microviscosity; however, when considering the effects of additives or external agents, complementary experiments and a cautious interpretation would be suggested.

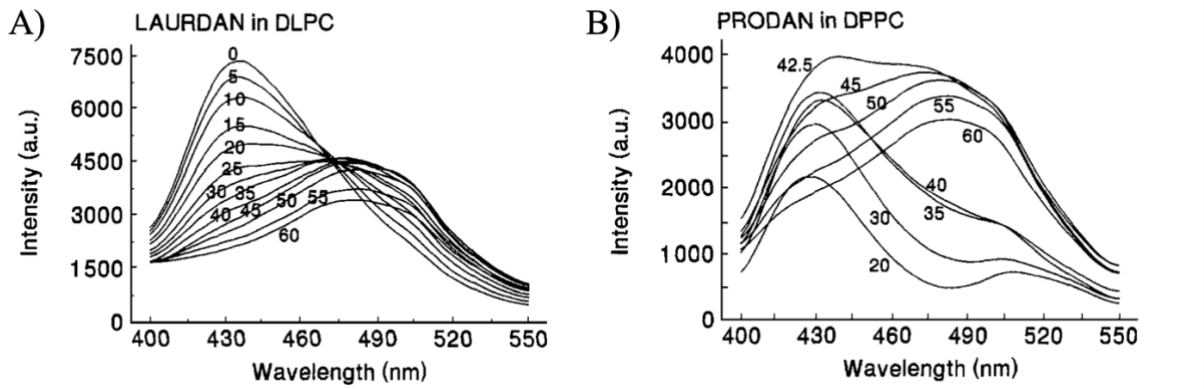

Figure 1.23. The emission spectra of A) laurdan in dilauroyl-phosphatidylcholine (DLPC) liposomes, and B) prodan in dipalmitoyl-phosphatidylcholine (DPPC) liposomes with increasing temperatures, and shows the shifting of the maximum emission as a function of temperature. (Parasassi *et al.*, 1998).

Weber designed two naphthalene derivatives, laurdan and prodan, to observe the phenomena of dipolar relaxation (Weber and Farris, 1979). Laurdan and prodan are fluorescent probes sensitive to polarity changes in their environment. The partial charge separation between 2-dimethylamino, and the 6-carbonyl residues in the probes

produce a dipole moment. The electronic excitation of the probe affects the local dipole moment and causes dipole reorientation of polar solvents. Dipolar relaxation of these probes' naphthalene residue can occur depending on the reorientation of water molecules in their surroundings. This results to either red or blue shift of the probe's steady-state emission. In a phospholipid bilayer, the prominent emission maxima depend on the overall phase state – blue for a rigid membrane (~440 nm), and red for a fluid one (~490 nm). *Fig. 1.23* shows the emission spectra of laurdan, and prodan in DLPC, and DPPC membranes, respectively. Above the Tm, a temperature-dependent spectral shift can be observed for both probes, which are attributed to the dipolar relaxation prominently occurring in the fluid phase. A continuous increase in membrane fluidity reflects in a continuous red shift of the emission (Parasassi *et al.*, 1998). In addition, generalized polarization (GP) values obtained from the measurement reflect the phase state, and hydration of the probe's surroundings. A high GP value signifies a more dense and less hydrated environment; while low GP values signify a more fluid and more hydrated environment. The lauric acid tail of laurdan allows it to sit deeper into the bilayer compared to prodan. Thus, the emission of laurdan reports for the environment of the membrane's hydrophobic core. On the other hand, the shorter chain of prodan prevents its further insertion into the bilayer; hence, it anchors shallowly to the membrane and is exposed to a more polar environment. Located closer to the water interface, prodan reports for the environment of the membrane's headgroup (Krasnowka *et al.*, 1998). These probes distribute well in the membrane regardless of its local phase state and show hydration- or phase-dependent emission spectra.

1.5.2.3. Confocal Fluorescence Microscopy

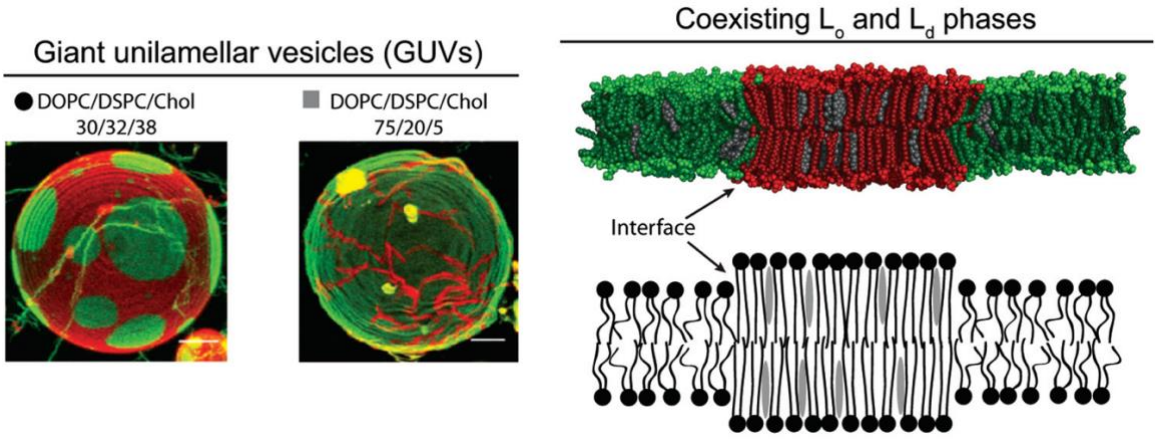

Figure 1.24. (left) Merged 3D micrographs of DOPC/DSPC/Chol GUVs labelled with C20:0-DiI and (16:0-Bodipy)-PC; (right) MD snapshot of DOPC/DSPC/Chol bilayer with coexisting Lo and Ld phases (Dick and Vogt, 2014).

Confocal fluorescence microscopy is a conventional technique for the three-dimensional imaging of cells and model membranes. With the appropriate fluorescent marker, this technique captures various membrane behaviors, and lipid organizations. Giant unilamellar vesicle (GUV) is a molecular assembly with an equivalent size of ~10 to 100 µm, and fluidic properties making it a suitable cellular model for imaging techniques. There are several ways to prepare GUVs, which include gentle hydration and the electroformation method. The gentle hydration technique is suitable when incorporating high ratios of negatively charged lipids in the GUVs; however, a disadvantage of this technique is its low yield. On the other hand, electroformation tends to have a higher GUV

yield but can be limited to the use of neutral lipids. In this study electroformation was utilized in generating GUVs with different compositions and phase states. This method generally involves the suspension of a lipid film in a glass chamber with an appropriate electrode material (e.g., platinum, ITO electrodes, *etc.*). The film is then hydrated at subjected to alternating current at an elevated temperature, allowing the lipid film to swell. The cooling rate of the vesicles is a crucial step in providing equilibrium conditions, especially when generating phase-separated vesicles. For example, abrupt cooling would lead to homogenous GUVs that are desired to be phase-separated in the microscale (Morales-Penningston *et al.*, 2010). There are several fluorescent probes that can be selected depending on the objective of utilization. For a detailed introduction and review of the widely-used fluorescent probes, refer to the review by Klymchenko and Kreder.

Variable information can be obtained using fluorescence microscopy in studying the effects of bioactive molecules to the model membranes. Changes in the morphology, lamellarity, bending, fluidity, and permeability of GUVs upon incubation with an external agent can be observed (Toyota and Zhang, 2022). In addition, the tweakable property of model membranes allows the generation of GUVs with different phase states. GUVs with microscale coexisting phases are a common complementary system in studying lipid rafts of biological membranes. A sample micrograph of a phase-separated GUV is shown in *Fig. 1.24* (left panel). This shows a color-merged fluorescence emission of C20:0-DiI (Lo marker), and 16:0-Bodipy-PC (Ld marker). The right panel shows the molecular dynamics snapshot of lipid segregation in a phase-separated bilayer (Dick and Vogt, 2014). Based on their chemical structure, the probes selectively segregate into different phases. Contributing structural factors include the probe's chain length, saturation, size, and functional groups of intercalating fluorophores (Baumgart *et al.*, 2007). Changes in the membrane properties due to temperature changes or molecular binding would also affect their partitioning.

1.5.2.4. Surface Pressure – Molecular Area Binding Assay

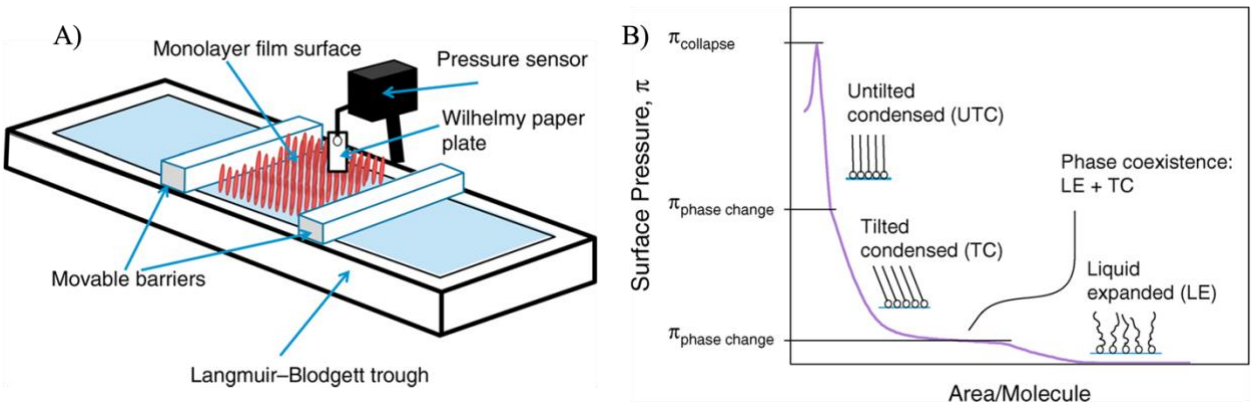

Figure 1.25. A) Schematic of a Langmuir−Blodgett trough; B) A typical pressure−area isotherm of a pure surfactant monolayer. Cartoons of the different phases and the pressures of where the phase changes and collapse occur are shown in the isotherm (Larsen, 2014).

Langmuir trough is a classic laboratory apparatus that is used to form Langmuir monolayers which is characterized by lipids or other amphipathic molecules partitioning between the air-water interface. This setup basically consists of a temperature-controlled trough filled with a solvent subphase (e.g., water), and a movable barrier that spans above the solvent (*Fig. 1.25A*). Langmuir monolayer is a platform that simulates lipid mechanisms occurring at the cell surface and has been extensively used in examining lipid interactions with bioactive molecules or proteins. A

lipid monolayer is formed by introducing a lipid mixture dissolved in a water-miscible, volatile solvent. As the organic solvent evaporates, homogenously lipids partition between the air-water interface. As an example, the phospholipid headgroup locates at the water interface, while the hydrophobic tails locate at the air interface. There are several physicochemical experiments that can be employed in Langmuir monolayers – one of which is the surface pressure-area isotherms. The Langmuir trough is commonly equipped with a pressure sensor and a Wilhelmy plate that monitors surface pressure. While decreasing the area of the monolayer by compressing the movable barriers, surface pressure is measured at constant temperature (Larsen, 2014) (Maget-Dana, 1999). This produces a basic compression isotherm that plots changes in the surface pressure (π) against the average molecular area (A). *Fig. 1.25B* shows a typical π-A isotherm of a pure lipid monolayer. At low pressure, the lipids are in the gaseous phase with little intermolecular interaction. Increasing the pressure leads to the formation of the liquid expanded phase, which eventually forms a kink in the isotherm, indicating phase transition. Then, the liquid condensed phase is formed, accompanied by the increase in surface pressure and packing of the lipids. The monolayer would eventually reach a collapse point upon the disruption of the monolayer. This gives information about the stability, phase transition, compressibility, and mixing behavior of the monolayer (Dynarowicz-Łątka *et al.*, 2001). The absorption of a surface-active molecule in the monolayer can be monitored in this technique. In addition, penetration in an ordered versus a disordered monolayer can be compared as well. The increase of surface pressure resulting from the interaction of the bioactive compound with the monolayer over time gives rise to the adsorption/penetration kinetics (Deleu *et al.*, 2014).

1.5.2.5. Solid-State Nuclear Magnetic Resonance

Solid-state Nuclear Magnetic Resonance (ss-NMR) spectroscopy is a powerful approach that, among its several applications, investigates the dynamics and integrity of biomimetic membranes. Furthermore, ss-NMR determines the localization and tilt-angle of constituent lipids and proteins. An advantage of ss-NMR is its capacity to provide information at the atomistic level that complements other approaches such as x-ray scattering and electronic spectroscopy. This technique relies on the abundance of inherent active atomic nuclei of interest (e.g., ^{1}H, ^{31}P, ^{14}N, ^{13}C, ^{19}F, *etc.*) (Deleu *et al.*, 2014). Site-specific isotope labeling (e.g., ^{2}H-labelled lipids) is another approach performed to achieve better sensitivity and resolution of ss-NMR measurements. Information on the structure and dynamics of lipids are established from the static or motion-averaged coupling tensors due to chemical shift or quadrupolar interactions of a specific nucleus. Tensor fluctuations based on mean-squared amplitudes and rates of the motions result in different line shapes and relaxation times characteristic of different dynamical information (Molugu *et al.*, 2017).

Phosphorus NMR is a well-established approach in biomembrane studies. The natural abundance of the ^{31}P isotope in phospholipids provides selectivity for the study of lipid structure and its local dynamics in membranes. In this notion, ^{31}P NMR spectroscopy of phospholipids can be used to study phase-states based on anisotropic line shapes and differentiation of individual phospholipids in mixtures based on their isotropic chemical shift (Filippov *et al.*, 2015). Different spectral line shapes observed in liquid-crystalline phases (i.e., lamellar, hexagonal, and isotropic) are illustrated in *Fig. 1.26.* In the lamellar phase, chemical shift anisotropy (CSA, $\Delta\delta$) value is defined as the

difference between the two asymmetric peaks in the spectra. It is a parameter sensitive to phase transitions elicited by an agent incorporated in the bilayer or due to changes in temperature.

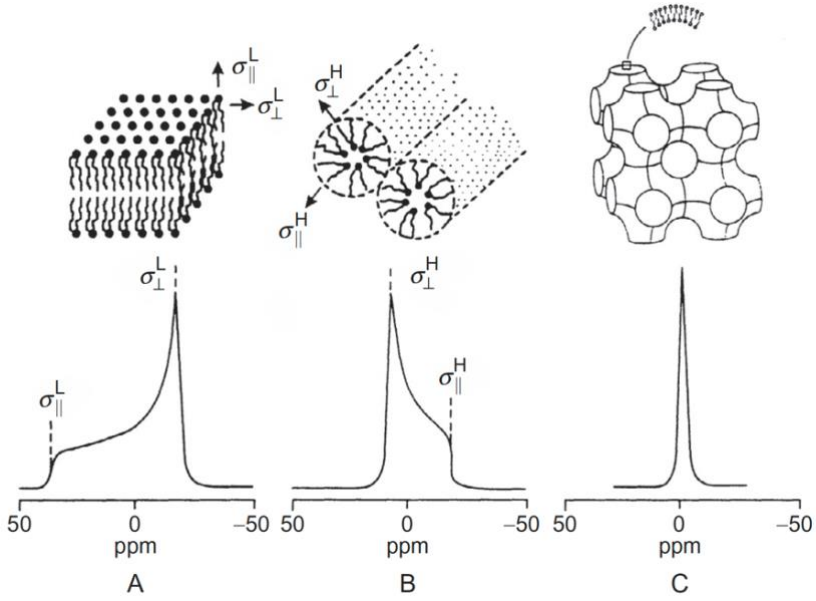

Figure 1.26. The ^{31}P powder NMR line shape of phospholipids is direct evidence for the class of liquid-crystalline phases: (A) lamellar, (B) hexagonal, and (C) isotropic (Filippov *et al.*, 2015).

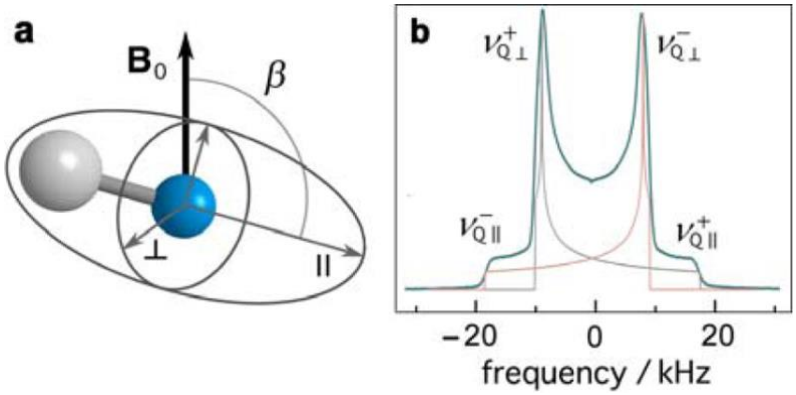

Figure 1.27. A) Illustration of the orientation of carbon-deuterium vector with respect to the magnetic field; and B) the corresponding spectra with a characteristic line shape resulting from the average orientations of the powder sample (Molugu *et al.*, 2017).

Solid-state deuterium (^2H) NMR is another useful method that provides information regarding lipid bilayers. Multi-deuteration or the site-specific labeling of Cho, and the acyl chains of phospholipids and sphingolipids have been a common protocol in ^2H NMR studies. This approach helps understand the dynamics and orientation of the labeled probes in different depths of the membrane. Quadrupolar coupling of the probe with respect to the C-^2H vector along the magnetic field is obtained from randomly oriented or aligned multilamellar lipids (*Fig. 1.27A*). *Fig. 1.27B* shows the characteristic spectral line shape of the lamellar phase (Molugu *et al.*, 2017). Pake doublet is the axially symmetric peaks in the spectra derived from the averaged orientations, and the difference along the peaks

corresponds to the quadrupolar splitting (Δν) value. Similar to the Δδ value, fluctuations in Δν value signify changes in the conformation of the probe within the membrane.

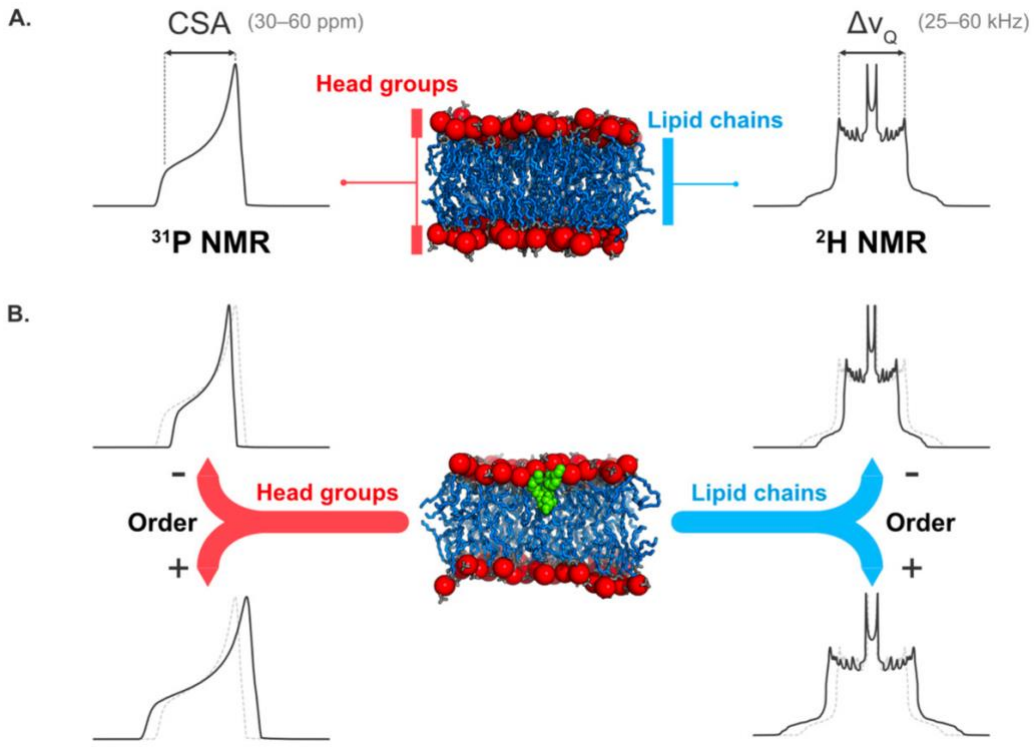

Figure 1.28. The dynamics of the membrane headgroup and interior determined by ^{31}P and ^{2}H solid-state NMR spectroscopy. A) typical ^{31}P NMR (left, CSA or Δδ) and ^{2}H NMR (right, quadrupolar splitting or $\Delta\nu_Q$) spectra for a bilayer; B) Alterations in membrane dynamics upon the inclusion of surface-active molecule (green beads) (Furlan *et al.*, 2020).

In the application ^{31}P and ^{2}H NMR in the study of lipid bilayers, changes in the local lipid environment due to membrane-active molecules (e.g., saponins) incorporated into the system would generally reflect on changes in the spectral widths. A sample interpretation of this effect is illustrated in *Fig. 1.28*. Extracted from the spectral widths and shapes characteristic of a bilayer, Δδ values give insight into the dynamics of the membrane headgroup, while the quadrupolar splitting values report for the hydrophobic core (depending on the location or degree of deuteration). An ordered environment would give rise to greater spectra widths and vice versa (Furlan *et al.*, 2020).

1.6. Significance and Objectives of the Study

Saponins are surface-active glycosides known for their significant immunological and pharmacological activities. Based on the structure of their aglycone moieties, they are classified into triterpenoid, and steroidal saponins. In the long history of saponin research, strong affinity with membrane cholesterol is often attributed to their significant hemolytic activity, toxicity, and surface activity. A classic example is the steroidal saponin, digitonin, which is identified to form complexes with cholesterol on the membrane surface consequently removing the sterol from the membrane core (Frenkel *et al.*, 2014). Triterpenoid saponins are generally recognized to instigate weaker pharmacological effects. However, in the case of active triterpenoid saponins, cholesterol or sphingolipid affinity is reported to be an important step in their mechanistic actions. The triterpenoid saponin, α-hederin, has been reported to bind with membrane cholesterol; accordingly, this interaction increases the spontaneous curvature of the membrane leading to pore- and bud-formations (Lorent *et al*., 2013). Therefore, there is a common implication that surface-active saponins instigate their effects by primarily interacting with the lipid constituents of the membrane (e,g., sterol, sphingolipids, *etc*.).

20(*S*)-ginsenoside Rh2 (Rh2), a rare type of triterpenoid saponin, is known for its potent biological effects. Rh2 has been reported to be recognized by cholesterol or sphingomyelin. Moreover, Rh2 was also proposed to act through cell rafts, a liquid-ordered domain enriched in cholesterol and sphingomyelin. However, the mechanism of these effects has not been precisely defined. Therefore, ***this research aims to apprehend the lipid-driven membrane interactions of Rh2 at the atomistic level to ensue wider applications of the saponin.*** Specific research objectives are (***i***) to assess the lipid-driven interactions and dependence of Rh2 to ***cholesterol*** or ***sphingomyelin***; and (***ii***) to compare the interaction with membranes of different phase states: homogenous liquid-ordered ***(Lo),*** liquid-disordered ***(Ld)***, and phase-separated ***Lo/Ld.***

Experimental approach

The approach is to use model membranes composed of 1-palmitoyl-2-oleoyl-sn-glycero-3-phosphorylcholine (***POPC***), N-palmitoyl-D-erythro-sphingosylphosphorylcholine (***PSM***), and cholesterol (***Cho***). With the appropriate physicochemical techniques, model membranes would help define Rh2's membrane disrupting effects, lipid interactions, and membrane orientations.

The first study focuses on evaluating the interactions of Rh2 with membrane PSM and Cho. The disrupting activities of the saponin was assessed using erythrocytes and model membranes. In the calcein leakage assay, lipid-driven membrane effects of Rh2 were investigated using POPC LUVs enriched with either PSM or Cho. Morphological changes on fluorescent labelled GUVs brought by Rh2 were examined using confocal microscopy. Moreover, the influences of Rh2 in MLVs at the atomistic level were evaluated in solid-state NMR. The ^{31}P NMR probes for alterations in the phospholipid headgroup, while deuterium labelled lipids (d_1-Cho and d_2-PSM) reports for the local environment of the membrane interior.

In the second study, the behavior of Rh2 towards model membranes with diverse phase states were examined using monolayers and bilayers. Based on the phase diagram reported for PSM, POPC, and Cho, different lipid mole ratios

were considered to generate homogenous Lo (PSM/POPC/Cho 35:25:40), homogenous Ld (PSM/POPC/Cho 17:75:8), and Lo-dominant phase separated membranes (PSM/POPC/Cho 1:1:1). DPH anisotropy, and the generalized polarizations of laurdan and prodan were measured to describes changes in the fluidity and hydration of LUVs incubated with Rh2. In addition, binding, and insertion of Rh2 were estimated in Langmuir monolayers. And the results gathered in these biophysical techniques were reinforced with MD simulations.

1.7. References

-Atkovska, K.; Klingler, J.; Oberwinkler, J.; Keller, S.; Hub, J. S. Rationalizing Steroid Interactions with Lipid Membranes: Conformations, Partitioning, and Kinetics. *ACS Cent. Sci.* **2018**, *4*, 1155−1165.

-Baeg, I. H.; So, S. H. The world ginseng market and the ginseng (Korea). *J Ginseng Res.* **2013**, *1*, 1-7.

-Bai, L.; Gao, J.; Wei, F.; Zhao, J.; Wang, D.; Wei, J. Therapeutic Potential of Ginsenosides as an Adjuvant Treatment for Diabetes. *Front. Pharmacol*. **2018**, *9*, 423.

-Bangham, A. D.; Horne, R. W.; Glauert, A. M.; Dingle, J. T.; Lucy, J. A. Action of saponin on biological cell membranes. *Nature*. **1962**. *196*, 952−955.

-Baumgart, T.; Hunt, G.; Farkas, E. R.; Webb, W. W. Feigenson, G. W. Fluorescence probe partitioning between Lo/Ld phases in lipid membranes. *Biochim. Biophys. Acta*. **2007.** *1768*, 2182-2194.

-Chen, X. J.; Zhang, X. J.; Shui, Y. M.; Wan, J. B.; Gao, J. L. Anticancer Activities of Protopanaxadiol- and Protopanaxatriol-Type Ginsenosides and Their Metabolites. *Evid. Based Complementary Altern. Med*. **2016**. *2016.*

-Claereboudt, E.J.S.; Eeckhaut, I.; Lins, L.; Deleu, M. *How different sterols contribute to saponin tolerant plasma membranes in sea cucumbers. Sci Rep.* **2018**. *8,* 10845.

-Deleu, M.; Crowet, J-M.; Nasir, M. N.; Lins, L. Complementary biophysical tools to investigate lipid specificity in the interaction between bioactive molecules and the plasma membrane: A review. *Biochim. Biophys. Acta*. **2014**. *1838*, 3171-3190.

-Dick, R. A.; Vogt, V. M. Membrane interaction of retroviral Gag proteins. *Front microbiol*. **2014**, *5*, 187.

-Dinda, B.; Debnath, S.; Mohanta, B. C.; Harigaya, Y. Naturally Occurring Triterpenoid Saponins. *Chem. Biodivers.* **2010**. *7.*

-Doogue, M. P.; Polasek, T. M.; The ABCD of clinical pharmacokinetics. *Ther Adv Drug Saf.* **2013**. *4*, 1, 5–7.

-Duc, N. M.; Kasai, R.; Ohtani, K.; Ito, A.; Nham, N. T.; Yamasaki, K.; Tanaka, O. Saponins from Vietnamese Ginseng, *Panax vietnamensis* Ha et Grushv. Collected in central Vietnam. II. *Chem. Pharm. Bull.* **1994**, *42*, 115-122.

-Duc, N. M.; Nham, N. T.; Kasai, R.; Ito, A.; Yamasaki, K.; Tanaka, O. Saponins from Vietnamese Ginseng, *Panax vietnamensis* Ha et Grushv. Collected in central Vietnam. I. *Chem. Pharm. Bull.* **1993**, *41*, 2010-2014.

-Dynarowicz-Łątka, P.; Dhanabalan, A.; Oliveira, O. N. Modern physicochemical research on Langmuir monolayers. *Adv. Colloid Interf. Sci.* **2001**. *91*, 221–293.

-Eeman, M.; Deleu, M. From biological membranes to biomimetic model membranes. *Biotechnol. Agron. Soc. Environ.* **2010**. *14*, 4, 719-736.

-El Aziz, M. M. A.; Ashour, A. S.; Melad, A. S. D. A review on saponins from medicinal plants: chemistry, isolation, and determination. *J Nanomed Res.* **2019**. *7*, 4, 282-288.

-Escriba, P. V.; Gonzalez-Ros, J. M.; Goni, F. M.; Kinnunen, P. K.; Vigh, L.; Sanchez-Magraner, L.; Fernandez, A. M.; Busquets, X.; Horvath, I.; Barcelo-Coblijn, G. Membranes: a meeting point for lipids, proteins and therapies. *J. Cell Mol. Med.* **2008**. *12*, 829–875.

-Filippov, A. V.; Khakimov, A. M.; Munavirov, B. V. Chapter 2 - ^{31}P NMR Studies of Phospholipids. *Annual Reports on NMR Spectroscopy.* **2015**. *85*, 27-92.

-Frenkel, N.; Makky, A.; Sudji, I. R.; Wink, M.; Tanaka, M. Mechanistic Investigation of Interactions between Steroidal Saponin Digitonin and Cell Membrane Models. *J. Phys. Chem. B.* **2014**. *118*, 14632−14639.

-Fukuma, S.; Shimanouchi, T.; Hayashi, K.; Kimura, Y. Calcein Leakage Behavior from Vesicles Induced by Protein-Vesicle Interaction: A Study by Surface Pressure-Area Isotherms. *Chem. Lett.* **2017**. *46*, 1036–1039.
-Furlan, A. L.; Laurin, Y.; Botcazon, C.; Rodriguez-Moraga, N.; Rippa, S.; Deleu, M.; Lins, L.; Sarazin, C.; Buchoux, S. Contributions and Limitations of Biophysical Approaches to Study of the Interactions between Amphiphilic Molecules and the Plant Plasma Membrane. *Plants*. **2020**, *6*, 648.
-Gao, S.; Kushida, H.; and Makino, T. Ginsenosides, ingredients of the root of Panax ginseng, are not substrates but inhibitors of sodium-glucose transporter 1. *J. Nat. Med*. **2017.** *71*, 131–138.
-Gauthier, C.; Legault, J.; Girard-Lalancette, K.; Mshvildadze, V.; Pichette, A. Haemolytic activity, cytotoxicity and membrane cell permeabilization of semi-synthetic and natural lupane- and oleanane-type saponins. *Bioorg. Med. Chem.* **2009.** *17*, 2002–2008.
-Ha, Y. W.; Ahn, K. S.; Lee, J. C.; Kim, S. H.; Chung, B. C.; Choi, M. H. Validated quantification for selective cellular uptake of ginsenosides on MCF-7 human breast cancer cells by liquid chromatography-mass spectrometry. *Anal Bioanal Chem.* **2010,** *396*, 3017–25.
-Hong, H.; Baatar, D.; Hwang S. G. Anticancer Activities of Ginsenosides, the Main Active Components of Ginseng. *Evid-Based Compl Alt.* **2021,** *2021*, 8858006.
-Hsieh, Y.; Deng, J.; Chang, Y.; Huang, G. Ginsenoside Rh2 Ameliorates Lipopolysaccharide-Induced Acute Lung Injury by Regulating the TLR4/PI3K/Akt/mTOR, Raf-1/MEK/ERK, and Keap1/Nrf2/HO-1 Signaling Pathways in Mice. *Nutrients*. **2018**. *10*, 1208.
-Jacobson, K.; Mouritsen, O.G.; Anderson, R.G. Lipid rafts: at a crossroad between cell biology and physics. *Nat Cell Biol.* **2007.** *9*, 1, 7-14.
-Jeong, S. M.; Lee, J. H.; Kim, J. H.; Lee, B. H.; Yoon, I. S.; Kim, D. H.; Rhim, H.; Kim, Y.; Nah, S. Y. Stereospecificity of ginsenoside Rg3 action on ion channels. *Mol Cells.* **2004**, *18*, 383–389.
-Jeong, Y.; Ku, S.; You, H. J.; Ji, G. E. A stereo-selective growth inhibition profile of ginsenoside Rh2 on human colon cancer cells. *CYTA J Food*. **2019**, *17*, 488-493.
-Jia, W. W. G.; Bu, X.; Philips, D.; Yan, H.; Liu, G.; Chen, X.; Bush, J. A.; Gang, L. Rh2, a compound extracted from ginseng, hypersensitizes multidrug-resistant tumor cells to chemotherapy. *Can. J. Physiol. Pharmacol.* **2004.** *82*, 431–437.
-Jiang, Y. S.; Jin, Z. X.; Umehara, H.; Ota, T. Cholesterol-dependent induction of dendrite formation by ginsenoside Rh2 in cultured melanoma cells. Int. J. Mol. Med. **2010**, *26*, 787-793.
-Kang, D.I.; Lee, J.Y.; Yang, J.Y.; Jeong, S.M.; Lee, J.H.; Nah, S.Y.; Kim, Y. Evidence that the tertiary structure of 20(S)-ginsenoside Rg(3) with tight hydrophobic packing near the chiral center is important for Na^+ channel regulation. *Biochem Bioph Res Co*. **2005**; *333*, 1194–1201.
-Kang, K. S.; Kim, H. Y.; Yamabe, N.; Yokozawa, T. Stereospecificity in hydroxyl radical scavenging activities of four ginsenosides produced by heat processing. *Bioorg Med Chem Lett.* **2006**, *16*, 5028–31.
-Karra, A. G.; Konstantinou, M.; Tzortziou, M.; Tsialtas, I.; Kalousi, F. D.; Garagounis, C.; Hayes, J. M.; Psarra, A. M. G. Potential Dissociative Glucocorticoid Receptor Activity for Protopanaxadiol and Protopanaxatriol. *Int. J. Mol. Sci*. **2019**, *20*, 94.
-Kikuchi, Y.; Sasa, H.; Kita, T.; Hirata, J.; Tode, T.; Nagata, I. Inhibition of human ovarian cancer cell proliferation *in vitro* by ginsenoside Rh2 and adjuvant effects to cisplatin *in vivo*. *Anticancer Drugs*. **1991**. *2*,63-67.

-Kim, Y. S.; Kim, D. S.; Kim, S. I. Ginsenoside Rh2 and Rh3 induce differentiation of HL-60 cells into granulocytes: modulation of protein kinase C isoforms during differentiation by ginsenoside Rh2. *Int J Biochem Cell Biol*. **1998**. *30*, 327–38.

-Klymchenko, A. S.; Kreder, R. Fluorescent Probes for Lipid Rafts: From Model Membranes to Living Cells. *Chemistry & Biology*. **2014.** *21*.

-Kohda, H.; Tanaka, S.; Yamaoka, Y.; Izumi, H.; Nuno, M.; Isoda, S.; Gotoh, K.; Watanabe, T.; Katsuki, S.; Satake, M. Chikusetsusaponin. VI. A new saponin from the rhizome of *Panax pseudo-ginseng* var. *angustatus* Hara. *Chem. Pharm. Bull.* **1991,** *39,* 1588-1590.

-Kranenburg, M.; Smit, B. Phase behavior of model lipid bilayers. *J Phys Chem B*. **2005**, *109*, 14, 6553-63.

-Krasnowska, E. K.; Gratton, E.; Parasassi, T. Prodan as a Membrane Surface Fluorescence Probe: Partitioning between Water and Phospholipid Phases. *Biophys J.* **1998**. *74*, 1984-1993.

-Larsen, M. C. Binary Phase Diagrams at the Air−Water Interface: An Experiment for Undergraduate Physical Chemistry Students. *J. Chem. Educ*. **2014**. *91*, 597−601.

-Lee, Y. N.; Lee, H. Y.; Chung, H. Y.; Kim, S. I.; Lee, S. K.; Park, B. C.; Kim, K. W. In vitro induction of differentiation by ginsenosides in F9 teratocarcinoma cells. *Eur. J. Cancer*. **1996**, *32*, 1420-1428.

-Lee, Y. N.; Lee, H. Y.; Lee, Y. M.; Chung, H. Y.; Kim, S. I.; Lee, S. K.; Park, B. C.; Kim, K. W. Involvement of Glucocorticoid Receptor in the Induction of Differentiation by Ginsenosides in F9 Teratocarcinoma Cells. *J. Steroid Biochem. Molec. Biol*. **1998**, *67*, 2, 105- 111.

-Lee, Y.J.; Kim, H.Y.; Kang, K.S.; Lee, J.G.; Yokozawa, T.; l, J.H. The chemical and hydroxyl radical scavenging activity changes of ginsenoside-Rb-1 by heat processing. *Bioorg Med Chem Lett*. **2008**, *18*, 4515–4520.

-Leung, K. W.; Wong, A. S. T. Pharmacology of ginsenosides: a literature review. *Chin. Med.* **2010**, *5*, 20.

-Li, W.; Liu, Y.; Zhang, J. W.; Ai, C. Z.; Xiang, N.; Liu, H. X.; Yang, L. Anti-androgen-independent prostate cancer effects of ginsenoside metabolites in vitro: mechanism and possible structure–activity relationship investigation. *Arch Pharm Res.* **2009**, *32*, 49–57.

-Li, X.; Chu, S.; Lin, M.; Gao, Y.; Liu, Y.; Yang, S.; Zhou, X.; Zhang, Y.; Hu, Y.; Wang, H.; Chen, N. Anticancer property of ginsenoside Rh2 from ginseng. *Eur. J. Med. Chem*. **2020.** *203.*

-Lingwood, D.; Simons, K. Lipid rafts as a membrane-organizing principle. *Science*. **2010**. *327*, 46−50.

-Lorent, J.; Le Duff, C. S.; Quetin-Leclercq, J.; Mingeot-Leclercq, M. P. Induction of Highly Curved Structures in Relation to Membrane Permeabilization and Budding by the Triterpenoid Saponins, α- and δ-Hederin. *J Biol Chem.* **2013.** *288*, 20, 14000-14017.

-Lorent, J. H.; Quetin-Leclercq, J.; Mingeot-Leclercq, M. P. The amphiphilic nature of saponins and their effects on artificial and biological membranes and potential consequences for red blood and cancer cells. *Org. Biomol. Chem*. **2014**, *12*, 8803.

-Maget-Dana, R. The monolayer technique: a potent tool for studying the interfacial properties of antimicrobial and membrane-lytic peptides and their interactions with lipid membranes. *Biochim. Biophys. Acta Biomembr.* **1999.** *1462*, 109–140.

-Mohan, V. R.; Tresina, P. S.; Daffodil, E. D. *Antinutritional Factors in Legume Seeds: Characteristics and Determination*. Encyclopedia of Food and Health; Academic Press, 2016; pp 211-220.

-Molugu, T. R.; Lee, S.; Brown, M. F. Concepts and Methods of Solid-State NMR Spectroscopy Applied to Biomembranes. *Chem. Rev*. **2017**. *117*, 12087−12132.

-Morales-Penningston, N. F.; Wu, J.; Farkas, E. R.; Goh, S. L.; Konyakhina, T. M.; Zheng, J. Y.; Webb, W. W.; Feigenson, G. W. GUV preparation and imaging: Minimizing artifacts. Biochim Biophys Acta. **2010.** *1798*, 1324-1332.

-Nakata, H.; Kikuchi, Y.; Tode, T.; Hirata, J.; Kita, T.; Ishii, K.; Kudoh, K.; Nagata, I.; Shinomiya, N. Inhibitory effects of ginsenoside Rh2 on tumor growth in nude mice bearing human ovarian cancer cells. *Jpn. J. Cancer Res.* **1998**. *89*, 733-740.

-Niu, T., Smith, D. L., Yang, Z., Gao, S., Yin, T., Jiang, Z. H., You, M., Gibbs, R. A., Petrosino, J. F., & Hu, M. Bioactivity and bioavailability of ginsenosides are dependent on the glycosidase activities of the A/J mouse intestinal microbiome defined by pyrosequencing. *Pharmaceutical research*. **2013**, *30*, 3, 836–846.

-Odashima, S.; Ohta, T.; Kohno, H.; Matsuda, T.; Kitagawa, I.; Abe, H.; Arichi, S. Control of Phenotypic Expression of Cultured B16 Melanoma Cells by Plant Glycosides. *Cancer Res.* **1985.** *45*, 2781-2784.

-Oh, M.; Choi, Y.H.; Choi, S.; Chung, H.; Kim, K.; Kim, S.I.; Kim, D. K.; Kim, N. D. Anti-proliferating effects of ginsenoside Rh2 on MCF-7 human breast cancer cells. *Int. J. Oncol.* **1999.** *14*, 869-875.

-Ondevilla, J. C.; Hanashima, S.; Mukogawa, A.; Umegawa, Y.; Murata, M. Diosgenin-induced physicochemical effects on phospholipid bilayers in comparison with cholesterol. *Bioorg. Med. Chem. Lett.* **2021**. *36*, 127816.

-Ota, T.; Fujikawa-Yamamoto, K.; Zong, Z. P.; Yamazaki, M,; Odashima, S.; Kitagawa, I.; Abe, H.; Arichi, S. Plant-glycoside modulation of cell surface related to control of differentiation in cultured B16 melanomacells. *Canc. Res.* **1987**. *47*, 3863-3867.

-Parasassi, T.; Krasnowska, E. K.; Bagatolli, L.; Gratton, E. Laurdan and Prodan as Polarity-Sensitive Fluorescent Membrane Probes. *J. Fluoresc.* **1998**. *8*, 4.

-Park, E. K.; Lee, E. J.; Lee, S. H.; Koo, K. H.; Sung, J. Y.; Hwang, E. H.; Park, J. H.; Kim, C. W.; Jeong, K. C.; Park, B. K.; Kim, Y. N. Induction of apoptosis by the ginsenoside Rh2 by internalization of lipid rafts and caveolae and inactivation of Akt. *Br. J. Pharmacol.* **2010**. *160*, 5, 1212–1223.

-Peetla, C.; Stine, A.; Labhasetwar, V. Biophysical Interactions with Model Lipid Membranes: Applications in Drug Discovery and Drug Delivery. *Molecular Pharmaceutics.* **2009.** *6*, 5, 1264-1276.

-Piao, X. M.; Huo, Y.; Kang, J. P.; Mathiyalagan, R.; Zhang, H.; Yang, D. U.; Kim, M.; Yang, D. C.; Kang, S. C.; Wang, Y. P. Diversity of Ginsenoside Profiles Produced by Various Processing Technologies. *Molecules.* **2020**, *25*, 4390.

-Poojari, C.; Wilkosz, N.; Lira, R. B.; Dimova, R.; Jurkiewicz, P.; Petka, R.; Kepczynski, M.; Róg, T. Behavior of the DPH fluorescence probe in membranes perturbed by drugs. *Chem. Phys. Lipids*. **2019**. *223*, 104784.

-Popovich, D. G.; Kitts, D. D. Structure–function relationship exists for ginsenosides in reducing cell proliferation and inducing apoptosis in the human leukemia (THP-1) cell line. *Arch. Biochem. Biophys.* **2002**. 406, 1-8

-Qi, L. W.; Wang, C. Z.; Yuan, C. S. American ginseng: Potential structure–function relationship in cancer chemoprevention. *Biochem. Pharmacol.* **2010**, *80*, 947-954.

-Qi, L.; Wang, C.; Yuan, C. Ginsenosides from American ginseng: Chemical and pharmacological diversity. *Phytochemistry*. **2011**, *72*, 689-699.

-Ratan, Z. A.; Haidere, M. F.; Hong, Y. H.; Park, S. H.; Lee, J. O.; Lee, J. S.; Cho, J. Y. Pharmacological potential of ginseng and its major component ginsenosides. *J Ginseng Res.* **2021**, *45*, 199-210.

-Salassi, S.; Simonelli, F.; Bartocci, A.; Rossi, G. A Martini coarse-grained model of the calcein fluorescent dye. *J. Phys. D: Appl. Phys*. **2018.** *51*, 384002.

-Shen, L.; Haas, M.; Wang, D. H. Q.; May, A.; Lo, C. C.; Obici, S.; Tso, P.; Woods, S. C.; Liu, M. Ginsenoside Rb1 increases insulin sensitivity by activatingAMP-activated protein kinase in male rats. *Physiol Rep*. **2015**, *3*, *9*.

-Shi, Z.; Zeng., J.; Wong, A. S. T. Chemical Structures and Pharmacological Profiles of Ginseng Saponins. *Molecules*. **2019**, *24*, 2443.

-Shibata, S. Chemistry and Cancer Preventing Activities of Ginseng Saponins and Some Related Triterpenoid Compounds. *J Korean Med Sci*. **2001**. *16*, S28-37.

-Shibata, S.; Tanaka, O.; Soma, K.; Ando, T.; Iida, Y.; Nakamura, H. Studies on saponins and sapogenins of ginseng. The structure of panaxatriol. *Tetrahedron Lett.* **1965**, *42*, 207-213.

-Shimanouchi, T.; Ishii, H.; Yoshimoto, N.; Umakoshi, H.; Kubo, R. Calcein permeation across phosphatidylcholine bilayer membrane: Effects of membrane fluidity, liposome size, and immobilization. *Colloids and Surfaces B: Biointerfaces. 2009, 73,* 156–160.

-Sovadinova, I.; Palermo, E. F.; Huang, R.; Thoma, L. M.; Kuroda, K. Mechanism of Polymer-Induced Hemolysis: Nanosized Pore Formation and Osmotic Lysis. *Biomacromolecules.* **2011**. *12*, 260–268.

-Tasker, J. G.; Joëls, M. *Chapter 3*: *The Synaptic Physiology of the Central Nervous System Response to Stress, Neuroendocrinology of Stress*, 1st ed.; John and Wiley & Sons, Ltd., 2015.

-Tero, R. Substrate Effects on the Formation Process, Structure and Physicochemical Properties of Supported Lipid Bilayers. *Materials*. **2012**. 5, 2658-2680.

-Toyota, T.; Zhang, Y. Identifying and Manipulating Giant Vesicles: Review of Recent Approaches. *Micromachines.* **2022**. *13*, 644.

-Tsuchiya, H. Membrane Interactions of Phytochemicals as Their Molecular Mechanism Applicable to the Discovery of Drug Leads from Plants. *Molecules*. **2015**, *20.*

-van Meer, G.; Voelker, D. R.; Feigenson, G. W. Membrane lipids: where they are and how they behave. *Nat. Rev. Mol. Cell Biol.* **2008**. *9*, 112–124.

-Verstraeten, S. L.; Deleu, M.; Janikowska-Sagan, M.; Claereboudt, E. J. S.; Lins, L.; Tyteca, D; Mingeot-Leclercq, M. P. The activity of the saponin ginsenoside Rh2 is enhanced by the interaction with membrane sphingomyelin but depressed by cholesterol. *Sci. Rep.* **2019**. 9, 1-14.

-Weber, G. and Farris, F. J. Synthesis and spectral properties of a hydrophobic fluorescent probe: 6-propionyl-2 (dimethylamino)naphthalene. *Biochemistry.* **1979**. *18*, 3075-3078.

-Winter, W. P. Mechanism of saponin induced red cell hemolysis: Evidence for the involvement of aquaporin CHIP28. *Blood.* **1994**. *84*, 445.

-Wong, A. S. T.; Che, C.; Leung, K. Recent Advances in ginseng as cancer therapeutics: a functional and mechanistic overview. *Nat. Prod. Rep.* **2015**, *32*, 256

-Xiang, Y. Z.; Shang, H. C.; Gao, X. M.; Zhang, B. L. L: A comparison of the ancient use of ginseng in traditional Chinese medicine with modern pharmacological experiments and clinical trials. *Phytother Res.* **2008**, *22*, 851-858.

-Xu, W.; Choi, H.; Huang, L. State of *Panax* ginseng Research: A Global Analysis. *Molecules*. **2017**, *22*, 1518.

-Xu, X.; Li, T.; Fong, C. M. V.; Chen, X.; Chen, X.; Wang, Y.; Huang, M.; Lu, J. Saponins from Chinese Medicines as Anticancer Agents. *Molecules*. **2016**. *21*, 1326.

-Yang, W. Z.; Hu, Y.; Wu, W. Y.; Ye, M.; Guo, D. A. Saponins in the genus *Panax* L. (Araliaceae): A systematic review of their chemical diversity. *Phytochemistry*. **2014**, *7*, 24.

-Yi, J. S.; Choo, H. J.; Cho, B. R.; Kim, H. M.; Kim, Y. N.; Ham, Y. M.; Ko, Y. G. Ginsenoside Rh2 induces ligand-independent Fas activation via lipid raft disruption. *Biochem. Biophys. Res. Commun.* **2009**. *385*, 154−159.

-Yoshizaki, K.; Yahara, S. New triterpenoid saponins from fruits specimen of *Panax japonicus* collected in Kumamoto and Miyazaki Prefectures. *Chem. Pharm. Bull.* **2012**, *60*, 354-362.

-Zare-Zardini, H.; Taheri-Kafrani, A.; Amiri, A.; Bordbar, A. K. New generation of drug delivery systemsbased on ginsenoside Rh2-, Lysine- and Arginine-treated highly porous graphene for improving anticancer activity. *Sci Rep*. **2018.** *8*, 586.

-Zhang, C.; Yu, H.; Hou, J. Effects of 20 (S)-ginsenoside Rh2 and 20 (R)-ginsenoside Rh2 on proliferation and apoptosis of human lung adenocarcinoma A549 cells. *Zhongguo Zhong Yao Za Zhi*. **2011**, *36*, 1670-1674. (article in Chinese)

-Zhang, F.; Li, M.; Wu, X.; Hu, Y.; Cao, Y.; Wang, X.; Xiang, S.; Li, H.; Jiang, L.; Tan, Z.; Lu, W.; Weng, H.; Shu, Y.; Gong, W.; Wang, X.; Zhang, Y.; Shi, W.; Dong, P.; Gu, J.; Liu, Y. 20(S)-ginsenoside Rg3 promotes senescence and apoptosis in gallbladder cancer cells via the p53 pathway. *Drug Design, Development and Therapy*. **2015**. *9*, 3969-3987.

-Zhang, H.; Abid, S.; Ahn, J. C.; Mathiyalagan, R.; Kim, Y.; Yang, D.; Wang, Y. Characteristics of *Panax ginseng* Cultivars in Korea and China. *Molecules*. **2020**, *25*, 2635.

-Zhang, L.; Virgous, C.; Si, H. How Does Ginsenoside Rh2 Mitigate Adipogenesis in Cultured Cells and Obese Mice? *Molecules*. **2020**. *25*, 2412.

-Zhao, H.; Lappalainen, P. A simple guide to biochemical approaches for analyzing protein–lipid interactions. *Mol. Biol. Cell*. **2012**. *23*, 15, 2823-2830.

-Zou, K.; Zhu, S.; Tohda, C.; Cai, S. Q.; Komatsu, K. Dammarane-type triterpene saponins from *Panax japonicus*. *J. Nat. Prod.* **2002**, *65*, 346-351.

~ Chapter 2 ~

The cholesterol- and sphingomyelin-driven membrane effects of ginsenoside Rh2

2.1. Introduction

Apprehending the cellular mechanism of a bioactive molecule is crucial in discerning its pharmacokinetic properties accurately. A common target for molecular messengers is receptors embedded in the plasma membrane. Other hydrophobic messengers diffuse through the plasma membrane first, then bind to intracellular receptors that are either floating freely in the cytoplasm or embedded on the organelle's membrane. Apart from receptor recognition, the association of these molecules with membrane lipids is equally crucial. Since specific receptors are a minute portion of the overall components of the membrane, a ligand precisely hitting its target protein is less probable (Vauquelin and Packeu, 2009) (Vauquelin and Charlton, 2010). The lipophilic structure of bioactive molecules promotes binding and diffusion through the lipid bilayer (Payandeh and Volgraf, 2021) (Kimura and Cheng, 2009).

Ginsenoside Rh2 (***Rh2***) is a triterpenoid saponin from *Panax ginseng* known for its extensive pharmacological effects. Structural similarities of Rh2 with corticosteroids (e.g., dexamethasone) led to the investigation of its potential mechanism through the glucocorticoid receptor (GR) (Lee *et al.,* 1998) (Chen *et al.,* 2016) (Karra *et al.,* 2019). Immunocytochemistry assay showed that Rh2 was on par with dexamethasone in increasing the nuclear translocation of the GR, and confirmed the transactivation of the glucocorticoid responsive element (GRE) (Lee *et al.*, 1998). GR is a nuclear receptor residing either in the cell cytoplasm or embedded in the plasma membrane. It controls the expression of several target genes resulting in inflammation, growth, and apoptotic events in cellular systems (Karra *et al.*, 2019). The general cellular mechanism of corticosteroids involves the diffusion of the molecule through the phospholipid bilayer, consequently recognizing GR in the cytoplasm. The steroid–receptor complex dimerizes and enters the nucleus, where they serve as transcription factors. On the other hand, the intracellular signaling cascade is also stimulated when corticosteroids bind to the phospholipid bilayer, activating membrane-associated receptors (Tasker and Joëls, 2015) (Barnes, 2006). Similar to corticosteroids, Rh2 may interact with biomembranes in a bimodal manner to exert its biological activities. A common denominator to these proposed pathways is the binding and crossing of the Rh2 through the lipid bilayer.

Several saponins were reported to have binding capacities with membrane lipids such as cholesterol and sphingomyelin. This lipid-specific action of saponins is correlated to their significant hemolytic activity, toxicity, and surface activity. Digitonin has been identified to form complexes with cholesterol on the membrane surface, consequently removing the sterol from the membrane core (Frenkel *et al*., 2014). The triterpenoid saponin, α-hederin, was also reported to bind with cholesterol; accordingly, increasing the spontaneous curvature of the membrane leading to pore- and bud-formations (Lorent *et al*., 2013). Rh2 has been reported to be recognized by cholesterol or sphingomyelin (Verstraeten *et al.,* 2019). It was also proposed to act through cell rafts, a liquid-ordered domain enriched in cholesterol and sphingomyelin. On the other hand, saponins with weak pharmacological effects (commonly triterpenoids, e.g., glycyrrhizin) are attributed to their inadequate interactions

with cholesterol (Malabed *et al.*, 2017). Therefore, a common implication is that surface active saponins instigate their effects by primarily interacting with the lipid constituents of the membrane (e,g., sterol, sphingolipids, *etc.*).

Since the mechanism of Rh2 towards the lipid bilayer has not been precisely defined; the aim of this first study is to understand lipid-driven interactions and the dependence of Rh2 on cholesterol or sphingomyelin. The approach is to use biomimetic membranes and create a more specific analysis of the lipid interactions of Rh2. Here, different types of bilayers (LUV, GUV, MLV) composed of 1-palmitoyl-2-oleoyl-sn-glycero-3-phosphorylcholine (***POPC***), 1,2-dipalmitoyl-sn-glycero-3-phosphorylcholine (***DPPC***) or N-palmitoyl-D-erythro-sphingosylphosphorylcholine (***PSM***), and cholesterol (***Cho***) were utilized. Different mole ratios of PSM and Cho were incorporated into the bilayers to differentiate the effects of Rh2 in membranes enriched with these lipids.

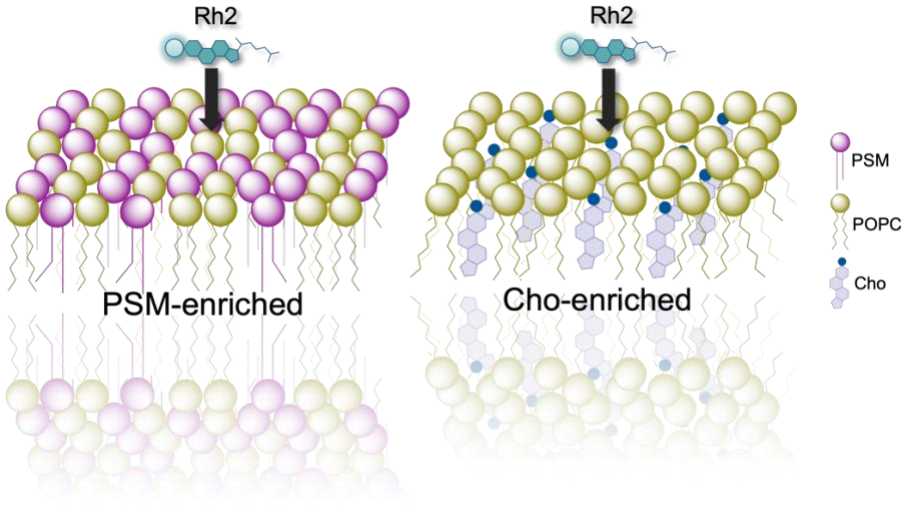

Fig. 2.1. A representation of POPC membrane enriched with PSM (left), and Cho (right) utilized in the investigation of the membrane effects of Rh2.

2.2. Results

2.2.1. Hemolytic assay and Liposome Leakage Assay

Biological membranes and model bilayers were used to investigate the effects of Cho, PSM, and other lipids on the permeability and fluidity of Rh2. As Cho-containing biological membranes, erythrocytes were adopted to examine the hemolytic activity of Rh2 in comparison to two triterpenoid saponins, α-hederin and glycyrrhizin. Similar to Rh2, both α-hederin and glycyrrhizin are monodesmosidic saponins (*Fig. 2.2*), but with a disaccharide unit at 3C. Glycyrrhizin is regarded as a low-permeabilizing and low-lytic saponin (Malabed *et al.*, 2017) (Bailly and Vergoten, 2020). On the other hand, α-hederin is reported as a high-permeabilizing saponin dependent on the membrane Cho (Lorent *et al.*, 2013). In the hemolytic assay, the amount of hemoglobin released from ruptured erythrocytes incubated with saponins was spectrophotometrically quantified (Sovadinova *et al.*, 2011). This serves as a measure for the potency of the saponins and expressed as percent hemolysis. Results in *Fig. 2.3A* showed that Rh2 and α-hederin exhibited significant % hemolysis with increasing saponin concentrations, rendering greater lytic efficacy compared to glycyrrhizin. Results obtained for the control saponins agree with previous studies (Malabed *et al.*, 2020) (Gilabert-Oriol *et al.*, 2013) (Gauthier *et al.*, 2009). In addition, α-hederin has greater potency (lower EC_{50}) than Rh2 and glycyrrhizin. The half maximal effective concentration (EC_{50}, μM) values of Rh2, α-hederin, and glycyrrhizin were 25.0, 6.0, and >100 μmol/L, respectively (*Table S1, Fig. S2.2*).

The liposome leakage assay was performed to evaluate the lipid-dependent permeabilizing activity of Rh2. Here, self-quenching calcein (*Figure S2.1A*, ~ 60 mM) was entrapped in LUVs enriched with Cho and PSM, then incubated with 10 µM saponin. The amount of fluorescent calcein released from disrupted vesicles is expressed as percent leakage and serves as a metric for the activity of the saponin. In *Fig. 2.3B*, even in pure POPC LUVs, Rh2 showed significant percent leakage and was not influenced by the addition of Cho or SM. The activity of α-hederin showed sterol-dependence with the upsurge in % leakage on vesicles with 10 mol % Cho. In contrast, the activity of glycyrrhizin was consistently low in all the liposomal preparations.

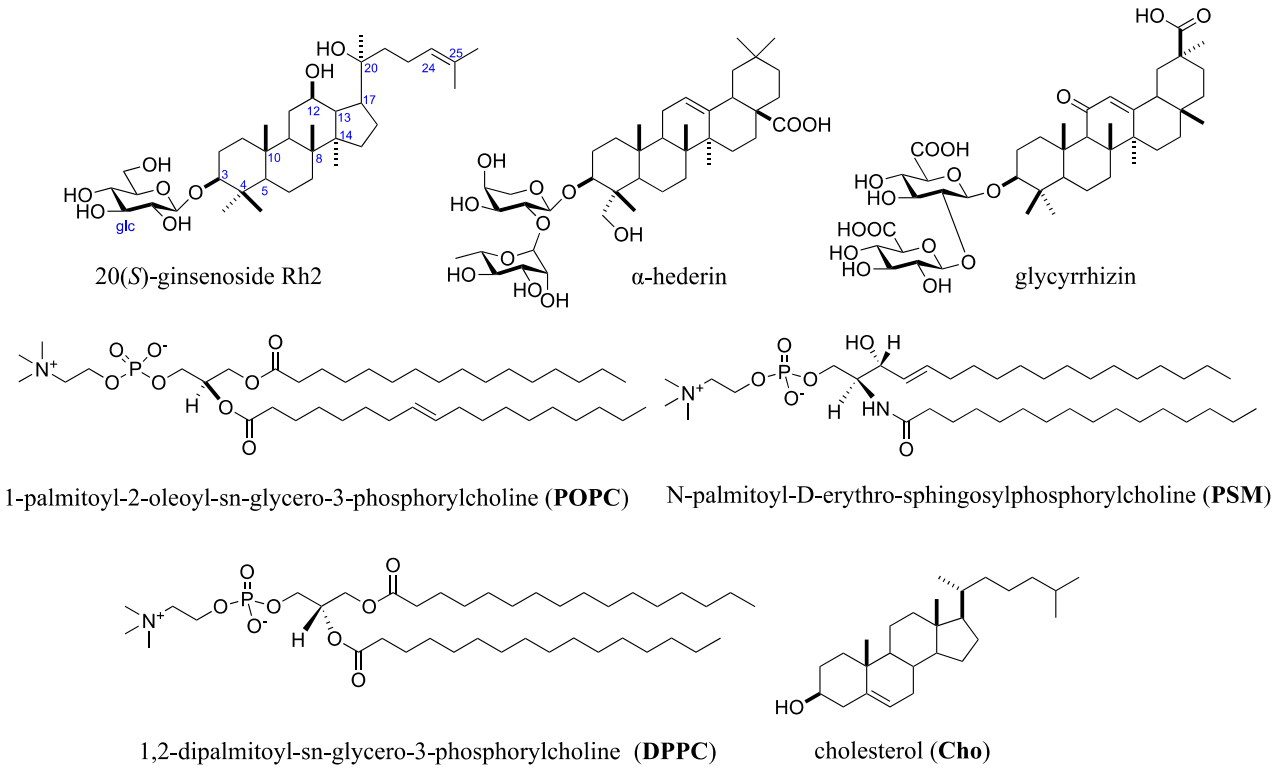

Figure 2.2. Structure of saponins, and the lipids used in this study.

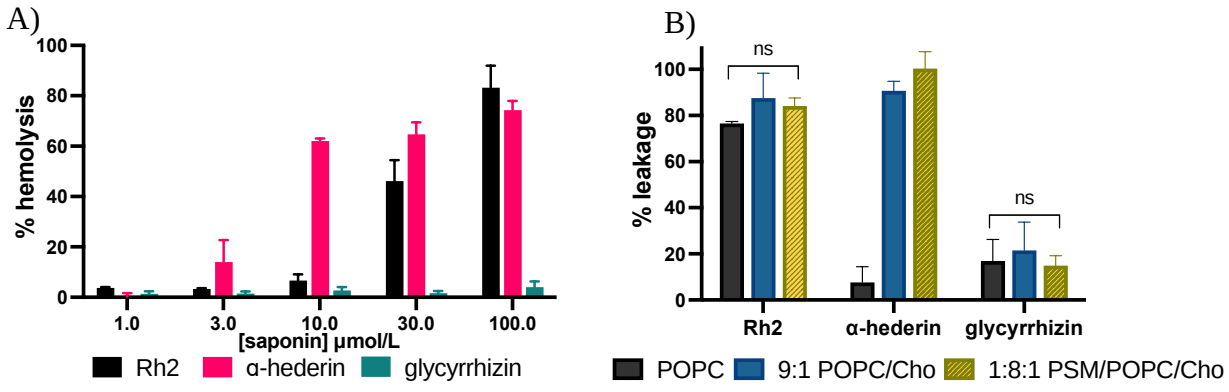

Figure 2.3. A) Hemolytic activity of Rh2, α-hederin, and glycyrrhizin measured at 37°C. B) Leakage activity of 10 µM saponin from various POPC LUVs incubated for 5 mins at 30ºC. ns p>0.05 (one-way ANOVA, n=3). Rh2 [F(2,6)=2.25, p=0.19], glycyrrhizin [F(2,6)= 0.39,p=0.69].

To further differentiate the sterol and sphingolipid dependence of Rh2, binary POPC LUVs with 10 and 30 mol% Cho or PSM were subjected to the leakage assay. In this experiment, vesicles were incubated with increasing

amounts of Rh2 (1 to 100 µM). In *Fig. 2.4*, it is evident that leakage activity of Rh2 is concentration-dependent. At 10 µM Rh2, an upsurge in % leakage was observed in all liposome preparations. Interestingly, binary systems with Cho and PSM, regardless of the lipid mole ratio, displayed similar activities with pure POPC liposomes (black columns).

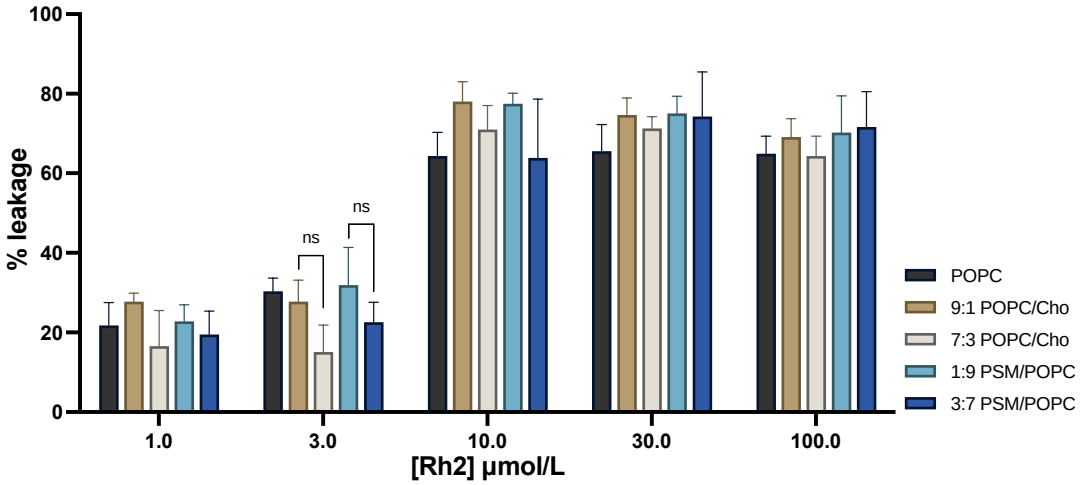

Figure 2.4. Dye leakage activity of Rh2 from various PC LUVs. Rh2 concentration in all liposome preparations ranges from 1 to 100 µM, incubated for 5 mins at 30°C. ns $p>0.05$ (t-test, n = 3). 9:1 and 7:3 POPC/Cho [$t(3) = 2.53$, $p = 0.06$]; 1:9 and 3:7 PSM/POPC [$t(3) = 1.50$, $p = 0.21$].

2.2.2. Confocal Fluorescence Microscopy

Vesicle deformations brought by Rh2 were investigated using confocal fluorescence microscopy. GUVs labeled with ~1 mol % β-BODIPY C_5-HPC (*Fig. S2.1E*) were incubated with Rh2, and monitored for morphological changes. In *Fig. 2.5*, time-lapse images illustrate typical structural changes in POPC GUVs after incubation with 30 µM Rh2. Here, vesicle elongation took place (B) followed by the formation of a biconcave discocyte (C), and a stomatocyte (D). This observation depicts that Rh2 induces morphological changes and membrane curvature. Similar deformations occurred for binary and ternary GUVs composed of 9:1 POPC/Cho and 1:8:1 PSM/POPC/Cho at a faster rate (*Fig. S2.3*).

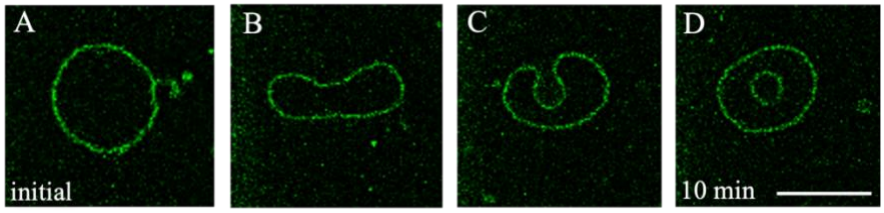

Figure 2.5. Fluorescent micrographs of POPC GUVs that underwent a series of morphological changes after incubation with 30 µM Rh2. Images are captured at 23ºC. (scale bar 10µm)

2.2.3. ^{31}P Solid-state NMR to Examine the Effects of Rh2 on Phospholipid Headgroups

Static ^{31}P NMR was measured to understand the influence of Rh2 on the headgroup environment of POPC liposomes with different concentrations of Cho and PSM. Alterations in the mobility and orientation of the phospholipid headgroup reflect on the chemical shift anisotropy (Δδ) that is determined by the signal widths under axial symmetric rotation. An increase in the Δδ value usually indicates a stronger ordering effect; conversely, a

decrease in the Δδ value indicates disordering (Cullis *et al.,* 1976) (Ondevilla *et al.,* 2021). The sample preparation for solid-state NMR is different from the rest of the experiments performed in this study. Here, 10 mol % Rh2 was mixed into the lipid film prior to the hydration and production of MLVs, and the resulting spectra were compared to liposomes without Rh2. Therefore, Rh2 was already incorporated in the bilayers and not introduced from the exterior of the membrane. Judging from lipid compositions, all bilayer systems in the NMR experiments were supposed to be liquid-disordered phase (Ld) (de Almeida *et al.,* 2013).

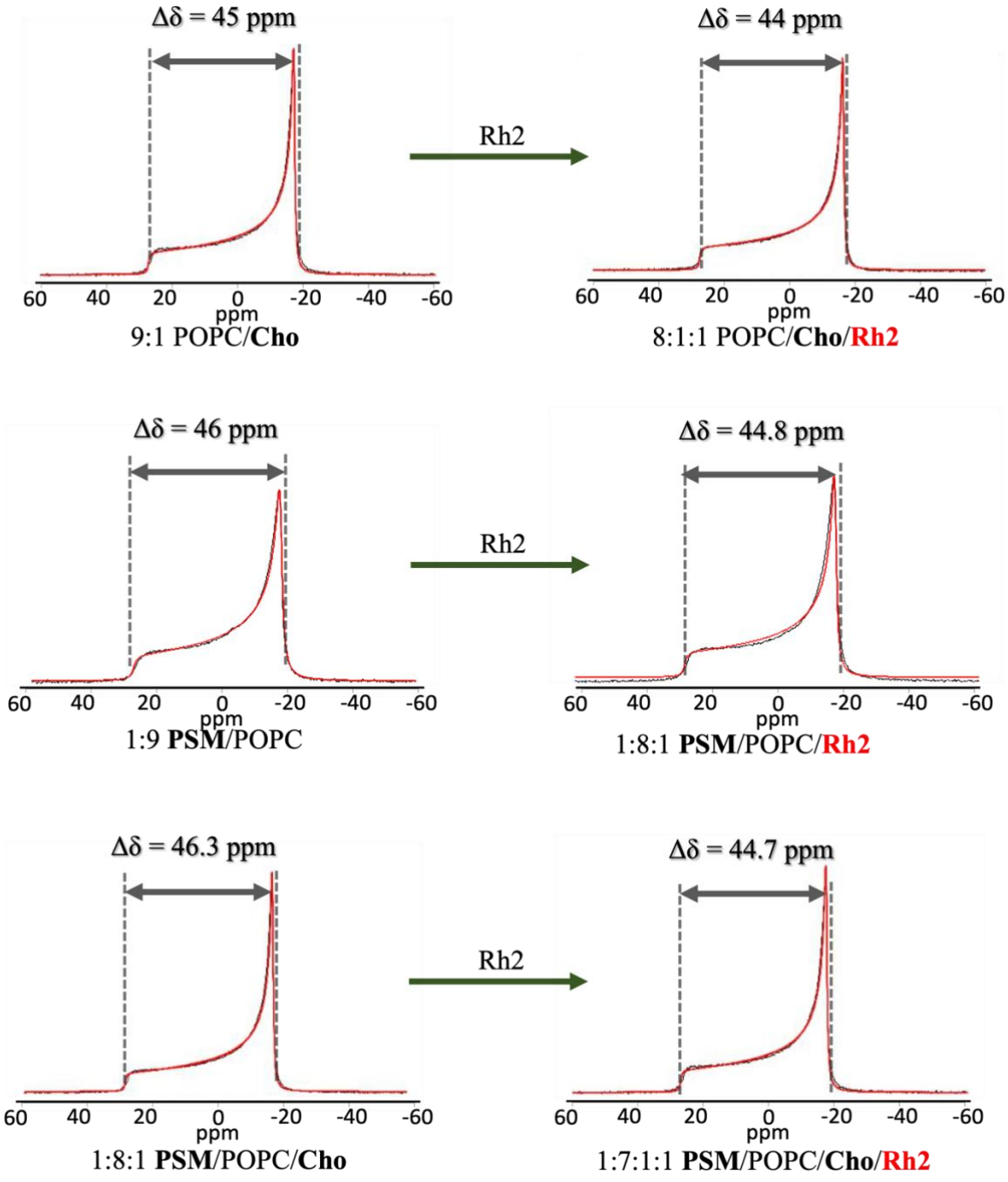

Figure 2.6. ^{31}P ss-NMR spectra and Δδ values for various POPC MLVs. Left spectra: without Rh2; right spectra panel: with 10 mol % Rh2. Black spectra correspond to the experimental data, while red spectra correspond to the simulated data. NMR spectra were referenced from 85% H_3PO_4 peak set at 0 ppm, and were measured at 30°C.

POPC MLVs with either 10 mol % Cho, PSM, and equimolar ratios of both lipids were subjected to ^{31}P ss-NMR measurements. Their corresponding Δδ values are shown in *Fig. 2.6* (left spectra). The ordering effect of PSM reflects in the higher Δδ values obtained in PSM-containing liposomes. The incorporation of 10% Rh2 (*Fig. 2.6,* right spectra) consequently decreased the Δδ values in all the liposome systems illustrating a disordered membrane headgroup with Rh2. With 30% of Rh2 in the POPC/Cho bilayer, membrane curvature was induced as represented by the emergence of an axially symmetric signal with a smaller Δδ value of about 43.2 ppm (*Fig S2.4*, left spectra). While the addition of 30% Rh2 in a PSM/POPC bilayer did not insinuate further decrease in membrane headgroup disorder (45 ppm), and an isotropic peak was not observed in the spectra (*Fig S2.4*, right spectra). In general, Rh2 ensued greater fluidity in the local environment of the membrane headgroup. Because of the polarity of glucose in the saponin, this moiety of Rh2 may preferentially situate close to the membrane-water interface. Depending on the tilt angle, depth, and orientation of Rh2 in a Ld membrane, its glucose moiety perturbs intermolecular forces between phospholipids which results to a greater area per lipid. Cholesteryl-β-D-glucoside (ChoGlc) is a cholesterol derivative that contains β-D-glucose at C3 similar to Rh2, and it is abundantly expressed in the brain tissue. The behavior of ChoGlc in a rigid stearoyl-sphingomyelin (SSM) membrane relative to Cho was examined through MD simulations. The results illustrated that ChoGlc and Cho are embedded at a comparable depth in the SSM membrane; however, the presence of glucose in ChoGlc near the membrane surface brings it closer to phosphate ester moiety of SSM, and prevents the headgroups from interacting with each other. This causes a larger fluctuation of the phosphate ester moiety and a slightly smaller angle of the headgroups (the angle between the P-N vector and the membrane normal). As the umbrella effect of the SSM phosphocholine headgroup towards ChoGlc is reduced, the overall proximity of the two lipids is consequently reduced as well (Hanashima *et al.*, 2021). The effect of the sugar moiety at C3 is a plausible rationalization for the Rh2-induced decrease in Δδ value of ^{31}P NMR.

2.2.4. ^{2}H Solid-state NMR to Examine the Effects of Rh2 on Phospholipid Acyl Chains

The effects of Rh2 on the hydrocarbon chains of PSM and the sterol core of Cho were examined through deuterium (^{2}H) NMR experiments. Labeled lipids, 3-d_1-Cho or 10',10'-d_2-PSM (*Fig S2.1B and C*), were incorporated into POPC bilayers with and without Rh2. Cho was labeled at the C3 position of the rigid ring system that would be sensitive to changes of the sterol core orientation. PSM was labeled at the 10' position and would report for the local environment of the hydrophobic interior (Matsumori *et al.,* 2012) (Hanashima *et al.,* 2021). Site-specific isotope labeling beneficially minimizes perturbation to ideally mimic the physicochemical properties of the native lipids. Alterations in the environment of the probes would influence the wobbling and tilt of the C-D vector with respect to the membrane normal. This reflects in the splitting widths of the Pake doublet from the resulting spectra. A low quadrupolar splitting (Δν) indicates high mobility of the probe; conversely, greater quadrupolar splitting indicates lower mobility of the probe.

Fig. 2.7 shows the spectra and Δν values for binary POPC MLVs with 3-d_1-Cho or 10',10'-d_2-PSM. The difference in the quadrupolar splitting between 10',10'-d_2-PSM and 3-d_1-Cho prior to the addition of Rh2 reflects the dissimilar local properties of the isotopes. The initial Δν value, 26.5 kHz, for the labeled PSM chain implies greater fluidity in the deeper regions of the hydrophobic core in Ld phase. In comparing the effects of Rh2 in these MLVs, a greater effect is evident in POPC/d_2-PSM. The 2.7 kHz decrease in Δν (*Fig. 2.7, lower spectra*)

implies the disordering effects of Rh2 towards the acyl chains of the bilayer, and further disordering was recorded with 30 mol % Rh2 (*Fig. S2.6, right spectra*). On the other hand, minimal changes in the Δν value (around 40 kHz) of d_1-Cho were observed with 10% Rh2 (*Fig. 2.7, upper spectra*), and 30% Rh2 (*Fig. S2.6, left spectra*). These results are summarized in *Fig. S2.7.*

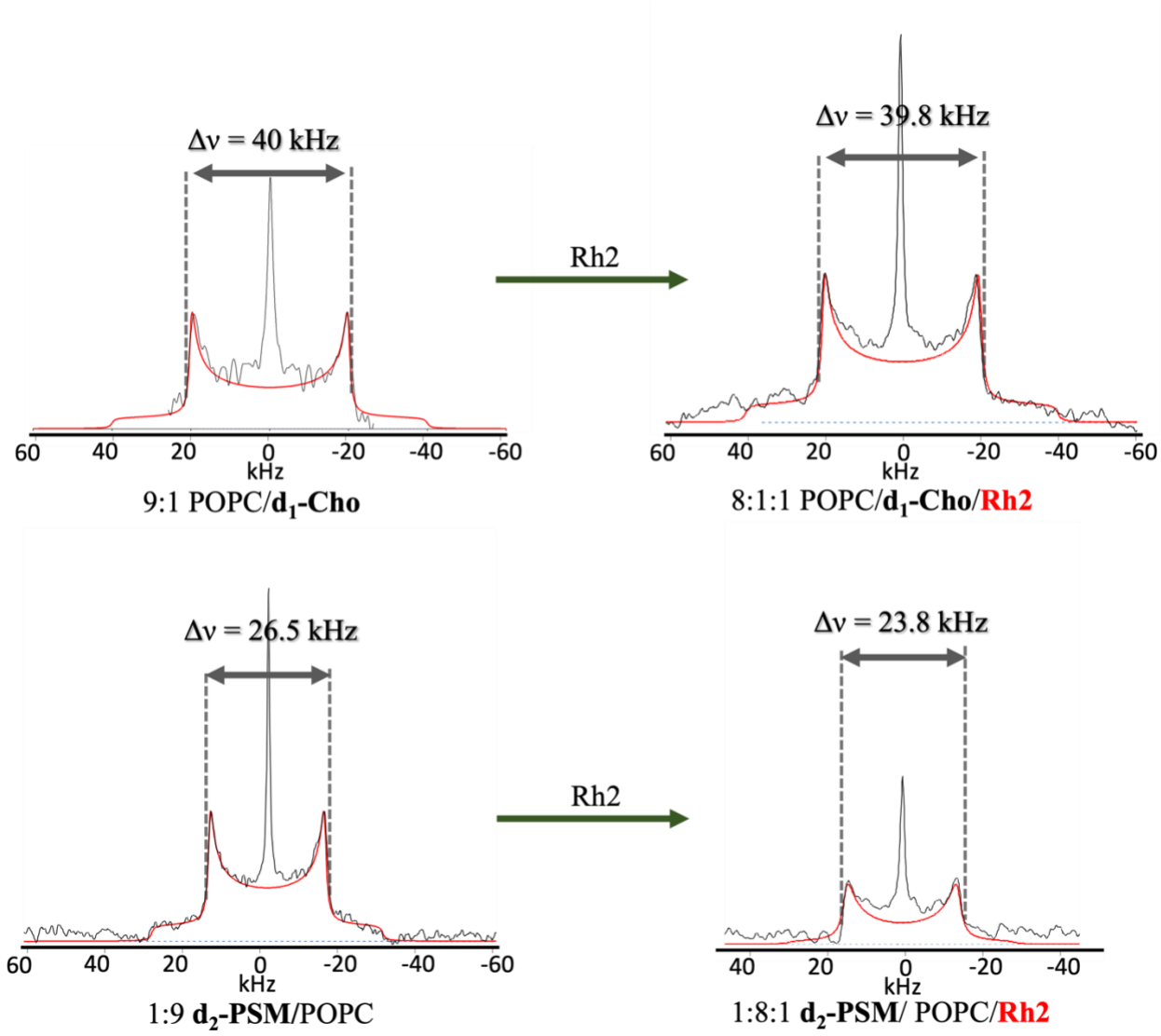

Figure 2.7. ^{2}H ss-NMR spectra and Δν values for POPC MLVs labeled with d_1-Cho and d_2-PSM measured at 30°C. Left spectra: without Rh2; right spectra panel: with 10 mol % Rh2. Black spectra correspond to the experimental data, while red spectra correspond to the simulated data.

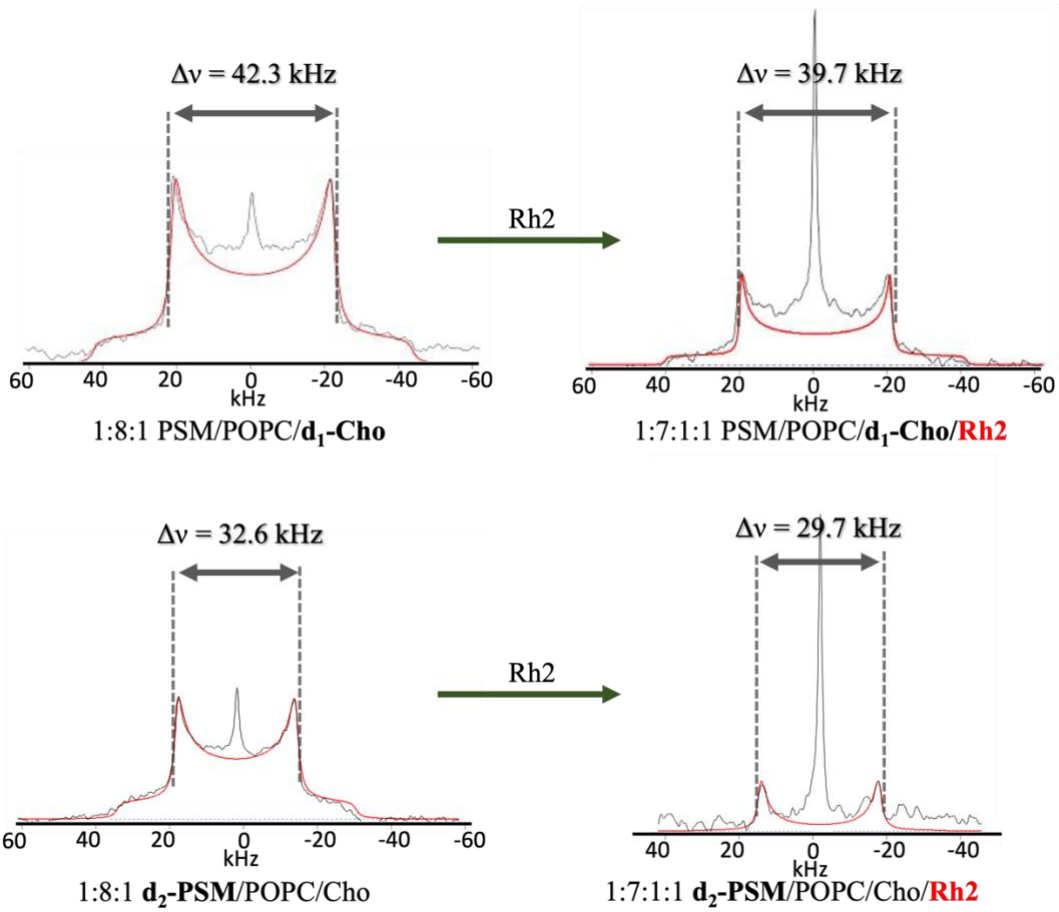

Figure 2.8. ^{2}H ss-NMR spectra and Δν values for POPC ternary MLVs labelled with d_1-Cho and d_2-PSM measured at 30°C. Left spectra: without Rh2; right spectra panel: with 10 mol % Rh2. Black spectra correspond to the experimental data, while red spectra correspond to the simulated data.

The effects of Rh2 on with respect to the deuterium-labeled lipids in ternary Ld systems containing PSM were examined as well. Changes upon the addition of Rh2 in bilayers composed of 1:8:1 PSM/POPC/Cho were monitored by replacing PSM or Cho with their equivalent deuterated compounds. The combination of Cho and PSM in the MLVs instigated ordering effects as shown by the increase of Δν values of both probes (*Fig. 2.8, left panel)*, compared to the values in the binary membranes in *Fig. 2.7.* In the presence of Rh2, the quadrupolar splitting of both probes in the ternary system decreased (*Fig. 2.8, right spectra*) by roughly 3 kHz. Since Cho is known to favorably interact with PSM, the decrease in Δν suggests the disruption of PSM-Cho network by Rh2 in the bilayer (Sodt *et al.,* 2015) (Ahmed *et al.,* 1997) (Matsumori *et al.,* 2011) (Róg and Pasenkiewicz-Gierula, 2006).

2.3. Discussion

This study demonstrates the membrane disrupting and modulating the activity of Rh2 in model membranes. High leakage of calcein was induced by the saponin, even with the unitary POPC bilayer, and the potency was not greatly affected by the inclusion of Cho and PSM. This poses reservations about the dependence of Rh2 on these lipids. These observations are contrary to most saponins that compel the support of sterols to induce potent activity. Well-known examples are digitonin and α-hederin, where calcein leakage activity became remarkable only in the presence of Cho in POPC bilayers (Malabed *et al.*, 2017).

The leakage activity of Rh2 increased in the presence of eggSM (Verstraeten *et al.*, 2019), but our findings show otherwise. In addition, their study utilized eggSM and eggPC mixtures, which may cause the different behavior of the saponin, especially when the objective is comparing direct interactions with specific membrane components. EggPC (Avanti) contains other PCs, such as those bearing C18:2 and C16:0 fatty acyl groups. Besides POPC, eggSM contains ineligible amounts of SMs bearing very long acyl chains.

Because minimal discrepancies were observed in the leakage activity of Rh2 in LUVs containing either PSM or Cho, the rate of leakage in these systems was considered. In the time-course assay, it was observed that the incubation period (1, 5, and 10 mins) did not significantly affect the % leakage in all Ld systems (POPC, 9:1 POPC/Cho, 1:9 PSM/POPC, 1:8:1 PSM/POPC/Cho), as shown in *Fig. S2.10 A-D*. On the other hand, in LUVs with two-phase coexisting bilayers (de Almeida *et al.*, 2003), such as the Ld/Lo phases in 7:3 POPC/Cho and the Ld/So phases in 3:7 PSM/POPC, calcein leakage increases over time (*Fig. S2.10 E, F, and G*). This result further suggests that the behavior of Rh2 differs between Lo and Ld. This will be highlighted in the next chapter.

In confocal fluorescence microscopy experiments, Rh2 induced vesicular deformation on homogenous bilayers of POPC, POPC/Cho, and POPC/PSM/Cho. Interestingly, Rh2 stimulates membrane curvature even in unitary POPC bilayers. This agrees with the result of transmission electron microscopy for POPC LUVs treated with 30µM Rh2 (*Fig. S2.11*). Time-course morphological changes in the vesicles were not observed akin to confocal microscopy; yet, it is noteworthy that Rh2 was able to induce changes in the physical state of the LUVs after incubation. Moreover, the investigation of calcein permeation in GUVs entailed that the morphological changes are not exclusively associated with the internalization of the dye, and these results are in line with the observations of Verstraeten *et al.* (*Figures S2.12 and S2.13*). Rh2 can stimulate the disruption and possible pore-formation on the bilayer with and without instigating drastic morphological changes on the membrane.

The fluidity of the model membrane allows it to undergo elastic deformations (e.g., bending and stretching) depending on the interplay between spontaneous curvature, bending rigidity, and mechanical tension applied to the vesicle. In *Fig. 2.5*, membrane curvature was observed, transitioning from a sphere to a biconcave discocyte. Acccording to Lipowsky, membrane boundaries appear to be 'smooth' at the micron scale under the optical microscope; however, this smoothness does not persist at the molecular level especially when bioactive molecules or proteins are unevenly distributed between leaflets of the membrane (Lipowksy, 2014). Molecules or proteins from the external aqueous solution that binds to the outer leaflet create transbilayer asymmetry between leaflets, and augments the unevenness of the membrane at the molecular scale. This can result to the spontaneous curvature of the membrane (Różycki and Lipowsky, 2015) as observed in *Fig. 2.5* for GUVs incubated with Rh2. In this case, outer leaflet-bound Rh2 molecules are likely to induce transbilayer asymmetry as the polar moieties in the saponin can restrict its flip-flop rate towards the inner leaflet. A similar limitation of the flip-flop transition is observed in steroidal hormones with several polar functional groups (Atkovska *et al.*, 2018). In addition, hydrophobic mismatch leading to membrane bending was entropically induced by cylindrical proteins as observed in coarse-grained simulations (Brannigan and Brown, 2006). It was also observed that the overall membrane symmetry was preserved as the GUV incubated with Rh2 undergo deformation, and this was to minimize the bending energy and lateral tension in the membrane (Berndl *et al.*, 1990). In line with the leakage assay, the release of calcein from the Ld-phase LUVs may be brought by changes in membrane fluidity as well as pore formation when Rh2 attaches to the membrane (Shimanouchi *et al.*, 2009).

The interaction and ordering effects of Rh2 in bilayers were examined at the atomistic level in the NMR experiments. The chemical shift anisotropy values for ^{31}P NMR measurements describes the local environment of the membrane headgroup. In general, the addition of 10% Rh2 in the MLVs increased the fluidity of the bilayer headgroup. This effect is mutual for binary and ternary POPC membranes with Cho or SM in the Ld phase. The bulky sugar moiety of the saponin is presumed to perturb the hydrogen bonding network between phospholipids which loosen the density of the headgroup (Dave *et al.,* 2004). This supports the results for calcein leakage assay, and microscopy, where leakage and permeation stemmed from the labile and disordered headgroup. Further increase of Rh2 concentration to 30% in POPC/Cho and PSM/POPC membranes did not disrupt the lamellar structure but had distinct effects. At this point, the ability of Rh2 to disrupt the network of the phospholipid headgroup has been discerned. Therefore, increasing the concentration of the saponin to 30 mol % in the membrane is expected to further disrupt the membrane headgroup, and decrease Δδ values. The chemical shift anisotropy value of 48 ppm was previously reported for pure POPC bilayers (Cullis *et al.,* 1976). The addition of 10% Cho decreased the Δδ value of POPC membrane to 45 ppm, and further declined to 44 and 43.2 ppm with 10% and 30% Rh2, respectively (*Figure S2.4*). The addition of Cho and increasing amounts of Rh2 progressively perturbed the intermolecular forces between POPC headgroup; as a result, the area between phosphate esters, and the wobbling of the P-N vector both increased. Apart from the structural properties of the headgroup, the mono-unsaturated acyl chain of POPC has weak interactions with the rigid ring of Cho and this is further perturbed in the presence of Rh2 (Halling *et al.,* 2008) (Aittoniemi *et al.,* 2007). Furthermore, the glucose moiety of Rh2 is likely to exhibit a weak umbrella effect from the phospholipids; hence, delivering a similar effect with ChoGlc towards membrane headgroup. The addition of 10% PSM in POPC membranes also decreased Δδ value (from 48 ppm in pure POPC membrane to 46 ppm with 10% PSM); however, this decline is not as much as with 10% Cho. PSM has a comparable phosphocholine headgroup as POPC, unlike Cho which has a smaller polar headgroup that would not only induce greater gap between headgroup but also increase tilting of the P-N vector to instigate the umbrella effect. In addition, PSM has amide, hydroxyl and carbonyl groups that serve as hydrogen bond donor and acceptor towards other PSM or POPC molecules, and reduces the wobbling of the P-N vector; hence, creating a less fluid headgroup than POPC/Cho membrane (Saito *et al.,* 2018). Interestingly, Δδ value in PSM/POPC did not further decrease with 30% Rh2, and plateaued to ~45 ppm (data summary in *Fig. S2.5*). One rationalization is the thorough miscibility of PSM in POPC membrane. In the event of lipid and Rh2 mixing during vesicle preparation, strong hydrogen bonding between PSM and POPC headgroups could retain greater PSM-PSM and PSM-POPC networks, hence, less decrease in the wobbling of the P-N vector regardless of the amount of Rh2 in the system. However, these presumptions have to be further examined.

Next, 3-d_1-Cho and 10',10'-d_2-PSM were incorporated in bilayers to examine changes in the orientation and wobbling of the sterol core, and acyl chains. In this experiment, Ld bilayers composed of POPC/d_1-Cho and d_2-PSM/POPC were utilized. Rh2 had distinct effects on these binary POPC membranes. Increasing Rh2 concentrations (10 and 30 mol %) did not induce substantial wobbling effects of d_1-Cho as reported by the sustained Δν values (*Fig. S2.7A*). On the other hand, Δν values of d_2-PSM decreased continuously with Rh2 concentration (*Fig. S2.7B*). A hypothesis for the unchanged splitting widths of d_1-Cho is its minimal interactions of Rh2. Rh2 has a bifacial rough face with methyl and hydroxyl groups in its triterpenoid core, and such property may restrict its interaction with Cho. Furthermore, Cho may have preferred binding with POPC during the process of lipid mixing to sustain the umbrella effect (Huang and Feigenson, 1999). In the case of d_2-PSM/POPC, the presumption

regarding the decrease in Δν is the increase in wobbling of PSM acyl chains as Rh2 effectively increases the gap between lipids. This is in line with the results for ^{31}P ss-NMR wherein Rh2 substantially disorders the membrane headgroup.

In ternary systems, changes in bilayers composed of 1:8:1 PSM/POPC/Cho were monitored by replacing PSM or Cho with their equivalent deuterated compounds. Since Cho and PSM are miscible, an increase in Δν value with respect to d_1-Cho and d_2-PSM were observed compared to the binary systems. Hydrogen bonding of the hydroxyl group of Cho with the phosphate or amide group of PSM triggered these observations (umbrella effect) (Huang and Feigenson, 1999) (Smith *et al.,* 2020). The addition of Rh2 increased the wobbling of both probes suggesting that Rh2 may have the capacity to disrupt PSM-Cho network in the membrane, and it may have a slightly higher affinity for PSM. This entails that Rh2 decrease the acyl chain ordering in the hydrophobic interior, and somewhat interrupts PSM-PSM/Cho-PSM interplay. *Fig. S2.8* and *S2.9* illustrates the changes in the splitting widths of d_1-Cho and d_2-PSM with increasing temperature (20 to 50^{o}C). The addition of 10% Rh2 in Ld mixture of POPC/PSM/Cho slightly increased the mobility of d_1-Cho; however, increasing the temperature did not significantly affect the splitting widths. While Rh2 increased the wobbling of d_2-PSM with increasing temperature which entails the disordering of the acyl chains.

2.4. Conclusion

Rh2 is a rare type of saponin comprised of a triterpene backbone and a glucose unit. It was proposed that Rh2 was recognized by Cho or SM; however, this has not been precisely established. The approach was to use model membranes of different lipid composition to create a lipid-driven analysis with respect to the totality of the membrane, and at the atomistic scale. Different concentrations of Cho and PSM in models were utilized and compared towards the activity of Rh2. Permeability studies revealed that Rh2 may not exclusively depend on membrane Cho or PSM. This is evidenced by significant leakage activity, and membrane deformations of pure POPC vesicles incubated with Rh2. Experiments at the atomistic level reported for the membrane headgroup disordering effects of Rh2 in both Cho and PSM-containing bilayers. In the sample preparation for ss-NMR, Rh2 was incorporated in the lipid mixture prior to the formation of MLVs; therefore, the saponin is driven towards the membrane interior. At this point, the locality of Rh2 in a Ld membrane is still elusive. However, since results indicate that it perturbs interaction at the environment of the phospholipid headgroup, it has the capacity to increase junction between lipids. This is presumed to result in splayed acyl chains and reflects in the increased wobbling of labelled PSM tail with Rh2 concentration. In contrast, deuterium labelling at the rigid ring of Cho reported limited changes in its orientation with increasing Rh2 concentration. This can be rationalized by the constrained interactions of Rh2 with Cho. Rh2's core has a bifacial rough face enriched with methyl and hydroxyl groups that may restrict its binding with Cho. Furthermore, Cho may prefer mixing with POPC or PSM to uphold the umbrella effect. Comparable selectivity of Rh2 towards PSM or Cho inside the membrane, and at the atomistic level is still ambiguous, and requires further assessment. In the case of the permeability assay, Rh2 anchors from the exterior of the membrane, and this is reported to not be lipid specific. In the time-course leakage assay, Rh2 was described to have different leakage rates in liquid-ordered, and -disordered membranes. Since Rh2 was also reported to

disrupt lipid rafts in cell membranes, its interaction and activity towards different liquid phase states may be noteworthy of investigative research.

2.5. References

-Ahmed, S. N.; Brown, D. A.; London, E. On the origin of sphingolipid/cholesterol-rich detergent-insoluble cell membranes: physiological concentrations of cholesterol and sphingolipid induce formation of a detergent-insoluble, liquid-ordered lipid phase in model membranes. *Biochemistry*. **1997**. *36,* 10944–10953.

-Aittoniemi, J.; Niemelä, P. S.; Hyvönen, M. T.; Karttunen, M.; Vattulainen, I. Insight into the Putative Specific Interactions between Cholesterol, Sphingomyelin, and Palmitoyl-Oleoyl Phosphatidylcholine. *Biophys. J.* **2007.** *92,* 1125-1137.

-Atkovska, K.; Klingler, J.; Oberwinkler, J.; Keller, S.; Hub, J. S. Rationalizing Steroid Interactions with Lipid Membranes: Conformations, Partitioning, and Kinetics. *ACS Cent. Sci*. **2018**, *4*, 1155−1165.

-Bailly, C.; Vergoten, G. Glycyrrhizin: An alternative drug for the treatment of COVID-19 infection and the associated respiratory syndrome? *Pharmacology & Therapeutics*. **2020.** *214*, 107618.

-Barnes, P. J. Corticosteroid effects on cell signalling. *Eur. Respir. J.* **2006.** *27,* 413-426.

-Berndl, K.; Käs, J.; Lipowsky, R.; Sackmann, E.; Seifert, U. Shape transformations of giant vesicles: extreme sensitivity to bilayer asymmetry. *Europhys Lett.* **1990**, *13*, 659–64.

-Brannigan, G.; Brown, F. L. H. A Consistent Model for Thermal Fluctuations and Protein-Induced Deformations in Lipid Bilayers. *Biophys J.* **2006**. *90,* 1501-1520.

-Chen, X. J.; Zhang, X. J.; Shui, Y. M.; Wan, J. B.; Gao, J. L. Anticancer Activities of Protopanaxadiol- and Protopanaxatriol-Type Ginsenosides and Their Metabolites. *eCAM.* **2016.** *2016*, 1-19.

-Cullis, P. R., and B. de Kruijff. 1979. Lipid polymorphism and the functional roles of lipids in biological membranes. *Biochim. Biophys. Acta.* **1979.** *559*, 399–420.

-Cullis, P. R.; De Kruyff, B.; Richards, R. E. Factors affecting the motion of the polar headgroup in phospholipid bilayers. A ^{31}P NMR study of unsonicated phosphatidylcholine liposomes. *Biochim. Biophys. Acta*. **1976.** *426*, 433-446.

-Dave, P. C.; Tiburu, E. K.; Krishnan D.; Lorigan, G. A. Investigating Structural Changes in the Lipid Bilayer upon Insertion of the Transmembrane Domain of the Membrane-Bound Protein Phospholamban Utilizing ^{31}P and ^{2}H Solid-State NMR Spectroscopy. *Biophys J*. **2004**. *86,* 1564–1573.

-de Almeida, R. F. M.; Federov, A.; Prieto, M. Sphingomyelin/phosphatidylcholine/cholesterol phase diagram: Boundaries and composition of lipid rafts. *Biophys J.* **2003.** *85*, 2406-2416.

-Frenkel, N.; Makky, A.; Sudji, I. R.; Wink, M.; Tanaka, M. Mechanistic Investigation of Interactions between Steroidal Saponin Digitonin and Cell Membrane Models. *J. Phys. Chem. B.* **2014**. *118*, 14632−14639.

-Gauthier, C.; Legault, J.; Girard-Lalancette, K.; Mshvildadze, V.; Pichette, A. Haemolytic activity, cytotoxicity, and membrane cell permeabilization of semi-synthetic and natural lupane- and oleanane-typesaponins. *Bioorg. Med. Chem.* **2009.** *17*, 2002–2008

-Gilabert-Oriol, R.; Mergel, K.; Thakur, M.; von Mallinckrodt, B.; Melzig, M. F.; Fuchs, H.; Weng, A. Real-time analysis of membrane permeabilizing effects of oleanane saponins. *Bioorg. Med. Chem*. **2013.** *21*,2387–2395.

-Halling, K. K.; Ramstedt, B.; Nyström, J. H.; Slotte, J. P.; Nyholm, T. K. M. Cholesterol Interactions with Fluid-Phase Phospholipids: Effect on the Lateral Organization of the Bilayer. *Biophys. J.* **2008**. *95,* 3861-3871

-Hanashima, S.; Fukuda, N.; Malabed, R.; Murata, M.; Kinoshita, M.; Greimel, P.; Hirabayashi, Y. β-Glucosylation of cholesterol reduces sterol-sphingomyelin interactions. *BBA – Biomembranes.* **2021**. *1863*, 18349

-Huang, J.; Feigenson, G. W. A microscopic interaction model of maximum solubility of cholesterol in lipid bilayers. *Biophys. J.* **1999.** *76*, 2142–2157.

-Karra, A. G.; Konstantinou, M.; Tzortziou, M.; Tsialtas, I.; Kalousi, F. D.; Garagounis, C.; Hayes, J. M.; Psarra, A. M. G. Potential Dissociative Glucocorticoid Receptor Activity for Protopanaxadiol and Protopanaxatriol. *Int. J. Mol. Sci.* **2019**. *20*, 94, 1-19.

-Kimura, T.; Cheng, K.; Rice, K. C.; Gawrisch, K. Location, Structure, and Dynamics of the Synthetic Cannabinoid Ligand CP-55,940 in Lipid Bilayers. *Biophys. J*. **2009**. *96*, 4916-4924.

-Lee, Y. N.; Lee, H. Y.; Lee, Y. M.; Chung, H. Y.; Kim, S. I.; Lee, S. K.; Park, B. C.; Kim, K. W.Involvement of glucocorticoid receptor in the induction of differentiation by ginsenosides in F9 teratocarcinoma cells. *J. Steroid Biochem. Molec. Biol.* **1998**. *67*, 2, 105-111.

-Lipowsky, R. Coupling of bending and stretching deformations in vesicle membranes. *Adv. Colloid Interface Sci*. **2014.** *208*, 14-24.

-Lorent, J.; Le Duff, C. S.; Quetin-Leclercq, J.; Mingeot-Leclercq, M. P. Induction of highly curved structures in relation to membrane permeabilization and budding by the triterpenoid saponins, α- and δ-hederin. *J. Biol. Chem.* **2013**. *288, 20*, 14000-14017.

-Malabed, R.; Hanashima, S.; Murata, M.; Sakurai, K. Interactions of OSW-1 with lipid bilayers in comparison with digitonin and soyasaponin. *Langmuir*. **2020.** *36*, 3600-3610.

-Malabed, R.; Hanashima, S.; Murata, M.; Sakurai, K. Sterol-recognition ability and membrane- disrupting activity of *Ornithogalum* saponin OSW-1 and usual 3-*O*-glycosyl saponins. *Biochim. Biophys.Acta.* **2017**, *1859*, 2516-2525.

-Matsumori, M., Yasuda, T., Okazaki, H., Suzuki, T., Yamaguchi, T., Tsuchikawa, H., Doi, M., Oishi, T. and Murata, M. Comprehensive molecular motion capture for sphingomyelin by site-specific deuterium labeling. *Biochemistry* **2012.** *51*, 8363-8370.

-Matsumori, N.; Tanada, N.; Murata, M. Design and synthesis of sphingomyelin-cholesterol conjugates and their formation of ordered membranes. *Chem. Eur. J*. **2011**. *17*, 8568–8575.

-Ondevilla, J. C.; Hanashima, S.; Mukogawa, A.; Umegawa, Y.; Murata, M. Diosgenin-induced physicochemical effects on phospholipid bilayers in comparison with cholesterol. Bioorg. Med. Chem. Lett. **2021**. *36*, 127816.

-Payandeh, J.; Volgraf, M. Ligand binding at the protein-lipid interface: strategic considerations for drug design. *Nat. Rev. Drug Discov*. **2021**. https://doi.org/10.1038/s41573-021-00240-2.

-Róg, T.; Pasenkiewicz-Gierula, M. Cholesterol-sphingomyelin interactions: a molecular dynamics simulation study. *Biophys. J.* **2006**. *91*, 3756–3767.

-Różycki, B.; Lipowsky, R. Spontaneous curvature of bilayer membranes from molecular simulations: Asymmetric lipid densities and asymmetric adsorption. *J. Chem. Phys.* **2015**. *142*, 054101.

-Saito, H.; Morishita, T.; Mizukami, T.; Nishiyama, K.; Kawaguchi, K.; Nagao, H. Molecular dynamics study of binary POPC bilayers: molecular condensing effects on membrane structure and dynamics. *J. Phys.: Conf. Ser.* **2018.** *1136*, 012022.

-Shimanouchi, T.; Ishii, H.; Yoshimoto, N.; Umakoshi, H.; Kubo, R. Calcein permeation across phosphatidylcholine bilayer membrane: Effects of membrane fluidity, liposome size, and immobilization. *Colloids and Surfaces B: Biointerfaces.* **2009**. *73,* 156–160.

-Smith, P.; Quinn, P. J.; Lorenz, C. D. Two Coexisting Membrane Structures Are Defined by Lateral and Transbilayer Interactions between Sphingomyelin and Cholesterol. *Langmuir*. **2020**. 36, 9786-9799

-Sodt, A. J.; Pastor, R. W.; Lyman, E. Hexagonal substructure and hydrogen bonding in liquid-ordered phases containing palmitoyl sphingomyelin. *Biophys. J.* **2015.** *109*, 948–955.

-Sovadinova, I.; Palermo, E. F.; Huang, R.; Thoma, L. M.; Kuroda, K. Mechanism of Polymer-Induced Hemolysis: Nanosized Pore Formation and Osmotic Lysis. *Biomacromolecules.* **2011**. *12,* 260–268.

-Tasker, J. G.; Joëls, M. *The Synaptic Physiology of the Central Nervous System Response to Stress*, Neuroendocrinology of Stress, 1st ed.;John and Wiley & Sons, Ltd., **2015**, 43-70.

-Vauquelin, G.; Charlton, S. J. Long-lasting target binding and rebinding as mechanisms to prolong *in vivo* drug action. *Br. J. Pharmacol.* **2010**. *161,* 488-508.

-Vauquelin, G.; Packeu, A. Ligands, their receptors and…plasma membrane. *Mol. Cell. Endocrinol.* **2009**. *311,* 1-10.

-Verstraeten, S. L.; Deleu, M.; Janikowska-Sagan, M.; Claereboudt, E. J. S.; Lins, L.; Tyteca, D; Mingeot-Leclercq, M. P. The activity of the saponin ginsenoside Rh2 is enhanced by the interaction with membrane sphingomyelin but depressed by cholesterol. *Sci. Rep.* **2019**. *9*, 1-14.

2.6. Supporting Materials

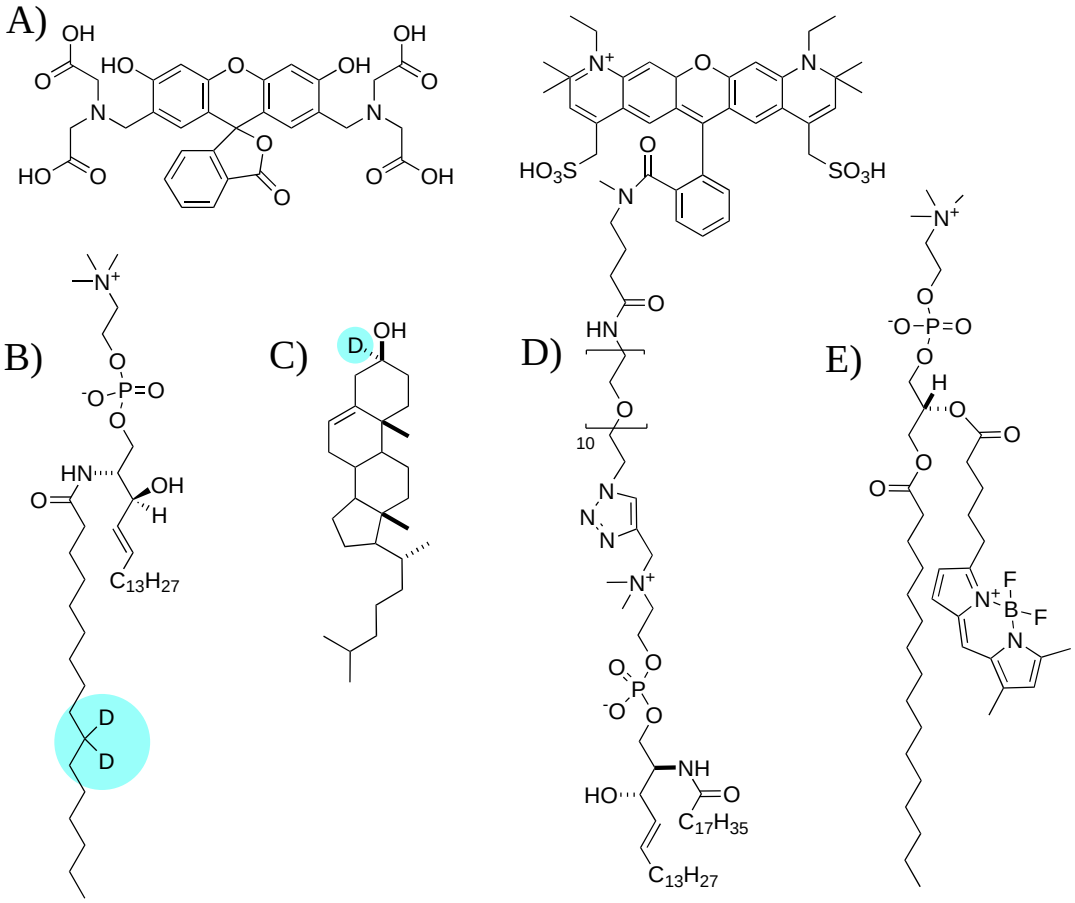

Figure S2.1. Structure of fluorescent dyes, and deuterated lipid probes used in this study. For leakage assay: ***A)*** 2,7-bis[bis(carboxymethyl)aminomethyl] fluorescein (**calcein**); For solid-state NMR: ***B)*** 10', 10'-d_2-PSM and ***C)*** 3-d_1-Cho; For confocal fluorescence microscopy*:* ***D)*** 594-neg-N-stearoylsphingomyelin (**594-neg-SSM**) and ***E)*** β-BODIPY FL C5-HPC.

Table S1. EC_{50} in hemolytic activity of Rh2 and other saponins

	Rh2	*α-hederin*	*glycyrrhizin*
EC_{50} (μM)	25.0	6.0	> 100

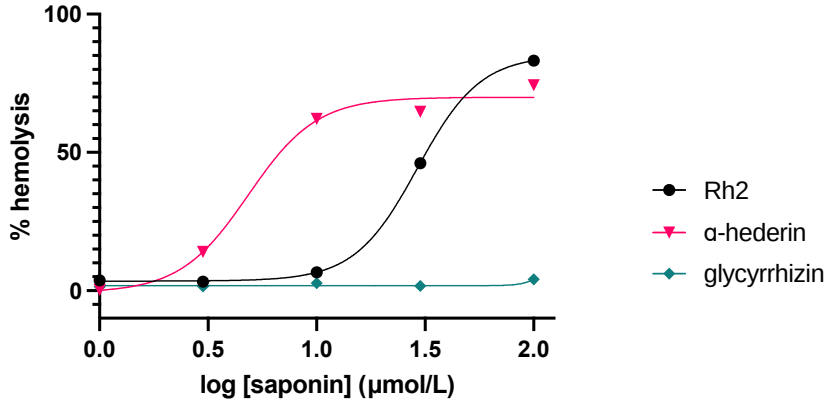

Figure S2.2. Log concentration vs response (% hemolysis) curve for Rh2 and other saponins measured at 37°C.

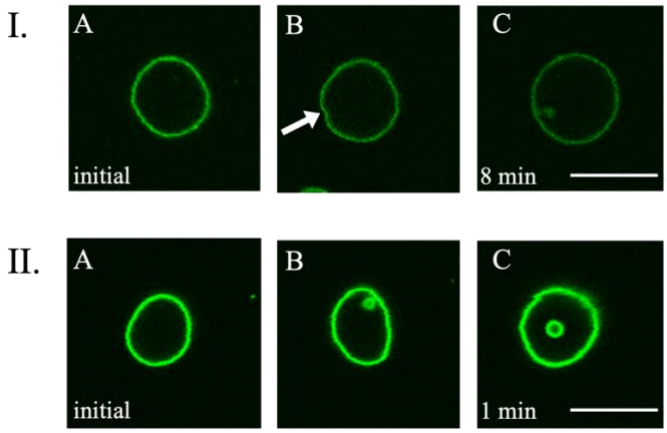

Figure S2.3. Micrographs of GUVs that underwent fluctuation and internalization after incubating with Rh2 (30μM) I. Binary GUV composed of POPC/Cho 9:1; II. Ternary GUV composed of PSM/POPC/Cho 8:1:1. GUVs labelled with 1 mol% β-BODIPY C_5-HPC. White arrow in panel I-B depicts internalization. A Images are captured at 23ºC. (scale bar 10μm)

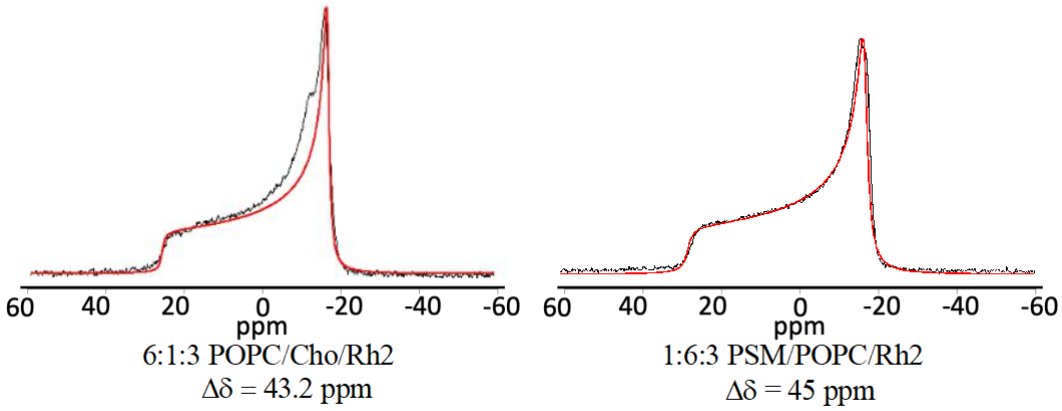

Figure S2.4. ^{31}P NMR spectra and Δδ values of various POPC MLVs with 30 mol % Rh2. Left spectra: with 10 mol % Cho; Right spectra panel: with 10 mol % PSM. Black spectra correspond to the experimental data, while red spectra correspond to the simulated data. NMR spectra were referenced from 85% H_3PO_4 peak set at 0 ppm, and were measured at 30°C.

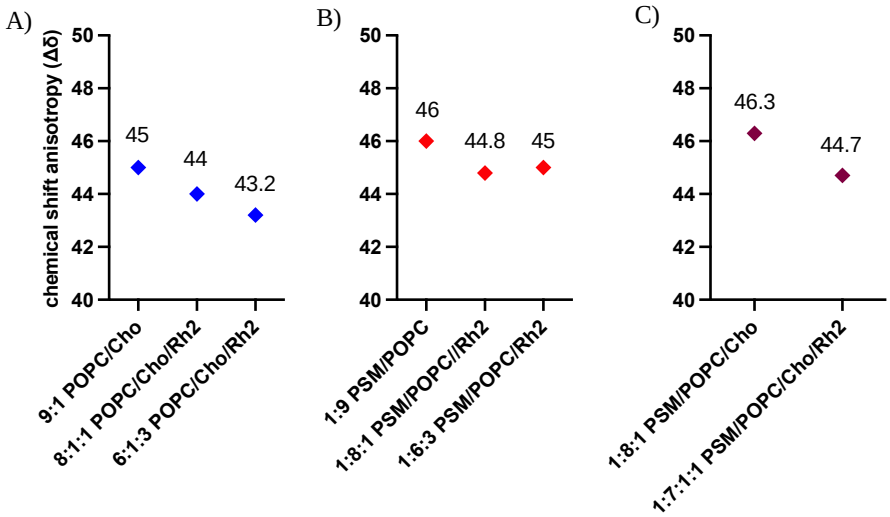

Figure S2.5. Summary of Δδ values of ^{31}P ss-NMR for liposomes with 10 % Cho, 10% PSM and equimolar ratios of both lipid, with and without Rh2.

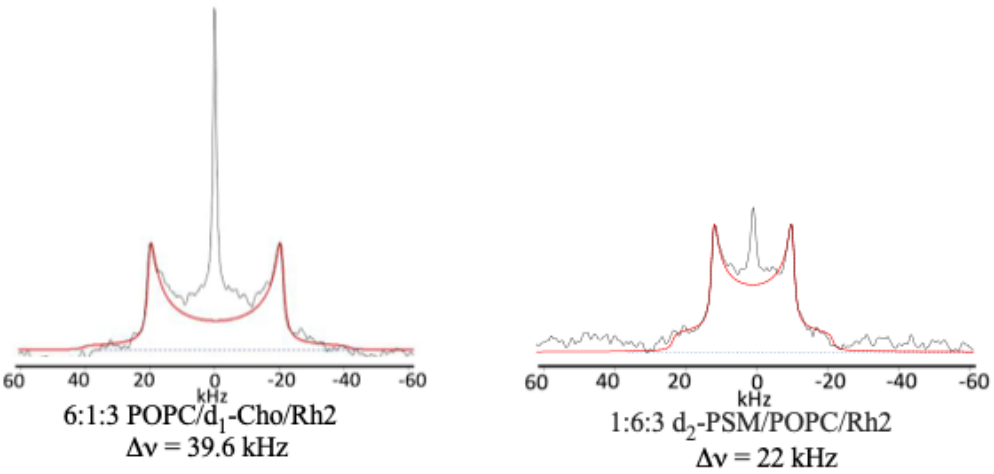

Figure S2.6. ^{2}H NMR spectra and Δν values of POPC MLVs with 30 mol % Rh2 measured at 30°C. Left spectra: with 10 mol % d_1-Cho; Right spectra panel: with 10 mol % d_2-PSM. Black spectra correspond to the experimental data, while red spectra correspond to the simulated data.

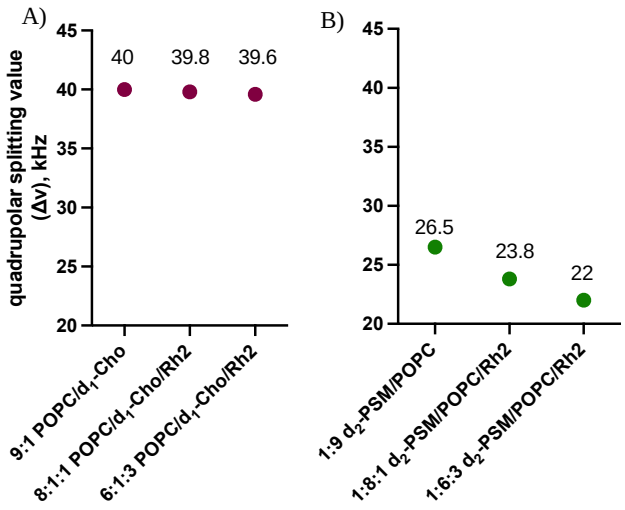

Figure S2.7. Summary of Δν values of liposomes with 10% d_1-Cho, 10% d_2-PSM, with and without Rh2.

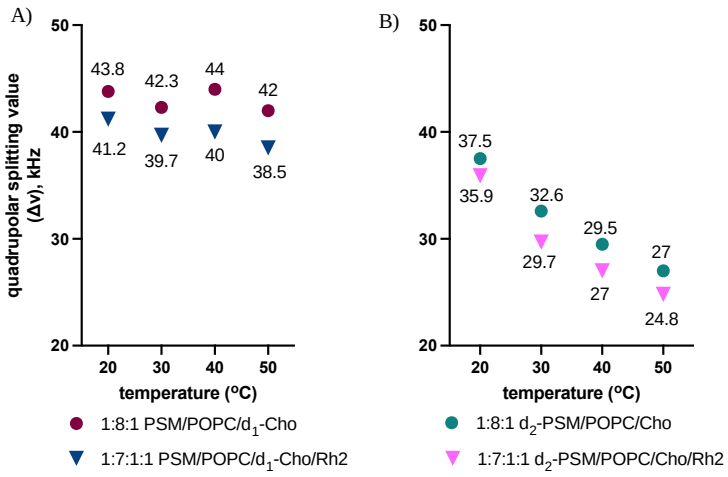

Figure S2.8. Summary of quadrupolar splitting values (Δν) for ^{2}H NMR data. a) 3-d_1-Cho, b) 10',10'-d_2-PSM with increasing temperature (20-50ºC).

1:8:1 PSM/POPC/d_1-Cho

1:7:1:1 PSM/POPC/d_1-Cho/Rh2

20°C

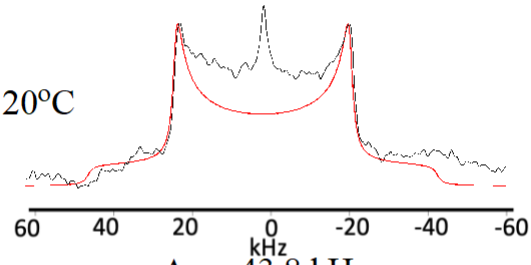

$\Delta\nu = 43.8$ kHz

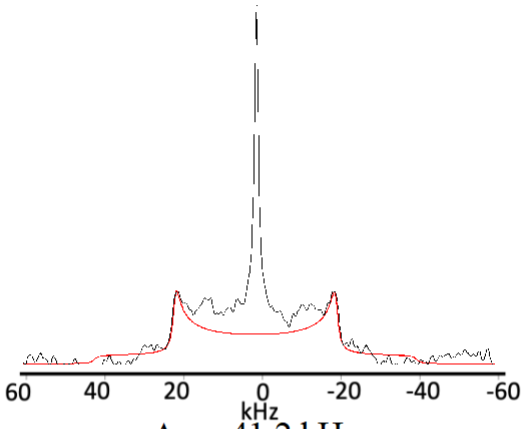

$\Delta\nu = 41.2$ kHz

30°C

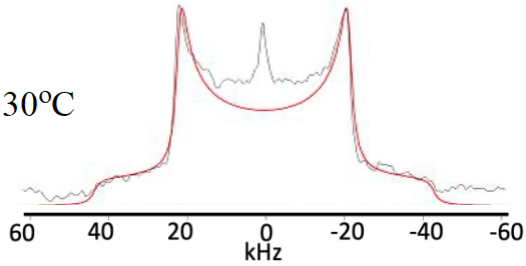

$\Delta\nu = 42.3$ kHz

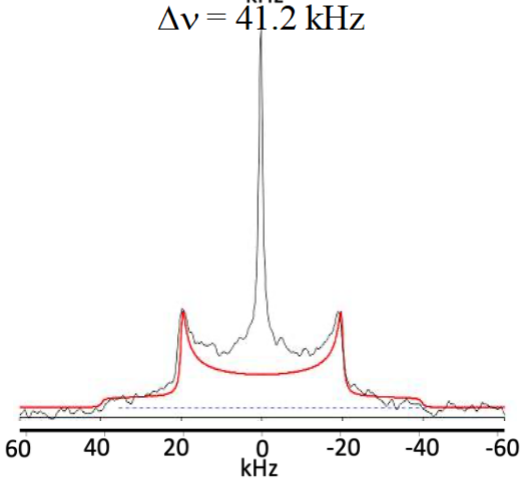

$\Delta\nu = 39.7$ kHz

40°C

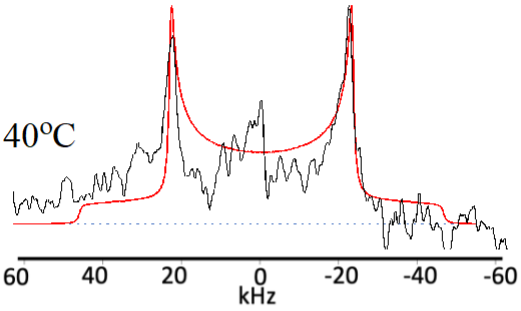

$\Delta\nu = 44$ kHz

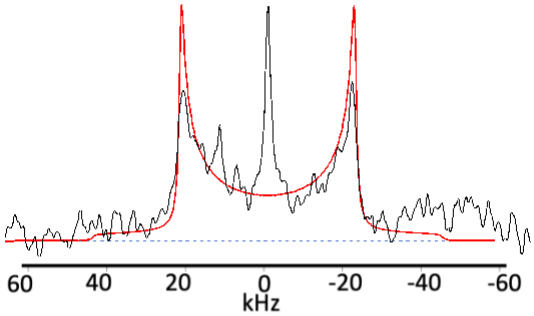

$\Delta\nu = 40$ kHz

50°C

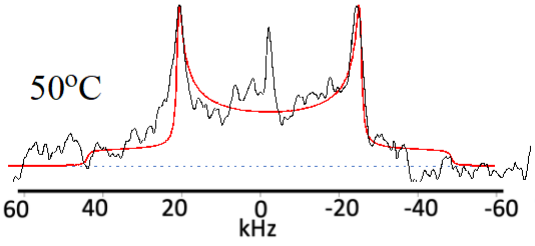

$\Delta\nu = 42$ kHz

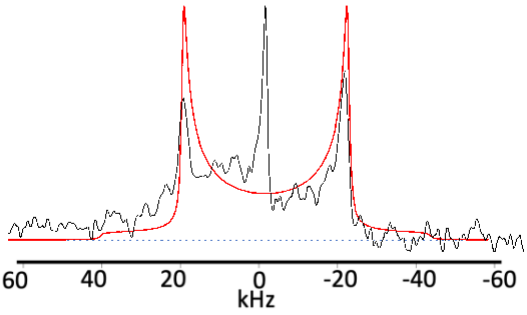

$\Delta\nu = 38.5$ kHz

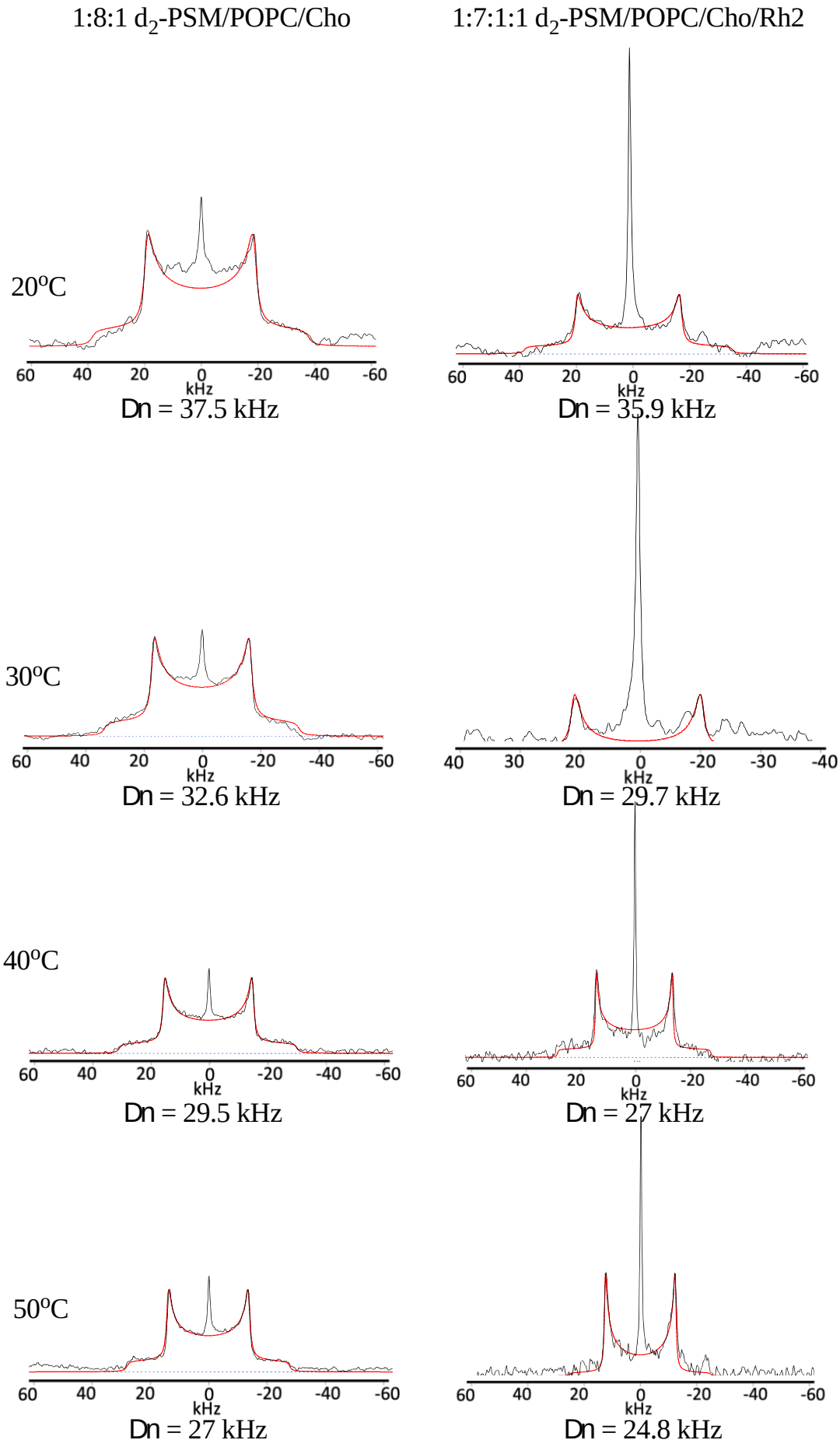

Figure S2.9. ^{2}H NMR spectra using d_1-Cho and d_2-PSM probes, varying temperatures

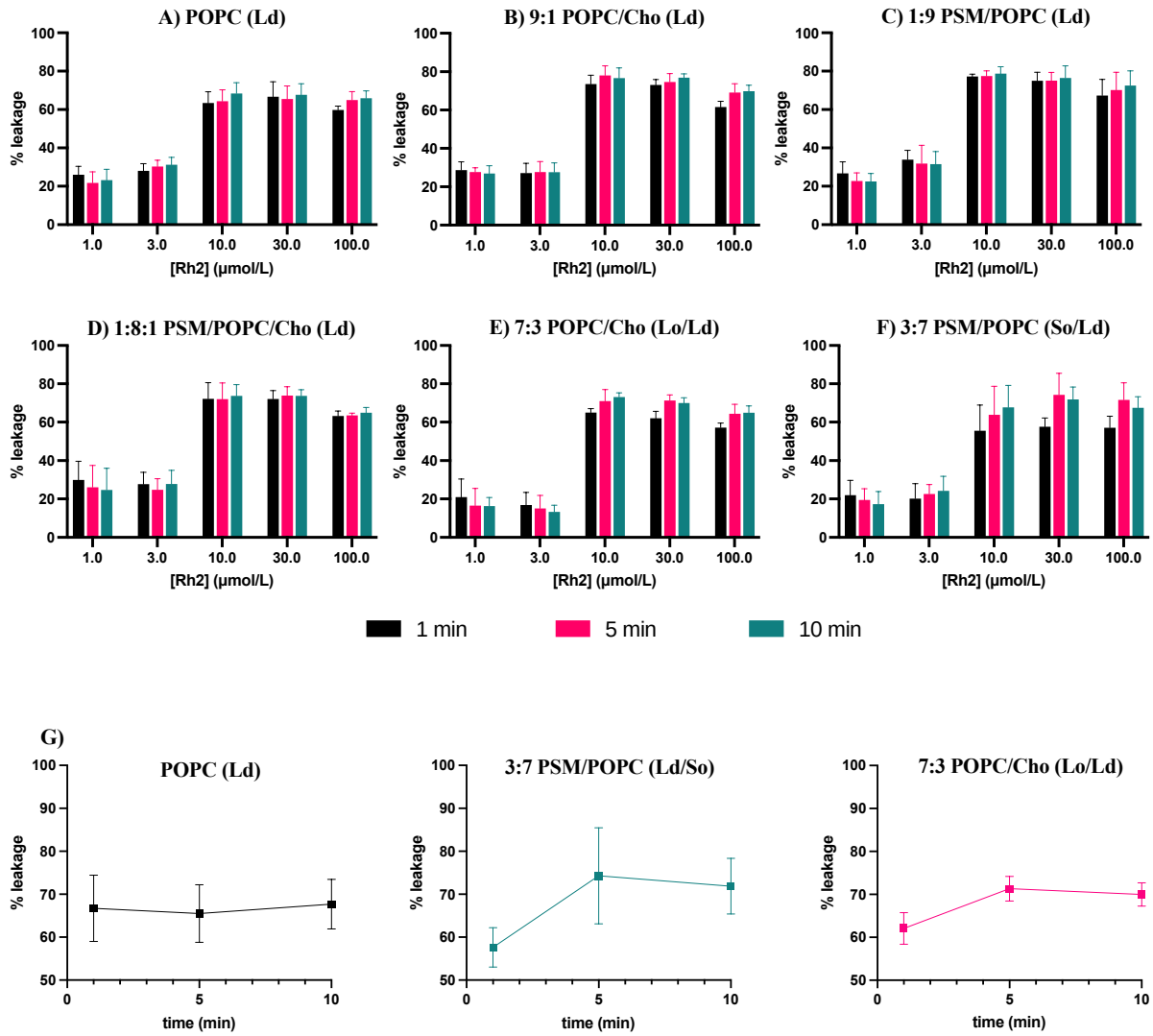

Figure S2.10. Leakage activity of Rh2 in various PC LUVs. A) POPC; B) 9:1 POPC/Cho; C) 1:9 PSM/POPC; D) 1:8:1 PSM/POPC/Cho; E) 7:3 POPC/Cho; F) 3:7 PSM/POPC incubated for 1, 5 and 10 mins. G) Comparison of percent leakage induced by Rh2 at 30 μmol/L in PC LUVs of different phase states, Ld (POPC), Ld/Lo (7:3 POPC/Cho), and Ld/So (3:7 PSM/POPC), over time (1, 5 and 10 mins).

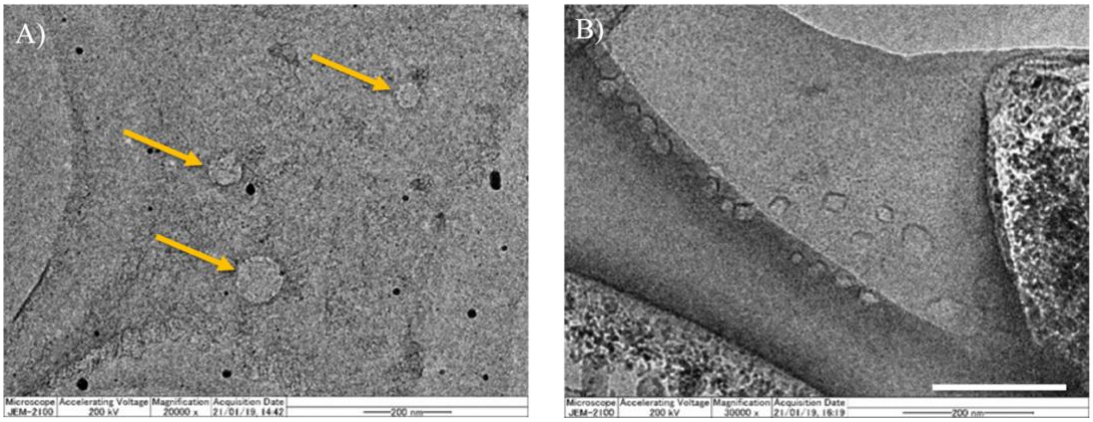

Figure S2.11. Transmission Electron Microscopy. A) untreated POPC LUVs (depicted by yellow arrow); Average LUV diameter is ~120nm. B) LUVs treated with Rh2, and shows smaller particles of various shapes, and sizes having an average diameter less than the LUVs from *panel A*. In addition, LUV structures of about 100 nm were not observed. Scale bars = 200 nm.

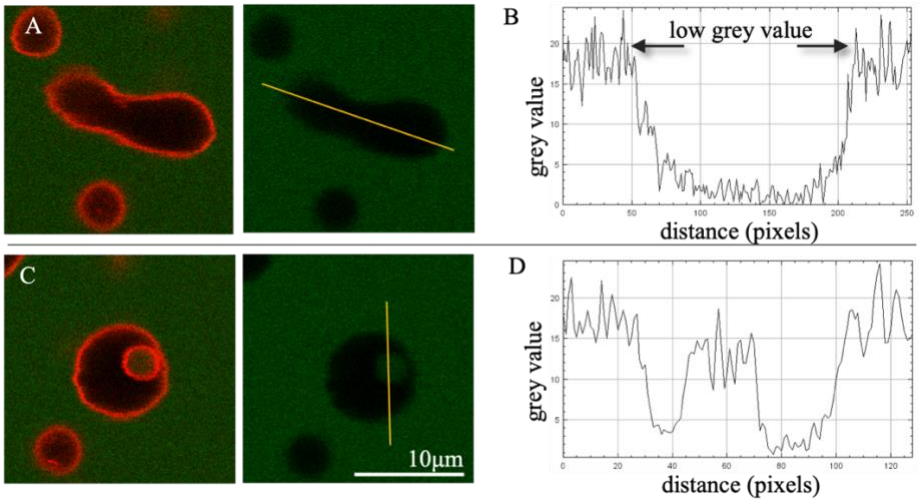

Figure S2.12. (A, C) POPC GUV labelled with TR-DPPE undergoing vesicular internalization (stomatocyte); (B, D) fluorescence intensity profile of calcein along the yellow line.

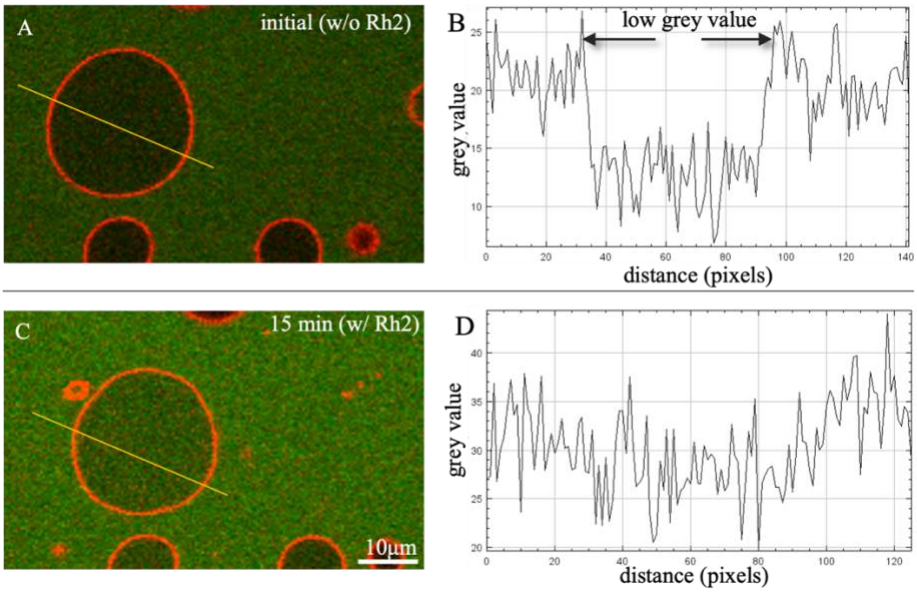

Figure S2.13. (A, C) Calcein permeation in POPC GUVs; (B, D) fluorescence intensity

~ Chapter 3 ~

The behavior of Rh2 in liquid-ordered and -disordered model membranes comprised of sphingomyelin, phosphatidylcholine, and cholesterol

3.1. Introduction

The complexity of eukaryotic membranes amassed from the multifaceted spatial organization and behavior of its constituents. Lipids that span along the membrane have an array of molecular and physicochemical properties that allows the formation of different phase states, which contribute to several membrane functions. The wide variety of lipid structures influence the formation of liquid phases, such as liquid-ordered (Lo), liquid-disordered (Ld), and the coexistence of the two (Lo/Ld). Besides the charge and polarity of the headgroup, saturated hydrocarbon chains of sphingolipids (e.g., sphingomyelin) promote the tightly packed, solid (So) and Lo phases. On the other hand, unsaturated hydrocarbon chains of phospholipids tend to enrich the more fluid Ld phase. Cholesterol (Cho) predominates the nonpolar lipids of the cell membrane. The functionalities of Cho are crucial as it can fluidize an ordered phase and rigidify a liquid phase (van Meer *et al.,* 2008). Together with sphingomyelin, Cho is reported to form lipid rafts, which are described as ordered domains serving as platforms for signaling pathways and other cellular functions (Kaiser *et al.,* 2009) (Sevcsik and Schütz, 2016). Furthermore, Cho creates compositional phase separation – which are coexisting fragments of sterol-rich Lo phase and sterol-poor Ld phase (Sevcsik and Schütz, 2016). Due to the sharp disparities in the physical properties of a phase-separated system, they partake in different cellular functions such as protein localization (van Meer *et al.,* 2008) (Sych *et al.,* 2021).

Different cellular organelles possess distinct lipid compositions that are essential to their behavior and function. As an example, because of the different lipids present in the plasma membrane (PM) and the endoplasmic reticulum (ER), their membrane properties differ as well. The PM is understood to be built for stability as it is the main barrier of the cell. It is mainly enriched in sphingolipids and sterols, especially in the outer leaflet, to increase packing and resist mechanical stress. In addition, a variety of liquid phases exist in the PM. On the other hand, ER is presumed to have a homogeneous Ld membrane at physiological temperatures. The ER functions as one of the main Cho-producing organelles, and its fluid membrane aids in the penetration and transport of newly synthesized molecules. Also, the mitochondria have generally low Cho content as they function in conjunction with the ER (van Meer *et al.,* 2008) (Jackson *et al.,* 2016).

In many cases, Lo and Lo/Ld domains in the membrane are recognized for the mechanistic actions of bioactive molecules and proteins. Saponins are no exception to this. Some saponins have been established for their Cho dependence. From the previous chapter, Rh2 was reported to have marginal selectivity towards Cho or PSM. Results for the calcein leakage assay revealed that the activity of Rh2 does not highly depend on the membrane Cho or SM (*Fig. 2.4*), unlike other saponins, such as α-hederin and digitonin (Malabed *et al.,* 2017) (Lorent *et al.,* 2013). However, the time-course leakage assay showed different leakage rates of Rh2 with different membrane phase states. The Lo/Ld coexisting systems presented an increasing trend in terms of leakage over time, while a constant rate was observed in the Ld system. This implies that Rh2 may quickly instigate its effects in a more fluid

system and that different phase states may affect the activity of Rh2 to a greater degree rather than individual lipid components.

This chapter assessed the different behavior of Rh2 in ternary systems of different phase states. Ternary bilayers were expected to reproduce lipid rafts and surrounding areas occurring in biological membranes better than Cho-containing binary systems. Different ratios of PSM, POPC, and Cho were adopted to generate liposomes with homogenous Lo and Ld phases and the Lo/Ld-coexisting states where the activity of Rh2 will be (illustrated below).

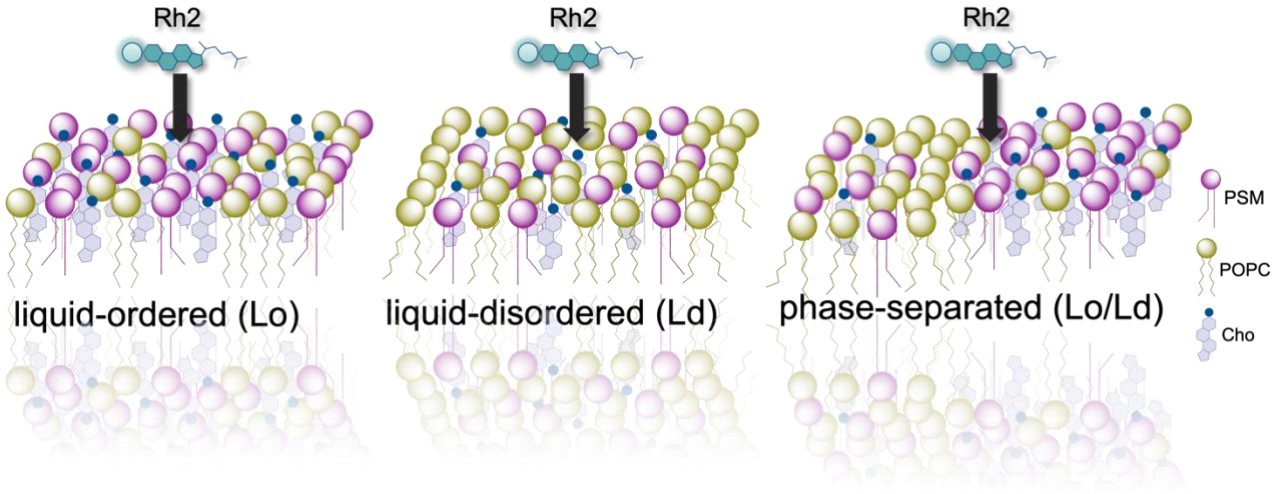

Figure 3.1. A representation of homogenous liquid-Ordered (Lo), liquid-disordered (Ld), and Lo/Ld PSM/POPC/Cho membranes utilized in the investigation of the membrane effects of Rh2.

Conferring to the phase diagram of the ternary system reported by de Almeida *et al.* in *Fig. 3.2,* the equimolar ratios of PSM/POPC/Cho reproduce the Lo/Ld coexisting bilayers, for which we examined the effect of Rh2 on the phase boundaries. The molar ratio of Lo/Ld lipids in this system is about 8:2 (de Almeida *et al.*, 2003) (Silva *et al.*, 2007), indicating that the Lo phase is dominant in this equimolar system. Along the extremes of the tie line for the ternary system, PSM/POPC/Cho 35:25:40 and 17:75:8 compositions were chosen for the homogenous Lo and Ld phases, respectively. The effects of Rh2 to these homogenous and phase-separated membranes will be investigated using various biophysical techniques and molecular dynamics simulation.

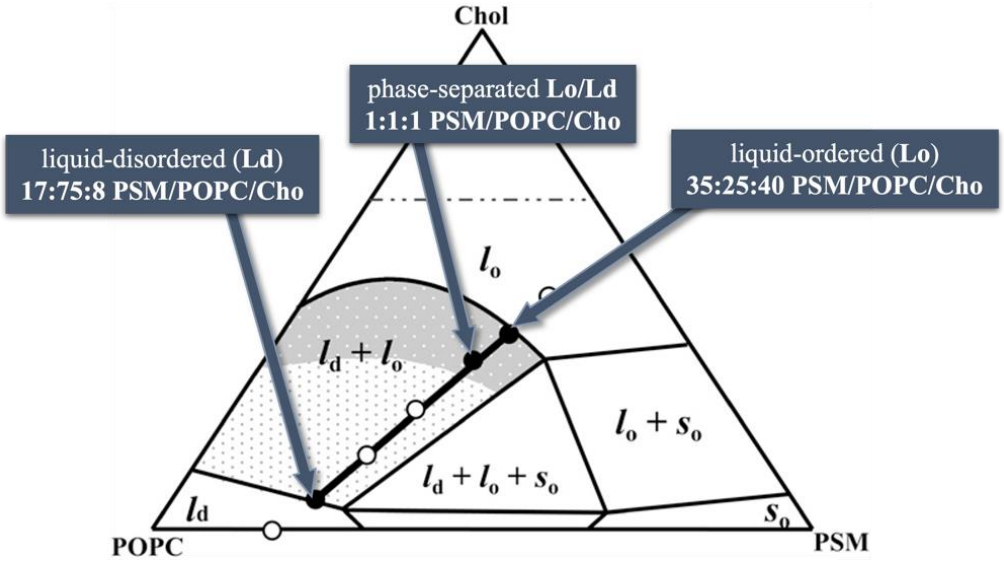

Figure 3.2. Ternary phase diagram of PSM/POPC/Cho. The black bold line corresponds to the tie line of 1:1:1 PSM/POPC/ Cho mixture. Light gray area: small raft domains (<20 to ~75 nm); dark gray area: large raft domains (>100 nm) (Silva *et al.*, 2007) (image modified to give emphasis on the lipid systems used in this study)

3.2. Results

3.2.1. DPH Anisotropy of Ternary Bilayers in the Presence of Rh2

The mobility and dynamic properties of the interior of the model and cellular bilayers can be determined through diphenylhexatriene (DPH) fluorescence anisotropy measurements. In this study, DPH (*Fig. S3.1A*) was pre-mixed into the lipid film (PSM/POPC/Cho 35:25:40, 17:75:8, 1:1:1) followed by the formation of LUVs. The LUV suspension labeled with 0.5% DPH was incubated with Rh2 of increasing concentrations. The steady-tate anisotropy, the *r* value calculated from the fluorescence measurements, describes the microviscosity of the membrane core (Poojari *et al.*, 2019). DPH was reported to have an average distance from the bilayer center (z_{cf}) of 6.7 Å, relatively deep into the membrane (Kaiser and London, 1998). A high anisotropy value represents the high chain ordering of the bilayer interior.

The result of the anisotropy measurements (*Fig. 3.3*) revealed that the phase-separated (Lo/Ld, 1:1:1 PSM/POPC/Cho) and Lo (35:25:40 PSM/POPC/Cho) systems did not show a substantial increase in the *r* value with increasing Rh2 concentration. As expected, the chain ordering in the Lo and Lo-dominant Lo/Ld systems is markedly high. Thus, the Cho-like ordering effect of membrane-bound sapogenin is not clearly reflected in the *r* values. On the other hand, the *r* values for Ld system significantly increased with Rh2 concentration. A straightforward interpretation of this upsurge in anisotropy is due to the ordering effects of Rh2 in the membrane core. However, the conjecture is that Rh2 binds and accumulates on the membrane surface in a parallel orientation to the surface. Consequently, water molecules are restricted from penetrating the interior of the membrane and enhance the ordering of the acyl chains. This hypothesis will be elaborated on the *Discussion.*

The specific interaction of Rh2 with eggSM has been reported by Verstraeten *et al*. However, results for the calcein leakage experiment from the previous chapter (*Fig. 2.3B* and *Fig. 2.4*) revealed that the effect of PSM, the major constituent of eggSM, is marginal. To further investigate this aspect, anisotropy measurements were carried out in POPC bilayers containing either PSM or DPPC. DPPC is a glycerophospholipid that has acyl chains similar

to PSM and forms the Lo phase as well. Similarly, this experiment determined the mobility of the hydrophobic interior of Lo, Ld and Lo/Ld bilayers in the presence of Rh2. *Fig. S3.2* shows negligible differences in the *r* value between the PSM and DPPC-containing bilayers upon increasing the Rh2 concentration.

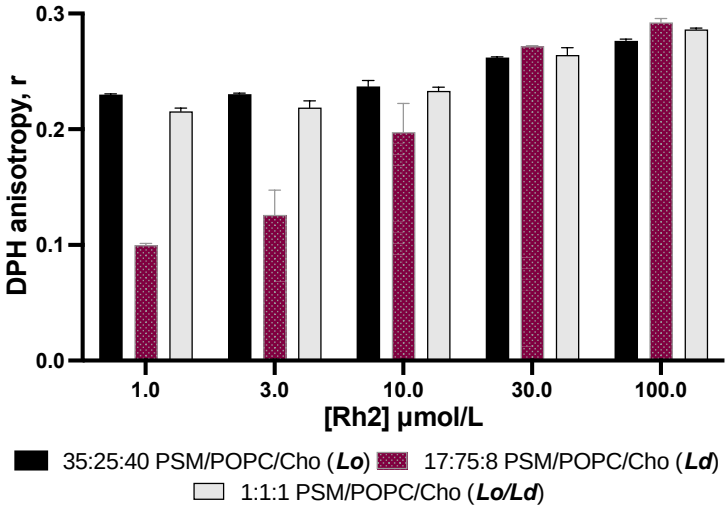

Figure 3.3. A) DPH anisotropy measurements of Rh2 in phase-separated, Lo and Ld systems composed of PSM/POPC/Cho at 30°C with Rh2 (1-100 µM).

3.2.2. Generalized Polarization of Laurdan and Prodan in the Presence of Rh2

Laurdan and prodan are fluorescent probes sensitive to polarity changes in their environment (*Fig. S3.1B and C*). The lauric acid tail of laurdan allows setting in hydrophobic areas of the bilayer compared to prodan. Thus, the emission spectrum of laurdan reflects the hydration extent and chain packing of the shallow/middle portions of the bilayer interior. On the other hand, the shorter chain of prodan prevents its insertion into the bilayer; hence, it anchors shallowly to the membrane and is exposed to a more polar environment. Overall, laurdan and prodan report changes in the fluidity of the membrane interior and headgroup, respectively (Parasassi *et al*., 1998) (Krasnowka *et al.*, 1998). In a phospholipid bilayer, the prominent emission maxima of the probes depend on the overall phase state. The emission maxima (λ_{em}) of the fluorescent compounds vary depending on the hydration and phase-state of the system. A shorter wavelength is observed for a rigid, less hydrated system (~440 nm) and a longer wavelength for a fluid, well-hydrated environment (~490 nm). Spectral shifting (e.g., blue and red shifts) monitors phospholipid phase transitions or changes in hydration levels of the probe. For example, decreasing the temperature of a phospholipid bilayer would lead to a phase transition from the liquid crystalline to gel phase, which would be reflected in changes to λ_{em} of the fluorescent probe from a long to a shorter wavelength, that is, a blue shift. An opposite scenario applies during a red shift (Parasassi *et al.*,1998). Generalized polarization (GP or GP_{340}) is a parameter that provides a quantitative index of the changes in membrane hydration and fluidity by utilizing the peak emission wavelengths from the two phases at 440 and 490 nm (Jay and Hamilton, 2017) (Chenioura *et al*., 2016). A high GP_{340} value signifies a denser, less hydrated environment; while low GP_{340} values signify a more fluid, more hydrated environment.

Laurdan and prodan GP_{340} values were also assessed in the three liposome systems (PSM/POPC/Cho 35:25:40, 17:75:8, 1:1:1). Preparation of LUVs is similar to DPH anisotropy where the fluorescent probes are pre-mixed in the

lipid film. Results in *Fig. 3.4A* show that with an increasing Rh2, laurdan GP_{340} also increased, suggesting diminished hydration of the membrane interior with Rh2. This is more evident in the fluid Ld system compared to the phase-separated (Lo/Ld) and Lo systems, which is similar to the result of DPH anisotropy. In the emission spectra in *Fig. S3.5A, C, E*, it is observed that the maximum (λ_{em}) of laurdan is approximately 440 nm for both phase-separated and Lo systems without Rh2 and with an increasing Rh2 concentration. This indicates that the pre- and post-Rh2-incubation states of these liposomes are dominantly ordered and less hydrated. While in the Ld system, the initial λ_{em} is at 490 nm shifted to 440 nm, with the Rh2 concentration illustrating a more apparent blue shift, as well as changes in the mobility and the number of water molecules surrounding laurdan. This implies that Rh2 induces a more substantial change in the hydration of the surface and/or shallow interior of the Ld bilayers than those of the Lo counterpart. Results in *Fig. 3.4B* show prodan GP_{340} in the same ternary bilayers with increasing Rh2 concentrations. In all systems, it is evident that GP_{340} values increased with the Rh2 concentration, showing a similar trend regardless of the phase state, i.e., Lo, Ld, or Lo/Ld coexisting bilayers. The emission spectra of prodan in *Fig. S3.6A, C, E* illustrate a blue shift in all systems with an increasing Rh2 concentration, indicating changes in the mobility and hydration of prodan in all liposome systems. In this case, the liposome headgroup may have achieved a more dense and less hydrated state with a high Rh2 concentration.

The density and hydration level of the bilayer's interior and headgroup were further assessed using the same liposome systems comparing PSM and DPPC. Results in *Fig. S3.3* illustrate that with an increasing Rh2 concentration, laurdan and prodan GP_{340} values also increase (emission spectra are shown in *Fig. S3.5B, D, F* and *Fig. S3.6B, D, F*). This signifies that the hydration of the bilayer core and headgroup was reduced, and interestingly, there was no significant difference from the results obtained for the PSM- and DPPC-containing bilayers. These results indicate that Rh2 does not interact strongly with SM, but almost equally with DPPC. Judging from the marked differences in DPH anisotropy and laurdan GP values in Lo and Ld phases shown in the following sections, the results suggest that Rh2 has a different interaction with Lo lipids, including SM and DPPC, than with Ld lipids, such as POPC.

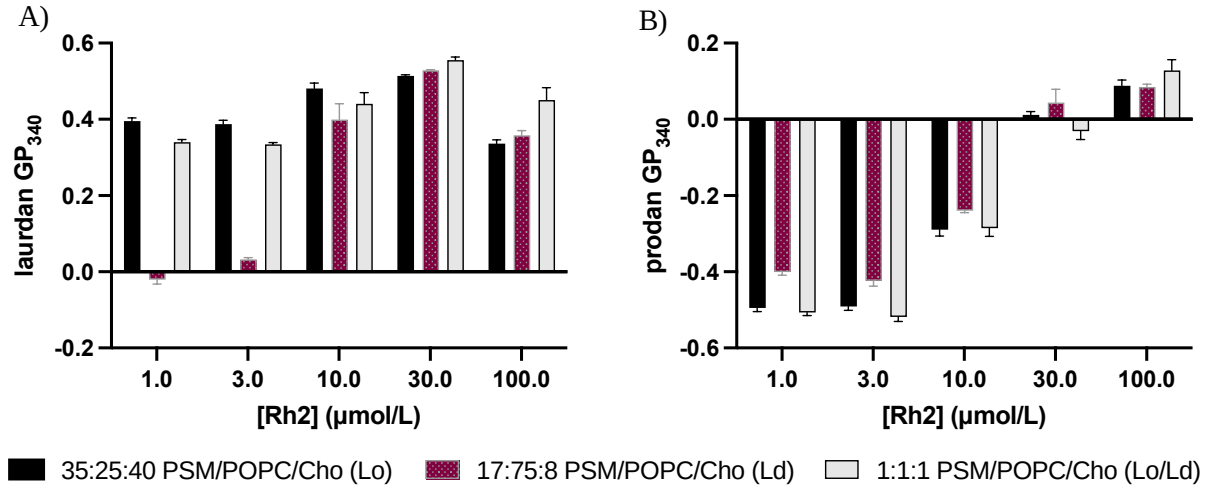

Figure 3.4. Laurdan and prodan GP_{340} values of bilayers containing different ratios of PSM/POPC and Cho, incubated with increasing concentrations of Rh2 (1-100 µM) measured at 30°C. The average GP_{340} values without Rh2 for laurdan and prodan experiments were remarkably close to those with 1 µmol/L Rh2.

3.2.3. Surface Pressure-Area (π-A) Binding Isotherm with Monolayer in the Presence of Rh2 (performed by Dr. Masanao Kinoshita (Kyushu University))

The binding of Rh2 to the Lo and Ld phases and their coexisting phases was examined. Langmuir monolayers of the ternary systems were formed on the surface of the subphase (milliQ), containing increasing amounts of Rh2. The surface pressure area (π-A) was measured after lateral compression. The reproducibility of monolayer isotherms was first evaluated. As shown in *Fig. S3.7*, two measurements were performed under the same conditions and in the absence of Rh2 in the subphase. The resulting isotherms for each lipid system had a marginal difference of 0.006 $Å^2$. *Fig. 3.5* shows π-A isotherms of Lo, Ld, and phase-separated systems with Rh2 on the subphase. Black, red, and blue isotherms stood for 0, 0.63, and 1.25 μM Rh2, respectively. Measured under the same conditions, it is evident that the monolayer for the Ld system expanded laterally to a greater degree relative to the Lo and phase-separated systems. The isotherm shifting towards the right revealed that Rh2 is more efficiently taken into the Ld phase than the Lo phase of the ternary bilayers. Overall, resulting π-A isotherms showed the probability of Rh2 binding in these lipid systems.

The 'collapse point' in the black isotherms at 40–50 mN/m (*Fig. 3.5A*, 0 μM Rh2, and *Fig. S3.7*) represents the 'collapse point' for the monolayers. However, a kink was also observed in the blue isotherms with 1.25 μM Rh2 at 18 mN/m. These kinks indicate coexisting phases in the monolayer (de Groot and Müller-Goymann, 2016). Next, the π-A isotherms of Rh2 alone were measured and compared to the isotherms of the Lo, Ld, and phase-separated systems with Rh2 in the subphase (*Fig. 3.5B*). Results showed that Rh2 (green isotherm) was able to generate an isotherm comparable to lipid monolayers (*Fig. S3.7* and *Fig. 3.5A*, 0 μM Rh2), indicating that Rh2 possibly forms monolayers on the water interface. Since Cho and ChoGlc did not cause such a phase transition (kink) (Hanashima *et al.*, 2021), this phase transition of the Rh2 phase may not be a change in the order of the side chains, but change in molecular orientation that reduces the molecular cross-sectional area. The pressure of pure Rh2 also shifted at a surface pressure π = 18 mN/m (green arrow), which was about the same π where kinks formed in the Lo, Ld, and phase-separated lipid monolayers (blue arrows), implying that Rh2 partially underwent phase separation from the lipid monolayer in the low surface pressure range. A similar premise as in *Fig. 3.5A* can be adapted to the scenario for the isotherms for pure Rh2 systems. The different orientations (e.g., binding parallel to the surface and/or full insertion parallel to phospholipid acyl chains) of Rh2 in the monolayer resulted in phase separation and the appearance of a kink in the isotherm. The kink appeared in all ternary monolayers at higher Rh2 concentrations despite being less prominent in the Lo system. This suggests that, at low surface pressure, the Lo-phase monolayer can take a fluid state, thus allowing Rh2 to situate itself within the monolayer. The possible orientations of Rh2 may cause the difference in the π-A isotherm curves of the Lo and Ld monolayers.

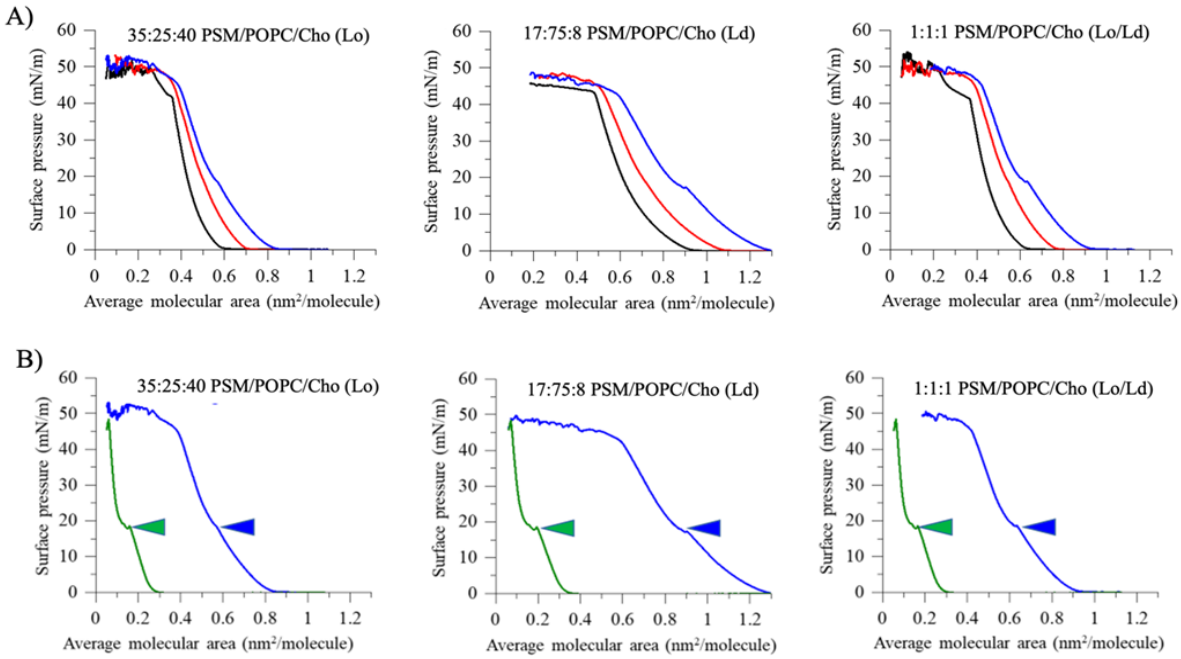

Figure 3.5. Surface tension measurements (π-A isotherms) of ternary monolayers with an Rh2 aqueous solution as the subphase. A) Isotherms in the presence of 0, 0.63, and 1.25 μM Rh2 are shown by the black, red and blue lines, respectively. The black isotherms are the same as with *Fig. S3.7*. B) The isotherm of a 1.25 μM Rh2 aqueous solution as the subphase (green). The isotherms for lipid monolayers are the same data from panel A (blue line).The phase shift in these respective isotherms is depicted by the green and blue arrows.

3.2.4. Liposome Morphological Changes Induced by Rh2 under Confocal Fluorescence Microscopy

To inspect and visualize the effects of Rh2 on phase-separated systems, giant unilamellar vesicles (GUVs) composed of 1:1:1 POPC/PSM/Cho were used. Here, BODIPY FL C5-HPC as the Ld marker, and 594neg-SSM as Lo marker (*Fig. S3.1D-E*), were incorporated in lipid films prior to the electrofomation of GUVs. Rh2 solution was carefully injected into the GUV suspension, garnering a final concentration of ~ 30 μM (based on the EC50 of Rh2 determined from the hemolysis assay in the previous chapter). Kinoshita *et al.* synthesized 594neg-SSM, a fluorescent sphingomyelin analogue that was reported to partition effectively into the Lo phase. The hydrophilic fluorophore, ATTO594, was conjugated at a certain distance into the choline moiety of SSM via the nonaethylene glycol linker. This process allowed SSM to retain the positive charge of its choline group, thus mimicking native SM interactions (Kinoshita *et al.*, 2017).

In *Fig. 3.6*, while coexisting domains were distinguished by the Ld and Lo-specific probes, morphological changes occurred over time in the presence of 30 μM Rh2. Initial micrographs were captured before the addition of Rh2 into the GUV suspension. In the one-minute column, it was observed that the Lo phase started to exhibit positive curvature. Over time, this progressed to the budding of the Lo domain, and 'neck' emerged. Here, the phase boundary shortens, and the line tension and energy decrease. As reported in the π-A binding assay, affinity and possible insertion of Rh2 may differ between Lo and Ld domains. In addition, binding of Rh2 on the outer leaflet may create transbilayer asymmetry. The nanoscopic changes in the domains brought by Rh2 can induce such morphological changes in the GUV. Furthermore, in the 15-minute panel, it seemed that the Lo vesicle had separated from the main GUV; however, the 'neck' started to open, and the vesicle merged or fused back into the

main GUV. It was a continuous, back and forth process of budding and fusing observed for several GUVs. The plausible competing factor is spontaneous curvature between domains. The assumption that Rh2 inserts to Ld phase easily rather than Lo phase may evoke different extrinsic tension in these domains, causing a series of membrane bending. A similar experiment (*Fig. S3.8)* was performed and garnered the same effect using only β-BODIPY FL C5-HPC as the lipid-order sensitive probe. Different local environment in membrane, such as fluid ordered and disordered domains, allows changes in the absorption dipole orientation of BODIPY FL C_5-HPC (Lesoine *et al.*, 2012). The GUV shown in *Fig. S3.9* contains multiple microdomains, contrary to the other GUVs presented in this study that has at least two macrodomains. The addition of Rh2 resulted in the coalescence of the microdomains, forming larger segregation in the vesicle. By and large, these observations stress that Rh2 has diverse interactions with different domains of the membrane.

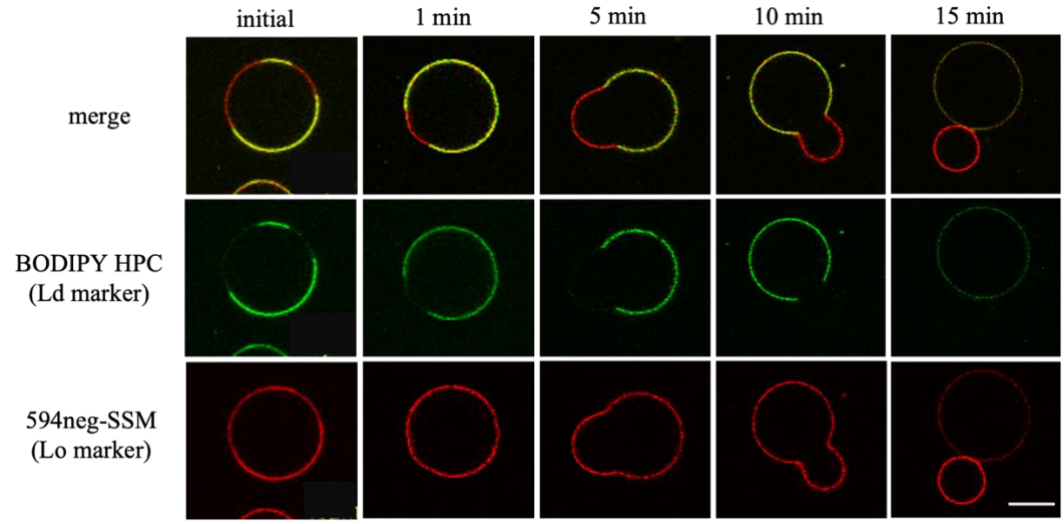

Figure 3.6. 2D micrographs of phase-separated GUVs (1:1:1 POPC/PSM/Cho) labeled with 0.4mol % β-BODIPY FL C5-HPC (green) and 0.2 mol% 594neg-SSM (red), and incubated with 30 μM Rh2. Micrographs were images captured at room temperature. Initial images were captured before the addition of Rh2. Scale bar = 10 μm.

3.2.5. Molecular Dynamics Simulation of Rh2-Incorporated Lipid Bilayers (performed by Dr. Peter Greimel (RIKEN CBS))

Molecular Dynamics (MD) simulation was performed to determine the different orientations of Rh2 in a fluid POPC bilayer VS a rigid PSM bilayer. Briefly, parameterization was performed using CHARMM36, and the bilayer was assembled in VMD using 36 lipids per leaflet. Simulations were performed using NAMD (CUDA acceleration), and Langevin dynamics (NPT 1atm, 312K), and the simulation temperature was set to 37°C (Hanashima *et al.*, 2021). In the electron density profiles (EDP) in *Fig. 3.7*, black peaks represent the phosphorus atoms in POPC and PSM headgroups, while the other peaks are for the different moieties in Rh2. In the EDP for PSM, multiple peaks per section in Rh2 molecules were observed as opposed to Rh2 in the POPC bilayer. This indicates that the majority of Rh2 in POPC may adapt a single overall orientation compared to Rh2 molecules in a rigid, PSM bilayer. In both profiles, glucose locates below the phosphorus atoms of POPC and PSM, and the sterol

backbone of Rh2 locates below glucose. In addition, the membrane thickness of both membranes with and without Rh2 averages 4 nm from the center of the bilayer (*Fig. S3.10*).

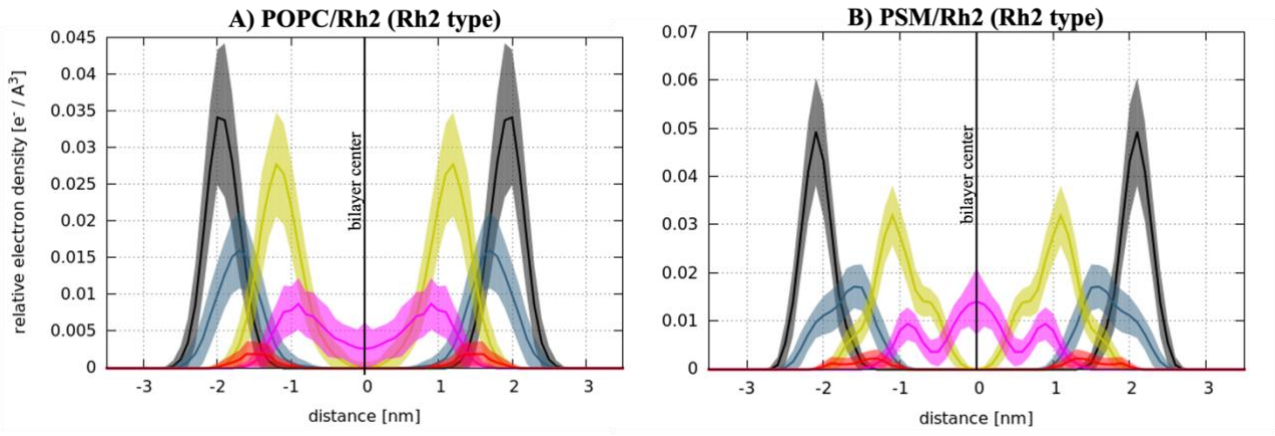

Figure 3.7. Electron density profiles POPC (A), PSM (B) and 10% Rh2 from MD simulations. Black: phosphorus atom in POC and PSM; blue: glucose from Rh2; red: oxygen link from sterol backbone and glucose; yellow: sterol backbone of Rh2; pink: a tail of Rh2.

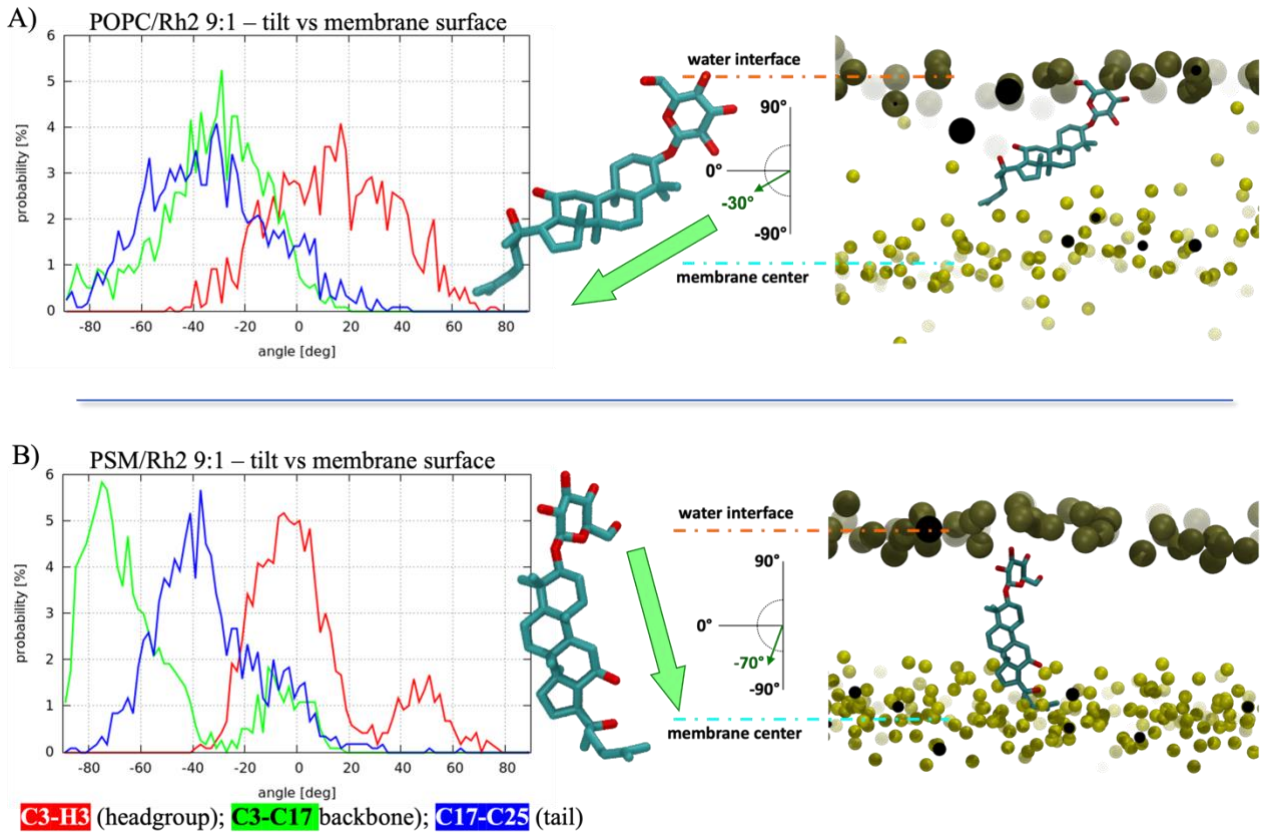

Figure 3.8. Snapshots of MD simulation showing the orientation of 10% Rh2 in bilayers consisting of A) POPC, and B) PSM. The green arrows indicate the orientation of the C3-C17 sterol core of Rh2. The phospholipid headgroups and terminal methyl groups in membranes were shown in large and small gold balls.

In a POPC bilayer (*Fig. 3.8A*), the overall tilt angle of the sapogenin is roughly -30°, and Rh2 lies almost parallel to the membrane surface. It is also noticeable that glucose is situated close to the headgroup, and the two hydroxyl groups of C12 and C20 point toward the polar headgroup. The fluidity in a POPC bilayer may have allowed glucose to sit closer to the membrane headgroup. In the case of PSM bilayer, there are two probable orientations of Rh2 based on the low- and high-probability EDPs, and tilt angle distributions. *Fig. 3.8B* shows the high probability orientation of Rh2 in PSM bilayer. Here, the overall tilt angle of the sapogenin is roughly -70°, and Rh2 lies almost parallel to the phospholipid acyl chains and locates slightly further down the membrane interior.

3.3. Discussion

In the previous chapter, high calcein leakage induced by Rh2 was reported even in unitary POPC bilayers, and its potency was not considerably affected by adding up of Cho and PSM into the membrane. Such information poses reservations about the proposed lipid-selective membrane activity of Rh2. Furthermore, these observations are contrary to most saponins that compel the support of sterols to induce potent activity. The time-course leakage assay described in the previous chapter implies that Rh2 may easily instigate its effects in a more fluid system, and different phase states may affect the activity of Rh2 to a greater degree rather than individual lipid components. In addition to that experiment, the leakage activity of Rh2 was compared in the ternary systems used in this chapter (PSM/POPC/Cho 35:25:40 (Lo), 17:75:8 (Ld), 1:1:1 (Lo/Ld)) against PSM/Cho 1:1, a Lo bilayer without POPC. Results in *Fig. S3.4A* revealed no significant differences observed among the three ternary systems above 10 µM Rh2. However, the binary Lo phase (*Fig, S3.4B*) showed markedly small increments in % leakage, considering a high background leakage of roughly 30%. This implies that Ld lipid, such as POPC, enhances the membrane activity of Rh2.

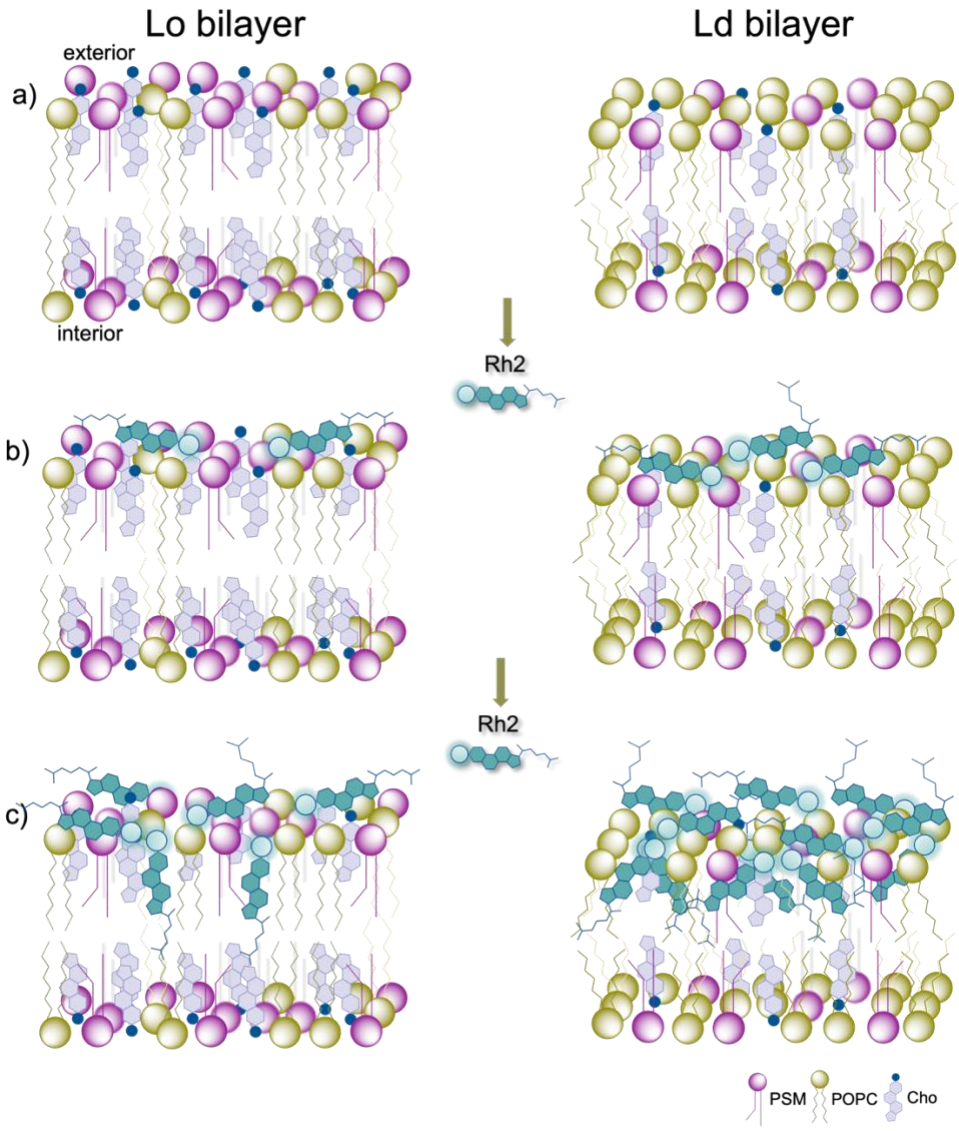

Figure 3.9. Schematic diagram of the proposed Rh2 interaction in Lo and Ld systems. a) absence of Rh2, b) small amount of Rh2introduced to the membrane, c) higher amounts of Rh2.

In this chapter, the behavior of Rh2 was investigated in liquid-ordered and -disordered membranes composed of PSM, POPC and Cho. The collective data and MD simulation led to the hypothesis that Rh2 binds into the membrane in a bimodal manner (*Fig. 3.9*). This is introduced early in this discussion to serve as a guide in deliberating the other experiments. Initially, Rh2 binds to the shallow peripheral of the membrane, regardless of its phase state, in a more parallel direction with respect to the bilayer surface (*Fig. 3.9B*). Postulated driving force is the hydrophilic interactions between the headgroup of the membrane and the polar moieties in Rh2 (glucose, and C12 and C20 hydroxyl groups). As Rh2 saturates the membrane surface, the penetration of water molecules into the membrane becomes restricted. The surface binding of Rh2 in Lo and Ld bilayers can set off different effects especially at elevated concentrations. In the Lo phase (*Fig. 3.9C*), where the acyl chains are tightly packed due to the high content of SM (*Fig. 3.9A*), it is difficult for Rh2 to penetrate the bilayer interior relative to a Ld phase; thus, a large proportion of Rh2 resides on the bilayer surface. However, once an Rh2 molecule penetrates the membrane, its sapogenin adopts an orientation of about ~70^{o} relative to the membrane surface, almost parallel to the acyl chains of the phospholipids (*Fig 3.8B*). In the Ld phase, where the acyl chains are loosely packed, Rh2 can partly penetrate the bilayer interior with more ease (*Fig. 3.9A*). Inside a fluid Ld phase, Rh2 tilts at about ~30^{o}

where the sugar moiety locates closer to the polar headgroup of the membrane (*Fig 3.8A*). The highly tilted orientation of Rh2 favors simultaneous contact of the C12 and C20 hydroxyl groups of Rh2 with the hydrophilic membrane surface. This interaction mode may cause the abundant binding of Rh2 to Ld phase in Cho-poor membranes. In POPC and eggPC bilayers, Rh2 is able to insert itself more easily into the bilayer interior. As the amount of bound Rh2 increases, the membrane surface becomes more crowded with Rh2, and the overall structure becomes more unstable. As in the case with membrane-inserting saponins, membrane lesions, such as toroidal pores, are more likely to occur. This has been reported with other saponins, such as pavoninin-1, OSW-1, and cholesteryl glucoside (Malabed *et al.,* 2020) (Hanashima *et al.,* 2021) (Ohnishi and Tachibana, 1997). In addition, the respective stimulatory and inhibitory effects of SM and Cho reported by Verstraeten *et al.* can be explained by the difference in membrane effects due to whether Rh2 binds to the bilayer surface or is inserted into the bilayers (Verstraeten *et al.,* 2019).

DPH anisotropy measurements showed that *r* values increased with Rh2 concentration notably for homogenous Ld bilayers. On the other hand, the initial high *r* values for the Lo and Lo-dominant phase-separated systems exhibited nominal changes with increasing Rh2 concentrations (*Fig. 3.3*). To investigate this proposition further, the GP values of the fluorescence probes, laurdan and prodan, were measured exploiting the same liposome systems (*Fig. 3.4*). Laurdan signifies the changes in polarity and hydration of the hydrophobic interior, whilst prodan sits closer to the water interface and reports for the environment of the lipid headgroups. As expected, the resulting trend for laurdan GP_{340} is grossly parallel with DPH anisotropy up to 30 μmol/L since both probes delve into the local environment of the membrane interior and accounts for chain ordering and hydration events. Similarly, the increase in GP_{340} from 10 μmol/L Rh2 was more prominent in the Ld bilayer. These results are the plausible outcomes for a membrane surface saturated with Rh2. As Rh2 crowds on the surface, water molecules hydrating the membrane interior is reduced. Hence, acyl chain ordering in the bilayer is enhanced and reflected by the increase in *r* values with more Rh2 molecules introduced into the matrix (*Fig. 3.3*). This is further supported by the results obtained in the laurdan GP measurements (*Fig. 3.4A*). Moreover, this observation is prominent in a rather fluid Ld system than in the rigid phase-separated or Lo systems, which indicates the ease of Rh2 binding, depending on the fluidity of the bilayers. However, there was a decrease in the laurdan GP_{340} at 100 μmol/L that was not observed in DPH anisotropy. The abundant binding of Rh2 to bilayers was assumed to increase the area per lipid and the gap between lipid molecules, as supported by the solid-state NMR data from the previous chapter. These effects induced laurdan to move to the shallower and more hydrated portion of the bilayer. A likely reason for these inconsistent results is the structural difference between these probes. Laurdan has a polar amine moiety that would allow it to interact with the polar headgroup of lipids in the shallower area, while DPH lacks polar functionality and tends to reside in the deeper portion of the acyl chains, where it is less susceptible to the effects of Rh2. A reduction in GP_{340} values at a high Rh2 concentration was also observed in the Ld and Lo phases, respectively (*Fig. 3.4A*).

The results for prodan (*Fig. 3.4B*) displayed a similar amount of change in terms of the GP_{340} value across all the liposomal preparations and a strikingly distinctive trend from laurdan and DPH. A plausible justification is that at 10 μmol/L, Rh2 extensively covers the membrane surface to prevent water penetration into the membrane surface. Thus, the reduced hydration state resulting from the abundant binding of Rh2 to the Ld phase, as shown in the laurdan experiment, was not clearly indicated in the GP values of prodan. If Rh2 binds or inserts exclusively into the hydrophobic interior and not the bilayer surface (similar to Cho), unblocked and disordered lipid headgroups are likely to expose the probe to the water interface, thus producing a negative GP value. Hence, the increased

values in *Fig. 3.4B* indicate that the lipid headgroups in the fluid phase are covered with Rh2. These effects of Rh2 to laurdan and prodan are illustrated in *Fig. S3.11*.

The results for DPH anisotropy and laurdan GP_{340} measurements seemingly implies an ordering effect of Rh2 in the interior of the Ld membrane, and appears to contradict the disordering effect of Rh2 in the membrane interior as determined from ^{2}H NMR in the previous chapter. However, the results gathered from these techniques are rather complementary. One of the possible explanations is that $\Delta\nu$ of ^{2}H NMR reflects the wobbling of the acyl chains of lipids whereas DPH anisotropy (and laurdan GP_{340}) values can be partly (and entirely) influenced by hydration in the bilayer interior. The high concentrations of Rh2 on the membrane surface in these fluorescence experiments prevent penetration of water molecules into the bilayer interior, particularly leading to the higher GP_{340} values in laurdan and prodan experiments up to 30 μmol/L, whereas not many Rh2 molecules possibly penetrate the deeper interior. Another thing to consider is the effects of the surface covering Rh2 on the phase segregation. The Rh2 on the surface of bilayers may decrease the diffusion speed of lipids and induce phase separation. In particular, the lipid composition of the Ld phase in *Fig. 3.3* and *3.4* is very close to the phase boundary on the phase diagram (*Fig. 3.2*); thus, this mixed bilayer could undergo phase separation by the slower diffusion of the lipids induced by Rh2 surface binding. Consequently, the order Lo phase is generated to which DPH and laurdan are preferentially transferred giving rise to higher *r* and GP_{340} values. The second reason may be the difference in the lipid-water ratios and membrane preparation methods between NMR and DPH. In the case of NMR, Rh2 is more efficiently incorporated into the membrane interior because of intensive mixing during vesicle preparation and a very small volume of aqueous media. As Hanashima *et al.* (2021) reported, ChoGlc bearing the same glucose unit insert into bilayer with a vertical orientation, thus efficiently orders the acyl chains of POPC under the Ld environment as seen for Cho. On the other hand, Rh2 binds to the shallow interior of the Ld phase with a tilted orientation (*Fig. 3.8A*), which enhances the space gap between the shallower and deeper interiors and induces disordering of the C10 position of the PSM acyl chain (*Fig. S2.7B*). A similar disordering effect of Rh2 can be seen for 100 μmol/L Rh2 in *Fig. 3.4*; the laurdan GP that becomes level-off at 100 μmol/L in the Ld phase may be due to the same reason. Thus, the apparent discrepancy between the NMR and DPH/laurdan results can be partly accounted for by these notions.

The effect of Rh2 in the ternary monolayers was also evaluated using a surface pressure-molecular area binding assay. The presence of Rh2 in the subphase expanded the isotherms for the Ld, Lo, and Ld/Lo systems (*Fig. 3.5A*). In addition, kinks appeared at about π = 18 mN/m noticeably at the highest concentration of Rh2. These results indicate the probability of Rh2 inserting in the monolayers. The resulting isotherms for Rh2-containing lipid monolayers in *Fig. 3.5B* indicate: 1) Rh2 binds more effectively to the Ld (fluid) monolayer; 2) a segregated Rh2 layer is partially formed at least within a low surface-tension range; 3) the kink at 18 mN/m indicates a phase transition of the Rh2 monolayer. In MD simulation, the triterpenoid core of Rh2, illustrated by the C3-C17 vector, is highly tilted, which may explain the formation of Rh2 layer in the monolayer experiments. This effect is summarized in an illustration in *Fig. S3.12.* To validate that Rh2 is also abundantly bound in the Ld phase of the *bilayer*, we estimated the binding affinity of Rh2 using the results of DPH anisotropy in *Fig. 3.3* (Huang and Haughland, 1991). The plot shown in *Fig. S3.13* allowed for the determination of the partition coefficient, K_p, of Rh2 in the L_d, L_o, and phase-separated bilayers. The K_p values were estimated by considering the amount of Rh2 bound to the liposomes relative to the free Rh2 in the aqueous solution (Eq. S3.4). As expected, the Ld phase has the greatest membrane-bound Rh2 ($K_p = 13.07 \times 10^6$), followed by the Ld/Lo ($K_p = 7.85 \times 10^6$) and Lo phases (K_p =

2.01×10^6). Thus, the Rh2 was shown to have a 6- to 7-fold higher affinity for the Ld phase than the Lo phase. The estimated K_p values support the premise and the results for the π-A binding assay, where Rh2 easily binds to or inserts into the Ld-type monolayer.

In confocal fluorescence microscopy, although DOPC may provide greater immiscibility between Lo and Ld phases, POPC is more biologically relevant, and this would be consistent with the lipid compositions in our experiments (Veatch and Keller, 2003). *Fig. 3.6* shows a phase-separated liposome undergoing budding or fission upon the addition of Rh2 into the GUV suspension. The domain boundaries are characterized by hydrophobic mismatch that is prone to the insertion of line-active molecules (Baumgart *et al.,* 2003) (Yang *et al.,* 2015). Like the conjecture for Rh2 in homogenous Ld systems, domain boundaries that are prone to bending may be a good target for insertion, consequently expanding Ld domains and reducing line tension. With sufficient membrane area and greater line tension, GUV in *Fig. 3.6* was driven to a spherical bud minimizing line tension and neck radius (*Fig. 3.6*, 15 min). Moreover, a back-and-forth motion of budding and fusion was observed. A possible explanation for such is the difference in the amount of Rh2 that is interacting in the Lo and Ld domains (*Fig. 3.5A, Fig. S3.13*). The assumption that Rh2 inserts to Ld phase easily rather than Lo phase may evoke different extrinsic tension to these individual sections, causing a series of membrane bending. Therefore, it is another indication of the phase-selective effects of Rh2.

3.4. Conclusion

Rh2 is a unique saponin that renders diverse effects on different membrane phases. The presence of the hydroxy groups at the 12 and 20 positions allows Rh2 to bind to the polar membrane surface. Based on the fluorescence measurements (DPH, laurdan and prodan GP), saturation of the membrane surface results in the partial dehydration of the membrane interior and in the reinforced hydrophobic interactions of the lipid chains. At higher saponin concentrations, Rh2 inserts effectively into the fluid Ld phase compared to the Lo phase. This is supported by the π-A isotherms revealing that Rh2 binds more abundantly to the monolayers of the Ld lipid composition than to those of the Lo lipid composition. In addition, imaging of phase-separated vesicles incubated with Rh2 illustrates the deformations brought by distinct binding of the saponin in Ld and Lo domains. MD simulations also suggest that the sapogenin portion of Rh2 is located in a relatively shallow (or boundary) region of the hydrophobic interior of the Ld phase. These results disclosed the unique mechanism in the efficient membrane permeabilization by Rh2; the saponin accumulates asymmetrically on the surface and in the shallow interior of the less ordered bilayers such as the Ld phase to cause membrane disruption.

3.5. References

-Baumgart, T.; Hess, S. T.; Webb, W. W. Imaging coexisting fluid domains in biomembrane models coupling curvature and line tension. *Nature.* **2003**. *42*, 821-824.

-Chenioura, M.; Gueyrard, D.; Goekjiana, P. G.; Granjona, T.; Marcillata, O. A convenient and versatile synthesis of Laurdan-like fluorescent membrane probes: characterization of their fluorescence properties. ***RSC Adv.*** **2016**. ***6,*** 5547-5557.

-de Almeida, R. F. M.; Federov, A.; Prieto, M. Sphingomyelin/phosphatidylcholine/cholesterol phase diagram: Boundaries and composition of lipid rafts. *Biophys J.* **2003.** *85*, 2406-2416.

-de Groot, C.; Müller-Goymann, C. C. Saponin Interaction with Model Membrane Systems – Langmuir Monolayer Studies, Hemolysis and Formation of ISCOMs. *Plant Med*. **2016**. *82*, 1496-1512.

-Hanashima, S.; Fukuda, N.; Malabed, R.; Murata, M.; Kinoshita, M.; Greimel, P.; Hirabayashi, Y. β-Glucosylation of cholesterol reduces sterol-sphingomyelin interactions. *Biochim. Biophys. Acta*. **2021**. *1863*, 183496

-Huang, Z., Haughland, R. P., Partition coefficients of fluorescent probes with phospholipid membranes. *Biochim. Biophys. Res. Commun.* **1991,** *181*, 166-171.

-Jackson, C. L.; Walch, L.; Verbavatz, J-M. Lipids and Their Trafficking: An Integral Part of Cellular Organization. *Dev. Cell.* **2016.** *39*, 139-154.

-Jay, A. G.; Hamilton, J. A. Disorder Amidst Membrane Order: Standardizing Laurdan Generalized Polarization and Membrane Fluidity Terms. *J Fluoresc.* **2017**.*27*, 243–249.

-Kaiser, H-J.; Lingwood, D.; Levental, I.; Sampaio, J. L.; Kalvodova, L.; Rajendran, L.; Simons, K. Order of lipid phases in model and plasma membranes. *PNAS*. **2009**. *106*, 39, 16645-16650.

-Kaiser, R. D.; London, E. Location of Diphenylhexatriene (DPH) and Its Derivatives within Membranes: Comparison of Different Fluorescence Quenching Analyses of Membrane Depth. *Biochemistry*. **1998**. *37*, 8180-8190.

-Kinoshita, M.; Suzuki, K. G. N.; Matsumori, N.; Takada, M.; Ano, H.; Morigaki, K.; Abe, M.; Makino, A.; Kobayashi, T.; Hirosawa, K. M.; Fujiwara, T. K.; Kusumi, A.; Murata, M. Raft-based sphingomyelin interactions revealed by new fluorescent sphingomyelin analogs. *J. Cell Biol.* **2017**. *216*, 1183–1204.

-Krasnowska, E. K.; Gratton, E.; Parasassi, T. Prodan as a Membrane Surface Fluorescence Probe: Partitioning between Water and Phospholipid Phases. *Biophys J.* **1998**. *74*, 1984-1993.

-Lesoine, J. F.; Lee, J. Y.; Krogmeier, J. R.; Kang, H.; Clarke, M. L.; Chang, R.; Sackett, D. L.; Nossal, R.; Hwang, J. Quantitative scheme for full-field polarization rotating fluorescence microscopy using a liquid crystal variable retarder. *Rev Sci Instrum*. **2012**. *83*, 053705.

-Lorent, J.; Le Duff, C. S.; Quetin-Leclercq, J.; Mingeot-Leclercq, M. P. Induction of highly curved structures in relation to membrane permeabilization and budding by the triterpenoid saponins, α- and δ-hederin. *J. Biol. Chem.* **2013**. *288*, *20*, 14000-14017.

-Malabed, R.; Hanashima, S.; Murata, M.; Sakurai, K. Interactions of OSW-1 with lipid bilayers in comparison with digitonin and soyasaponin. *Langmuir*. **2020.** *36*, 3600-3610.

-Malabed, R.; Hanashima, S.; Murata, M.; Sakurai, K. Sterol-recognition ability and membrane- disrupting activity of *Ornithogalum* saponin OSW-1 and usual 3-*O*-glycosyl saponins. *Biochim. Biophys.Acta.* **2017**, *1859*, 2516-2525.

-Ohnishi, Y.; Tachibana, K. Synthesis of Pavoninin-1, a shark repellant substance, and its structuralanalogues toward a mechanistic study on their membrane perturbation. *Pergamon*. **1997**. *12*, 2251-2265.

-Ondevilla, J. C.; Hanashima, S.; Mukogawa, A.; Umegawa, Y.; Murata, M. Diosgenin-induced physicochemical effects on phospholipid bilayers in comparison with cholesterol. *Bioorg. Med. Chem. Lett.***2021**. *36*, 127816.

-Parasassi, T.; Krasnowksa, E. W.; Bagatolli, L.; Gratton, E. Laurdan and Prodan as Polarity-sensitiveFluorescent Membrane Probes. *J. Fluoresc.* **1998**. *8*, 365-373.

-Poojari, C.; Wilkosz, N.; Lira, R. B.; Dimova, R.; Jurkiewicz, P.; Petka, R.; Kepczynski, M.; Róg, T. Behavior of the DPH fluorescence probe in membranes perturbed by drugs. *Chem. Phys. Lipids*. **2019**. *223*, 104784.

-Sevcsik, E.; Schütz, G. J. With or without rafts? Alternative views on cell membranes. *Bioessays*. **2016**. *38*, 2, 129-139.

-Silva, L. C.; de Almeida, R. F. M.; Castro, B. M.; Fedorov, A.; Prieto, M. Ceramide-Domain Formation and Collapse in Lipid Rafts: Membrane Reorganization by an Apoptotic Lipid. *Biophys J.* **2007**. *92*, 502-516.

-Sych, T.; Gurdap, C. O. Wedemann, L.; Sezgin, E. How Does Liquid-Liquid Phase Separation in Model Membranes Reflect Cell Membrane Heterogeneity? *Molecules*. **2021**. *11*, 323.

-van Meer, G.; Voelker, D. R.; Feigenson, G. W. Membrane lipids: where they are and how they behave. *Nat Rev Mol Cell Biol*. **2008**. *9*, 2, 112–124.

-Veatch, S. L.; Keller, S. L. Separation of Liquid Phases in Giant Vesicles of Ternary Mixtures of Phospholipids and Cholesterol. *Biophys. J.* **2003.** *85*, 5, 3074–3083.

-Verstraeten, S. L.; Deleu, M.; Janikowska-Sagan, M.; Claereboudt, E. J. S.; Lins, L.; Tyteca, D; Mingeot-Leclercq, M. P. The activity of the saponin ginsenoside Rh2 is enhanced by the interaction with membrane sphingomyelin but depressed by cholesterol. *Sci. Rep.* **2019**. *9*, 1-14.

-Yang, S. T.; Kiessling, V.; Tamm, L. K. Line Tension at lipid phase boundaries as driving force for HIV fusion peptide-mediated fusion. *Nat. Commun.* **2015.** *11401*.

3.6. Supporting Materials

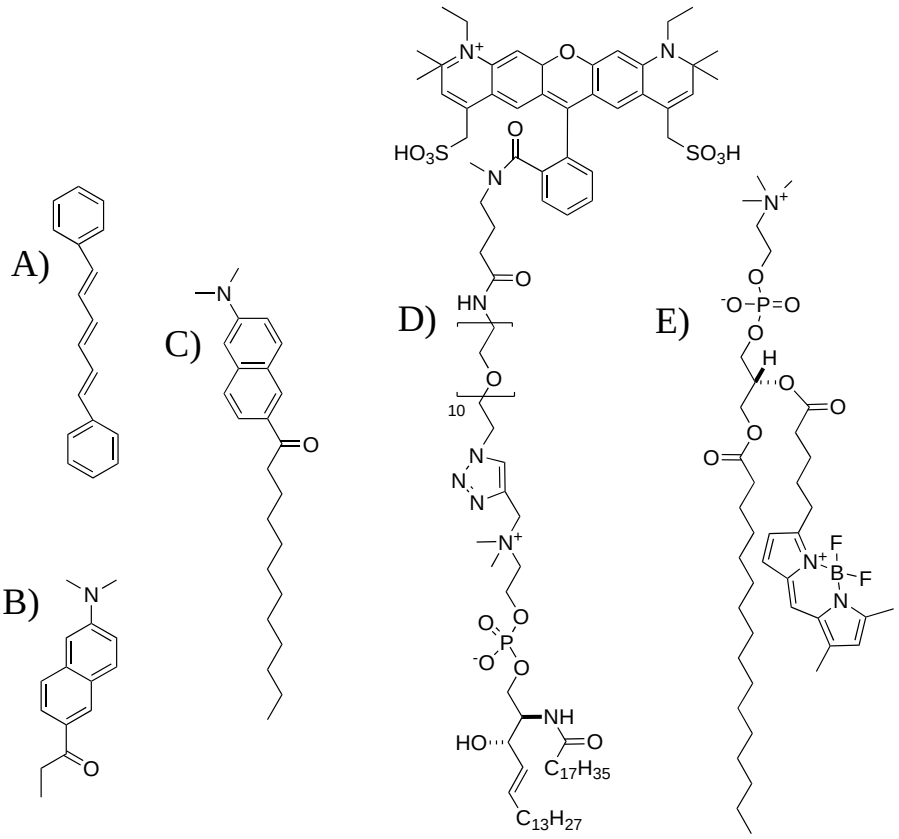

Figure S3.1. Structure of fluorescent probes used in this study. For anisotropy/generalized polarization measurements: ***A)*** 1,6-diphenylhexatriene (DPH), ***B)*** 2-dimethylamino-6- propionylnaphthalene (prodan), and ***C)*** 2-dimethylamino-6-lauroylnaphthalene (laurdan). For confocal fluorescence microscopy*:* ***D)*** 594-neg-N-stearoylsphingomyelin (**594neg-SSM**) and ***E)*** β-BODIPY FL C5-HPC.

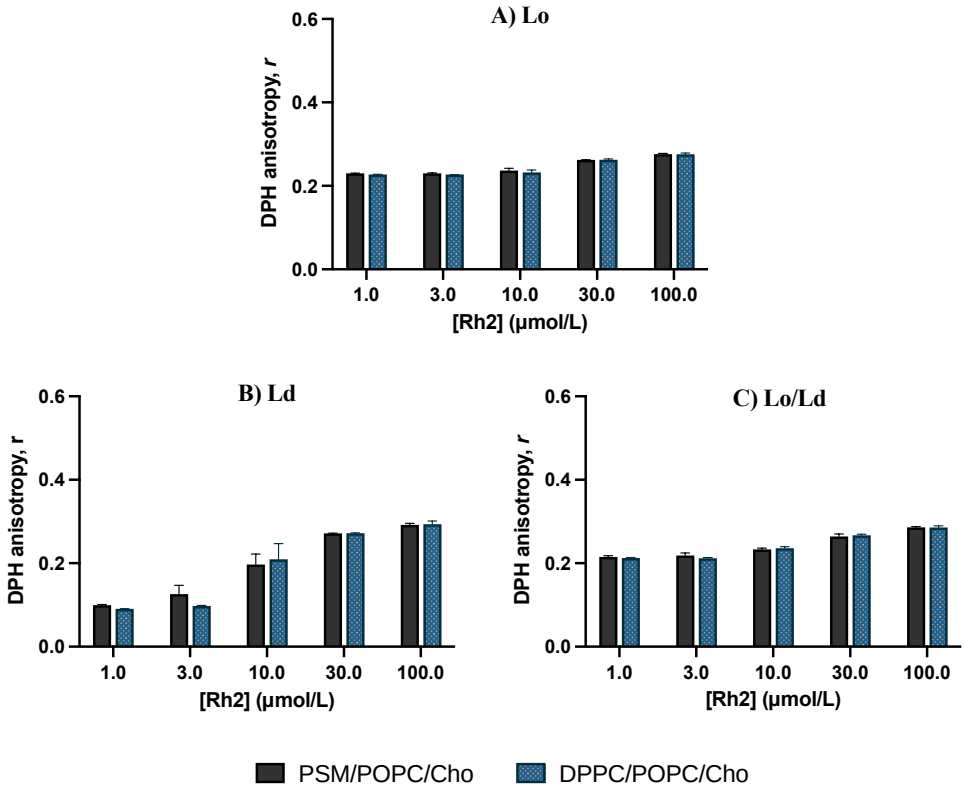

Figure S3.2. DPH anisotropy in POPC and Cho bilayers with either PSM or DPPC. Measurements were performed in homogenous A) Lo, B) Ld, and phase-separated Lo/Ld incubated with Rh2 (1-100μM) at 30°C.

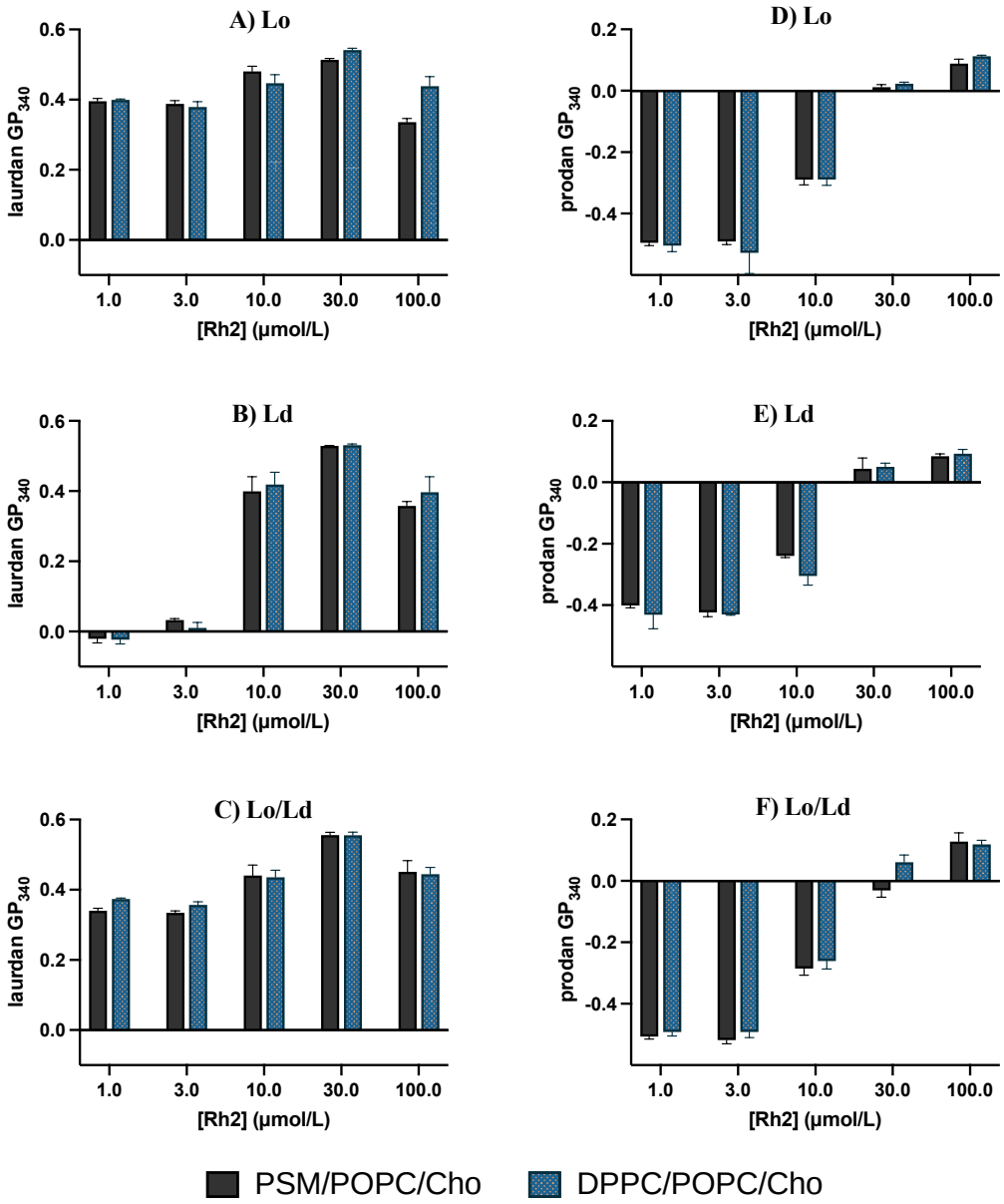

Figure S3.3. Hydration levels of PSM and DPPC bilayers, as evaluated by GP values for laurdan (A-C) and prodan (D-F). The experiments were carried out at 30°C.

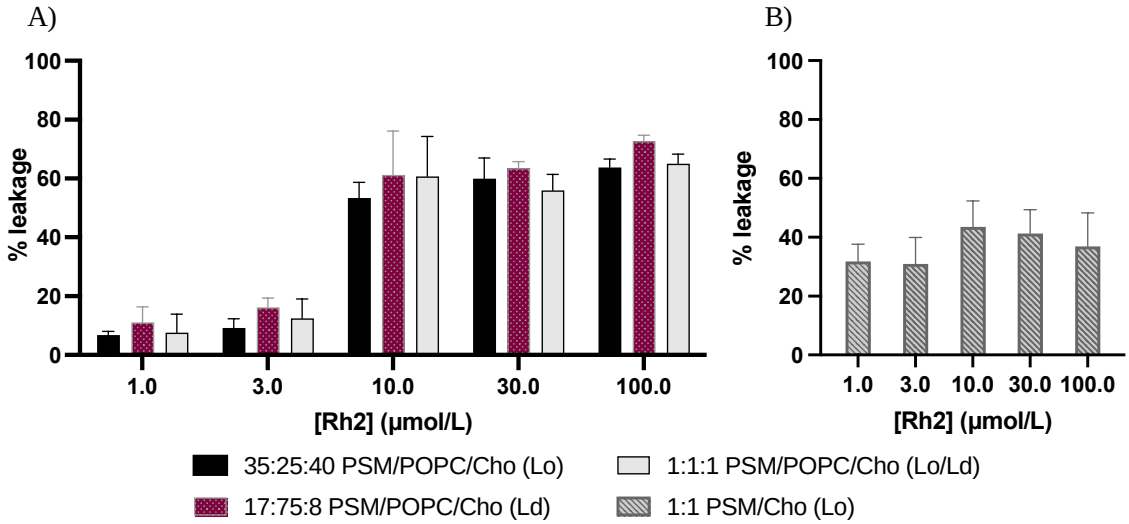

Figure S3.4. Calcein leakage of Lo and Ld phases. (A) Lo, Ld, and coexisting phases. (B) Lo model bilayers without POPC. The leakage was measured at 30°C. The average control values of calcein without Rh2 for these experiments were remarkably close to those with 1 μmol/L Rh2. Percent leakage in 5B shows no statistically significant differences across concentrations of Rh2 (ns $p<0.05$ (one-way ANOVA, n = 5), [$F(4,10) = 1.219$, $p = 0.36$]).

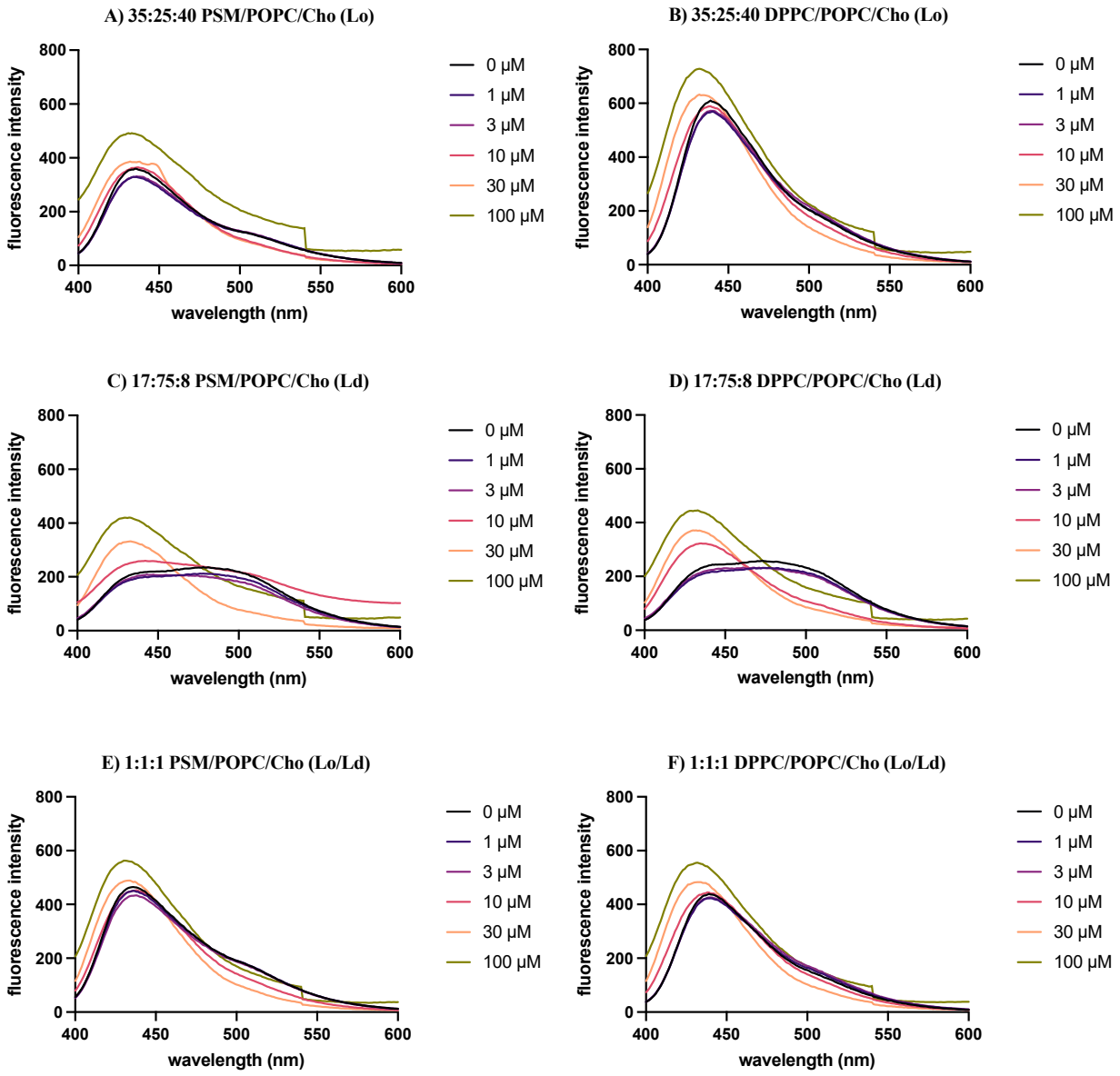

Figure S3.5. Emission spectra of laurdan in various POPC bilayers with increasing Rh2 concentration. A, B) homogenous Lo, C, D) homogenous Ld, and E, F) phase-separated Lo/Ld.

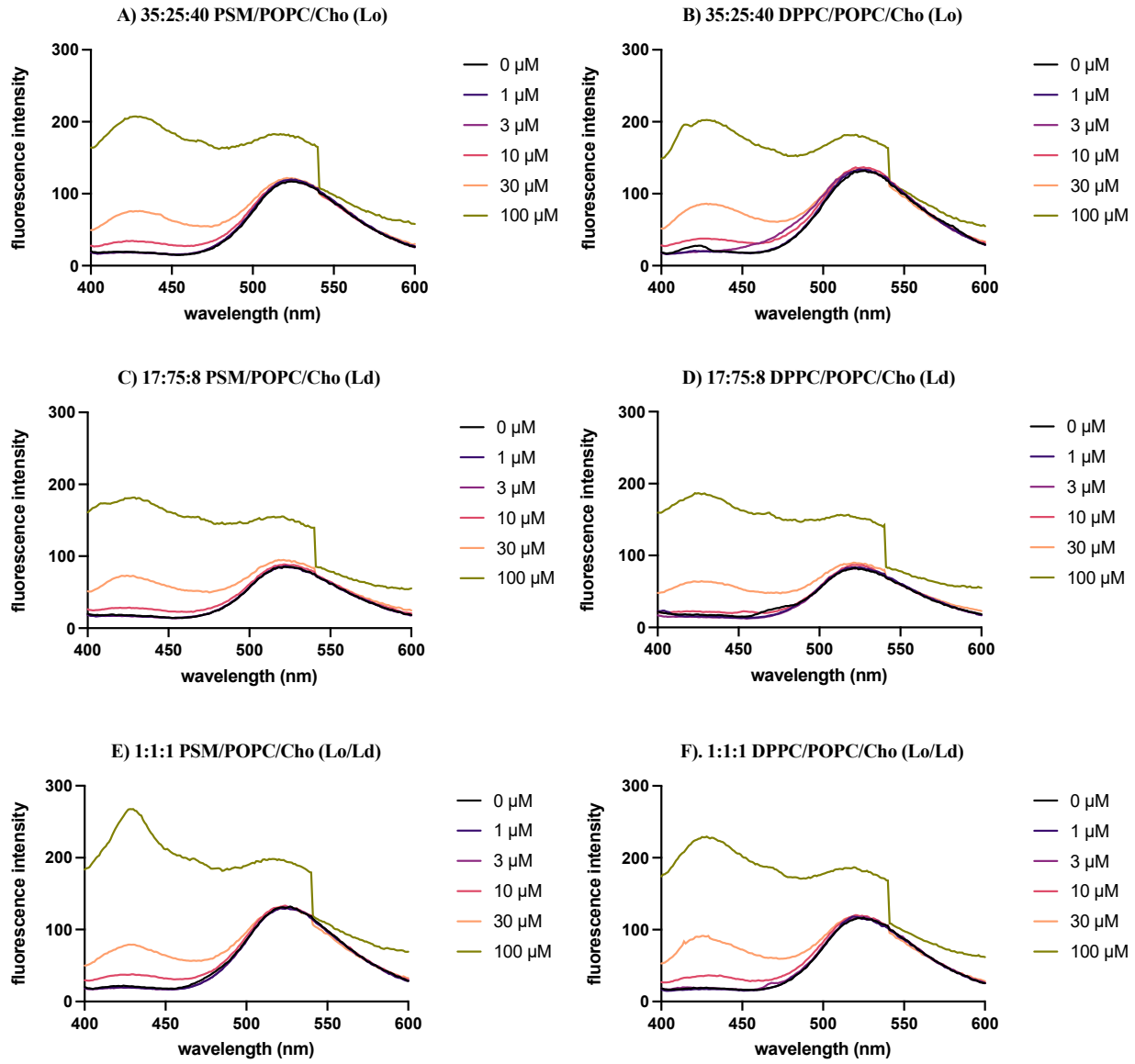

Figure S3.6. Emission spectra of prodan in various POPC bilayers with increasing Rh2 concentration. A, B) homogenous Lo, C, D) homogenous Ld, and E, F) phase-separated Lo/Ld.

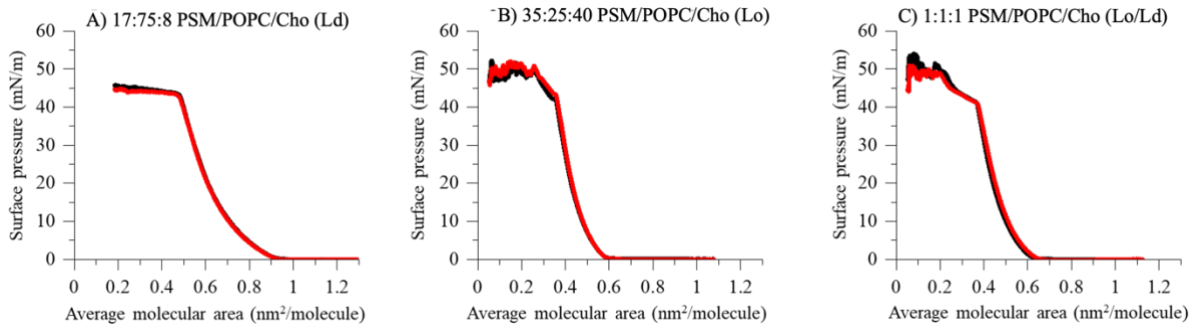

Figure S3.7. Reproducibility of π-A isotherm. POPC/PSM/Cho monolayer isotherms with milliQ as the subphase. A) 75:17:8 POPC/PSM/Cho (Ld), B) 25:35:40 POPC/PSM/Cho (Lo), C) 1:1:1 POPC/PSM/Cho (Ld/Lo). Black and red isotherms show the first and second actual results when measured under the same conditions, respectively.

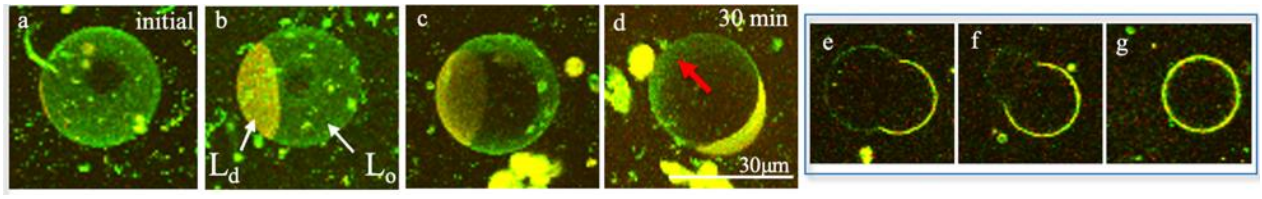

Figure S3.8. 3D micrographs of phase-separated GUVs labelled with β-BODIPY FL C_5-HPC (λ_{ex} 488 nm; λ_{em} 522 nm), and incubated with 30 µM Rh2; budding of the Lo phase (d, red arrow); e-g – 2D cross-section showing vesicle budding. Micrographs were captured at room temperature. Scale bar = 30 µm.

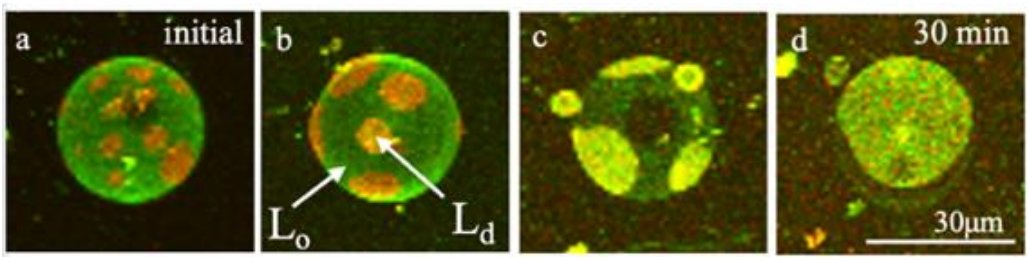

Figure S3.9. 3D micrographs of phase-separated GUVs labelled with β-BODIPY FL C_5-HPC incubated with 30 µM Rh2. Microdomains were observed to coalesce. Micrographs were captured at room temperature. Scale bar = 30 µm.

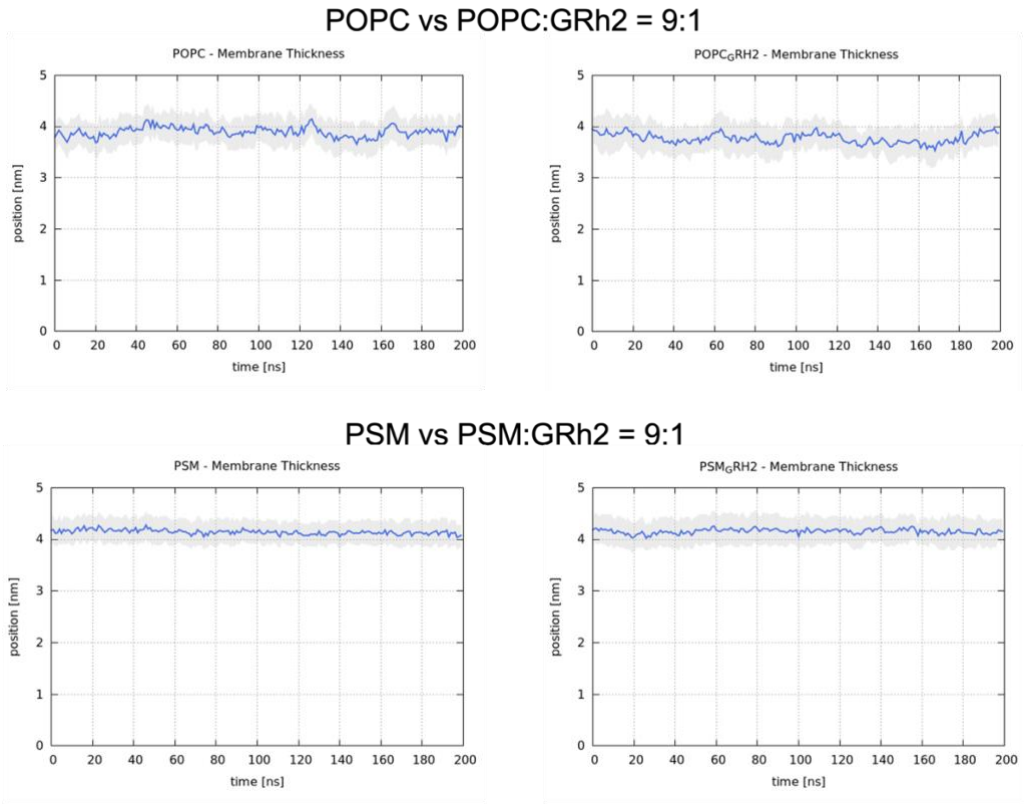

Figure S3.10. Membrane thickness of POPC (upper panel), and PSM (lower panel), with and without Rh2.

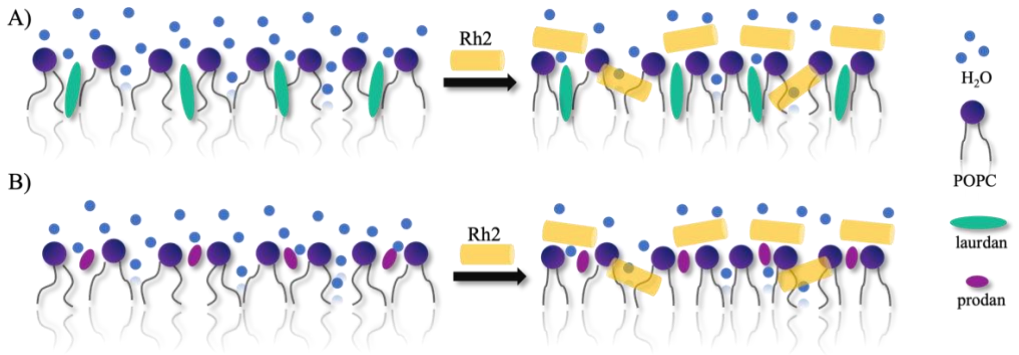

Figure. S3.11. Hypothetical illustration for the effects of Rh2 in Ld membrane enriched with A) laurdan, and B) prodan. Surface crowding of Rh2 decreases hydration of membrane core, and causes disorder of membrane headgroup, and prevents further exposure of prodan to the water interface. This illustration represents the outer leaflet of the membrane, and only POPC was used for simplification.

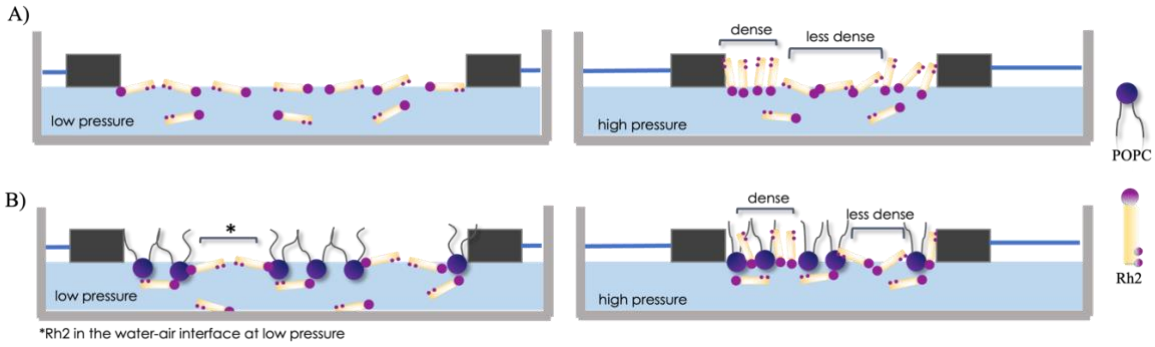

Figure S3.12. Hypothetical illustration of A) 1.25µM Rh2 (*Fig. 3.5B*, green isotherm) in the subphase of a Langmuir trough forming its own monolayer (no preformed lipid monolayer), and B) Ld Langmuir monolayer with 1.25µM Rh2 in the subphase (*Fig. 3.5B*, blue isotherm). This figure represents events at low and high pressures. Only POPC was used for simplification.

Membrane binding rate estimated by DPH anisotropy

Membrane binding rate of Rh2 was estimated using the results gathered for DPH anisotropy in ternary systems (Huang and Haughland, 1991). The partition coefficient, Kp, was calculated to assess the amount of Rh2 bound to the membrane, and is given by Eq. S3.1, where $[Rh2]_b$ and $[Rh2]_f$ are the concentration of Rh2 bound and unbound to the membrane, respectively, and L and W are the molar concentration of phospholipid and water, respectively. First, the amount of Rh2 bound to the liposomes (α) at different phase states (Ld, Lo and Ld/Lo) after a 15-min incubation at 37°C was estimated using Eq. S3.2, where r_o is the anisotropy value prior to incubation of liposomes with Rh2, and r_{max} is the maximum value of r in the measurement (in this case, r_{max} corresponds to the anisotropy value of DPH with 500µM Rh2). The calculated α value was plotted against Rh2 concentration (1-300 µM) to obtain *Figure S3.8A*.

$$Kp = \frac{\frac{[Rh2]_b}{L}}{\frac{[Rh2]_f}{W}} \quad \text{(S3.1)} \qquad \alpha = \frac{r\,(x) - r\,(x)_o}{r\,(x)_{max} - r\,(x)_o} \quad \text{(S3.2)}$$

x = Ld, Lo, Ld/Lo

$$\alpha = \frac{[Rh2]}{\frac{W}{Kp} + [Rh2]} \quad \text{(S3.3)} \qquad \frac{1}{\alpha} = \frac{W}{Kp} \times \frac{1}{[Rh2]} \quad \text{(S3.4)}$$

W = 55.6M

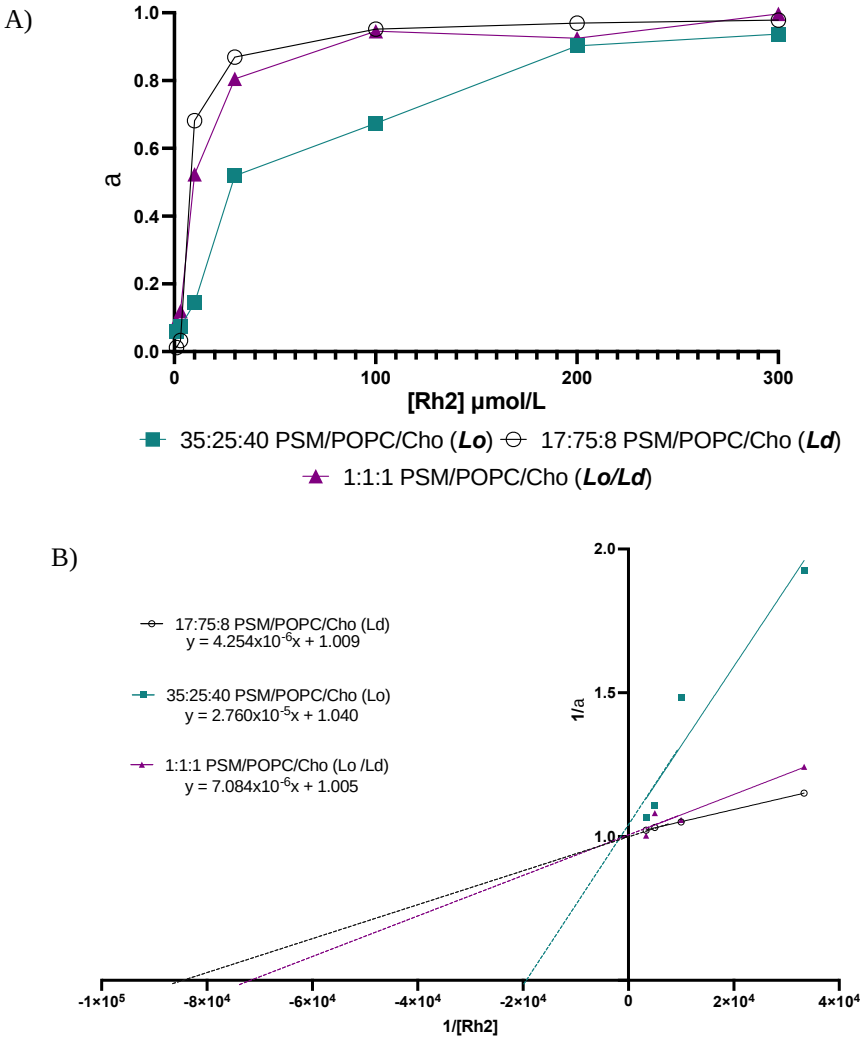

Figure S3.13. A) α vs Rh2 concentration.; B) double reciprocal plot of 1/α and 1/[Rh2]

To better estimate the Kp value, the double reciprocal plot was generated using Eq. S3.3 to give Eq. S3.4 which resulted to a linear curve shown in *Figure S3B*. The value of Kp was calculated using the slope of the line and given that W is equal to 55.6M. The estimated Kp values for the Ld, Lo and Ld/Lo systems are **13.07, 2.01,** and **7.85 x 10^6,** respectively. The order of Ld>Ld/Lo>Lo implies that Ld systems has the highest amount of Rh2 bound to the membrane.

~ Chapter 4 ~

General Discussion and Conclusions

4.1. General Discussions

Ginsenoside Rh2 is a rare type of saponin extracted from *Panax ginseng*. Oftentimes, saponin research delves into steroidal saponins for their significant pharmacological activities, and apart from their potential interactions with membrane proteins, their potency is frequently associated with membrane lipids (e.g., Cho). The weak biological potential of several triterpenoid saponins, on the other hand, is accounted for their inadequate capacity for lipid recognition. The uniqueness of Rh2 as a triterpenoid saponin comes from its ability to evoke significant pharmacological behaviors, while reported to interact with lipids and modulate the physical properties of cellular and model membranes. In this study, the lipid-driven and phase-selective effects of Rh2 in model membranes were investigated. The effects of Rh2 at the atomistic scale, and on the entirety of the membrane were examined on lipid monolayers and bilayers using several biophysical techniques coupled with MD simulations.

Since Rh2 was previously reported to prompt its biological responses through membrane cholesterol, sphingomyelin (SM), the initial approach of this study was to scrutinize its lipid-driven effects (Verstraeten *et al.*, 2019). Liposome leakage assay, as the preliminary analysis, revealed that Rh2 can induce significant leakage activity even in unitary POPC. The overall leakage effects of Rh2 in this pure system were at par with POPC liposomes containing Cho and PSM. This poses a reservation of its dependence to specific lipids of the membrane. In a time-course assay, POPC in the Ld phase was compared with POPC LUVs containing 30 mol% Cho and 30 mol% PSM, corresponding to the Ld/Lo and Ld/So phases, respectively. The coexisting systems presented an increasing trend in terms of leakage over time, while a constant rate was observed in the Ld system. This shows that Rh2 has varying influences on different phase states of the membrane, and implies that it may easily influence a more fluid system. This led to the investigation of the effects of Rh2 in Lo, Ld, and Lo/Ld membranes composed of PSM/POPC/Cho.

The microviscosity and hydration of the membrane interior were determined to be influenced by Rh2 through anisotropy measurements employing the fluorescent probes, DPH and laurdan. As Rh2 binds to the surface of the liposome, it effectively shields the membrane interior from hydration. Consequently, the hydrophobic interactions along lipid acyl chains are reinforced causing a decrease in the mobility of DPH (an increase in the *r* value) and decrease in the hydration of laurdan (an increase in the GP value). This effect is more pronounced in Ld systems than in Lo and Lo/Ld, which shows the phase-specific activity of Rh2. At higher concentrations of Rh2 (100 μM), an increase in hydration of laurdan was observed in all phases. As Rh2 crowds the membrane surface, it could disrupt the network of the membrane headgroup promoting greater hydration in peripheral sections of the membrane. The polar moiety of laurdan may steer the position of the probe to the shallower, and more hydrated portions of the membrane, consequently increasing the polarity of its local environment (decrease in GP). Prodan was also utilized to probe for the hydration changes in the membrane headgroup. After incubation with the saponin, prodan GP values increased with Rh2 concentration in all phases, which implies the dehydrating capacity of when

interacting with the surface of Lo, Ld, and Lo/Ld bilayers. Membrane surface saturated with bound Rh2 may prevent the exposure of prodan to the water interface (increase in GP). In contrast to the prominent differences between the Lo and Ld phases in the DPH and laurdan experiments, the difference in membrane-permeabilizing activity is less pronounced, particularly at higher concentrations of Rh2. One possible explanation is that Rh2 binds to the surface of the Lo and Ld bilayers to a similar extent as implied in prodan experiments. In the toroidal mechanism, an external agent accumulates on the surface of the bilayers and is occasionally inserted vertically to form transient pores when the surface becomes crowded. Therefore, under high-density conditions, the tight lipid–lipid packing in the Lo phase is somewhat loosened, as inferred from the laurdan experiment. Thus, when a significant amount of Ld lipids, such as POPC, is contained in the Lo phase, Rh2 may favorably interact with Ld lipids to form membrane-permeabilizing pores. Moreover, a common trend in these initial experiments (calcein leakage, and fluorescence measurements of DPH anisotropy and laurdan GP in Ld phase) is the upsurge in activity starting 10 μmol/L Rh2. At elevated concentrations of surface-active compounds, such as saponins, these molecules start to aggregate and form micelles. The critical micelle concentration (CMC) of Rh2 was estimated to be about 10 μmol/L using a pyrene method (data not shown). The results indicate that Rh2 above CMC efficiently binds to lipid membranes as generally seen for surfactants, and exhibits membrane permeabilizing activity. This trend has been observed for other saponins such as α-hederin (Lorent *et al.*, 2013).

Binding isotherms of Lo, Ld, and Lo/Ld monolayers also revealed that Rh2 binds and inserts in the fluid phase more efficiently. This is in line with the estimated partition coefficient (*K*p value) of Rh2 based on DPH anisotropy values, wherein the Ld phase garnered the highest membrane-bound Rh2. At low surface pressure, a layer of Rh2 is presumed to partially segregate at the air-water interface. This creates phase-separation upon lateral compression of the monolayer and reflects in the appearance of a kink in the isotherm at 18 mN/m.

Confocal fluorescence microscopy revealed the capacity of Rh2 to induce deformations in unilamellar vesicles. The premise of Rh2 binding differently in Ld and Lo bilayers based on the π-A isotherms upholds the morphological changes observed in phase separated GUVs. The constant bending and budding of the Ld and Lo domains are presumed to be an outcome of discrepancies in Rh2 inserting in these domains. In addition, the formation of stomatocyte-like Ld vesicles supports the proposed membrane surface binding of Rh2. As Rh2 saturates the outer leaflet of the membrane and creates nanoscopic protrusions, it enhances the asymmetry between leaflets resulting in this unique type of membrane deformation.

Solid-state NMR tackles the interactions of Rh2 in an Ld membrane at the atomistic level. This assay is from the perspective of Rh2 already incorporated into the bilayer and not coming from the membrane exterior. The local environment of the membrane headgroup was found to increase in fluidity with 10 % Rh2 in the bilayer. The glucose moiety of Rh2 is postulated to perturb the intermolecular forces between the phosphocholine headgroup PSM and POPC, a similar effect observed with ChoGlc (a cholesterol derivative bearing a glucose unit at C3). This results to a greater gap between phosphate esters, and the increase in wobbling of the P-N vector. In addition, the order of lipid acyl chains was disrupted based on ^{2}H NMR experiments. This implies that Rh2 does not portray a cholesterol-like ordering effect in the membrane interior. This seemingly contradicts the results from DPH anisotropy where Rh2 prompted an ordering effect in the interior of an Ld membrane. The following presumptions could account for the discrepancies between the NMR and DPH/laurdan results. First, there is a difference in the lipid-water ratios and membrane preparations between the two techniques. In the case of NMR experiments, Rh2 was abundantly incorporated in the bilayer interior, unlike in the other biophysical techniques where Rh2 emerged

from the outer leaflet. Therefore, data gathered in the NMR experiments reflects the wobbling of the acyl chains, and lacks the 'surface-crowding' effects of Rh2. Meanwhile, fluorescence anisotropy measurement is influenced by the hydration of the bilayer interior due to Rh2 molecules saturating the membrane surface. In ^{2}H NMR, Rh2 locates at the shallow portion of the Ld membrane with a tilted orientation, and effectively increases the gap between lipids. This causes the PSM acyl chains to be disordered and splay to occupy the interstices which may restrict further penetration of water molecules. When coupled with the effects of Rh2 saturating the membrane peripheral, a disordered membrane can have modulated hydration, and this complements the increase in DPH anisotropy and laurdan GP_{340} values. In the second presumption, binding of Rh2 in the membrane surface decreases the diffusion speed of lipids, and induce phase separation especially in a Ld membrane. As an effect, fluorescent probes (i.e., DPH and laurdan) can relocate to the ordered phase generated by Rh2, thereby increasing anisotropy and GP values.

Overall, this study presumes that Rh2 binds to the surface of the membrane in a parallel manner, driven by hydrophilic interactions between the polar headgroup and the polar constituents of Rh2. Due to the greater gap between lipids in a fluid phase, Rh2 can insert easily compared to a rigid phase. Once inside the Ld membrane, MD simulations revealed that the sapogenin of Rh2 adopts a tilted orientation of about ~30° relative to the membrane surface and that the glucose moiety locates closely to the phospholipid headgroup. The hydroxyl groups in Rh2 may prevent the side chains from inserting deeply into the bilayer, and it may be possible that the orientation of glucose changes when Rh2 is perpendicular to the membrane surface compared to when it is parallel. The phosphate and ester groups of POPC can form hydrogen bonds with the sugar moiety of Rh2 in either a parallel or vertical orientation. On the other hand, due to the close-fitting lipid environment in the Lo phase, Rh2 is pushed almost parallel to the lipid acyl chains, and its sapogenin adopts a ~70° angle.

Other triterpenoid saponins also show an affinity for Cho in membranes, and they exert membrane activity by inserting deeply into the bilayers and interacting with Cho. By contrast, Rh2 is unique in interacting with membrane lipids without Cho and in preferring Cho-poor Ld phase than Cho-rich Lo phase. In addition, the effects of these Rh2 behaviors in lipid bilayers on biological activity is an interesting topic. The glucocorticoid receptor (GR), a putative target of Rh2, is present in the plasma membrane, cytoplasm, and nucleus, and binds to steroid hormones, which are small lipophilic molecules and diffuse relatively freely through the cell membranes. On the other hand, Rh2 bearing a sugar unit shows higher hydrophilicity and probably binds to and permeates membrane systems more slowly than the hormones. While many saponins exhibit a high affinity for Cho, Rh2 binds more likely to the Ld phase with a lower Cho content. Since there are large differences in the distribution of Cho in the intracellular membrane system, it is likely that Rh2 preferentially accumulates in mitochondria and Golgi/ER membranes, where the amount of Cho is much lower than at the plasma membrane. The Lo/Ld phase-dependent affinity of Rh2 elucidated in this study can be useful information for improving the selectivity of pharmacological effects and suppressing side effects. To this end, it is necessary to clarify the structural factors of Rh2 that cause its membrane behavior to differ from that of Cho-selective saponins.

4.2. Conclusions

The ginsenoside Rh2 (Rh2), extracted from *Panax ginseng*, is a rare type of saponin. Its amphiphilic structure consists of a triterpene backbone and a glucose moiety in the 3 positions. Our approach to using model bilayers of

different lipid compositions and properties involves a specific analysis of the membrane effects of Rh2. The presence of the hydroxy groups at the 12 and 20 positions allows Rh2 to bind to the polar membrane surface. At higher saponin concentrations, Rh2 inserts effectively into the fluid Ld phase compared to the Lo phase. In POPC-based bilayers, the addition of Cho or SM did not significantly affect the membrane permeation activity of Rh2. In addition, there were no significant differences between the SM and saturated PC (DPPC) bilayers when examined according to the effects of Rh2 on acyl chain packing (DPH anisotropy) or water molecule permeability (laurdan and prodan GP values). Fluorescence experiments revealed the mode of interaction between Rh2 and the bilayer lipids. The hydration state of the bilayer estimated from the GP340 values implied that Rh2 tends to bind to the surface of the Lo and Ld bilayers, while in the Ld phase, Rh2 tends to be located in the relatively shallow interior of the bilayer. Surface tension-area isotherms revealed that Rh2 binds more abundantly to the monolayers of the Ld lipid composition than to those of the Lo lipid composition. MD simulations also suggest that the sapogenin portion of Rh2 is located in a relatively shallow (or boundary) region of the hydrophobic interior of the Ld phase. These results disclosed the unique mechanism in the efficient membrane permeabilization by Rh2; the saponin accumulates asymmetrically on the surface and in the shallow interior of the less ordered bilayers such as the Ld phase to cause membrane disruption. Understanding the molecular mechanism of Rh2 is advantageous in ensuring wider applications of the saponin. The importance of determining the precise mechanism of Rh2 concerns its applications, as Rh2 can be devised as an adjuvant in liposomal drug delivery systems. More generally, knowledge of the affinity of saponins for the membrane allows us to modify their structure for improving specific recognition by target cells. A better comprehension of their activities will tailor to factors of drug development, such as structure modification for longer bioavailability and lower hemolytic capacity.

~ Chapter 5 ~

Experimental Section

5.1. Materials

1-Palmitoyl-2-oleoyl-sn-glycero-3-phosphorylcholine **(**POPC) and 1,2-Dipalmitoyl-sn-glycero-3-phosphorylcholine (DPPC) were purchased from NOF Corp., Japan (Coatsome ®). N-palmitoyl-D-erythro-sphingosylphosphorylcholine (PSM) was purified from the Egg Yolk Sphingomyelin Mix purchased from Nagara Science Co., Ltd (Gifu, Japan). Then, 20(*S*)-ginsenoside Rh2 was obtained from Toronto Research Chemicals Inc. (North York, ON, Canada); glycyrrhizin from Wako Pure Chemical Industries, Ltd. (Osaka, Japan); and α-hederin from BLD Pharmtech Ltd. (Shanghai, China). Structures of 20(*S*)-ginsenoside Rh2, glycyrrhizin, and α-hederin are shown in *Fig. 2.2*. Chol, diphenylhexatriene (DPH), and prodan were purchased from Sigma-Aldrich (St. Louis, MO, USA). Laurdan was obtained from Cayman Chemicals (Ann Arbor, Michigan, USA), and calcein was purchased from Nacalai Tesque (Kyoto, Japan). Texas Red – DPPE and β-BODIPY FL C5-HPC were purchased from Thermo Fisher Scientific (Waltham, MA, USA), and Invitrogen, respectively. Kinoshita *et al.* synthesized 594neg-SSM, and deuterated probes, 3-d_1-cholesterol 10',10'-d_2-palmitoyl sphingomyelin (c/o Ayana Yamanaka) were synthesized from a previous protocol in our laboratory. All other chemicals used were of standard analytical quality.

5.2. Instruments

Microplate Reader	Corona Electric Microplate Reader MTP-800
Fluorescence Spectrofluorometer	Jasco FP-8500
High Performance Liquid Chromatography	Shimadzu SCL-10AVP
Mass Spectrometer	Thermo Scientific LTQ Orbitrap XL
Nuclear Magnetic Resonance Spectrometer	JEOL ECS400 and ECA500
	Varian CMX300
	Bruker Avance 400MHz
Confocal Fluorescence Microscope	FLUOVIEW FV1000D
Arbitrary Waveform Generator	33220A, Agilent Technologies
UV Spectrophotometer	Shimadzu UV-2500
Polycarbonate Extruder	LiposoFast Basic (200 and 100 nm pore size)

5.3. Experimental Methods

5.3.1. Hemolytic Assay

To evaluate the hemolytic capacity of saponins, the amount of hemoglobin released from the red blood cells incubated with saponin was quantified spectrophotometrically. In the hemolysis assay, 3 mL of freshly obtained human blood samples was washed with 10 mM phosphate buffered saline (PBS) at pH 7.4 and centrifuged at 2,000 rpm for 5 min to remove plasma. The pellet was resuspended in PBS to obtain a 10% (v/v) red blood cell (RBC) solution, and 1% (v/v) solution was prepared from the 10% (v/v) RBC solution. In an Eppendorf tube, 190 µL 1% (v/v) RBC suspension and 10 µL saponin of concentrations ranging from 1 to 100 µM were combined. The mixture was vortexed, incubated at 37 °C for 18 h, and centrifuged at 2,000 rpm for 5 min. The supernatant was carefully transferred into a 96-well microplate (Greiner Bio-one, PS-U), and absorbance of the samples was measured at 450 nm using a microplate reader (Corona Electric). A mixture of milliQ water/10% RBC (v/v; 9:1 volume ratio) was used as a positive control, and 1% (v/v) RBC/PBS (18:1 volume ratio) was used as the blank. Triplicate samples were prepared for each saponin concentration (Malabed *et al.,* 2017). The degree of hemolysis was calculated with the absorption at 450 nm, according to the formula:

$$\%hemolysis = \frac{A_{sample} - A_{blank}}{A_{positive\ control}}\ x\ 100 \qquad (1)$$

5.3.2. Calcein Leakage Assay

Vesicle disruption induced by saponins was assessed through a calcein leakage assay. Here, self-quenching calcein is entrapped in large unilamellar vesicles (LUVs) of different lipid compositions. The fluorescence intensity of calcein released through membrane disruption after incubating with saponin is monitored and quantified. In the assay, lipid film was produced by dissolving 10 mg of lipid mixture (POPC, POPC/Cho 9:1, PSM/POPC 1:9, PSM/POPC/Cho 1:8:1) in $CHCl_3$. The solvent was carefully removed using a rotary evaporator, and the film was dried overnight under vacuo. The lipid film was rehydrated with 60 mM calcein in Tris-HCl buffer (pH 7.4, 150mM NaCl, 1mM EDTA) and subjected to five freeze-thaw cycles to generate multilamellar vesicles (MLVs). The solution was filtered through the LiposoFast Basic Extruder (pore size 200 nm) 19 times and purified using Sepharose 4B to obtain homogenous LUVs containing calcein. The size of the LUVs ranged from 100 nm to 200 nm with the average value of 120 nm according to microscopic (TEM) observations. The lipid concentration of purified LUVs was quantified using the Phospholipid C test kit (Fujifilm Wako). The LUV solution was transferred into a 96-well microplate (Corning®, PS-F black, ref 3915) having a final concentration of 27 µM in each well. The initial fluorescence was measured using the Corona Electric Microplate Reader MTP-800 (λ_{ex} of 490 nm and λ_{em} of 517 nm). Then, saponins of different concentrations (1, 3, 10, 30, and 100 µM final concentrationin microplate) were added into the wells and mixed at a low speed for 30 s. Fluorescence intensity was measured after 5 min incubation at room temperature, and 10% Triton-10X was added to the saponin-lipid mixture to obtain thecondition of 100% leakage followed by fluorescence measurements (Malabed *et al.,* 2017). The measurements were done in triplicate and the % calcein leakage was calculated using the following equation; given that I_0, I_S, and I_T are

fluorescence intensities before saponin addition, after saponin incubation, and after 100% leakage with Triton-10X, respectively.

$$\% \, calcein \, leakage = \frac{I_S - I_0}{I_T - I_0} \, x \, 100 \qquad (2)$$

I_S – saponin addition; I_T – 100% leakage; I_0 – background

5.3.3. Confocal Fluorescence Microscopy

Preparation of Giant Unilamellar Vesicles (GUVs). Potential morphological changes induced by Rh2 to giant unilamellar vesicles of different lipid compositions was observed through confocal fluorescence microscopy. Using the electroformation method (Angelova and Dimitrov, 1986), GUVs composed of POPC, POPC/Cho 9:1 and POPC/PSM/Cho 8:1:1 (total of 1mg/mL) with 1% β-BODIPY FL C5-HPC (λ_{ex} of 488 nm and λ_{em} of 522 nm) were generated. Pt wires (φ = 100 µm; Nilaco Corp.) were fixed parallel onto a microscope cover glass (NEO, 0.12-0.17 mm). Between the Pt wires, about 5 µL aliquot of lipid and dye mixture was added and dried overnight under vacuo. A rubber spacer with a gap was secured to the cover glass using grease and was filled with milliQ water or 300mM sucrose to rehydrate the lipid film and a narrower microscope cover glass was used to seal the solution. The slide was placed in a temperature-controlled stage, and electroformation was induced by applying alternating current of 10 V (sinusoidal current) and 10 Hz (low frequency) (arbitrary waveform generator 33220A, Agilent Technologies) for 50 min at 50ºC and cooled to 25ºC for 30 min prior to microscopic observations. GUVs were viewed at room temperature using FLUOVIEW FV1000D scanning unit with an Olympus IX81 inverted microscope equipped with PLAPON 60× semi-apochromat objective lens (numerical aperture of 1.40). The acquisition speed was 10 µs/pixel. Images were captured before and after the addition of Rh2 solution (30µM final concentration on the glass plate) using FV10-ASW-3.0 software (Malabed *et al.,* 2020).

Calcein permeation through GUVs. This experiment was performed to determine whether morphological changes induced by Rh2 is relative to the permeation of calcein through the membrane. Briefly, GUVs were incubated with calcein prior to the addition of the saponin in the suspension. The fluorescence intensity of calcein in the interior and exterior of the vesicles was monitored (Verstraeten *et al.,* 2019). GUVs composed of POPC, POPC/Cho 9:1 and POPC/PSM/Cho 8:1:1 (total of 1mg/mL) with 0.5% Texas Red – DPPE (λ_{ex} of 586 nm and λ_{em} of 603 nm) were prepared through electroformation method described in the previous section. MilliQ water was used to rehydrate the lipid film in the glass slide. Initial images of GUVs were captured at room temperature, then calcein (10µM final concentration, λ_{ex} of 490 nm and λ_{em} of 517 nm) was added to the mixture, and allowed to disperse throughout the slide. Images were captured before and after the addition of Rh2 solution (30µM final concentration on the glass slide). Fluorescence intensity of calcein inside and outside of the vesicles were determined using ImageJ software.

Phase-separated GUVs. The effect of Rh2 to Lo and Ld domains were investigated by generating phase separated GUVs. In this experiment, GUVs composed of 1:1:1 POPC/PSM/Cho (total of 1mg/mL) labelled with 0.5% β-BODIPY FL C5-HPC as the Ld marker, and 594-neg-N-stearoylsphingomyelin (594-neg-SSM) (λ_{ex} of 601 nm and

λ_{em} of 627 nm) as the Lo marker (Lesoine *et al.*, 2012) (Kinoshita *et al.*, 2017). 3D images of phase separated GUVs were captured at room temperature before and after the addition of Rh2 solution.

5.3.4. Solid-state ^{31}P and ^{2}H Nuclear Magnetic Resonance Spectroscopy

Appropriate amounts of POPC, Cho, PSM and Rh2, and the deuterated probes 3-d_1-Cho, 10', 10'-d_2-PSM (total of 20 mg) were added in a flask and dissolved in HPLC grade 1:1 $CHCl_3$/MeOH. Solvent was evaporated to make homogenous and thin lipid film. The lipid film is dried under vacuo overnight. About 1 ml of deuterium depleted water was added in portions to the lipid film. The film was ripped from the flask by vortex and by warming the flask. The solution was transferred in the pre-weighed Eppendorf tube and subjected to 15 freeze (-20°C) and thaw (65°C) cycles to generate MLVs. The sample was lyophilized overnight and rehydrated with deuterium depleted water (50% hydration). The hydrated sample was subjected to a series of ripping, freezing, thawing, and mixing cycles until homogenous, and transferred in an NMR tube (Bruker HR-MAS insert). Sample tube was sealed using epoxy glue, dried overnight, and analyzed in the Bruker AVANCE 400WB spectrometer (400 MHz) (Billerica, MA, USA). The aforementioned sample preparation applies to both ^{2}H and ^{31}P NMR experiments.

For ^{2}H NMR, the spectrometer was equipped with a 5mm rotor 2H static probe, and the temperature was set at 20, 30, 40 and 50 °C. Under static conditions, solid-echo pulse sequence with a 90° pulse width at 5 µs was used, and operated at an interpulse delay of 30 µs, echo delay of 24 µs, and repetition delay of 5 ms. The sweep width of 250 kHz covered 4096 points, with scans ranging from 150,000 to 300,000.

$$\Delta\nu = \frac{3}{4} Q \times S_{mol} \times \frac{3\cos^2\theta - 1}{2} \quad (3)$$

Quadrupolar coupling widths ($\Delta\nu$) of the bilayer were calculated based on the equation above; given that Q is the quadrupolar splitting constant, S_{mol} is the order parameter, and θ is the angle between the C-D vector and outer magnetic field. The ^{31}P experiments were acquired using a triple resonance 4mm HXY MAS probe under static conditions with a 4.35 µs 90° pulse width, and relaxation delay of 2 s. Spinal-64 proton decoupling was performed at 30 kHz. The sweep width was 64 kHz covering 4096 repetition points totaling of 4000 scans. The probe temperature was set to 30°C. FID and spectra were processed using Delta NMR Software (Jeol USA, Inc., Peabody, MA, USA).

5.3.5. Fluorescence Anisotropy and Generalized Polarization of Laurdan and Prodan

To determine the mobility of the hydrophobic interior of the bilayers, diphenylhexatriene (DPH) fluorescence anisotropy measurements were carried out. DPH was pre-mixed into the lipid film composedof POPC/or PSM/Cho (total lipid: DPH 200:1 ratio) and dried overnight under vacuo. The lipid-probe film was rehydrated with 1 mL PBS (10 mM, pH 7.4), and LUVs were prepared in a similar way as described above. Liposomes containing the final lipid concentration of about 50 µM in PBS were mixed with Rh2 (0, 1, 3, 10, 30, and 100 µM total concentrations) and incubated at 37°C for 15 min, with occasional mixing prior to analysis (Ondevilla *et al.*, 2021). The mixture was transferred into a quartz cell, and fluorescence measurements were performed using the JASCO FP-8500

spectrofluorometer equipped with an automatic polarizer, a Peltier stirrer, and a thermostat cell holder. Anisotropy was measured at 30°C with excitation at 358 nm and fluorescence observation at 430 nm. Steady-state dye anisotropy was determined using the following equation:

$$r = \frac{I_{vv} - GI_{vh}}{I_{vv} + 2GI_{vh}} \qquad (4)$$

where *I* represents the fluorescent intensities of the *v* (vertical) and *h* (horizontal) settings of the excitation and emission polarizers, respectively. $G = I_{hv}/I_{hh}$ is an instrumental correction factor calculated individually for each sample, where I_{hv} and I_{hh} are intensities when the emission polarizer is set in the vertical and horizontal directions, respectively, relative to the horizontal excitation (Lakowicz, 2006).

Generalized polarization of laurdan and prodan. In this experiment, 2-dimethylamino-6-lauroylnaphthalene (laurdan) and 2-dimethylamino-6- propionylnaphthalene (prodan) were utilized, as they respond to the changes in membrane solvent polarity. Laurdan and prodan were premixed in separate batches of lipid films to have a final ratio of 200:1 (lipid/probe). Liposomes were prepared and incubated with Rh2, as described in the DPH anisotropy experiment (see Supplementary Materials). Using the FP-8500 spectrofluorometer (JASCO, Tokyo, Japan), the fluorescence emission of the probes was measured from 400 to 600 nm (λ_{ex} = 340 nm) at 30°C. The generalized polarization (GP_{ex}) was calculated using the following equation:

$$GP_{ex} = \frac{I_{440} - I_{490}}{I_{440} + I_{490}} \qquad (5)$$

where I_{440} and I_{490} are the emission intensities at 440 and 490 nm (Ondevilla *et al.,* 2021) (Parasassi *et al.*, 1990).

5.3.6. Surface Pressure-Molecular Area (π-A) Binding Assay (Dr. Masanao Kinoshita (Kyushu University))

Appropriate amounts of PSM, POPC, and Cho were dissolved in $CHCl_3$/MeOH (4:1 v/v, 1 mg/mL) and then, the lipid solution (30 μL) was spread onto the subphase (100 mm × 290 mm) using a glass micropipette (Drummond Scientific Company, Pennsylvania). The subphases were 250 mL of milli-Q water in the absence and presence of 0.63 μM and 1.25 μM Rh2. After an initial delay of 15 min to evaporate the organic solvent, the monolayer was compressed at a rate of 20 mm^2/s. The surface pressure of the lipid monolayer (π) was measured by Langmuir film balance (USI System, Fukuoka, Japan), and the average molecular area of lipids (*A*) was calculated by dividing the surface area of the subphase by the number of lipid molecules. The π–*A* isotherm of Rh2 alone was gained by laterally compressing the lipid-free Rh2 solution (1.25 μM). The vertical axis (*A*) of the Rh2 solution was calculated by dividing the surface area of the subphase by the number of lipid molecules to evaluate the influence of Rh2, which is originally deposited on the water surface, on the isotherm of the lipid monolayers. The subphase temperature and ambient temperature were kept at 25.0±0.1°C and 25±1°C, respectively. The measurements were repeated thrice under the same conditions to obtain reliable data (Kinoshita *et al.,* 2020).

5.3.7. Molecular Dynamics Simulation (Dr. Peter Greimel (RIKEN CBS))

The Ginsenoside Rh2 molecule was built based on the reported x-ray structure of ginsenoside compound K (20-O-β-glucopyranosyl-20(S)-protopanaxadiol) (Chen *et al.,* 2019) and parametrized using the CHARMM General FF (Soteras Gutiérrez *et al.,* 2016) based on the CHARMM36 lipid force field (Klauda *et al.,* 2010) and carbohydrate force fields, as well as and the previously reported cholesteryl-β-glucopyranoside (Hanashima *et al.,* 2021).

All systems were composed of a total of 36 lipids (33 phospholipids and 3 Rh2 molecules) per leaflet and . Pure phospholipid systems were hydrated with at least 33 water molecules per lipid, while Ginsenoside Rh2 containing systems were hydrated with up to 69 water molecules per lipid. The relatively small size of the membrane patch was confirmed to behave normally based on the results of test systems composed of pure phospholipids. Two Rh2 containing systems were constructed featuring exclusively vertical or horizontal initial orientation of the Rh2 triterpenoid core respectively. Each system was fully equilibrated at 37°C in NAMD (Phillips *et al.,* 2005) using NPT ensemble at 1atm, 2 fs time steps and cubic periodic boundary conditions. Pressure was controlled by Nose-Hoover Langevin-pistion and temperature was maintained via Langevin dynamics with a damping constant of 1.0 ps-1. Van der Waal interactionis were modeled with a Lennard-Jones potential with a force switching range of 10-12 Å, long-range electrostatic interactions were evaluated by the particle-mesh Ewald (PME) method and hydrogen bond lengths were kept constant by the RATTLE algorithm. All systems were simulated for a total of 500 ns, with the final 250 ns as production run. Pre and post processing was performed with the Visual Molecular Dynamics (VMD) package (Humphrey *et al.,* 1996) in part utilizing in-house scripts.

5.4. References

-Angelova, M.I.; Dimitrov, D. S. Liposome electroformation. *Faraday Discuss. Chem. Soc.* **1986**. *81*, 303–311.

-Chen, J.; Zhu, W.; Ji, W.; Zhu, B.; Guo, C.; Qi, M.; Ren, G. Crystal structure and physical stability of ginsenoside compound-K solvates. *CrystEngComm*. **2019**, *21*, 7313-7321.

-Hanashima, S.; Fukuda, N.; Malabed, R.; Murata, M.; Kinoshita, M.; Greimel, P.; Hirabayashi, Y. β-Glucosylation of cholesterol reduces sterol-sphingomyelin interactions. *Biochim. Biophys. Acta*. **2021**. *1863*, 183496

-Humphrey, W.; Dalke, A.; Schulten, K. VMD: Visual Molecular Dynamics. *J Mol Graph*, **1996.** *14*, 1, 33-38.

-Kinoshita, M.; Suzuki, K. G. N.; Matsumori, N.; Takada, M.; Ano, H.; Morigaki, K.; Abe, M.; Makino, A.; Kobayashi, T.; Hirosawa, K. M.; Fujiwara, T. K.; Kusumi, A.; Murata, M. Raft-based sphingomyelin interactions revealed by new fluorescent sphingomyelin analogs. *J. Cell Biol.* **2017**. *216*, 1183–1204.

-Kinoshita, M.; Yamaguchi, S.; Matsumori, N. Low-flux scanning electron diffraction reveals substructuresinside the ordered membrane domain. *Sci Rep.* **2020**, *10*, 1.

-Klauda, J. B.; Venable, R. M.; Freites, J. A.; O'Connor, J. W.; Tobias, D. J.; Mondragon-Ramirez, C.; Vorobyov, I.; MacKerell Jr, A. D. Update of the CHARMM all-atom additive force field for lipids: Validation on six lipid types. *J Phys Chem B.* **2010**, *114*, 7830–7843.

-Lakowicz, J. R. *Principles of fluorescence spectroscopy*, 3rd ed.; Springer, **2006**, 353-382.

-Lesoine, J. F.; Lee, J. Y.; Krogmeier, J. R.; Kang, H.; Clarke, M. L.; Chang, R.; Sackett, D. L.; Nossal, R.; Hwang, J. Quantitative scheme for full-field polarization rotating fluorescence microscopy using a liquid crystal variable retarder. *Rev Sci Instrum*. **2012**. *83*, 053705.

-Malabed, R.; Hanashima, S.; Murata, M.; Sakurai, K. Interactions of OSW-1 with Lipid Bilayers in Comparison with Digitonin and Soyasaponin. *Langmuir*. **2020.** *36*, 3600-3610.

-Malabed, R.; Hanashima, S.; Murata, M.; Sakurai, K. Sterol-recognition ability and membrane- disrupting activity of *Ornithogalum* saponin OSW-1 and usual 3-*O*-glycosyl saponins. *Biochim. Biophys.Acta.* **2017**, *1859*, 2516-2525.

-Ondevilla, J. C.; Hanashima, S.; Mukogawa, A.; Umegawa, Y.; Murata, M. Diosgenin-induced physicochemical effects on phospholipid bilayers in comparison with cholesterol. *Bioorg. Med. Chem. Lett.* **2021**. *36*, 127816.

-Parasassi, T.; De Stasio, G.; d'Ubaldo, A.; Gratton, E. Phase fluctuation in phospholipid membranesrevealed by Laurdan fluorescence. *Biophys. J.* **1990**. *57*, 1179-1186.

-Phillips, J. C.; Braun, R.; Wang, W.; Gumbart, J.; Tajkhorshid, E.; Villa, E.; Chipot, C.; Skeel, R. D.; Kalé, L.; Schulten, K. Scalable molecular dynamics with NAMD. *J. Comput. Chem.* **2005**. *26*, 16, 1781-1802.

-Soteras Gutiérrez, I.; Lin, F. Y.; Vanommeslaeghe, K.; Lemkul. J. A.; Armacos, K. A.; Brooks III, C. L.; MacKerell Jr, A. D. Parametrization of halogen bonds in the CHARMM general force field: Improved treatment of ligand-protein interactions. *Bioorg Med Chem*. **2016**, *24*, 20, 4812–4825.

-Verstraeten, S. L.; Deleu, M.; Janikowska-Sagan, M.; Claereboudt, E. J. S.; Lins, L.; Tyteca, D; Mingeot-Leclercq, M. P. The activity of the saponin ginsenoside Rh2 is enhanced by the interaction with membrane sphingomyelin but depressed by cholesterol. *Sci. Rep.* **2019**. *9*, 1-14.

~ Reprint Permissions ~

ELSEVIER ORDER DETAILS

Jul 12, 2022

This Agreement between Darcy L. Garza ("You") and Elsevier ("Elsevier") consists of your order details and the terms and conditions provided by Elsevier and Copyright Clearance Center.

Order Number	501745543
Order date	Jul 12, 2022
Licensed Content Publisher	Elsevier
Licensed Content Publication	Phytochemistry
Licensed Content Title	Saponins in the genus Panax L. (Araliaceae): A systematic review of their chemical diversity
Licensed Content Author	Wen-zhi Yang,Ying Hu,Wan-ying Wu,Min Ye,De-an Guo
Licensed Content Date	October 2014
Licensed Content Volume	106
Licensed Content Issue	n/a
Licensed Content Pages	18
Start Page	7
End Page	24
Type of Use	reuse in a thesis/dissertation
Portion	figures/tables/illustrations
Number of figures/tables/illustrations	1
Format	both print and electronic
Are you the author of this Elsevier article?	No
Will you be translating?	No
Title	Investigation of the behavior and interaction of ginsenoside Rh2 in model membranes containing cholesterol and sphingomyelin
Institution name	Osaka University
Expected presentation date	Sep 2022
Portions	Table 1.1
Requestor Location	Ms. Darcy Garza Shibaharacho 4-8-8 202 Socia Hill Shibaharacho 4 - chome 8-8 Toyonaka, Osaka 560-0055 Japan Attn: Ms. Darcy Garza
Publisher Tax ID	JP00022
Billing Type	Invoice
Billing Address	Ms. Darcy Garza Shibaharacho 4-8-8 202 Socia Hill Shibaharacho 4 - chome 8-8 Toyonaka, Japan 560-0055 Attn: Ms. Darcy Garza
Total	**0 JPY**
Terms and Conditions	

INTRODUCTION

1. The publisher for this copyrighted material is Elsevier. By clicking "accept" in connection with completing this licensing transaction, you agree that the following terms and conditions apply to this transaction (along with the Billing and Payment terms

ELSEVIER LICENSE TERMS AND CONDITIONS

Jul 12, 2022

This Agreement between Ms. Darcy Garza ("You") and Elsevier ("Elsevier") consists of your license details and the terms and conditions provided by Elsevier and Copyright Clearance Center.

License Number	5346811113499
License date	Jul 12, 2022
Licensed Content Publisher	Elsevier
Licensed Content Publication	Biochemical and Biophysical Research Communications
Licensed Content Title	Evidence that the tertiary structure of 20(S)-ginsenoside Rg3 with tight hydrophobic packing near the chiral center is important for Na+ channel regulation
Licensed Content Author	Dong-Il Kang,Jee-Young Lee,Ji-Young Yang,Sang Min Jeong,Jun-Ho Lee,Seung-Yeol Nah,Yangmee Kim
Licensed Content Date	Aug 12, 2005
Licensed Content Volume	333
Licensed Content Issue	4
Licensed Content Pages	8
Start Page	1194
End Page	1201
Type of Use	reuse in a thesis/dissertation
Portion	figures/tables/illustrations
Number of figures/tables/illustrations	1
Format	both print and electronic
Are you the author of this Elsevier article?	No
Will you be translating?	No
Title	Investigation of the behavior and interaction of ginsenoside Rh2 in model membranes containing cholesterol and sphingomyelin
Institution name	Osaka University
Expected presentation date	Sep 2022
Portions	Fig. 1.11
Requestor Location	Ms. Darcy Garza Shibaharacho 4-8-8 202 Socia Hill Shibaharacho 4 - chome 8-8 Toyonaka, Osaka 560-0055 Japan Attn: Ms. Darcy Garza
Publisher Tax ID	JP00022
Total	**0 JPY**
Terms and Conditions	

INTRODUCTION

1. The publisher for this copyrighted material is Elsevier. By clicking "accept" in connection with completing this licensing transaction, you agree that the following terms and conditions apply to this transaction (along with the Billing and Payment terms and conditions established by Copyright Clearance Center, Inc. ("CCC"), at the time that you opened your Rightslink account and that are available at any time at http://myaccount.copyright.com).

GENERAL TERMS

2. Elsevier hereby grants you permission to reproduce the aforementioned material subject to the terms and conditions indicated.

CCC Marketplace™

Order Date	13-Jul-2022	Type of Use	Republish in a thesis/dissertation
Order License ID	1246799-1		
ISSN	0265-0568	Publisher	ROYAL SOCIETY OF CHEMISTRY,
		Portion	Chart/graph/table/figure

LICENSED CONTENT

Publication Title	Natural product reports : a journal of current developments in bio-organic chemistry	Rightsholder	Royal Society of Chemistry
		Publication Type	Journal
		Start Page	256
Article Title	Recent advances in ginseng as cancer therapeutics: a functional and mechanistic overview.	End Page	272
		Issue	2
		Volume	32
Author/Editor	ROYAL SOCIETY OF CHEMISTRY (GREAT BRITAIN)		
Date	01/01/1984		
Language	English		
Country	United Kingdom of Great Britain and Northern Ireland		

REQUEST DETAILS

Portion Type	Chart/graph/table/figure	Distribution	Worldwide
Number of charts / graphs / tables / figures requested	1	Translation	Original language of publication
		Copies for the disabled?	No
Format (select all that apply)	Print, Electronic	Minor editing privileges?	No
Who will republish the content?	Academic institution	Incidental promotional use?	No
Duration of Use	Life of current edition	Currency	JPY
Lifetime Unit Quantity	Up to 499		
Rights Requested	Main product		

NEW WORK DETAILS

Title	Investigation of the behavior and interaction of ginsenoside Rh2 in model membranes containing cholesterol and sphingomyelin	Institution name	Osaka University
		Expected presentation date	2022-09-01

Instructor name	Prof. Michio Murata

ADDITIONAL DETAILS

Order reference number	N/A	The requesting person / organization to appear on the license	Darcy Lacanilao Garza

REUSE CONTENT DETAILS

Title, description or numeric reference of the portion(s)	Fig. 1.13	Title of the article/chapter the portion is from	Investigation of the behavior and interaction of ginsenoside Rh2 in model membranes containing cholesterol and sphingomyelin
Editor of portion(s)	Wong, Alice S T; Che, Chi-Ming; Leung, Kar-Wah	Author of portion(s)	Wong, Alice S T; Che, Chi-Ming; Leung, Kar-Wah
Volume of serial or monograph	32	Issue, if republishing an article from a serial	2
Page or page range of portion	256-272	Publication date of portion	2015-02-01

Marketplace Order General Terms and Conditions

The following terms and conditions ("General Terms"), together with any applicable Publisher Terms and Conditions, govern User's use of Works pursuant to the Licenses granted by Copyright Clearance Center, Inc. ("CCC") on behalf of the applicable Rightsholders of such Works through CCC's applicable Marketplace transactional licensing services (each, a "Service").

1) **Definitions.** For purposes of these General Terms, the following definitions apply:

"License" is the licensed use the User obtains via the Marketplace platform in a particular licensing transaction, as set forth in the Order Confirmation.

"Order Confirmation" is the confirmation CCC provides to the User at the conclusion of each Marketplace transaction. "Order Confirmation Terms" are additional terms set forth on specific Order Confirmations not set forth in the General Terms that can include terms applicable to a particular CCC transactional licensing service and/or any Rightsholder-specific terms.

"Rightsholder(s)" are the holders of copyright rights in the Works for which a User obtains licenses via the Marketplace platform, which are displayed on specific Order Confirmations.

"Terms" means the terms and conditions set forth in these General Terms and any additional Order Confirmation Terms collectively.

"User" or "you" is the person or entity making the use granted under the relevant License. Where the person accepting the Terms on behalf of a User is a freelancer or other third party who the User authorized to accept the General Terms on the User's behalf, such person shall be deemed jointly a User for purposes of such Terms.

"Work(s)" are the copyright protected works described in relevant Order Confirmations.

2) **Description of Service.** CCC's Marketplace enables Users to obtain Licenses to use one or more Works in accordance with all relevant Terms. CCC grants Licenses as an agent on behalf of the copyright rightsholder identified in the relevant Order Confirmation.

3) **Applicability of Terms.** The Terms govern User's use of Works in connection with the relevant License. In the event of any conflict between General Terms and Order Confirmation Terms, the latter shall govern. User acknowledges that Rightsholders have complete discretion whether to grant any permission, and whether to place any limitations on any grant, and that CCC has no right to supersede or to modify any such discretionary act by a Rightsholder.

4) **Representations; Acceptance.** By using the Service, User represents and warrants that User has been duly authorized by the User to accept, and hereby does accept, all Terms.

CCC Marketplace™

Order Date	13-Jul-2022	Type of Use	Republish in a thesis/dissertation
Order License ID	1246801-1		
ISSN	1477-0520	Publisher	ROYAL SOCIETY OF CHEMISTRY
		Portion	Chart/graph/table/figure

LICENSED CONTENT

Publication Title	Organic & biomolecular chemistry	Rightsholder	Royal Society of Chemistry
		Publication Type	Journal
Article Title	The amphiphilic nature of saponins and their effects on artificial and biological membranes and potential consequences for red blood and cancer cells.	Start Page	8803
		End Page	8822
		Issue	44
		Volume	12
Author/Editor	Royal Society of Chemistry (Great Britain)		
Date	01/01/2003		
Language	English		
Country	United Kingdom of Great Britain and Northern Ireland		

REQUEST DETAILS

Portion Type	Chart/graph/table/figure	Distribution	Worldwide
Number of charts / graphs / tables / figures requested	1	Translation	Original language of publication
		Copies for the disabled?	No
Format (select all that apply)	Print, Electronic	Minor editing privileges?	No
Who will republish the content?	Academic institution	Incidental promotional use?	No
Duration of Use	Life of current edition	Currency	JPY
Lifetime Unit Quantity	Up to 499		
Rights Requested	Main product		

NEW WORK DETAILS

Title	Investigation of the behavior and interaction of ginsenoside Rh2 in model membranes containing cholesterol and sphingomyelin	Institution name	Osaka University
		Expected presentation date	2022-09-01
Instructor name	Prof. Michio Murata		

ADDITIONAL DETAILS

Order reference number	N/A	**The requesting person / organization to appear on the license**	Darcy Lacanilao Garza

REUSE CONTENT DETAILS

Title, description or numeric reference of the portion(s)	Fig 1.15	**Title of the article/chapter the portion is from**	The amphiphilic nature of saponins and their effects on artificial and biological membranes and potential consequences for red blood and cancer cells.
Editor of portion(s)	Lorent, Joseph H.; Quetin-Leclercq, JoÃ«lle; Mingeot-Leclercq, Marie-Paule	**Author of portion(s)**	Lorent, Joseph H.; Quetin-Leclercq, JoÃ«lle; Mingeot-Leclercq, Marie-Paule
Volume of serial or monograph	12	**Issue, if republishing an article from a serial**	44
Page or page range of portion	8803-8822	**Publication date of portion**	2014-11-28

Marketplace Order General Terms and Conditions

The following terms and conditions ("General Terms"), together with any applicable Publisher Terms and Conditions, govern User's use of Works pursuant to the Licenses granted by Copyright Clearance Center, Inc. ("CCC") on behalf of the applicable Rightsholders of such Works through CCC's applicable Marketplace transactional licensing services (each, a "Service").

1) **Definitions.** For purposes of these General Terms, the following definitions apply:

"License" is the licensed use the User obtains via the Marketplace platform in a particular licensing transaction, as set forth in the Order Confirmation.

"Order Confirmation" is the confirmation CCC provides to the User at the conclusion of each Marketplace transaction. "Order Confirmation Terms" are additional terms set forth on specific Order Confirmations not set forth in the General Terms that can include terms applicable to a particular CCC transactional licensing service and/or any Rightsholder-specific terms.

"Rightsholder(s)" are the holders of copyright rights in the Works for which a User obtains licenses via the Marketplace platform, which are displayed on specific Order Confirmations.

"Terms" means the terms and conditions set forth in these General Terms and any additional Order Confirmation Terms collectively.

"User" or "you" is the person or entity making the use granted under the relevant License. Where the person accepting the Terms on behalf of a User is a freelancer or other third party who the User authorized to accept the General Terms on the User's behalf, such person shall be deemed jointly a User for purposes of such Terms.

"Work(s)" are the copyright protected works described in relevant Order Confirmations.

2) **Description of Service.** CCC's Marketplace enables Users to obtain Licenses to use one or more Works in accordance with all relevant Terms. CCC grants Licenses as an agent on behalf of the copyright rightsholder identified in the relevant Order Confirmation.

3) **Applicability of Terms.** The Terms govern User's use of Works in connection with the relevant License. In the event of any conflict between General Terms and Order Confirmation Terms, the latter shall govern. User acknowledges that Rightsholders have complete discretion whether to grant any permission, and whether to place any limitations on any grant, and that CCC has no right to supersede or to modify any such discretionary act by a Rightsholder.

4) **Representations; Acceptance.** By using the Service, User represents and warrants that User has been duly authorized by the User to accept, and hereby does accept, all Terms.

JOHN WILEY AND SONS LICENSE TERMS AND CONDITIONS

Jul 12, 2022

This Agreement between Ms. Darcy Garza ("You") and John Wiley and Sons ("John Wiley and Sons") consists of your license details and the terms and conditions provided by John Wiley and Sons and Copyright Clearance Center.

License Number	5346821025269
License date	Jul 12, 2022
Licensed Content Publisher	John Wiley and Sons
Licensed Content Publication	Wiley Books
Licensed Content Title	The Synaptic Physiology of the Central Nervous System Response to Stress
Licensed Content Author	Marian Joëls, Jeffrey G. Tasker
Licensed Content Date	Aug 21, 2015
Licensed Content Pages	28
Type of Use	Dissertation/Thesis
Requestor type	University/Academic
Format	Print and electronic
Portion	Figure/table
Number of figures/tables	1
Will you be translating?	No
Title	Investigation of the behavior and interaction of ginsenoside Rh2 in model membranes containing cholesterol and sphingomyelin
Institution name	Osaka University
Expected presentation date	Sep 2022
Portions	Fig. 1.14
Requestor Location	Ms. Darcy Garza Shibaharacho 4-8-8 202 Socia Hill Shibaharacho 4 - chome 8-8 Toyonaka, Osaka 560-0055 Japan Attn: Ms. Darcy Garza
Publisher Tax ID	EU826007151
Billing Type	Invoice
Billing Address	Ms. Darcy Garza Shibaharacho 4-8-8 202 Socia Hill Shibaharacho 4 - chome 8-8 Toyonaka, Japan 560-0055 Attn: Darcy L. Garza
Total	**0 JPY**
Terms and Conditions	

TERMS AND CONDITIONS

This copyrighted material is owned by or exclusively licensed to John Wiley & Sons, Inc. or one of its group companies (each a"Wiley Company") or handled on behalf of a society with which a Wiley Company has exclusive publishing rights in relation to a particular work (collectively "WILEY"). By clicking "accept" in connection with completing this licensing transaction, you agree that the following terms and conditions apply to this transaction (along with the billing and payment terms and conditions established by the Copyright Clearance Center Inc., ("CCC's Billing and Payment terms and conditions"), at the time that you opened your RightsLink account (these are available at any time at http://myaccount.copyright.com).

Terms and Conditions

ELSEVIER LICENSE TERMS AND CONDITIONS

Jul 12, 2022

This Agreement between Ms. Darcy Garza ("You") and Elsevier ("Elsevier") consists of your license details and the terms and conditions provided by Elsevier and Copyright Clearance Center.

License Number	5346830357922
License date	Jul 12, 2022
Licensed Content Publisher	Elsevier
Licensed Content Publication	Biochemical and Biophysical Research Communications
Licensed Content Title	Ginsenoside Rh2 induces ligand-independent Fas activation via lipid raft disruption
Licensed Content Author	Jae-Sung Yi,Hyo-Jung Choo,Bong-Rae Cho,Hwan-Myung Kim,Yong-Nyun Kim,Young-Mi Ham,Young-Gyu Ko
Licensed Content Date	Jul 24, 2009
Licensed Content Volume	385
Licensed Content Issue	2
Licensed Content Pages	6
Start Page	154
End Page	159
Type of Use	reuse in a thesis/dissertation
Portion	figures/tables/illustrations
Number of figures/tables/illustrations	1
Format	both print and electronic
Are you the author of this Elsevier article?	No
Will you be translating?	No
Title	Investigation of the behavior and interaction of ginsenoside Rh2 in model membranes containing cholesterol and sphingomyelin
Institution name	Osaka University
Expected presentation date	Sep 2022
Portions	Fig. 1.16
Requestor Location	Ms. Darcy Garza Shibaharacho 4-8-8 202 Socia Hill Shibaharacho 4 - chome 8-8 Toyonaka, Osaka 560-0055 Japan Attn: Ms. Darcy Garza
Publisher Tax ID	JP00022
Total	**0 JPY**
Terms and Conditions	

INTRODUCTION

1. The publisher for this copyrighted material is Elsevier. By clicking "accept" in connection with completing this licensing transaction, you agree that the following terms and conditions apply to this transaction (along with the Billing and Payment terms and conditions established by Copyright Clearance Center, Inc. ("CCC"), at the time that you opened your Rightslink account and that are available at any time at http://myaccount.copyright.com).

GENERAL TERMS

2. Elsevier hereby grants you permission to reproduce the aforementioned material subject to the terms and conditions indicated.

ELSEVIER LICENSE TERMS AND CONDITIONS

Jul 12, 2022

This Agreement between Ms. Darcy Garza ("You") and Elsevier ("Elsevier") consists of your license details and the terms and conditions provided by Elsevier and Copyright Clearance Center.

License Number	5346841318432
License date	Jul 12, 2022
Licensed Content Publisher	Elsevier
Licensed Content Publication	Biochimica et Biophysica Acta (BBA) - Biomembranes
Licensed Content Title	Complementary biophysical tools to investigate lipid specificity in the interaction between bioactive molecules and the plasma membrane: A review
Licensed Content Author	Magali Deleu,Jean-Marc Crowet,Mehmet N. Nasir,Laurence Lins
Licensed Content Date	Dec 1, 2014
Licensed Content Volume	1838
Licensed Content Issue	12
Licensed Content Pages	20
Start Page	3171
End Page	3190
Type of Use	reuse in a thesis/dissertation
Portion	figures/tables/illustrations
Number of figures/tables/illustrations	1
Format	both print and electronic
Are you the author of this Elsevier article?	No
Will you be translating?	No
Title	Investigation of the behavior and interaction of ginsenoside Rh2 in model membranes containing cholesterol and sphingomyelin
Institution name	Osaka University
Expected presentation date	Sep 2022
Portions	Fig. 1.20
Requestor Location	Ms. Darcy Garza Shibaharacho 4-8-8 202 Socia Hill Shibaharacho 4 - chome 8-8 Toyonaka, Osaka 560-0055 Japan Attn: Ms. Darcy Garza
Publisher Tax ID	JP00022
Total	**0 JPY**
Terms and Conditions	

INTRODUCTION

1. The publisher for this copyrighted material is Elsevier. By clicking "accept" in connection with completing this licensing transaction, you agree that the following terms and conditions apply to this transaction (along with the Billing and Payment terms and conditions established by Copyright Clearance Center, Inc. ("CCC"), at the time that you opened your Rightslink account and that are available at any time at http://myaccount.copyright.com).

GENERAL TERMS

2. Elsevier hereby grants you permission to reproduce the aforementioned material subject to the terms and conditions indicated.

ELSEVIER LICENSE TERMS AND CONDITIONS

Jul 13, 2022

This Agreement between Ms. Darcy Garza ("You") and Elsevier ("Elsevier") consists of your license details and the terms and conditions provided by Elsevier and Copyright Clearance Center.

License Number	5346860122395
License date	Jul 13, 2022
Licensed Content Publisher	Elsevier
Licensed Content Publication	Bioorganic & Medicinal Chemistry Letters
Licensed Content Title	Diosgenin-induced physicochemical effects on phospholipid bilayers in comparison with cholesterol
Licensed Content Author	Joan Candice Ondevilla,Shinya Hanashima,Akane Mukogawa,Yuichi Umegawa,Michio Murata
Licensed Content Date	Mar 15, 2021
Licensed Content Volume	36
Licensed Content Issue	n/a
Licensed Content Pages	1
Start Page	127816
End Page	0
Type of Use	reuse in a thesis/dissertation
Portion	figures/tables/illustrations
Number of figures/tables/illustrations	1
Format	both print and electronic
Are you the author of this Elsevier article?	No
Will you be translating?	No
Title	Investigation of the behavior and interaction of ginsenoside Rh2 in model membranes containing cholesterol and sphingomyelin
Institution name	Osaka University
Expected presentation date	Sep 2022
Portions	Fig. 1.22
Requestor Location	Ms. Darcy Garza Shibaharacho 4-8-8 202 Socia Hill Shibaharacho 4 - chome 8-8 Toyonaka, Osaka 560-0055 Japan Attn: Ms. Darcy Garza
Publisher Tax ID	JP00022
Total	**0 JPY**
Terms and Conditions	

INTRODUCTION

1. The publisher for this copyrighted material is Elsevier. By clicking "accept" in connection with completing this licensing transaction, you agree that the following terms and conditions apply to this transaction (along with the Billing and Payment terms and conditions established by Copyright Clearance Center, Inc. ("CCC"), at the time that you opened your Rightslink account and that are available at any time at http://myaccount.copyright.com).

GENERAL TERMS

2. Elsevier hereby grants you permission to reproduce the aforementioned material subject to the terms and conditions indicated.
3. Acknowledgement: If any part of the material to be used (for example, figures) has appeared in our publication with credit or acknowledgement to another source, permission must also be sought from that source. If such permission is not obtained then

SPRINGER NATURE LICENSE TERMS AND CONDITIONS

Jul 13, 2022

This Agreement between Ms. Darcy Garza ("You") and Springer Nature ("Springer Nature") consists of your license details and the terms and conditions provided by Springer Nature and Copyright Clearance Center.

License Number	5346860328293
License date	Jul 13, 2022
Licensed Content Publisher	Springer Nature
Licensed Content Publication	Journal of Fluorescense
Licensed Content Title	Laurdan and Prodan as Polarity-Sensitive Fluorescent Membrane Probes
Licensed Content Author	Tiziana Parasassi et al
Licensed Content Date	Jan 1, 1998
Type of Use	Thesis/Dissertation
Requestor type	academic/university or research institute
Format	print and electronic
Portion	figures/tables/illustrations
Number of figures/tables/illustrations	1
Will you be translating?	no
Circulation/distribution	1 - 29
Author of this Springer Nature content	no
Title	Investigation of the behavior and interaction of ginsenoside Rh2 in model membranes containing cholesterol and sphingomyelin
Institution name	Osaka University
Expected presentation date	Sep 2022
Portions	Fig. 1.23
Requestor Location	Ms. Darcy Garza Shibaharacho 4-8-8 202 Socia Hill Shibaharacho 4 - chome 8-8 Toyonaka, Osaka 560-0055 Japan Attn: Ms. Darcy Garza
Total	**0 JPY**
Terms and Conditions	

Springer Nature Customer Service Centre GmbH
Terms and Conditions

This agreement sets out the terms and conditions of the licence (the **Licence**) between you and **Springer Nature Customer Service Centre GmbH** (the **Licensor**). By clicking 'accept' and completing the transaction for the material (**Licensed Material**), you also confirm your acceptance of these terms and conditions.

1. Grant of License

1. 1. The Licensor grants you a personal, non-exclusive, non-transferable, world-wide licence to reproduce the Licensed Material for the purpose specified in your order only. Licences are granted for the specific use requested in the order and for no other use, subject to the conditions below.

1. 2. The Licensor warrants that it has, to the best of its knowledge, the rights to license reuse of the Licensed Material. However, you should ensure that the material you are requesting is original to the Licensor and does not carry the

ELSEVIER LICENSE TERMS AND CONDITIONS

Jul 13, 2022

This Agreement between Ms. Darcy Garza ("You") and Elsevier ("Elsevier") consists of your license details and the terms and conditions provided by Elsevier and Copyright Clearance Center.

License Number	5346860716746
License date	Jul 13, 2022
Licensed Content Publisher	Elsevier
Licensed Content Publication	Elsevier Books
Licensed Content Title	Annual Reports on NMR Spectroscopy
Licensed Content Author	Andrei V. Filippov,Aidar M. Khakimov,Bulat V. Munavirov
Licensed Content Date	Jan 1, 2015
Licensed Content Pages	66
Start Page	27
End Page	92
Type of Use	reuse in a thesis/dissertation
Portion	figures/tables/illustrations
Number of figures/tables/illustrations	1
Format	both print and electronic
Are you the author of this Elsevier chapter?	No
Will you be translating?	No
Title	Investigation of the behavior and interaction of ginsenoside Rh2 in model membranes containing cholesterol and sphingomyelin
Institution name	Osaka University
Expected presentation date	Sep 2022
Portions	Fig. 1.26
Requestor Location	Ms. Darcy Garza Shibaharacho 4-8-8 202 Socia Hill Shibaharacho 4 - chome 8-8 Toyonaka, Osaka 560-0055 Japan Attn: Ms. Darcy Garza
Publisher Tax ID	JP00022
Total	**0 JPY**
Terms and Conditions	

INTRODUCTION

1. The publisher for this copyrighted material is Elsevier. By clicking "accept" in connection with completing this licensing transaction, you agree that the following terms and conditions apply to this transaction (along with the Billing and Payment terms and conditions established by Copyright Clearance Center, Inc. ("CCC"), at the time that you opened your Rightslink account and that are available at any time at http://myaccount.copyright.com).

GENERAL TERMS

2. Elsevier hereby grants you permission to reproduce the aforementioned material subject to the terms and conditions indicated.
3. Acknowledgement: If any part of the material to be used (for example, figures) has appeared in our publication with credit or acknowledgement to another source, permission must also be sought from that source. If such permission is not obtained then that material may not be included in your publication/copies. Suitable acknowledgement to the source must be made, either as a footnote or in a reference list at the end of your publication, as follows:

Concepts and Methods of Solid-State NMR Spectroscopy Applied to Biomembranes

Author: Trivikram R. Molugu, Soohyun Lee, Michael F. Brown
Publication: Chemical Reviews
Publisher: American Chemical Society
Date: Oct 1, 2017

LANGMUIR

pubs.acs.org/Langmuir Article

Behavior of Triterpenoid Saponin Ginsenoside Rh2 in Ordered and Disordered Phases in Model Membranes Consisting of Sphingomyelin, Phosphatidylcholine, and Cholesterol

Darcy Lacanilao Garza, Shinya Hanashima,* Yuichi Umegawa, Michio Murata,* Masanao Kinoshita, Nobuaki Matsumori, and Peter Greimel

Cite This: https://doi.org/10.1021/acs.langmuir.2c01261 Read Online

ACCESS | Metrics & More | Article Recommendations | Supporting Information

ABSTRACT: The ginsenoside Rh2 (Rh2) is a saponin of medicinal ginseng, and it has attracted much attention for its pharmacological activities. In this study, we investigated the interaction of Rh2 with biological membranes using model membranes. We examined the effects of various lipids on the membrane-disrupting activity of Rh2 and found that cholesterol and sphingomyelin (SM) had no significant effect. Furthermore, the effects of Rh2 on acyl chain packing (DPH anisotropy) and water molecule permeability (GP_{340} values) did not differ significantly between bilayers containing SM and saturated phosphatidylcholine. These results suggest that the formation of the liquid-ordered (Lo) phase affects the behavior of Rh2 in the membrane rather than a specific interaction of Rh2 with a particular lipid. We investigated the effects of Rh2 on the Lo and liquid-disordered (Ld) phases using surface tension measurements and fluorescence experiments. In the surface tension−area isotherms, we compared the monolayers of the Ld and Lo lipid compositions and found that Rh2 is abundantly bound to both monolayers, with the amount being greater in the Ld phase than in the Lo phase. In addition, the hydration state of the bilayers, mainly consisting of the Lo or Ld phase, showed that Rh2 tends to bind to the surface of the bilayer in both phases. At higher concentrations, Rh2 tends to bind more abundantly to the relatively shallow interior of the Ld phase than the Lo phase. The phase-dependent membrane behavior of Rh2 is probably due to the phase-selective affinity and binding mode of Rh2.

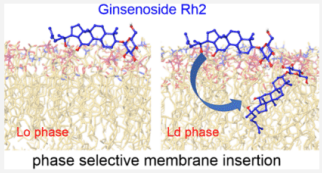

INTRODUCTION

Apprehending the molecular mechanisms of drugs is crucial to discern their pharmacokinetic properties and long-lasting actions accurately. Most synthetic and natural drugs target membrane proteins, such as G-protein-coupled receptors, ion channels, and transporters. A specific target protein is only a minute portion of the overall component of the plasma membrane; thus, the occurrence of a ligand precisely hitting its target protein is less probable. Ligands mostly diffuse through the phospholipid bilayer of the plasma membrane, prior to its interaction with a specific protein.[1,2] Along with the lipid matrix, the adsorbed ligand interacts with non-specific areas, anchors at a particular depth, and orients itself near the target protein. Several ligands were observed to be largely exposed to bulk lipid assembly rather than the target protein.[3] Therefore, apart from the ligand−protein association, it is equally critical to investigate the interaction of ligands with the lipid components of the membrane. The extent of ligand partitioning along the protein−lipid interface is driven by the structure and lipophilicity of drugs.[3,4] The amphiphilic characteristic of ligands is a vital factor that instigates direct integration and effective diffusion in the bilayers.

Saponins, a class of natural products, are known for their amphiphilic nature.[5,6] Ginsenosides are a class of bioactive saponins known as key components of the oldest and most-utilized herbal medicine, ginseng (*Panax* L.).[7−13] Stimulation of somatic and cognitive functioning and the alleviation of certain illnesses are attributed to ginsenosides. The ginsenoside Rh2 was first isolated and characterized with its structural isomer ginsenoside Rh1 (glucose is substituted at the C6 position of the triterpenoid sapogenin of Rh2) in 1985. These ginsenosides belong to triterpenoid saponins bearing the protopanaxadiol backbone, with β-glucose attached to its C6 and C3 position for Rh1 and Rh2, respectively.[14] Odashima et al. compared the effects of Rh1 and Rh2 in B16 melanoma cells, and despite their structural similarities, Rh2 instigated the inhibition of cell growth and melanogenesis, while Rh1 simply stimulated melanogenesis.[14,15] This striking difference in their biological effects has led to further scrutinization of Rh2. Cancer combination therapy studies have revealed the promising effects of incorporating Rh2 in current cancer medications. Its amphiphilic nature allows the formation of nanostructures, making it a potential adjuvant of drug carriers.[17,16]

Received: May 17, 2022
Revised: August 7, 2022

~ Acknowledgement ~

Moving to a foreign land is an enormous decision bound by excitement, fear, and expectations. At times, the disparity between two cultures and the pressure to adapt to a new environment hampers progress and diminishes self-assurance. However, it is through conquering adversities that we become resilient and wiser. And cultivating a grateful heart and appreciating the smallest blessings shift your perspective towards the positive. This journey is nothing but wonderful, and I wish to express my utmost gratitude to the people who gave me strength and encouragement.

To God, you have humbled me throughout this journey. You have showed me hope in times of despair, and how every day is beautiful in the simplest ways. Thank you for blessing me with this opportunity, and for guiding me throughout life.

To my mentor, Professor Michio Murata, I am grateful to you more than words could express. Thank you for not only accepting me in your research group, but for also being an understanding and a compassionate adviser. Your guidance and wisdom encouraged me to grow throughout this journey. To my supervisor, Dr. Shinya Hanashima, I truly appreciate your kindness and guidance. Thank you for always sharing your time and knowledge. And to Drs. Yuichi Umegawa and Tomokazu Yasuda, your assistance is always valuable and well-appreciated. If not for the great and inspiring mentors in this research group, this feat will be impossible.

To my family, thank you for showering me with unconditional love and support. To Mommy and Daddy, thank you for always believing in me – this achievement is a fruit of your immeasurable support for me. To Kuya Da, Kuya Den and Dana, Ate Bianca and Manu, thank you for always uplifting my spirit despite the distance. And to my fur babies, One and Chubby, your presence is a gift itself. I can't wait to be with you all again soon.

To my best college buddies, Therese, Ryan and Awe, you are indeed family, and I am forever grateful to have you guys in my life. You never failed to show your love and support despite us being scattered across continents. I look forward to making more memories (and getting more passport stamps) with you three.

To Ate Anna and Ms. Candy, I gained sisters because of you two. My move to Japan was more delightful because of the memories I share with you. I can't thank you enough for always looking after me. Our friendship has indeed become one of the safe spaces in my heart.

To Fatsy, Sittie and Jamie, our unexpected sisterhood holds a special place in my heart. Thank you for always reminding me to keep my faith grounded, and for remembering me in your prayers.

To my second home, the DLSU Chemistry Department family – Dr. J., Dr. Nancy, Dr. Alea, Dr. Jimmy, Dr. Guidote, Dr. Carmen, Sir Raymond, and to the rest – *Maraming Salamat po.* Thank you for all the prayers and encouragements. And a special thanks to Dr. Marissa Noel for not only being an amazing mentor but for also being a second mother to me.

To Yofu-san, from day one, I am always grateful not only for your unending assistance but also for the friendship we share. To my labmates, Senior, Kulos, Minamino-san, Nakano-san, Ohta-kun, Tomota-san, Yamanaka-san, Katayama-kun, Suzuki-kun, Fukuda-san, Moku-chan, and to the rest, I appreciate your hospitality, and I will forever treasure our happy memories.

And to my husband, Nampei Miyazato, your unfathomable love towards me has moved mountains. *Ang pagmamahal mo sa akin ay isang biyayang walang kapantay.*